2014 / Volume 52 / Number 4
ISSN 1641-4640

Folia NEUROPATHOLOGICA

www.folianeuro.termedia.pl

Official Journal of Mossakowski Medical Research Centre Polish Academy of Sciences
and
Polish Association of Neuropathologists

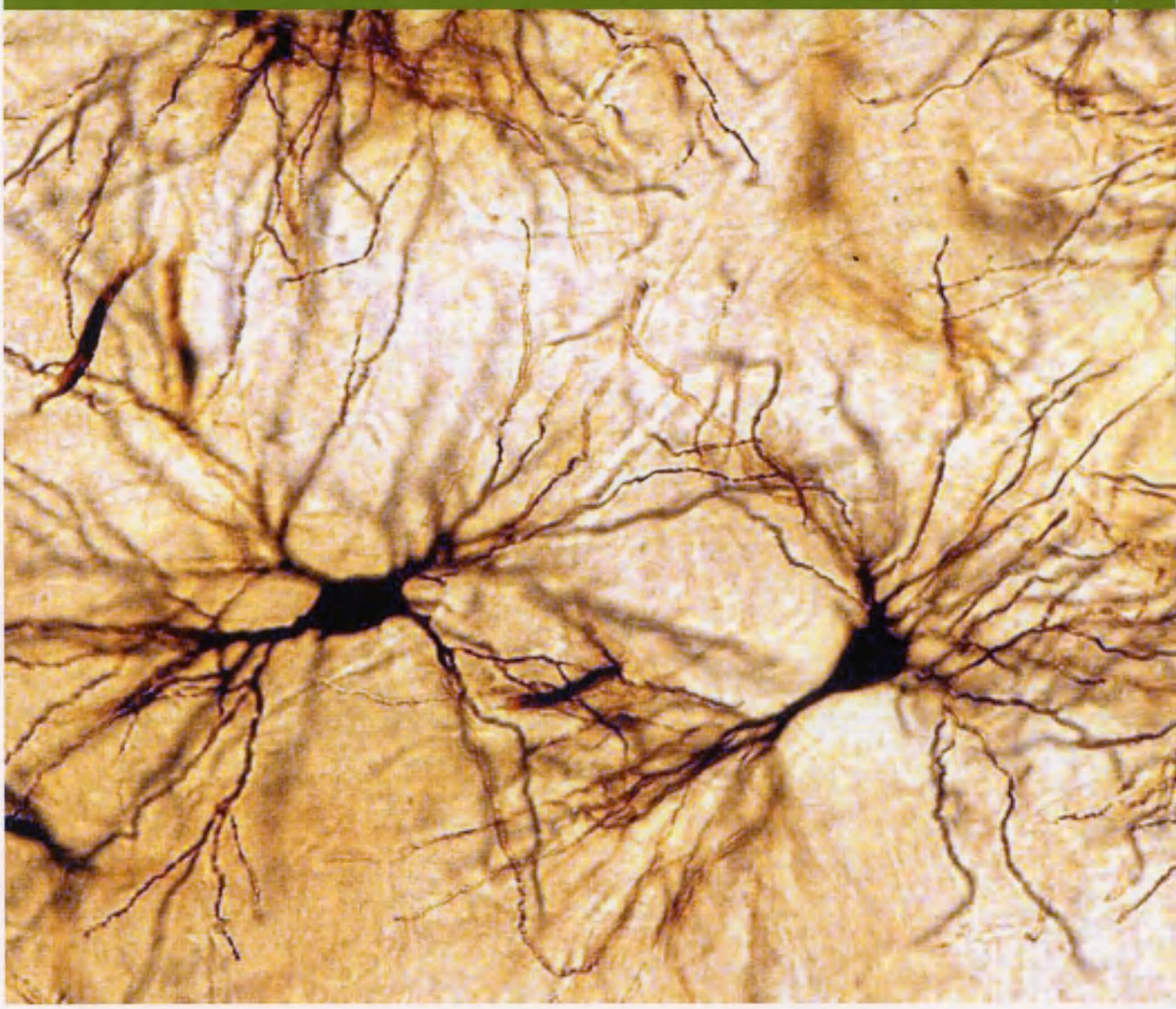

ISSN 1641-4640

Folia Neuropathologica

TERMEDIA Publishing House

Folia
Neuropathologica
former *Neuropatologia Polska*

Official Journal of Mossakowski Medical Research Centre Polish Academy of Sciences and Polish Association of Neuropathologists

The journal is partly financially supported by the Ministry of Science and Higher Education

termedia

Termedia Publishing House
Kleeberga 2, 61-615 Poznań, Poland
phone/fax: +48 61 822 77 81
e-mail: termedia@termedia.pl
www.termedia.pl
www.folianeuro.termedia.pl

Warsaw office
phone/fax: +48 22 827 75 14
e-mail: biuro.warszawa@termedia.pl

president of the management board
editor-in-chief of the Publishing House, director
Janusz Michalak
e-mail: j.michalak@termedia.pl

director of the Publishing House
Andrzej Kordas
e-mail: a.kordas@termedia.pl

Marketing and Advertising Department
Renata Dolata
phone: +48 61 822 77 81 ext. 508
e-mail: r.dolata@termedia.pl

Distribution Subscription Department
Jolanta Jankowiak
phone: +48 61 656 22 00
e-mail: prenumerata@termedia.pl

Impact Factor for Folia Neuropathologica equals 1.667
MNiSW score for Folia Neuropathologica equals 15.00
Index Copernicus score (2011) for Folia Neuropathologica equals 18.13
Position in Index Copernicus ranking systems available at http://www.indexcopernicus.pl

Abstracted and indexed in Index Medicus/MEDLINE, Neuroscience Citation Index, SciSearch, Research Alert, Chemical Abstracts, EMBASE/Excerpta Medica, Polish Medical Bibiography, Index Copernicus

The journal is financially supported by the Ministry of Sciences and Higher Education.

Print run: 450 copies

Folia
Neuropathologica
2014; 52/4: 377-482

Contents

Review paper

Folia Neuropathologica

Impairment of glutamine/glutamate-γ-aminobutyric acid cycle in manganese toxicity in the central nervous system

Marta Sidoryk-Wegrzynowicz

Department of Clinical Neurosciences, The Clifford Allbutt Building (CAB), University of Cambridge, Cambridge, United Kingdom

Folia Neuropathol 2014; 52 (4): 377-382 DOI: 10.5114/fn.2014.47838

Abstract

Manganese (Mn) is an essential trace element that is required for maintaining the proper function and regulation of many biochemical and cellular reactions. Despite its essentiality, at excessive levels Mn is toxic to the central nervous system. The overdose accumulation of Mn in specific brain areas, such as the substantia nigra, the globus pallidus and the striatum, triggers neurotoxicity resulting in a neurological brain disorder, referred to as manganism. Manganese toxicity is associated with the disruption of glutamine (Gln)/glutamate (Glu) GABA cycle (GGC). The GGC represents a complex process, since Gln efflux from astrocytes must be met by its influx in neurons. Mn toxicity is associated with the disruption of both of these critical points in the cycle. In cultured astrocytes, pre-treatment with Mn inhibits the initial net uptake of Gln in a concentration-dependent manner. Manganese added directly to astrocytes induces deregulation in the expression of SNAT3, SNAT2, ASCT2 and LAT2 transporters and significantly decreases in Gln uptake mediated by the transporting Systems N and ASC, and a decrease in Gln efflux mediated by Systems N, ASC and L. Further, Mn disrupts Glu transporting systems leading to both a reduction in Glu uptake and elevation in extracellular Glu levels. Interestingly, there appear to be common signaling targets of Mn in GGC cycling in glial cells. Namely, the PKC signaling is affected by Mn in Gln and Glu transporters expression and function. Additionally, Mn was identified to deregulate glutamine synthetase (GS) expression and activity. Those evidences could triggers depletion of Gln synthesis/metabolism in glia cells and consequently diminish astrocytic-derived glutamine, while disruption of Glu removal/transport can mediate dyshomeostasis in neurotransmission of functioning neurons. Overdose and excessive Mn accumulations in astrocytes not only culminate in pathology, but also affect astrocytic protective properties and defect or alternate astrocyte-neuronal integrity. Here we highlight the mechanistic commonalities inherent to Mn neurotoxicity related to the astrocyte pathology and GGC impairment.

Key words: *manganese, neurodegeneration, neurotoxicity, transporter, Gln, Glu, GABA.*

Manganese

Essentiality and toxicity

Manganese (Mn) is an essential trace metal commonly found in the environment. It is an important dietary nutrient, and as such is required for growth, development, and maintenance of normal physiological function. Manganese is necessary for a variety of metabolic functions, including lipid, protein, and carbohydrate metabolism. It is a critical component of numerous metalloenzymes, including Mn superoxide dismutase, arginase, glutamine synthetase and

Communicating author:

Marta Sidoryk-Wegrzynowicz, PhD, Department of Clinical Neurosciences, The Clifford Allbutt Building (CAB), University of Cambridge, Hills Road, Cambridge CB2 0QH, UK, e-mail: ms2069@cam.ac.uk

phosphoenolpyruvate decarboxylase [42], to name a few. However, excessive and prolonged exposure to Mn may lead to a neurological disorder that shares many similarities with Parkinson's disease (PD), and is referred to as manganism [15]. Exposure to Mn in the general population occurs from the automobile combustion of gasoline containing methylcyclopentadienyl manganese tricarbonyl (MMT) or from organic Mn-containing pesticides, such as manganese ethylene-bis-dithiocarbamate [8]. Chronic exposure to high levels of inhalable Mn (1-5 mg Mn/m^3), which is commonly associated with several occupations (e.g. mining, battery manufacturing, welding, ferroalloy smelting, and steel production), is believed to be the most frequent cause of Mn neurotoxicity [32]. Individuals with some medical conditions such as liver failure or total parenteral nutrition exhibit elevated Mn blood level and neurological dysfunctions [1]. The accumulation of Mn in basal ganglia is responsible for a form of parkinsonism with clinical features overlapping with, but distinct from, those observed in idiopathic PD [18]. Manganese-induced neurotoxicity affects mainly the globus pallidus as well as the cortex and hypothalamus [48,50], distinct from the striatal changes associated with PD. Excessive Mn deposition in the central nervous system (CNS) contributes to the pathogenesis of PD, causing loss of dopamine in the striatum, death of non-dopaminergic (DAergic) neurons in the globus pallidus, and damage to glutamatergic and GABAergic projections [25,39]. Manganese has also been shown to mediate fibril formation by α-synuclein along with its expression and aggregation [47]. A role for Mn has also been advanced in the etiology of a few neurodegenerative disorders, e.g. Huntington's disease, amyotrophic lateral sclerosis, prion diseases and Alzheimer's disease (AD), all of which rely on similar intracellular mechanisms involving oxidative stress, mitochondrial impairment, and protein aggregation.

Mitochondrial dysfunction was found to be a common effect in Mn toxicity [7]. A previous study showed that primary astrocytic cultures are highly sensitive to Mn and undergo apoptotic cell death involving mitochondrial dysfunction [51]. Manganese was found to be preferentially and rapidly transported into the mitochondrial matrix via the calcium (Ca^{2+}) uniporter, with relatively slow clearance, leading to the accumulation of Ca^{2+} [16]. Elevated matrix calcium increases formation of reactive oxygen species (ROS) by the electron transport chain and mediates inhibition of aerobic respiration [22]. Manganese was found to induce mitochondrial respiratory dysfunction *in vitro*, induce ROS, and inhibit the antioxidant system by depleting glutathione and glutathione peroxidase [26,52]. Additionally, activation of oxidative stress-sensitive kinases and transcription factors including nuclear factor (NF)-κB has been identified in cell lines exposed to Mn [31,51].

Manganese-mediated dysfunction of astrocytes and astrocyte-neuron integrity

Astrocytes play an essential role in the CNS by regulating and maintaining the extracellular environment and protective barriers, which include glia scars, the glia limitans and the blood-brain barrier. Astrocytes ensure trophic, energy and metabolic support to neurons. Glial cells actively participate in neuronal excitability and survival by modulating synaptic homeostasis and formation [38]. Astrocytes accumulate Mn up to 50-fold greater than neurons through a high-affinity transport mechanism [2] and hence are considered as an initial target for Mn-induced neurotoxicity. Chronic overexposure to Mn is associated with glial cell activation and is manifested with gliosis. As in neurons, albeit at higher concentrations, Mn is sequestered in mitochondria and disrupts astrocytic energy metabolism [6]. Importantly, the level of glutathione (GSH), the main cellular antioxidant, is significantly lower in neurons than in astrocytes. In general, neuronal stores of GSH are largely dependent upon astrocytic stores, and neurons are more sensitive than astrocytes to oxidative stress [33]. Several studies have demonstrated that Mn promotes failure of astrocytes to maintain antioxidant defense mechanisms via disruption of GSH synthesis [49]. *In vivo*, interneuron injury in striatal and pallidal regions of Mn-exposed mice is associated with an increased number of reactive astrocytes expressing inducible form of nitric oxide synthase (iNOS) in the same brain areas [41]. Treatment of astrocytes with Mn increases uptake of *L*-arginine, an iNOS substrate, leading to increased ROS generation as a consequence of nitric oxide (NO) production and deterioration of cellular antioxidant capacity and energy metabolism. Furthermore, as discussed below, Mn is believed to exert toxicity via disruptive effects on the synthesis of neurotransmitters. While Mn, at higher concentrations than in neurons, might be toxic to astrocytes themselves and the astrocytes

are crucial for its brain transport and accumulation, they are extremely important from a neuroprotection point of view. For example, Mn-induced neuronal injury in the striatum and the globus pallidus is associated with primary dysfunction of astrocytes via mechanisms involving NO [45]. In addition, Mn inhibits the ability of astrocytes to promote neuronal differentiation by a mechanism that involves oxidative stress and a reduction of the extracellular matrix protein, such as fibronectin [17].

Glutamine in general and in the glutamine/glutamate-γ-aminobutyric acid cycle

Glutamine (Gln) content in the extracellular fluid (microdialysates) (ECF) or in the cerebrospinal fluid (CSF) (~0.5-1 mM) exceeds, by at least one order of magnitude, the extracellular contents of other amino acids in these compartments. Glutamine is the most abundant amino acid in the plasma (at 600-800 µmol) and exhibits extremely rapid cellular turnover rates [9,10]. This amino acid serves multiple roles in the mammalian brain: as an essential precursor in nucleotide, glucose and amino sugar biosynthesis, glutathione homeostasis and protein synthesis. Glutamine transport across cell membranes has been extensively studied. In the past few years a number of glutamine carriers have been cloned, and their molecular and functional properties have been characterized. Glutamine transport systems in the mammalian brain are classified into two distinct groups termed sodium-dependent (systems A, ASC and N) and sodium-independent (system L). All of the glutamine transport systems has been identified in brain, indicating that the CNS possesses multiple pathways for Gln transportation across the plasma membrane [5].

In the mammalian brain, Gln functions via the complex glutamine/glutamate-γ-aminobutyric acid cycle (GGC), where Gln efflux from astrocytes must be met by its influx in neurons. After exocytotic release at synaptic terminals, glutamate (Glu) is taken up by surrounding astrocytes via the glia specific Glu transporter 1 GLT-1 and the Glu-aspartate transporter GLAST [29,43]. In astrocytes Glu is converted to Gln by glutamine synthetase (GS). Astrocytic Gln transporters with the predominant role of SNAT3 (system N) mediate its release into the extracellular space. In turn, Gln is transferred into the neurons mainly by SNAT1 and SNAT2 transporters belonging to system A. In neurons Gln is catalyzed to Glu via phosphate-dependent glutaminase (PAG). Glutamate is subsequently converted into GABA via decarboxylation by glutamic acid decarboxylase (GAD). In both astrocytes and neurons Glu is used for the synthesis of alpha-ketoglutaric acid, a substrate for the tricarboxylic acid cycle, by oxidative deamination mediated by Glu dehydrogenase (GDH) [3]. Furthermore, Glu is stored in synaptic vesicles at presynaptic terminals by the vesicular glutamate transporters VGluT1, VGluT2 and VGluT3 (SLC17A6, SLC17A7 and SLC17A8, respectively).

The glutamate-γ-aminobutyric acid cycle plays an essential role in recycling the excitatory neurotransmitter glutamate. High affinity glutamate transporters play essential roles in removing released glutamate from the synaptic cleft and for maintaining the extracellular glutamate concentration of the cerebrospinal fluid below neurotoxic levels. Glutamine transporters mediate uptake and release of glutamine and supply neurons with the primary neurotransmitter precursor. Disruption of GGC has been reported in numerous pathological conditions, such as epilepsy, cerebral ischemia, AD, PD and manganism [3].

Manganese and glutamine/glutamate-γ-aminobutyric acid cycle

Manganese and glutamine turnover

Studies have established that the effects of Mn inhalation on GGC vary greatly among different mammalian brain regions. For example, in the brain of monkeys exposed to airborne Mn, GS protein levels were found to be altered, with a strong decrease of GS protein expression in the cerebellum and the globus pallidus [11]. Monkeys exposed to Mn also had several other alterations including decreased caudate, globus pallidus, olfactory cortex, and cerebellum GLT-1 protein, decreased olfactory cortex and cerebellum GLAST protein. Other rodent models of manganese exposure have also pointed to alterations in GABA and GAD in the caudate and globus pallidus [19,46].

Manganese toxicity is associated with disruption of critical points in the GGC, such as glutamine translocation and glutamate uptake by astrocytes. In cultured astrocytes, pre-treatment with Mn inhibits the initial net uptake of Gln in a concentration-dependent manner. Manganese added directly to astrocytes induces deregulation in the expression of SNAT3,

SNAT2, ASCT2 and LAT2 transporters [34]. Corroborating the changes in transporter protein expression levels, astrocytes treated with Mn displayed a significant decrease in Gln uptake mediated by the transport systems N and ASC, and a decrease in Gln efflux mediated by systems N, ASC and L. PKC(s) signaling, with the predominant role of the PKCδ isoform, has been invoked as a potential mechanism leading to transporters inactivation and glial dysfunction in Mn-mediated disruption of Gln transport. Manganese exposure has been demonstrated to mediate the specific phosphorylation of PKCδ isozyme, and significantly increase PKC(s) activity. In addition, astrocytes transfected with shRNA against PKCδ are significantly less sensitive to Mn compared to those transfected with control shRNA [36]. Treatment of primary astrocyte cultures with a PKC(s) stimulator reduces Gln uptake mediated by systems ASC and N, and reduces expression of ASCT2 and SNAT3 protein levels in cell lysates and in plasma membranes [37]. Furthermore, increased binding of PKCδ to ASCT2 and SNAT3 upon exposure to Mn has been identified by a co-immunoprecipitation study. It is noteworthy that both Mn-affected transporters contain putative PKC phosphorylation sites, which are conserved in the human, rat and mouse [28,30].

SNAT3 (system N), selectively expressed on astrocytic processes ensheathing synapses, mediates release of glutamine and supplies neurons with the primary neurotransmitter precursor. Thus, functional integrity of SNAT3 may be a key regulator for the recycling of glutamate and GABA. SNAT3 exhibits a highly differential cellular and subcellular localization and the highest sensitivity to Mn exposure among all investigated Gln transporters. A recent *in situ* study revealed that PKC(s) activation induces phosphorylation of SNAT3 and regulates its membrane trafficking and protein degradation [28]. Notably, the study demonstrated that Mn-dependent PKC activation induces hyper-ubiquitination, and increases the association of SNAT3 with ubiquitin-protein ligase E3, Nedd4-2 (neuronal precursor cell expressed, developmentally down-regulated 4-2) in primary culture of astrocytes. In addition, internalization of SNAT3 upon PKC-dependent phosphorylation is corroborated by evidence from an *Xenopus laevis* oocyte model in which PKC activation reduced V_{max} of the Gln uptake activity [4]. Together, this evidence could represent a link of manganese to PKC(s) regulation in the GGC cycle, since phosphorylation by PKC stimulates transporters' internalization and/or ubiquitination and further lysosomal or proteasomal degradation.

Manganese and the glutamate transport system

The Glu transport system is essential for maintaining optimal extracellular Glu concentrations that do not activate Glu transporters and receptors. Rapid removal of glutamate from the extracellular space is required for survival and proper neuronal function. Impaired uptake of glutamate by astrocytes mediates excitotoxicity, slows the synthesis of glutathione and leaves the brain vulnerable to oxidative damage [24]. Several studies have demonstrated the propensity of Mn to disrupt the Glu transport system and other components of the GGC, leading to both a reduction in Glu uptake and elevation of extracellular Glu level [23]. Manganese has been widely reported to mediate the impairment of glutamate transporters, GLAST and GLT-1 expression and function [12,27]. Furthermore, Chinese hamster ovary cells transfected with GLAST or GLT-1 were found to fail to transport Glu after Mn exposure [27]. A recent finding has identified that PKC signaling is involved in Mn-induced deregulation of Glu turnover [35]. The study revealed that PKC(s) stimulation significantly reduces astrocytic Glu uptake, while treatment with a general PKC(s) inhibitor protects astrocytes from Mn-induced deregulation of Glu transport. Interestingly, co-immunoprecipitation studies demonstrated association of GLT-1, but not GLAST, with the PKCδ and PKCα isoforms and a Mn-induced specific increase in PKCδ-GLT-1 interaction [28,35]. This evidence combined with findings on Mn's influence on Gln transport is consistent with abnormal GGC cycling function caused by Mn at two key steps, including Gln and Glu transport, via a homologous, PKC(s)-dependent pattern.

A more recent study revealed the important role of the transcription factor Yin Yang 1 (YY1) in Mn-mediated disruption of GLT-1. Manganese increases YY1 promoter activity and, consequently, its mRNA and protein levels [20]. Manganese enhances YY1 binding to its consensus sites in the GLT-1 promoter, and, accordingly, mutations of YY1 binding sites attenuate the Mn-induced decrease in GLT-1 promoter activity, indicating that YY1 is a critical transcriptional mediator in Mn-induced repression of GLT-1. Manganese likely activates YY1 via proinflammatory mediators, such as tumor necrosis factor α (TNF-α), interleukin

(IL)-6 and IL-1β [13,14]. TNF-α and IL-1β are negative regulators of GLT-1, and they reduce GLT-1 mRNA and protein levels in astrocytes [21,40,44]. Recent studies have indicated that Mn increases production of TNF-α, which, in turn, increases YY1 promoter activity, and mRNA and protein levels [20], suggesting that TNF-α mediates Mn effects on reduction of GLT-1 expression via YY1 in astrocytes.

Concluding remarks

Manganism has been considered as a metabolic syndrome related to impairment of glutamate transport and, more recently, the glutamine/glutamate-γ-aminobutyric acid cycle. *In vivo* and *in vitro* studies have demonstrated that Mn evokes mitochondrial abnormalities, oxidative/nitrosative stress and morphological/functional changes of astrocytes, major players of the GGC. Manganese effectively increases abnormalities in the glutamine metabolism and turnover between glia and neurons. There appear to be common PKC(s) signaling targets of Mn in GGC cycling in glial cells. The astrocytic glutamate and glutamine transporters may be targeted by these regulatory mechanisms as a response to certain synaptic activity synergistically inhibiting glutamate recycling. The evidence discussed here not only contributes to understanding the mechanism by which Mn disrupts astrocyte function and astrocyte-neuron intercommunication but may potentially lead to the development of novel therapeutic interventions in animal models of manganese toxicity.

Disclosure

Author reports no conflict of interest.

References

1. Aschner JL, Aschner M. Nutritional aspects of manganese homeostasis. Mol Aspects Med 2005; 26: 353-362.
2. Aschner M, Gannon M, Kimelberg HK. Manganese uptake and efflux in cultured rat astrocytes. J Neurochem 1992; 58: 730-735.
3. Bak LK, Schousboe A, Waagepetersen HS. The glutamate/GABA-glutamine cycle: aspects of transport, neurotransmitter homeostasis and ammonia transfer. J Neurochem 2006; 98: 641-653.
4. Balkrishna S, Broer A, Kingsland A, Broer S. Rapid downregulation of the rat glutamine transporter SNAT3 by a caveolin-dependent trafficking mechanism in Xenopus laevis oocytes. Am J Physiol Cell Physiol 2010; 299: C1047-1057.
5. Bode BP. Recent molecular advances in mammalian glutamine transport. J Nutr 2001; 131: 2475S-2485S; discussion 2486S-2477S.
6. Chen CJ, Liao SL. Oxidative stress involves in astrocytic alterations induced by manganese. Exp Neurol 2002; 175: 216-225.
7. Cotzias GC, Greenough JJ. The high specificity of the manganese pathway through the body. J Clin Invest 1958; 37: 1298-1305.
8. Crump KS. Manganese exposures in Toronto during use of the gasoline additive, methylcyclopentadienyl manganese tricarbonyl. J Expo Anal Environ Epidemiol 2000; 10: 227-239.
9. Darmaun D, Matthews DE, Bier DM. Glutamine and glutamate kinetics in humans. Am J Physiol 1986; 251: E117-126.
10. Erecinska M, Silver IA. Metabolism and role of glutamate in mammalian brain. Prog Neurobiol 1990; 35: 245-296.
11. Erikson KM, Dorman DC, Lash LH, Aschner M. Manganese inhalation by rhesus monkeys is associated with brain regional changes in biomarkers of neurotoxicity. Toxicol Sci 2007; 97: 459-466.
12. Erikson KM, Suber RL, Aschner M. Glutamate/aspartate transporter (GLAST), taurine transporter and metallothionein mRNA levels are differentially altered in astrocytes exposed to manganese chloride, manganese phosphate or manganese sulfate. Neurotoxicology 2002; 23: 281-288.
13. Filipov NM, Dodd CA. Role of glial cells in manganese neurotoxicity. J Appl Toxicol 2012; 32: 310-317.
14. Filipov NM, Seegal RF, Lawrence DA. Manganese potentiates in vitro production of proinflammatory cytokines and nitric oxide by microglia through a nuclear factor kappa B-dependent mechanism. Toxicol Sci 2005; 84: 139-148.
15. Finkelstein MM, Jerrett M. A study of the relationships between Parkinson's disease and markers of traffic-derived and environmental manganese air pollution in two Canadian cities. Environ Res 2007; 104: 420-432.
16. Gavin CE, Gunter KK, Gunter TE. Manganese and calcium efflux kinetics in brain mitochondria. Relevance to manganese toxicity. Biochem J 1990; 266: 329-334.
17. Giordano G, Pizzurro D, VanDeMark K, Guizzetti M, Costa LG. Manganese inhibits the ability of astrocytes to promote neuronal differentiation. Toxicol Appl Pharmacol 2009; 240: 226-235.
18. Guilarte TR. Manganese and Parkinson's disease: a critical review and new findings. Cien Saude Colet 2011; 16: 4549-4566.
19. Gwiazda RH, Lee D, Sheridan J, Smith DR. Low cumulative manganese exposure affects striatal GABA but not dopamine. Neurotoxicology 2002; 23: 69-76.
20. Karki P, Webb A, Smith K, Johnson J, Jr., Lee K, Son DS, Aschner M, Lee E. Yin Yang 1 is a repressor of glutamate transporter EAAT2, and it mediates manganese-induced decrease of EAAT2 expression in astrocytes. Mol Cell Biol 2014; 34: 1280-1289.
21. Korn T, Magnus T, Jung S. Interaction with antigen-specific T cells regulates expression of the lactate transporter MCT1 in primary rat astrocytes: specific link between immunity and homeostasis. Glia 2005; 49: 73-83.
22. Kowaltowski AJ, Castilho RF, Vercesi AE. Ca(2+)-induced mitochondrial membrane permeabilization: role of coenzyme Q redox state. Am J Physiol 1995; 269: C141-147.
23. Lee ES, Sidoryk M, Jiang H, Yin Z, Aschner M. Estrogen and tamoxifen reverse manganese-induced glutamate transporter impairment in astrocytes. J Neurochem 2009; 110: 530-544.
24. Lewerenz J, Albrecht P, Tien ML, Henke N, Karumbayaram S, Kornblum HI, Wiedau-Pazos M, Schubert D, Maher P, Meth-

ner A. Induction of Nrf2 and xCT are involved in the action of the neuroprotective antibiotic ceftriaxone in vitro. J Neurochem 2009; 111: 332-343.
25. Li Y, Sun L, Cai T, Zhang Y, Lv S, Wang Y, Ye L. alpha-Synuclein overexpression during manganese-induced apoptosis in SH-SY5Y neuroblastoma cells. Brain Res Bull 2010; 81: 428-433.
26. Liccione JJ, Maines MD. Selective vulnerability of glutathione metabolism and cellular defense mechanisms in rat striatum to manganese. J Pharmacol Exp Ther 1988; 247: 156-161.
27. Mutkus L, Aschner JL, Fitsanakis V, Aschner M. The in vitro uptake of glutamate in GLAST and GLT-1 transfected mutant CHO-K1 cells is inhibited by manganese. Biol Trace Elem Res 2005; 107: 221-230.
28. Nissen-Meyer LS, Popescu MC, Hamdani el H, Chaudhry FA. Protein kinase C-mediated phosphorylation of a single serine residue on the rat glial glutamine transporter SN1 governs its membrane trafficking. J Neurosci 2011; 31: 6565-6575.
29. Northington FJ, Traystman RJ, Koehler RC, Martin LJ. GLT1, glial glutamate transporter, is transiently expressed in neurons and develops astrocyte specificity only after midgestation in the ovine fetal brain. J Neurobiol 1999; 39: 515-526.
30. Pawlik TM, Souba WW, Sweeney TJ, Bode BP. Phorbol esters rapidly attenuate glutamine uptake and growth in human colon carcinoma cells. J Surg Res 2000; 90: 149-155.
31. Prabhakaran K, Ghosh D, Chapman GD, Gunasekar PG. Molecular mechanism of manganese exposure-induced dopaminergic toxicity. Brain Res Bull 2008; 76: 361-367.
32. Santamaria AB, Cushing CA, Antonini JM, Finley BL, Mowat FS. State-of-the-science review: Does manganese exposure during welding pose a neurological risk? J Toxicol Environ Health B Crit Rev 2007; 10: 417-465.
33. Shih AY, Johnson DA, Wong G, Kraft AD, Jiang L, Erb H, Johnson JA, Murphy TH. Coordinate regulation of glutathione biosynthesis and release by Nrf2-expressing glia potently protects neurons from oxidative stress. J Neurosci 2003; 23: 3394-3406.
34. Sidoryk-Wegrzynowicz M, Lee E, Albrecht J, Aschner M. Manganese disrupts astrocyte glutamine transporter expression and function. J Neurochem 2009; 110: 822-830.
35. Sidoryk-Wegrzynowicz M, Lee E, Aschner M. Mechanism of Mn(II)-mediated dysregulation of glutamine-glutamate cycle: focus on glutamate turnover. J Neurochem 2012; 122: 856-867.
36. Sidoryk-Wegrzynowicz M, Lee E, Mingwei N, Aschner M. Disruption of astrocytic glutamine turnover by manganese is mediated by the protein kinase C pathway. Glia 2011; 59: 1732-1743.
37. Sidoryk-Wegrzynowicz M, Lee ES, Ni M, Aschner M. Manganese-induced downregulation of astroglial glutamine transporter SNAT3 involves ubiquitin-mediated proteolytic system. Glia 2010; 58: 1905-1912.
38. Sidoryk-Wegrzynowicz M, Wegrzynowicz M, Lee E, Bowman AB, Aschner M. Role of astrocytes in brain function and disease. Toxicol Pathol 2011; 39: 115-123.
39. Sikk K, Haldre S, Aquilonius SM, Taba P. Manganese-Induced Parkinsonism due to Ephedrone Abuse. Parkinsons Dis 2011; 2011: 865319.
40. Sitcheran R, Gupta P, Fisher PB, Baldwin AS. Positive and negative regulation of EAAT2 by NF-kappaB: a role for N-myc in TNFalpha-controlled repression. EMBO J 2005; 24: 510-520.
41. Spranger M, Schwab S, Desiderato S, Bonmann E, Krieger D, Fandrey J. Manganese augments nitric oxide synthesis in murine astrocytes: a new pathogenetic mechanism in manganism? Exp Neurol 1998; 149: 277-283.
42. Stallings WC, Metzger AL, Pattridge KA, Fee JA, Ludwig ML. Structure-function relationships in iron and manganese superoxide dismutases. Free Radic Res Commun 1991; 12-13 Pt 1: 259-268.
43. Storck T, Schulte S, Hofmann K, Stoffel W. Structure, expression, and functional analysis of a Na(+)-dependent glutamate/aspartate transporter from rat brain. Proc Natl Acad Sci U S A 1992; 89: 10955-10959.
44. Su ZZ, Leszczyniecka M, Kang DC, Sarkar D, Chao W, Volsky DJ, Fisher PB. Insights into glutamate transport regulation in human astrocytes: cloning of the promoter for excitatory amino acid transporter 2 (EAAT2). Proc Natl Acad Sci U S A 2003; 100: 1955-1960.
45. Tjalkens RB, Liu X, Mohl B, Wright T, Moreno JA, Carbone DL, Safe S. The peroxisome proliferator-activated receptor-gamma agonist 1,1-bis(3'-indolyl)-1-(p-trifluoromethylphenyl)methane suppresses manganese-induced production of nitric oxide in astrocytes and inhibits apoptosis in cocultured PC12 cells. J Neurosci Res 2008; 86: 618-629.
46. Tomas-Camardiel M, Herrera AJ, Venero JL, Cruz Sanchez-Hidalgo M, Cano J, Machado A. Differential regulation of glutamic acid decarboxylase mRNA and tyrosine hydroxylase mRNA expression in the aged manganese-treated rats. Brain Res Mol Brain Res 2002; 103: 116-129.
47. Uversky VN, Li J, Fink AL. Metal-triggered structural transformations, aggregation, and fibrillation of human alpha-synuclein. A possible molecular NK between Parkinson's disease and heavy metal exposure. J Biol Chem 2001; 276: 44284-44296.
48. Verina T, Schneider JS, Guilarte TR. Manganese exposure induces alpha-synuclein aggregation in the frontal cortex of non-human primates. Toxicol Lett 2013; 217: 177-183.
49. Weber S, Dorman DC, Lash LH, Erikson K, Vrana KE, Aschner M. Effects of manganese (Mn) on the developing rat brain: oxidative-stress related endpoints. Neurotoxicology 2002; 23: 169-175.
50. Yamada M, Ohno S, Okayasu I, Okeda R, Hatakeyama S, Watanabe H, Ushio K, Tsukagoshi H. Chronic manganese poisoning: a neuropathological study with determination of manganese distribution in the brain. Acta Neuropathol 1986; 70: 273-278.
51. Yin Z, Aschner JL, dos Santos AP, Aschner M. Mitochondrial-dependent manganese neurotoxicity in rat primary astrocyte cultures. Brain Res 2008; 1203: 1-11.
52. Zhang P, Hatter A, Liu B. Manganese chloride stimulates rat microglia to release hydrogen peroxide. Toxicol Lett 2007; 173: 88-100.

Original article

Folia Neuropathologica

In vitro pharmacological evaluation of the radiolabeled *C*-terminal substance P analogue Lys-Phe-Phe-Gly-Leu-Met-NH2: Does a specific binding site exist?

Aleksandra Tomczyszyn[1], Balazs Csibrany[2], Attila Keresztes[2], Jayapal Reddy Mallareddy[2], Jolanta Dyniewicz[3], Aleksandra Misicka[1,3], Geza Toth[2], Andrzej W. Lipkowski[3,4]

[1]Faculty of Chemistry, Biological and Chemical Research Centre, University of Warsaw, Warsaw, Poland, [2]Hungarian Academy of Sciences, Biological Research Center, Institute of Biochemistry, Szeged, Hungary, [3]Department of Neuropeptides, Mossakowski Medical Research Centre, Polish Academy of Sciences, Warsaw, Poland, [4]Tufts University School of Medicine, Boston, MA, USA

Folia Neuropathol 2014; 52 (4): 383-393 DOI: 10.5114/fn.2014.47839

Abstract

In the present paper, we report the synthesis, radiolabeling and comprehensive pharmacological evaluation of a C-terminally truncated tachykinin derivative, ^{3}H-KFFGLM-NH$_2$. The C-terminal fragments of endogenous tachykinins are pharmacophores responsible for interaction with the tachykinin receptors NK1, NK2 and NK3. The N-terminal fragments are responsible for modulation of receptor selectivity and interactions with other receptor systems. To evaluate and separate the function of an NK-pharmacophore from the activity of its parent neurokinin, KFFGLM-NH$_2$ was synthesized in both tritiated and unlabeled forms. It has been proposed that the obtained NK-binding profiles of specific reference ligands and KFFGLM-NH$_2$ differentiate monomeric and dimeric forms of NK receptors. We hypothesize that dimers of NK receptors could be specific receptor(s) for C-terminal fragments of all neurokinins as well as their C-terminal fragments, including H-KFFGLM-NH$_2$. Dissociation of dimers into monomers opens access to additional allosteric binding sites. Fully elongated undecapeptide substance P interacts with both the "tachykinin pocket" and the "allosteric pocket" on the monomeric NK1 receptor, resulting in high and selective activation. However, C-terminal hexapeptide fragment analogues, recognizing only the "tachykinin pocket", may have less specific interactions with all tachykinin receptors in both monomeric and dimeric forms.

Key words: *neurokinin (tachykinin), receptor binding, radioligand, GPCR monomer, dimer, allosteric modulation.*

Introduction

The history of mammalian tachykinin discovery begins in 1931, when von Euler and Gaddum isolated a peptide from a preparation of equine brain and intestine. They characterized this peptide and named it "substance P". Further studies revealed that substance P caused vasodilation and stimulation of gut motility in rabbits. It was another 40 years before the amino acid sequence of substance P was confirmed. At that time, it was recognized that the sequence of substance P is similar to those of the tachykinins eledoisin and physalaemin, which were isolated from invertebrates [28]. Other endogenous tachyki-

Communicating author:
Aleksandra Misicka, Department of Neuropeptides, Mossakowski Medical Research Centre, Polish Academy of Sciences, 5 Pawinskiego St., 02-106 Warsaw, Poland, e-mail: misicka@chem.uw.edu.pl

nins (neurokinins A and B and hemokinin-1) have been discovered more recently in vertebrates [19]. Primary structure activity relationship (SAR) studies on invertebrate tachykinins led to the conclusion that *C*-terminal hexapeptide amide fragments are fully responsible for the tachykinin-like properties [1]. Further SAR studies on mammalian tachykinins also confirmed that the active fragments of tachykinins (pharmacophores) have a common *C*-terminal sequence of Y-Phe-X-Gly-Leu-Met-NH_2, where Y is any non-lipophilic amino acid residue and X is a lipophilic alkyl (Val, Ile) or aromatic (Tyr, Phe) residue [11]. Three tachykinin receptors, termed NK_1, NK_2 and NK_3, were identified in the late 1980s as G-protein-coupled receptors (GPCR). The *N*-terminal fragments, as well as the type of lipophilic amino acid residue in the *C*-terminal fragments, modulate NK-receptor selectivity. The *N*-terminal fragments of tachykinins play a particularly important role in modulating selectivity. The nature of these fragments decreases or increases affinities to particular NK receptor types, resulting in highly selective endogenous ligands. The order of affinities for different tachykinin receptors toward mammalian tachykinins is as follows: for NK_1, SP>NKA>NKB; for NK_2, NKA>NKB>SP; for NK_3, NKB>NKA>SP. Recently, a new chimeric type of GPCR ligand has been proposed that hybridizes pharmacophores from different receptor types into one molecule [10]. The *C*-terminal fragments of tachykinins, or their analogues, have been hybridized with opioid pharmacophores to develop a new type of analgesic [6,7,11,15,16]. In multitarget receptor ligands it is important to evaluate the role of each separated target component. Therefore, we decided to synthesize and evaluate the *C*-terminal fragment of tachykinin to identify specific roles for tachykinin pharmacophores. The first amino acid in the *C*-terminal hexapeptide fragment is glutamine, which can be transformed easily to pyroglutamine. Both the *N*-terminal hexapeptide and its pyroglutamine analogue have very limited solubility in aqueous media. This creates the requirement that special solvents (DMSO or DMF) or carriers (dextran, cyclodextrin, albumin, etc.) be used for biological studies on these peptides. We thus decided to synthesize Lys-[SP_{7-11}] as a prospective tachykinin pharmacophore standard. This compound was originally synthesized as an analogue of the non-mammalian tachykinin eledoisin, long before the sequence of substance P had been established [12]. In comparison with the activity of substance P, Lys-[SP_{7-11}] shows a 200% greater hypotensive effect in dogs and 100% greater GPI contraction. These results suggest that the pharmacological properties of this compound are similar to those of substance P.

Material and methods

Chemicals

Protected amino acids were purchased from Sigma Aldrich, Merck Chemicals and Bachem. Coupling reagents were obtained from Sigma Aldrich. All reagents and solvents were of reagent grade and were used without further purification. The mobile phases for linear gradient elution in RP-HPLC contained 0.05% trifluoroacetic acid (TFA) in water or acetonitrile. The stationary phase was a Jupiter Proteo C12 column. A Shimadzu LC-MS liquid chromatograph with an attached ESI mass spectrometer was used to identify the peptides.

Selective neurokinin receptor ligands such as substance P, L-703,606, (Nle^{10})-neurokinin A (4-10), (Tyr^5,D-$Trp^{6,8,9}$,Lys-$NH_2{}^{10}$)-neurokinin A (4-10), (Pro^7)-neurokinin B and (Trp^7,β-Ala^8)-neurokinin A (4-10) were purchased from Bachem (Budapest, Hungary). Unlabeled H-Lys-Phe-Phe-Gly-Leu-Met-NH_2 (H-KFFGLM-NH_2) and its halogenated precursor were synthesized in our laboratories. Tris-hydroxymethylaminomethane (Tris, free base), polyethylenimine (PEI), ethylene glycol-bis(2-aminoethylether)-N,N,N',N'-tetraacetic acid (EGTA), guanosine-5'-diphosphate sodium salt (GDP), guanosine 5'-[γ-thio] triphosphate tetralithium salt (GTPγS), Bradford reagent, bovine serum albumin (BSA), magnesium chloride hexahydrate ($MgCl_2 \times 6H_2O$), protease inhibitor cocktail (P8340), manganese chloride tetrahydrate ($MnCl_2 \times 4H_2O$) and HCl (37%) were purchased from Sigma Aldrich, Ltd. (Budapest, Hungary). Sodium chloride (NaCl) and sucrose were obtained from Molar, Ltd. and Fluka (Budapest, Hungary). The tritiated radioligand [^{3}H]-KFFGLM-NH_2 (0.9 TBq/mmol, 24 Ci/mmol) was prepared locally (Hungarian Academy of Sciences, Biological Research Center, Institute of Biochemistry, Isotope Laboratory) using the appropriate halogenated peptide derivative. Stabilized [^{35}S]GTPγS (37 TBq/mmol, > 1000 Ci/mmol) was purchased from Isotope Institutes, Ltd. (Budapest, Hungary). The tritium used for the radiolabeling of the precursor peptides was imported from Techsnabexport (Moscow, Russia). All other reagents were of analytical grade.

Synthesis, purification and structure determination of H-KpIFpIFGLM-NH_2 and H-KFFGLM-NH_2

Peptides were synthesized manually on Rink Amide resin through a standard Fmoc/tBu solid phase protocol. N^{α}-Fmoc chemistry was employed using *N*-hydroxybenzotriazole and *O*-(benzotriazol-1-yl)-N,N,N'N'-tetramethyluronium tetrafluoroborate as the coupling reagents for peptide elongation. The peptide was cleaved from the resin with concomitant side chain deprotection by treatment of the resin with a solution of TFA/TIS/H_2O 19 : 1 : 1 (20 ml/1 g resin). HPLC analyses and purifications were carried out using C12 analytical (Jupiter 4u Proteo 90A, 250 × 4.6 mm, 4 µm) and C12 semipreparative (Jupiter 4u Proteo 90A, 250 × 10 mm, 4 µm) columns on a Shimadzu instrument. ESI-MS analyses were performed on a Shimadzu instrument.

Radiolabeling of the *N*-terminally truncated neurokinin hexapeptide derivative [^{3}H]-KFFGLM-NH_2

The halogenated hexapeptide precursor was tritiated by the general method reported previously [31]. The halogenated precursor H-Lys-*p*IPhe-pIPhe-Gly-Leu-Met-NH_2 (3.6 mg, 2.95 µmol) was dissolved in DMF (1 ml). To this solution was added PdO/$BaSO_4$ catalyst (10 mg) and triethylamine (TEA, 5 µl). The reaction mixture was stirred for 1 h in the presence of $^3H_2$ at room temperature. When the reaction was complete, the mixture was filtered through a Whatman GF/C glass fiber filter and washed several times with EtOH:H_2O (1 : 1, v/v) to remove the catalyst and labile tritium. The total activity of the crude product was determined in a toluene-based scintillation cocktail using a TRI-CARB 2100TR Liquid Scintillation Counter (Canberra-Packard, PerkinElmer Life Sciences, 549 Albany Street, Boston, MA 02118), and was found to be 110 mCi (4.1 GBq). The crude [^{3}H]-KFFGLM-NH_2 was then purified by RP-HPLC, and its purity was determined to be greater than 95%. Specific radioactivity was found to be 24 Ci/mmol (0.89 TBq/mmol). The radioligand was taken up in spectroscopic grade ethanol containing 0.1 mM L-Met and stored in liquid nitrogen.

Rat brain membrane preparation

Rats (male and female Wistar, 250-300 g, 2-3 months old) were kept in groups of four under standard conditions with access to food and water ad libitum. The animals were handled according to the guidelines of the European Communities Council Directives (86/609/ECC) and the Hungarian Act for the Protection of Animals in Research (XXVIII. tv. Section 32). Crude membranes of rat brains without cerebellums were prepared by a standard protocol as described earlier [2]. The brain homogenates were kept frozen in liquid nitrogen. On the day of the experiment, rat brain homogenates were thawed, diluted with working buffer and centrifuged at 20,000 × g to remove sucrose. The pellet was homogenized with a Dounce homogenizer in an appropriate volume of binding buffer (50 mM Tris-HCl, pH 7.4, 0.1% BSA, 3 mM $MnCl_2$ and protease inhibitor). Protein content was determined using the Bradford assay with BSA as the standard.

Radioligand binding assays

All binding experiments were carried out at 25°C in a final volume of 1 ml containing 0.3-0.5 mg/ml membrane in neurokinin buffer. This buffer consisted of 50 mM Tris-HCl (pH 7.4), 0.1% BSA, 3 mM $MnCl_2$ and protease inhibitor. In the kinetic experiments, the time course of association was measured by incubating 2.0 nM [^{3}H]-KFFGLM-NH_2 with the protein for 60 minutes. In the dissociation experiments, the radioligand was pre-incubated with the membrane until equilibrium was reached (60 minutes). A solution of 10 µM unlabeled H-KFFGLM-NH_2 was then added to induce dissociation of the radioligand. This process was typically complete after 60 minutes. Saturation binding experiments to determine the equilibrium dissociation constant (K_d) and maximum number of binding sites (B_{max}) were performed with increasing concentrations (0.1-10 nM) of [^{3}H]-KFFGLM-NH_2. Homologous and heterologous competition binding experiments were carried out by incubation of rat brain membranes with 3 nM [^{3}H]-KFFGLM-NH_2 in the presence of increasing concentrations (10^{-10}-10^{-5} M) of unlabeled neurokinin ligands. Non-specific binding was determined with 10 µM H-KFFGLM-NH_2 and subtracted from the total binding to obtain specific binding. Incubations were terminated by the addition of ice-cold buffer (50 mM Tris-HCl, pH: 7.4, 0.05% BSA). A Brandel Cell Harvester (Gaithersburg, MD, USA) was then used to filter cells rapidly with Whatman GF/B glass fiber filters pre-soaked in PEI. Filters were immersed directly in Optiphase Supermix scintillation cocktail

(PerkinElmer) and assessed in a TRI-CARB 2100TR liquid scintillation counter. The results presented are mean values ± SEM of at least five independent experiments, each performed in duplicate. Kinetic data were calculated to obtain the rate constants for association (k_a) and dissociation (k_d). Non-linear regression analysis of direct saturation isotherms was used to obtain values for the equilibrium dissociation constant (K_d) and receptor density (B_{max}). Inhibitory constants (K_i, nM) were calculated from competition binding experiments using non-linear least-square curve fitting and the Cheng-Prusoff equation with GraphPad Prism software (version 4.0, San Diego, CA, USA) [5].

Ligand-stimulated [^{35}S]GTPγS functional assay

Rat brain membrane homogenates (10-15 µg protein/tube) were incubated with 0.05 nM [^{35}S]GTPγS and 10^{-10}-10^{-5} M unlabeled ligand agonists and/or 10^{-6} M (final concentration) receptor specific antagonists in the presence of 30 µM GDP, 100 mM NaCl, 3 mM MgCl and 1 mM EGTA in Tris-HCl buffer (50 mM, pH: 7.4) for 60 minutes at 30°C. Basal binding was determined in the absence of ligands and normalized to 100%. Nonspecific binding was determined with 10 µM unlabeled GTPγS and subtracted from total binding to yield specific binding. Reaction mixtures were filtered onto GF/B glass fiber filters using a Brandel Cell Harvester (Gaithersburg, MD, USA). Filter-bound radioactivity was determined in Optiphase Supermix scintillation cocktail (PerkinElmer) using a TRI-CARB 2100TR Liquid Scintillation Counter (Canberra-Packard, PerkinElmer Life Sciences, 549 Albany Street, Boston, MA 02118). The data are presented as the percentage stimulation of specific [^{35}S]GTPγS binding over the basal activity and are expressed as the mean values ± SEM. Each measurement was taken in triplicate and analyzed with the sigmoid dose-response curve fitting option of the GraphPad Prism software (version 4.0, San Diego, CA, USA) to obtain values for potency (EC_{50}) and efficacy (E_{max}).

Results

The synthetic peptide was selected for tritium labeling (Table I). The precursor peptide H-Lys-pI-Phe-pIPhe-Gly-Leu-Met-NH_2 was catalytically dehalogenated under tritium gas to yield the radioligand H-Lys-[^{3}H]Phe-[^{3}H]Phe-Gly-Leu-Met-NH_2. This peptide was found to have a specific activity of 24 Ci/mmol (0.89 TBq/mmol). To prevent methionine oxidation and other side reactions, the radioligand was dissolved and stored in spectroscopic grade ethanol containing 0.1 mM L-Met as a stabilizing agent.

The kinetic and pharmacological properties of the new radioligand were defined using various receptor binding techniques in rat brain membrane homogenate as the biological matrix. Kinetic parameters (k_a and k_d rate constants, K_d and B_{max} values) were determined from association, dissociation and saturation experiments. Association binding experiments were carried out with 2.0 nM radioligand at 25°C in rat brain membrane homogenate. Specific binding reached a steady state within 20-30 minutes (Fig. 1A) and remained stable for 60 minutes. Non-specific binding was approximately 50-60% of total binding in all cases under equilibrium conditions (not shown). The pseudo-first order rate constant was found to be approximately 0.1805 ± 0.023 min^{-1}. The association rate constant, k_a, was determined from this value to be 0.0181 ± 0.0009 $nM^{-1}min^{-1}$ (Table II). Dissociation was measured by pre-incubating the radioligand with the receptor until equilibrium; subsequent addition of 10 µM unlabeled ligand initiated dissociation (Fig. 1B). The dissociation isotherm followed monophasic kinetics and provided a dissociation rate constant (k_d) of 0.1263 ± 0.0422 min^{-1}. The equilibrium dissociation constant (K_d), calculated from these two rate constants, was found to be 6.9 ± 1.8 nM. The saturation isotherm showed that the specific binding of [^{3}H]-KFFGLM-NH_2 was

Table I. Analytical data for synthetic peptides

Sequence of peptides	RT[a]	ESI-MS	
		$[M+H^+]_{calc}$	$[M+H^+]_{found}$
H-Lys-Phe-Phe-Gly-Leu-Met-NH_2	12.3	741.9	741.9
H-Lys-pIPhe-pIPhe-Gly-Leu-Met-NH_2	13.9	993.7	993.7

[a]*Gradient 3-97% ACN in 30 min, flow 1 ml/min, eluents: H_2O and ACN both containing 0.05% (v/v) TFA*

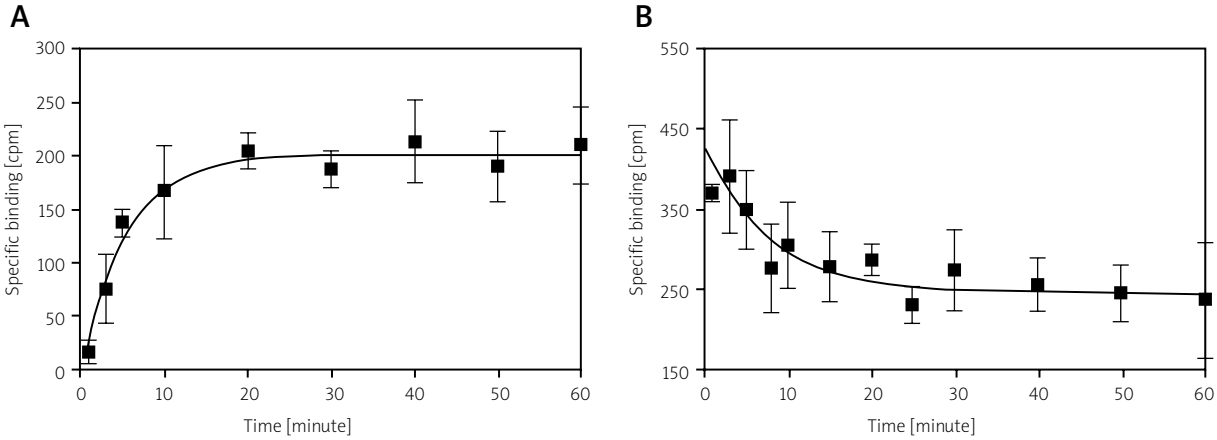

Fig. 1. Association and dissociation time courses of [^{3}H]-KFFGLM-NH_2 binding at 25°C. **A)** 2.0 nM radioligand was incubated with rat brain membrane for 60 minutes until the system reached equilibrium. **B)** 2.0 nM radioligand was pre-incubated with rat brain membrane for 60 minutes followed by addition of 10 µM unlabeled H-KFFGLM-NH_2 to induce dissociation. Dissociation was complete after 60 minutes. Only specific binding is reported.

a high-affinity, saturable interaction (Fig. 2). Fitting the direct saturation plot to a "one-site" binding model gave a K_d of 7.1 ± 2.2 nM, which was in good agreement with that determined from the kinetic curves (Table II). Receptor density (B_{max}) was calculated to be 257 ± 46 fmol × mg protein^{-1}, a value that is several orders of magnitude greater than those reported in the literature for substance P (SP) [20].

The sites on the receptor where the radioligand binds were characterized through displacement binding experiments using receptor selective competitors of the radioligand in rat brain membrane homogenates (Fig. 3A-C). The inhibitory constants (K_i) determined through these experiments are summarized in Table III. The majority of neurokinin receptor specific ligands displaced the radioligand with micromolar inhibitory constants (K_i – µM) reflecting the low affinity of the radioligand for these receptors. This contrasts markedly with literature data reported for SP [17,20]. The highest affinity was found for the non-peptidic NK-1 receptor antagonist

Table II. Kinetic binding parameters for [^{3}H]-KFF-GLM-NH_2

Kinetic parameters	
k_{obs} (min^{-1})	0.1805 ± 0.023
k_a (nM^{-1} × min^{-1})	0.0181 ± 0.0009
k_d (min^{-1})	0.1263 ± 0.0422
K_d (nM)	6.9 ± 1.8
K_d* (nM)	7.1 ± 2.2*
B_{max} (fmol × mg protein^{-1})	257 ± 46

The observed pseudo-first order rate constant (k_{obs}) was derived from the association curve. Values for the dissociation (k_d) and association (k_a) rate constants were calculated according to the following equation: $k_a = (k_{obs} - k_d)/$ [radioligand]. K_d was calculated as follows: $K_d = k_d/k_a$. Receptor density (B_{max}) and equilibrium dissociation constant (K_d^*) were calculated from the saturation plot. The data are expressed as the mean values ± SEM, n ≥ 5.

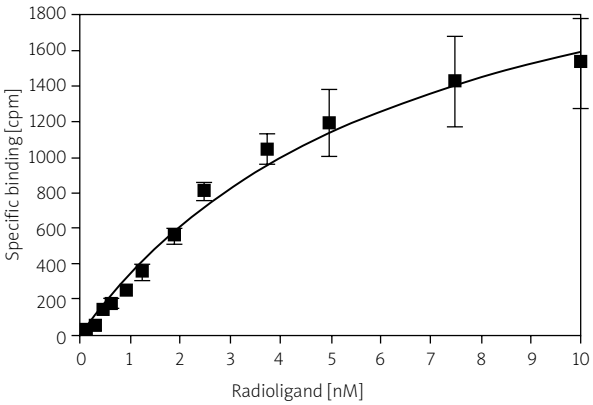

Fig. 2. Saturation isotherm of [^{3}H]-KFFGLM-NH_2. Increasing concentrations of radioligand (0.1-10 nM) were incubated with rat brain membrane as described in the Material and methods section. Values for the dissociation equilibrium constant (K_d) and receptor density (B_{max}) were determined directly from the saturation plot. The value of B_{max} was then converted to fmol × mg protein^{-1}. Only specific binding is reported.

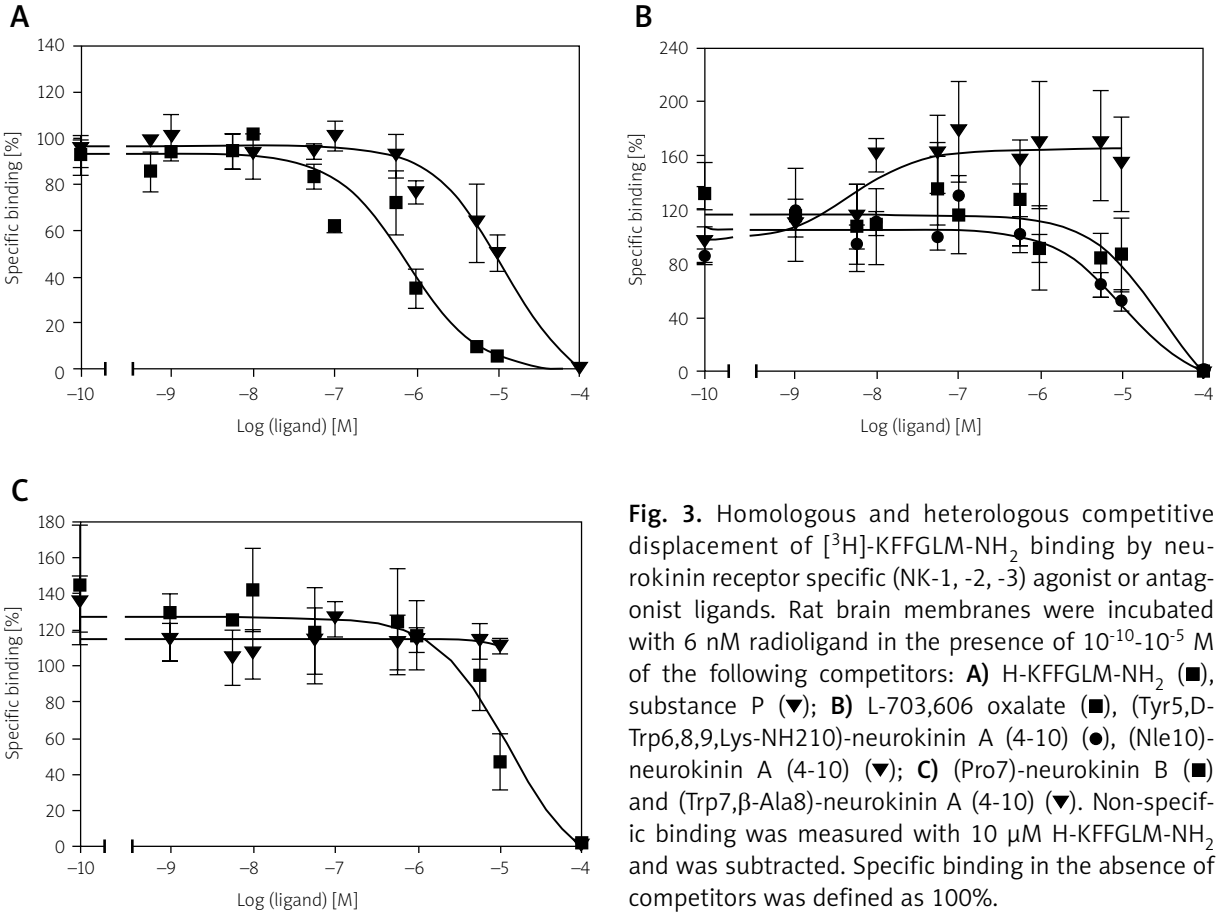

Fig. 3. Homologous and heterologous competitive displacement of [^{3}H]-KFFGLM-NH_2 binding by neurokinin receptor specific (NK-1, -2, -3) agonist or antagonist ligands. Rat brain membranes were incubated with 6 nM radioligand in the presence of 10^{-10}-10^{-5} M of the following competitors: **A)** H-KFFGLM-NH_2 (■), substance P (▼); **B)** L-703,606 oxalate (■), (Tyr5,D-Trp6,8,9,Lys-NH210)-neurokinin A (4-10) (●), (Nle10)-neurokinin A (4-10) (▼); **C)** (Pro7)-neurokinin B (■) and (Trp7,β-Ala8)-neurokinin A (4-10) (▼). Non-specific binding was measured with 10 µM H-KFFGLM-NH_2 and was subtracted. Specific binding in the absence of competitors was defined as 100%.

Table III. Inhibitory constants (K_i) for NK-1, -2 and -3 receptor specific unlabeled ligands against radiolabeled [^{3}H]-KFFGLM-NH_2

Ligands	K_i (µM)
H-Lys-Phe-Phe-Gly-Leu-Met-NH_2	0.58 ± 0.10
Substance P (NK-1 > NK-2 ≥ NK-3, non-selective agonist)	5.98 ± 1.39
L-703,606 oxalate (NK-1 antagonist)	0.08 ± 0.01
(Nle^{10})-neurokinin A (4-10) (NK-2 agonist)	–
(Tyr^5,D-$Trp^{6,8,9}$,Lys-NH_2^{10})-neurokinin A (4-10) (NK-2 antagonist)	1.39 ± 0.65
(Pro^7)-neurokinin B (NK-3 agonist)	3.78 ± 0.54
(Trp^7,β-Ala^8)-neurokinin A (4-10) (NK-3 antagonist)	–

Inhibitory constants (K_i) were calculated according to the Cheng-Prusoff equation: $K_i = EC_{50}/(1+[ligand]/K_d)$, where K_d = 7 nM was deduced from kinetic experiments. The data are expressed as the mean values ± SEM, n ≥ 5.

L-703,606 oxalate, which inhibits radioligand binding with a K_i value of 0.087 ± 0.016 µM. This K_i is more potent than that observed for the unlabeled analogue of the radioligand (K_i = 0.580 ± 0.103 µM). Other derivatives proved to be poor inhibitors of radioligand binding, suggesting that truncation of neurokinin N-terminal sequences is not favorable for selective receptor-ligand interactions. Interestingly, unusual behavior was observed for two receptor selective ligands and receptor types. Positive cooperativity could be observed for a peptidic NK-2 agonist, (Nle^{10})-neurokinin A (4-10) (Fig. 3B). Increasing the concentration of (Nle^{10})-neurokinin A (4-10) to 10^{-5} M while maintaining a constant radioligand concentration led to a massive accumulation of radioligand. This outcome manifests itself in an "inverse" behavior. This feature suggests the likelihood of positive allosteric modulation, the existence of multiple binding sites or multiple conformational states of the receptor protein. Any of these could trigger concomitant binding of two different ligands, likely at two distinct binding sites. This is very interesting given that the analysis of kinetic data using the "two site" binding model for the radioligand failed to provide

meaningful values. In contrast, no competition was observed between the radioligand and the NK-3 antagonist (Trp^7,β-Ala^8)-neurokinin A (4-10), whereas competition with an NK-3 selective agonist was observed. These results show that the antagonist cannot reverse the binding of the radioligand at any concentration. Consequently, the radioligand and antagonist may not occupy the same binding sites. This finding further supports the hypothesis that the radioligand may bind to distinct binding sites or conformational states of the receptor protein, different from those of the receptor selective competitors.

The functional properties of the H-KFFGLM-NH_2 hexapeptide were investigated in a ligand-stimulated [^{35}S]GTPγS functional binding assay, which revealed the ability of NK ligands to activate G proteins. Potency (EC_{50}) and efficacy (E_{max}) values were compared with those for the prototypic NK receptor agonist SP (Fig. 4, Table IV). Both ligands showed potency toward activation of G proteins, with EC_{50} values of 313 ± 36 nM (H-KFFGLM-NH_2) and 892 ± 65 nM (SP). The corresponding efficacies were found to be 142 ± 9% (H-KFFGLM-NH_2) and 120 ± 4% (SP). These results strongly suggest that the ligands are agonists of the NK receptors, indicating that targeted *N*-terminal truncation and modification of SP do not profoundly influence its functional properties. The relatively low efficacy found for SP may be attributed to the presence of fewer NK-1 binding sites in rat brain compared with the number of primary sites in the spinal cord. The functional data measured for the co-application of receptor antagonists and H-KFFGLM-NH_2 confirmed that the hexapeptide binds to neurokinin receptors and activates G-protein coupling that could be abrogated by the selective antagonists.

Discussion

Numerous structure-activity relationship studies have shown that the *C*-terminal component of neurokinin ligands (especially the *C*-terminal pentapeptide Phe-X-Gly-Leu-Met-NH_2 motif, where X is a hydrophobic amino acid residue) is critical for specific binding of high-affinity agonists to receptors in the tachykinin family [4,20,22,26,27,33].

All *C*-terminal tachykinin fragments interact with similar binding sites of their receptors. For these fragments there exist some common structural requirements. For example, peptide mapping studies of the NK_1 receptor have established that the site of interactions of both SP and NKA is located within the same segment of the receptor [3,33].

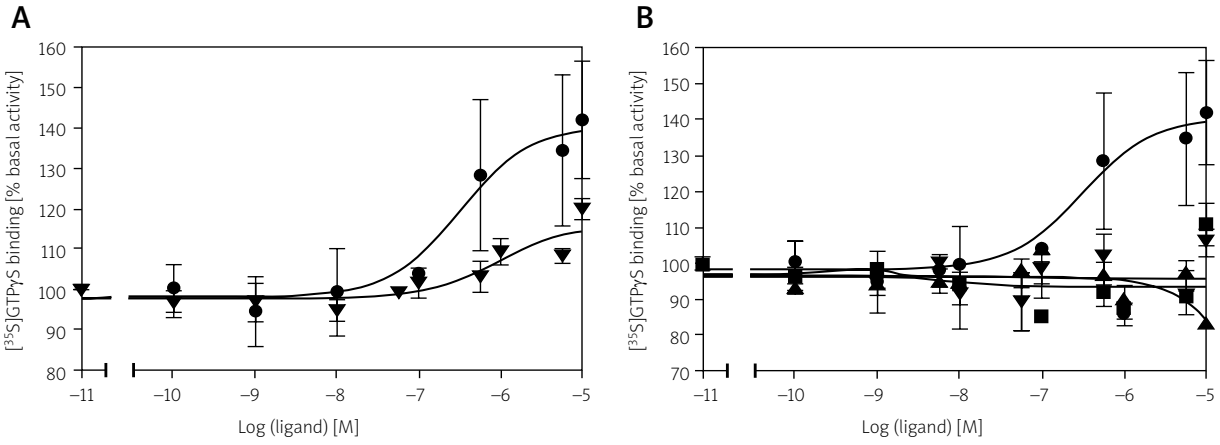

Fig. 4. Stimulation of guanine nucleotide binding to the NK receptors by H-KFFGLM-NH_2 and substance P in the absence or presence of receptor specific antagonists: **A)** H-KFFGLM-NH_2 (●) and substance P (▼); **B)** H-KFFGLM-NH_2 (●), H-KFFGLM-NH_2 and L-703,606-oxalate (NK-1 antagonist) (▼), H-KFFGLM-NH_2 and (Tyr^5,D-$Trp^{6,8,9}$,$Lys\text{-}NH2^{10}$)-neurokinin A (4-10) (NK-2 antagonist) (■); H-KFFGLM-NH_2 and (Trp^7,β-Ala^8)-neurokinin A (4-10) (NK-3 antagonist) (▼). Rat brain membranes were incubated with 0.05 nM [^{35}S]GTPγS and NK ligands at various concentrations. Stimulation of [^{35}S]GTPγS binding was measured and evaluated as described in the Material and methods section. The data are expressed as the percentage stimulation of basal activities and reported as the mean values ± SEM, $n \geq 4$, each performed in triplicate.

Table IV. Summary of [^{35}S]GTPγS functional assays performed with H-KFFGLM-NH_2 in the absence or presence of receptor selective antagonists in rat brain membrane preparation

Peptides	EC_{50} (nM)	E_{max} (%)
H-KFFGLM-NH_2	313 ± 36	142 ± 9
Substance P (NK-1 ≥ NK-2 ~ NK-3 agonist)	892 ± 65	120 ± 4
H-KFFGLM-NH_2 + L-703,606 (NK-1 antagonist)	n.a.	n.a.
H-KFFGLM-NH_2 + (Tyr^5,D-Trp^{6,8,9},Lys-NH2^{10})-neurokinin A (4-10) (NK-2 antagonist)	n.a.	n.a.
H-KFFGLM-NH_2 + (Trp^7,β-Ala^8)-neurokinin A (4-10) (NK-3 antagonist)	n.a.	n.a.

Values for EC_{50} and E_{max} were calculated by GraphPad Prism software using the "sigmoid dose-response" fitting option. All three antagonists could completely block the stimulatory effect of H-KFFGLM-NH_2 (no functional data could be determined) even at low (10^{-6} M) antagonist concentrations. The data are expressed as percentage stimulation of basal activities and are mean values ± SEM, n ≥ 4, each performed in triplicate.

The *N*-terminal fragments of tachykinins play a role in modulating the selectivity of endogenous ligands by decreasing or increasing affinities to particular NK receptor types. In addition, *N*-terminal fragments can carry out their independent neuromodulatory functions in intact endogenous peptides or as metabolites [8]. Our strategy was to truncate and modify the structure of the *C*-terminal fragment of an NK receptor agonist to prepare a tractable radioligand that could be used to investigate the tachykinin system. Our results further confirmed the fact that subtle differences in structure and chain length can result in striking changes in the mode of ligand binding, and presumably have an effect on GPCR signaling. The first intriguing finding came from kinetic experiments, which revealed unusually high receptor density (B_{max}) and a relatively high value for K_d compared with those reported for SP in rat brain [20]. Park *et al*. (1984) reported a single high affinity (K_d = 0.3 nM) and low density (B_{max} = 27.7 fmol mg protein^{-1}) class of binding sites for SP in rat brain. Additionally, the relative potencies of various SP fragments for [^{3}H]-SP binding sites were found to be roughly proportional to the length of the *C*-terminal fragments. We hypothesize from these data that the hexapeptide binds to multiple regions, conformational states or subtypes/splice variants of the receptor proteins. Some of these binding sites may not be identical to the "conventional" binding sites or conformational states for the endogenous neurokinin ligands or receptors. The existence of two different binding sites has already been proposed by Sagan *et al*. as the major binding site (labeled with [[^{3}H]Pro9]SP) and the minor binding site (labeled with [[^{3}H]propionyl-Met(O_2)11]SP-(7–11), respectively [24]. The differences have been further confirmed by displacement experiments, which revealed that binding of [^{3}H]-KFFGLM-NH_2 could be fully abrogated by the addition of H-KFFGLM-NH_2, but not by any of the antagonists. The micromolar inhibitory constants (K_i) measured for the radioligand in competition with receptor selective antagonists for binding to NK receptors also support this hypothesis. Indeed, there are several lines of evidence that support the existence of different binding sites, kinetically distinct states of receptors or the involvement of subtypes/splice variants of neurokinin receptors in ligand binding [9,13,14]. However, these possibilities have yet to be explored.

The *N*-terminally truncated and modified hexapeptide retained its functional agonist activity and stimulated G-protein coupling. Its overall behavior was similar to that observed for the parent peptide SP. The increased potency and efficacy of H-KFFGLM-NH_2 over those of SP also suggest a different mode of ligand binding. However, all of the NK-receptor antagonists could inhibit ligand activity at relatively low concentrations. While it has yet to be investigated, it is possible that ligand binding may alter G-protein signaling. It has also been demonstrated that the endogenous or exogenous ligands for neurokinin receptors can induce conformational state-dependent or ligand binding-dependent modulation of various signal transduction pathways. This can lead to such diverse responses as calcium release and cAMP production, or initiation of receptor desensitization [18,21,23,29]. In addition, derivatives of SP modified at the *C*-terminus have been described that can behave as both agonists and antagonists of the NK-1 receptor, depending on the second messenger pathway [18,23]. Taking the literature data and our findings together, we speculate that our ligand interacts with binding sites specific to *C*-terminal tachykinin binding sites ("tachykinin

pocket"). These sites are structurally similar for all tachykinin receptors. The endogenous ligands of at least three receptors (NK_1, NK_2 and NK_3) have *N*-terminal fragments that enhance affinity to one type of receptor while decreasing affinity for other types. Our results may also suggest the existence of other tachykinin binding sites that preferentially recognize the H-KFFGLM-NH_2 motif. However, this binding site (or sites) is characterized by broad recognition of all tachykinin ligands and attenuated recognition of the *N*-terminal fragments that usually increase ligand selectivity and affinity.

Mysteriously, two previously observed specific binding sites are not present in stable equivalent amounts, suggesting the influence of other modulatory elements [25]. All interpretations of previous observations of various binding sites have been constructed with prediction of tachykinin receptors' existence in monomeric form. However, in the light of our data, we hypothesize that dimers of NK receptors could be specific receptor(s) for *C*-terminal fragments, including H-KFFGLM-NH_2. Previous discussions on other types of GPCR led to the suggestion that dimerization of receptors may result in the formation of an additional allosteric binding site or sites [30]. It should also be considered that interaction of receptor domains in the dimerization process may also destroy "allosteric pockets" as the result of structural reorganization required to form a dimeric macromolecule (Fig. 5). In such a case, *C*-terminal hexapeptide fragment analogues may have less specific interactions with all tachykinin receptors in both monomeric and dimeric forms. Fully elongated undecapeptide substance P interacts with both the "tachykinin pocket" and the "allosteric pocket" on the monomeric NK1 receptor (Fig. 5A). Interactions with the dimeric form are limited to the "tachykinin pockets". The obtained results on pharmacological

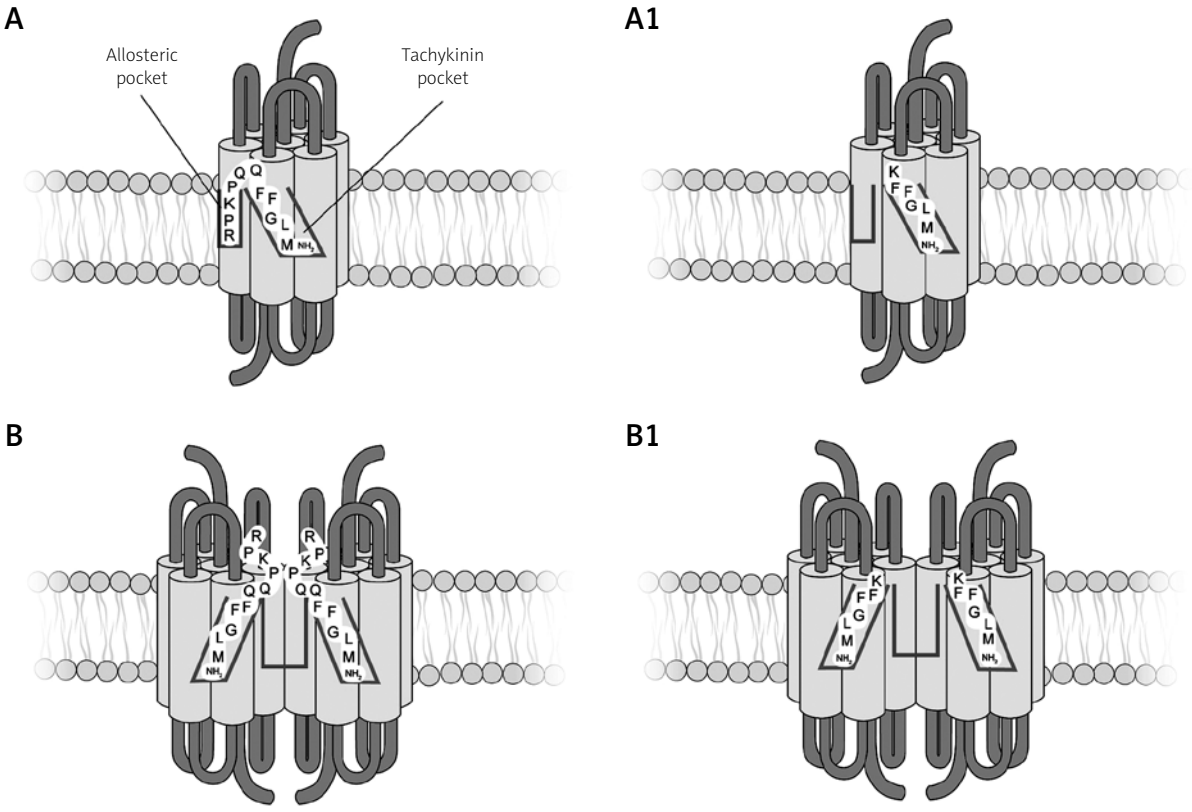

Fig. 5. Illustration of substance P interacting with monomeric and dimeric NK_1 receptor. In the monomer, the interaction of the *C*-terminal fragment of substance P with the "tachykinin pocket" is enhanced by allosteric interaction of the *N*-terminal fragment with the "allosteric pocket". Dimerization of receptors blocks the "allosteric pockets". "Tachykinin pockets" in the monomeric and dimeric forms are recognized equally well by KFFGLM-NH_2.

properties of H-KFFGLM-NH_2 were quite unexpected. This allowed us to construct the working hypothesis. However, for confirmation it is necessary to define a new avenue of investigation that will be explored in our further studies.

Acknowledgments

Aleksandra Tomczyszyn and Balazs Csibran contributed equally to this paper. The technical assistance of Ildiko Nemethne is acknowledged and greatly appreciated. This research was carried out using the TET 10-1-2011-055 grant, CePT infrastructure financed by the European Union – the European Regional Development Fund within the Operational Programme "Innovative Economy" for 2007-2013, Mazowia Peptide Klaster, a Polish-Hungarian bilateral collaboration program, a Polish-Hungarian bilateral collaboration program and COST Action CM1207-GLISTEN. Part of the study was carried out at the Biological and Chemical Research Centre, University of Warsaw, established within the project co-financed by the European Union from the European Regional Development Fund under the Operational Programme Innovative Economy, 2007-2013.

Disclosure

Authors report no conflict of interest.

References

1. Bernardi L, Bosisio G, Chillemi F, de Caro G, de Castiglione R, Erspamer V, Glaesser A, Goffredo O. Synthetic peptides related to eledoisin. Experientia 1964; 20: 306-309.
2. Bozó B, Fülöp F, Tóth GK, Tóth G, Szücs M. Synthesis and opioid binding activity of dermorphin analogues containing cyclic β-amino acids. Neuropeptides 1997; 31: 367-373.
3. Bremer AA, Leeman SE, Boyd ND. The common C-terminal sequences of substance P and neurokinin A contact the same region of the NK-1 receptor. FEBS Lett 2000; 486: 43-48.
4. Cascieri MA, Huang RR, Fong TM, Cheung AH, Sadowski S, Ber E, Strader CD. Determination of the amino acid residues in substance P conferring selectivity and specificity for the rat neurokinin receptors. Mol Pharmacol 1992; 41: 1096-1099.
5. Cheng Y, Prusoff WH. Relationship between the inhibition constant (K1) and the concentration of inhibitor which causes 50 percent inhibition (IC50) of an enzymatic reaction. Biochem Pharmacol 1973; 22: 3099-3108.
6. Foran SE, Carr DB, Lipkowski AW, Maszczynska I, Marchand JE, Misicka A, Beinborn M, Kopin A, Kream RM. Substance P-opioid chimeric peptide as a novel non-tolerance forming analgesic. Proc Natl Acad Sci USA 2000; 97: 7621-7626.
7. Foran SE, Carr DB, Lipkowski AW, Maszczynska I, Marchand JE, Misicka A, Beinborn M, Kopin A, Kream RM. Inhibition of morphine tolerance development by a substance P-opioid peptide chimera. J Pharmacol Exp Ther 2000; 295: 1142-1148.
8. Fransson R, Botros M, Sköld C, Nyberg F, Lindeberg G, Hallberg M, Sandström A. Discovery of dipeptides with high affinity to the specific binding site for substance P1-7. J Med Chem 2010; 53: 2383-2389.
9. Kim HR, Lavielle S, Sagan S. The two NK-1 binding sites are distinguished by one radiolabed substance P analogue. Biochem Biophys Res Com 2003; 306: 725-729.
10. Kleczkowska P, Lipkowski AW, Tourwe D, Ballet S. Hybrid opioid/non-opioid ligands in pain research. Curr Pharm Des 2013; 19: 7435-7450.
11. Lipkowski AW, Carr DB, Bonney I, Kosson P. Opioid-Substance P chimeric peptides. In: Kastin AJ (ed.). Handbook of Biologically Active Peptides. 2nd ed. Academic Press, San Diego 2013; pp. 1586-1591.
12. Lipkowski AW, Carr DB. Neuropeptides: Peptide and Neuropeptide Analogs. In: Peptides – Synthesis and Applications. In: Gutte B (ed.). Academic Press, London 1995; pp. 287-320.
13. Liu L, Markus I, Vandenberg RJ, Neilan BA, Murray M, Burcher E. Molecular identification and characterization of three isoforms of tachykinin NK(1)-like receptors in the cane toad Bufo marinus. Am J Physiol Regul Integr Comp Physiol 2004; 287: R575-585.
14. Maillet EL, Pellegrini N, Valant C, Bucher B, Hibert M, Bourguignon JJ, Galzi JL. A novel conformation-specific allosteric inhibitor of the tachykinin NK2 receptor (NK2R) with functionally selective properties. FASEB J 2007; 21: 2124-2134.
15. Maszczynska Bonney I, Foran SE, Marchand JE, Lipkowski AW, Carr DB. Spinal antinociceptive effects of AA501, a novel chimeric peptide with opioid receptor agonist and tachykinin receptor antagonist moieties. Eur J Pharmacol 2004; 488: 91-99.
16. Matalinska J, Skurzak H, Markowicz S, Lesniak A, Sacharczuk M, Molnar G, Varga E, Lipkowski AW. Opioid agonist – tachykinin antagonist as a new analgesic with adjuvant anticancer properties. Folia Neuropathol 2013; 51: 132-139.
17. Mazzone SB, Hinrichsen CF, Geraghty DP. Substance P receptors in brain stem centers of the rat: regulation of NK1 receptors by hypoxia. J Pharmacol Exp Ther 1997; 282: 1547-1556.
18. Michael-Titus AT; Blackburn D, Connolly Y, Priestley JV, Whelpton R. N- and C-terminal substance P fragments: differential effects on striatal [3H] substance P binding and NK1 receptor internalization. Neuroreport 1999; 10: 2209-2213.
19. Page NM. Brain Tachykinins. In: Kastin AJ (ed.). Handbook of Biologically Active Peptides. 2nd ed. Academic Press, San Diego 2013; pp. 943-950.
20. Park CH, Massari VJ, Quirion R, Tizabi Y, Shults CW, O'Donohue TL. Characteristics of 3H-substance P binding sites in rat brain membrane. Peptides 1984; 4: 833-836.
21. Perrine SA, Beard DJ, Young JK, Simmons MA. The role of the N-terminal and mid-region residues of substance P in regulation functional selectivity at the tachykinin NK1 receptor. Eur J Pharmacol 2008; 592: 1-6.
22. Quancard J, Karoyan P, Sagan S, Convert O, Lavielle S, Chassaing G, Lequin O. Characterization of the bioactive conformation of the C-terminal tripeptide Gly-Leu-Met-NH2 of substance P using [3-prolinoleucin10]SP analogues. Eur J Biochem 2003; 270: 2869-2878.

23. Sachon E, Girault-Lagrange S, Chassaing G, Lavielle S, Sagan S. Analogs of substance P modified at the C-terminus which are both agonist and antagonist of the NK-1 receptor depending on the second messenger pathway. J Pept Res 2002; 59: 232-240.
24. Sagan S, Beaujouan J-C, Torrens Y, Saffroy M, Chassaing G, Glowinski J, Lavielle S. High affinity binding of [3H]propionyl-[Met(O2)11] substance P(7–11), a tritiated septide-like peptide, in Chinese hamster ovary cells expressing human neurokinin-1 receptors and in rat submandibular glands. Mol Pharmacol 1997; 52: 120-127.
25. Sagan S, Karoyan P, Chassaing G, Lavielle S. Further delineation of the two binding sites (R*n) associated with tachykinin neurokinin-1 receptors using [3-prolinomethionine11]SP analogues. J Biol Chem 1999; 274: 23770-23776.
26. Sagan S, Quancard J, Lequin O, Karoyan P, Chassaing G, Lavielle S. Conformational analysis of the C-terminal Gly-Leu-Met-NH2 tripeptide of substance P bound to the NK-1 receptor. Chem Biol 2005; 5: 555-565.
27. Severini C, Improta G, Falconieri-Erspamer G, Salvatori S, Erspamer V. The tachykinin peptide family. Pharmacol Rev 2002; 54: 1-38.
28. Severini C, Improta G. Tachykinins. In: Handbook of Biologically Active Peptides. Kastin AJ (ed.). 2nd ed. Academic Press, San Diego 2013, pp. 391-399.
29. Simmons MA. Functional selectivity of NK1 receptor signaling: peptide agonist can preferentially produce receptor activation or desensitization. J Pharm Exp Ther 2006; 319: 907-913.
30. Smith NJ, Milligan G. Allostery at G protein-coupled receptor homo- and heteromers: uncharted pharmacological landscapes. Pharmacol Rev 2010; 62: 701-725.
31. Toth G, Mallareddy JR, Toth F, Lipkowski AW, Tourwe D. Radiotracers, tritium labelling of neuropeptides ARKIVOC 2012; 5: 163-174.
32. Valant C, Maillet E, Bourguignon JJ, Bucher B, Utard V, Galzi J. Allosteric functional switch of neurokininA-mediated signaling at the neurokinin NK2 receptor: Structural exploration. J Med Chem 2009; 52: 5999-6011.
33. Wang J-X, Dipasquale AJ, Bray AM, Maeji NJ, Spellmeyer DC, Geysen HM. Systematic study of substance P analogs. II. Rapid screening of 512 substance P stereoisomers for binding to NK1 receptor. Int J Pept Protein Res 1993; 42: 392-399.

Original article

Folia Neuropathologica

Assessment of antioxidative activity of alkaloids from *Huperzia selago* and *Diphasiastrum complanatum* using *in vitro* systems

Grzegorz A. Czapski[1], Wojciech Szypuła[2], Magdalena Kudlik[1], Beata Wileńska[3], Magdalena Kania[3], Witold Danikiewicz[3], Agata Adamczyk[1]

[1]Mossakowski Medical Research Centre Polish Academy of Sciences, Warsaw, [2]Medical University, Warsaw, [3]Institute of Organic Chemistry Polish Academy of Sciences, Warsaw, Poland

Folia Neuropathol 2014; 52 (4): 394-406 DOI: 10.5114/fn.2014.47840

Abstract

Free radical-induced oxidative damage is implicated in the pathogenesis of neurodegenerative disorders, and antioxidants are presumably of therapeutic value in such diseases. Our previous data indicated that free radicals are strongly associated with brain aging and also play an important role in cytotoxicity of amyloidogenic proteins including α-synuclein and amyloid β, which accumulate in brains during Parkinson's and Alzheimer's diseases. Disruption of the equilibrium of pro-oxidants and antioxidants results in oxidative stress that leads to the modification of DNA, proteins, carbohydrates, and lipids. It is widely accepted that antioxidants acting as radical scavengers protect the brain against oxidative damage in neurodegenerative diseases. Plant products are rich sources of phytochemicals and have been found to possess a variety of biological activities, including antioxidative potential.

The aim of this study was to analyse the antioxidative potential of alkaloid fractions from Huperzia selago and Diphasiastrum complanatum to protect macromolecules against oxidative damage. Thin layer chromatography (TLC) and high-performance liquid chromatography with diode array (HPLC-DAD) and electrospray ionisation mass spectrometric detection (ESI-MS/MS) were used to carry out a comprehensive characterization of alkaloids isolated from the plant material. The effect of the tested compounds on iron/ascorbate-induced lipid peroxidation and carbonyl group formation was analysed in the rat brain homogenate. Direct free radical scavenging (DPPH assay) and the effect on dityrosine formation were measured in cell-free systems.

Our results indicated that a number of alkaloid extracts at concentration of 25 μg/ml exhibited antioxidant activity as indicated by DPPH radical scavenging potential (up to 59% inhibition) and inhibition of dityrosine formation. Selected alkaloid fractions provided significant protection against lipid peroxidation and protein oxidation in rat brain tissue homogenate, reducing iron/ascorbate-induced damage by about 20% and 76%, respectively. Overall, the results indicated that selected alkaloids isolated from Huperzia selago effectively protect macromolecules from oxidative stress injury, which will give us an insight into the potential of alkaloids in terms of opening up a new therapeutic approach for oxidative stress-dependent disorders.

Key words: *oxidative damage, carbonyl groups, lipid peroxidation, antioxidant, free radical scavenger, Huperzia selago, Diphasiastrum complanatum.*

Communicating author:

Grzegorz A. Czapski, Mossakowski Medical Research Centre Polish Academy of Sciences, 5 Pawinskiego St., 02-106 Warsaw, Poland, e-mail: gczapski@imdik.pan.pl

Introduction

Free radical-induced oxidative damage is a component of the pathomechanism of many deleterious neurodegenerative disorders, such as Alzheimer's or Parkinson's disease [10]. The brain is an organ especially vulnerable to reactive oxygen species (ROS)-mediated injury for the following reasons: 1) high consumption of oxygen which is necessary for producing large amounts of ATP needed to maintain ion homeostasis, 2) neuronal membranes are rich in polyunsaturated fatty acids (PUFA), which are particularly vulnerable to free radical attack, 3) antioxidant defence mechanisms are modest, with low levels of catalase and glutathione peroxidase in particular, 4) the high Ca^{2+} traffic across neuronal membranes and interference of ion transport increase intracellular Ca^{2+}, often leading to oxidative stress, 5) iron is accumulated in the brain, and brain damage readily releases iron ions capable of catalysing free radical reactions [17]. Disruption of equilibrium of pro-oxidants and antioxidants results in oxidative stress that leads to the modification of DNA, proteins, carbohydrates, and lipids. Free radicals attack the unsaturated fatty acids in the biomembranes, resulting in lipid peroxidation, decrease in fluidity, loss of enzyme and receptor activity, and damage to membrane proteins, and ultimately leading to cell damage. Lipid peroxidation is strongly associated with brain aging and neurodegenerative disorders. It is suggested that antioxidants, acting as radical scavengers, protect the brain against free radicals involved in the pathomechanism of neurodegenerative disorders. Many studies have demonstrated the association between the risk of neurodegenerative diseases and the antioxidative status, suggesting the importance of antioxidants as disease-preventing agents [18,39,40,59]. Oxidative stress is a factor acting in the early stage of neurodegeneration, raising the possibility that protection of macromolecules against free radical damage may have a beneficial effect [1]. Plant products are rich sources of phytochemicals that have been found to possess antioxidative properties. Recently, there has been an upsurge of interest in the therapeutic potential of medicinal plants as antioxidants in reducing free radical-induced injury. In this regard, some plant species that possess medicinal and antioxidant properties have been identified, e.g. *Ginkgo biloba* [42,50], *Panax ginseng* [11,26], *Thea sinensis* [7,15], *Scutellaria baicalensis* [37,38] and *Curcuma longa* [22,44].

Huperzia selago (L.) Bernh. ex Schrank et Mart., a source of huperzine A (HupA) and other alkaloids commonly known as fir club moss (family *Huperziaceae*), is a plant of great interest that is used in combating a wide variety of diseases in European and Asian countries [30,32,48]. Plants of the species *Diphasiastrum complanatum* (L.) Holub (*Lycopodiaceae*) are rich in alkaloids, mostly lycopodine and its derivatives, generally biologically not yet investigated [30].

The *Huperzia* and *Diphasiastrum* alkaloids are of great importance due to their biological activity and unique chemical structures [24,30]. Various alkaloids derived from these plants and their therapeutic potentials have been characterized in several reports [8,30,57,60]. Pharmacological studies conducted since the 1980s have demonstrated that the therapeutic properties of *Huperzia serrata*, which has been used for centuries in traditional Chinese medicine, are due to the presence of many alkaloids, including HupA, which is a potent, reversible and selective acetylcholinesterase (AChE) inhibitor [30]. However, the neuroprotective action of these alkaloids goes beyond the inhibition of AChE. They may affect DNA synthesis, gene expression, mitochondrial function, oxidative stress, apoptosis and NGF signalling. Interestingly, HupA protects against liberation of amyloid beta peptides, which may be related to its beneficial effects on learning and memory deficiency in animal models and Alzheimer's disease patients [8,30,57,60].

Studies on the pharmacological properties of HupA are being conducted in many centres worldwide, and a comprehensive review of them has been published by Zhang and Tang [60] and Ma *et al*. [32]. Moreover, studies by Szypuła *et al*. [46-48] have shown that *H. selago* is a rich source of HupA and other alkaloids, which are much more abundant in this plant than in the Chinese club moss *H. serrata*.

The aim of our study was to investigate and compare antioxidative properties of *Huperzia selago* and *Diphasiastrum complanatum* alkaloids *in vitro*. We analysed the effect of alkaloid extracts and HupA, lycopodine and annotinine authentic standards on protein oxidation and lipid peroxidation. Our results indicated for the first time that some components of *H. selago* alkaloid extract possess potent antioxidative properties, scavenge free radicals and prevent

lipid and protein oxidation. These results indicated that *H. selago* might be a promising source of lead compounds for drug discovery.

Material and methods

Chemicals

Dimethyl sulfoxide (DMSO), 2,2-diphenyl-1-picrylhydrazyl (DPPH), 2,4-dinitrophenylhydrazine, sodium hexafluorophosphate and acetonitrile were purchased from Sigma Chemical Co., St. Louis, MO, USA. Ferrous chloride tetrahydrate was from Fluka Chemie AG, Buchs, Switzerland; L-(+)-ascorbic acid was from Avocado Research Chemicals Ltd.; L-tyrosine, 2-thiobarbituric acid, hydrogen peroxide and water of HPLC grade were purchased from Merck KGaA, Darmstadt, Germany; chloroform, diethyl ether, ammonium and sodium chloride were from POCH, Gliwice, Poland. All other common reagents were from Sigma-Aldrich (St. Louis, MO, USA). HupA was purchased from ChromaDex, Inc. (Laguna Hills, CA); the reference compounds lycopodine, alpha-obscurine and annotinine were obtained from the Department of Pharmacognosy and Molecular Basis of Phytotherapy, Medical University of Warsaw. For all standards at least ^{1}H NMR, ^{13}C NMR, 2D COSY, HMBC, UV- VIS and MS/MS spectra were recorded.

Animals

Male Wistar rats (200-250 g) were supplied by the Animal House of Mossakowski Medical Research Centre Polish Academy of Sciences, Warsaw, Poland. The animals (n = 5) were maintained at constant humidity, temperature and light cycle, and had free access to food and water. All experiments on animals were accepted by the Polish National Ethics Committee and were carried out in accordance with the European Communities Council Directive of 24 November 1986 (86/609/EEC).

Preparation of rat brain cortex homogenate

For analysis of protein and lipid oxidation, adult male Wistar rats were decapitated, their brains were removed, and brain cortices were isolated on ice and frozen at –80°C. Brain cortex was homogenized in ice-cold 50 mM Tris-HCl buffer, pH 7.4, to obtain 10% homogenate.

Acquisition of plant material

Aerial parts of *H. selago* were collected in the Babia Gora Biosphere Reserve (Poland) in September 2010. Aerial parts of *D. complanatum* were collected in the Masurian Lake District (Poland). A voucher collection permit of plants was obtained from the Ministry of Environment (Poland). Material was identified and authenticated by one of the authors (Wojciech Szypuła). Voucher specimens were deposited in the herbarium of the Department of Pharmaceutical Biology and Medicinal Plant Biotechnology, Medical University of Warsaw.

Preparation and purification of extracts

The extraction of alkaloids from *H. selago* was based on the protocol used by Wiedenfeld *et al*. [54] with modifications according to Szypula *et al*. [48]. A powdered plant sample of *H. selago* was accurately weighed (190 ± 0.01 g) and placed in a 5-L conical flask. Ultrasound extraction was carried out in an RK 100H ultrasonic cleaning bath (Bandelin Sonorex, Berlin, Germany), which had a mean operating frequency of 35 kHz, and the power was adjusted to 160 W. The extraction was performed at 40°C for 30 min, each time with 2 l of methanol of analytical purity grade until the eluate was negative to Dragendorff's reagent. The extracts were decanted through fluted filter paper into a 2 l round-bottomed flask. The combined methanol extracts were evaporated to dryness under reduced pressure at 40°C. The obtained residues were reconstituted into 1 l of 2.5% hydrochloric acid, transferred into a 2-l separator, and purified by extracting two times with 1 l of chloroform and once with 1 l of diethyl ether. The aqueous layer was adjusted to pH 9.0 with 25% ammonia solution and then extracted with chloroform (2 × 1-l). Next, sodium chloride was gradually added to the aqueous layer until a saturated solution was obtained and it was again extracted with chloroform, until the eluate was negative to Dragendorff's reagent. The chloroform extracts were combined and evaporated to dryness under decreased pressure at 40°C. The chloroformic extract was evaporated until dry in order to obtain 2.0 g of the crude total alkaloid extract E_1 (% w/w, 1.11; % w/w calculated relative to dry starting material).

A dried $CHCl_3$ extract (2.0 g) obtained from *H. selago* was chromatographed on Sephadex LH-20 in a glass column (30 × 2.5 cm), eluting with mixtures

of $CHCl_3$-MeOH (100 : 0 → 70 : 30 v/v in 16 steps) as the mobile phase to give 129 fractions pooled into 7 main fractions containing alkaloids: AEF-1 (63.4 mg), AEF-2 (178.31 mg), AEF-3 (335.4 mg), AEF-4 (90.13 mg), AEF-5 (124.84 mg), AEF-6 (125.9 mg) and AEF-7 (77.1 mg).

The extraction of alkaloids from sporophytes of *D. complanatum* was performed using our own method. The air-dried whole plants of *D. complanatum* (0.5 kg) were extracted with 96% EtOH twice. The extraction was performed at 25°C for 24 h, each time with 3.5 l of ethanol of analytical purity grade until the eluate was negative to Dragendorff's reagent. The extracts were decanted through fluted filter paper into a 2 l round-bottomed flask. The combined ethanol extracts were evaporated to dryness under reduced pressure at 40°C. The obtained residues were reconstituted into 0.7 l of 2% hydrochloric acid, transferred into a separator, and purified by extracting twice with benzene. Next, the aqueous layer was adjusted to pH 8.0 with 25% ammonia solution and then extracted a few times with benzene and chloroform. The combined extracts were evaporated until dry in order to obtain 0.95 g of the crude total alkaloid extract (% w/w, 0.19; % w/w calculated relative to dry starting material). A dried combined extract (0.95 g) from *D. complanatum* was chromatographed on an aluminium oxide column (30 × 2.5 cm), eluting with a mixture of n-hexane/benzene (100 : 0 → 0 : 100 v/v in 4 steps) to give 133 fractions pooled into 2 – AEF-8 (0.4 g) and AEF-9 (0.2 g) – main fractions. Fractions AEF-8-AEF-9 were purified by crystallization from acetone to give compounds AEF-8 (10 mg) and AEF-9 (5 mg). All AEF-1-AEF-7 and AEF-8-AEF-9 fractions were then submitted to TLC, HPLC-DAD and HPLC-ESI-MS/MS analysis.

Thin layer chromatography (TLC) analysis of alkaloids

The alkaloid extracts (20 µg/20 µl) and 10 µl of the separated (HupA, lycopodine, alpha-obscurine and annotinine) reference compounds in 1 ml of $CHCl_3$ were spotted on a silica gel plate (Merck Silica Gel 60F254, 10 cm x 10 cm). The mobile phase used was $CHCl_3$: MeOH : NH_4OH (70 : 7 : 1, v : v : v). After chromatography the TLC plate was removed from the tank and air-dried. It was then sprayed with modified Dragendorff's reagent or I_2 vapour. *Huperzia* and *Diphasiastrum* genus alkaloids showed up immediately as orange spots.

High performance liquid chromatography with diode array detection (HPLC-DAD) and high performance liquid chromatography-electrospray tandem mass spectrometry (HPLC-ESI-MS/MS) of alkaloids

Qualitative and quantitative HPLC-DAD analyses were performed on a Shimadzu system consisting of a UV-VIS and SPD-10A DAD 340S detector, LC-10AD pump and LC solution software. A Hypersil GOLD column, C_{18} 250 × 4.6 mm, and a Hypersil GOLD precolumn, 5 UM 10 × 4 mm, were used [48]. The mobile phase consisted of (A) water with the addition of 30 mM $NaPF_6$ and (B) acetonitrile. The following gradient was applied: 0-5 min 0 → 25% B, 5-20 min 25 → 45% B, 20-30 min 45 → 80% B [48]. Column temperature: 24 ± 1°C, flow rate of the mobile phase: 1.0 ml/min, analysis duration: 30 min, detection at wavelengths λ = 210, 230, 260, 310 nm.

Individual alkaloids were identified by the HPLC-ESI-MS/MS method. The measurements were carried out on a High-Performance Liquid Chromatograph Prominence LC-20 (Shimadzu) coupled with a 4000 QTrap mass spectrometer. The LC separation was performed on a Hydro RP C18 column (Phenomenex) using as a mobile phase 10 mM CH_3COONH_4 aqueous solution with HCOOH addition to obtain pH 4.3 (A) and MeCN (B), in the following linear gradient: 0-5 min 30 → 45% B, 5-40 min 45 → 95% B. Column temperature: 24 ± 1°C, flow rate of the mobile phase: 1.0 ml/min. The analysis was performed at 230 nm and 270 nm.

The electrospray ionisation mass spectrometry (ESI-MS) spectra were recorded in the positive ion mode, in the m/z range 100-1000. The source parameters set was as follows: IS 5500 V, DP 40 V, EP 10 V and the source temperature was 550°C.

The fragmentation spectra were performed also in the positive ion mode. The collision energy was optimized to obtain the most informative CID (collision-induced dissociation) spectra of investigated compounds.

Preparation of standard solution and sample solution

Standard solutions of HupA, lycopodine, alpha-obscurine and annotinine were prepared by weighing into an Eppendorf tube approximately 1 ± 0.1 mg of the standard substance, and a sample solution

was obtained by dissolving the alkaloid fraction isolated from the plant material in methanol of HPLC purity grade to a concentration of 1 mg/ml. Approximately 1 ± 0.1 mg was weighed using an analytical balance into Eppendorf tubes and reconstituted in methanol of HPLC purity grade to obtain a solution of 1 mg of extract in 1 ml of methanol. Aliquots of 20 µl of the solution were introduced into the column. To obtain the fragmentation spectra of HupA, lycopodine, alpha-obscurine and annotinine standard, the methanol extracts were injected directly into the electrospray interface of the mass spectrometer in positive ion mode ESI(+). To obtain the fragmentation spectra of HupA and other alkaloids from the plant material, appropriate solutions of the fraction (10 µl of the fraction solution corresponding to 10 µg of the fraction) were introduced into the chromatographic column. For all compounds at least UV-VIS and MS/MS spectra were recorded. Data obtained from all experiments (retention factor and retention time, UV spectrum, total ion chromatogram, selected ion chromatograms for specific m/z and comparison of the fragmentation quasi-molecular ion of the standards and the ion with m/z corresponding to the appropriate alkaloids in plant material) were compared with those reported in the literature (see Table I) and, if standards were available, comparison was made by HPLC-ESI-MS/MS method.

Preparation of alkaloid extracts (AEF) for biochemical studies

Samples were dissolved in DMSO at a concentration of 25 mg/ml, which roughly corresponds to molar concentration approximately 100 mM for this group of alkaloids. Then dilutions were prepared in the same DMSO concentration, and AEF were used in final concentrations of 0.25 µg/ml (approximately 1 µM), 2.5 µg/ml (approximately 10 µM) and 6.25 µg/ml (approximately 25 µM).

Determination of the antioxidant activity of AEF

The free radical scavenging properties of AEF were determined by analysis of the 2,2-diphenyl-1-picrylhydrazyl (DPPH) radical scavenging activity following the method reported by Blois [9] with some modifications [12]. The tested AEF (0-25 µg/ml) was mixed with 1 M Tris-HCl buffer (pH 7.9) and 50 µM solution of DPPH in methanol. The samples were incubated for 20 min at room temperature in the dark, and then the absorbance at 517 nm was determined on a Model 680 Microplate Reader (Bio-Rad). Samples with appropriate concentration of DMSO instead of AEF were used as the control, and samples without DPPH were used as blanks.

Determination of the effect of AEF on dityrosine formation

The effect of AEF on dityrosine formation was determined in a protein-free system according to the method described by Ferdinandy and Schulz [16] with some modifications [13]. L-tyrosine (0.5 mM) was incubated with $CuSO_4$ (100 µM) and H_2O_2 (100 mM) in the presence of AEF (2.5 µg/ml) for 10 min at room temperature. The fluorescence of formed dityrosine was determined spectrofluorimetrically at 325 nm excitation and 405 nm emission.

Determination of the effect of AEF on lipid peroxidation

The effect of AEF on lipid peroxidation was determined in the rat brain cortex homogenate incubated with $FeCl_2$ and ascorbic acid, as an ROS-generating system. The 10% homogenate was incubated with 25 µM $FeCl_2$ and 10 µM ascorbic acid in the presence of AEF (25 µg/ml) for 15 min at 37°C in a final volume of 0.2 ml. The level of thiobarbituric acid reactive substances (TBARS) was determined as an index of lipid peroxidation according to the method reported by Asakawa and Matsushita [2] with some modifications [14].

Determination of the effect of AEF on carbonyl group formation

The effect of AEF on protein oxidation was determined in the rat brain cortex homogenate incubated with $FeCl_2$ and ascorbic acid, as an ROS-generating system. Protein oxidation was analysed by determining the content of the carbonyl groups. The 10% homogenate was incubated with 25 µM $FeCl_2$ and 10 µM ascorbic acid in the presence of AEF (25 µg/ml) for 15 min at 37°C in a final volume of 0.2 ml. The carbonyl group concentration was determined by derivatization with dinitrophenylhydrazine (DNPH) according to the method described by Oliver *et al.* [35] with some modifications [14].

Table I. Composition of alkaloid fractions of *Huperzia selago* (L.) Bernh. ex Schrank et Mart. and *Diphasiastrum complanatum* (L.) Holub. The table shows formulas, and theoretical and empirical molecular masses of possible components for each fraction. AEF-1–AEF-7 refer to the alkaloids isolated from *H. selago*, and AEF-8 and AEF-9 are from *D. complanatum*

Fraction and compound number		Formula	$[M+H]^+$ (*m/z*, theoretical mass)	(+)-ESIMS (*m/z*, from spectrum)	Identification or possible alkaloid
AEF-1	1	$C_{17}H_{26}N_2O$	275.4011	275.3	Alpha-obscurine, confirmed using TLC, HPLC-DAD and ESI-MS method in the present study
	2	$C_{17}H_{30}N_2$	263.2482	263.3	Nankakurine A [23,24]
	3	$C_{16}H_{23}NO_2$	262.1801	262.3	Acrifoline, confirmed using TLC, HPLC-DAD and ESI-MS method in the present study and literature data according to [20,30]
	4	$C_{16}H_{22}N$	258.1734	257.1	Des-*N*-methyl-β-obscurine [3,31]
	5	$C_{17}H_{22}N_2O_2$	287.1754	287.1	Huperzine D [24]
	6	$C_{16}H_{21}N_2O$	257.1659	257.1	Lyconadin A [27]
	7	$C_{16}H_{25}NO_2$	264.3752	264.3	Lycodoline [21]
AEF-2	1	$C_{16}H_{20}N_2O$	257.1648	257.1	Huperzine B – confirmed using TLC, HPLC-DAD and ESI-MS method in the present study and literature data according to [24]
	2	$C_{16}H_{22}N$	258.1734	257.1	Des-*N*-methyl-β-obscurine [3,31]
	3	$C_{16}H_{23}N_2$	243.1861	243.1	Lycodine [30,58]
	4	$C_{16}H_{25}NO$	248.2009	248.3	Lycopodine confirmed using TLC, HPLC-DAD and ESI-MS method in the present study and literature data according to [24]
	5	$C_{16}H_{24}NO$	246.1852	246.1	Fawcettidine [29]
	6	$C_{16}H_{25}NO_2$	264.1968 or 264.1969	264.2	Lycoposerramine-L or lycoposerramine-M [49]
	7	$C_{16}H_{23}NO_2$	262.1801	262.1	Acrifoline confirmed using TLC, HPLC-DAD and ESI-MS method in the present study and literature data according to [20]
AEF-3	1	$C_{15}H_{18}N_2O$	243.1492	243.1	Huperzine A – confirmed using TLC, HPLC-DAD and ESI-MS method in the present study and literature data according to [48]
	2	$C_{16}H_{25}NO_3$	280.1893	280.1	Lycoposerramine-G or serratezamine C [45]
	3	$C_{16}H_{25}NO$	248.2009	248.3	Lycopodine confirmed using TLC, HPLC-DAD and ESI-MS method in the present study
	4	$C_{16}H_{26}NO_2$	264.3620	264.3	6-Hydroxylycopodine (flabelliformine) confirmed using ESI-MS method in the present study
	5	$C_{16}H_{20}N_2O$	257.1648	257.1	Huperzine B confirmed using TLC, HPLC-DAD and ESI-MS method in the present study and literature data according to [24]
	6	$C_{15}H_{18}N_2O$	259.1369	259.1	6-β-Hydroxyhuperzine [5,55]
	7	$C_{16}H_{25}NO_2$	264.1968 or 264.1969	264.2	Lycoposerramine-L or lycoposerramine-M [49]
AEF-4	1	$C_{15}H_{18}N_2O_2$	259.3156	259.3	6-β-Hydroxyhuperzine [5,55]
		$C_{15}H_{18}N_2O$	243.1492	243.1	Huperzine A confirmed using TLC, HPLC-DAD and ESI-MS method in the present study and literature data according to [48]
	2	$C_{16}H_{25}NO_2$	264.1968 or 264.1969	264.2	Lycoposerramine-L or lycoposerramine-M [49]
	3	$C_{16}H_{25}NO$	248.2009	248.1	Lycopodine confirmed using TLC, HPLC-DAD and ESI-MS method in the present study and literature data according to [24]
	4	$C_{16}H_{25}NO_3$	280.1893	280.1	Lycoposerramine-G [49]
	5	$C_{16}H_{20}N_2O$	257.1648	257.1	Huperzine B confirmed using TLC, HPLC-DAD and ESI-MS method in the present study and literature data according to [24]
	6	$C_{16}H_{24}NO_3$	278.1754	278.1	Probably 8b-hydroxylycoposerramine K [53]
	7	$C_{16}H_{23}N_2O$	259.1805	259.1	Lyconadin E [25]

Table I. Continue

Fraction and compound number		Formula	$[M+H]^+$ (*m/z*, theoretical mass)	(+)-ESIMS (*m/z*, from spectrum)	Identification or possible alkaloid
AEF-5	1	$C_{16}H_{25}NO$	248.2009	248.3	Lycopodine confirmed using TLC, HPLC-DAD and ESI-MS method in the present study and literature data according to [24]
	2	$C_{16}H_{24}NO_2$	262.1803	262.1	Serratidine [45]
	3	$C_{16}H_{25}NO_3$	280.1893	280.1	Lycoposerramine-G [49]
	4	$C_{17}H_{32}N_2$	265.3108	265.3	Probably cermizine B [33]
AEF-6	1	$C_{16}H_{27}NO$	250.3920	250.3	Dihydrolycopodine confirmed using TLC, HPLC-DAD and ESI-MS method in the present study and literature data according to [19]
	2	$C_{16}H_{25}NO_2$	264.1968 or 264.1969	264.2	Lycoposerramine-L or lycoposerramine-M [49] or flabelliformine
	3	$C_{16}H_{25}NO$	248.2009	248.3	Lycopodine confirmed using TLC, HPLC-DAD and ESI-MS method in the present study and literature data according to [24]
	4	$C_{16}H_{24}NO_2$	262.1803	262.1	Serratidine [45]
	5	$C_{16}H_{25}NO_3$	280.1893	280.1	Lycoposerramine-G or serratezamine C [45]
	6	$C_{16}H_{24}NO$	246.1852	246.1	Fawcettidine [36]
AEF-7	1	$C_{16}H_{27}NO$	250.3920	250.3	Dihydrolycopodine – confirmed using TLC, HPLC-DAD and ESI-MS method in the present study and literature data according to [19]
	2	$C_{16}H_{24}NO$	246.1852	246.1	Fawcettidine [36]
AEF-8	1	$C_{16}H_{25}NO$	248.2009	248.3	Lycopodine confirmed using TLC, HPLC-DAD and ESI-MS method in the present study and literature data according to [24]
AEF-9	1	$C_{16}H_{25}NO$	248.2009	248.3	Lycopodine confirmed using TLC, HPLC-DAD and ESI-MS method in the present study and literature data according to [24]
	2	$C_{16}H_{24}NO$	246.1852	246.1	Fawcettidine [36]
	3	$C_{16}H_{27}NO$	250.3920	250.3	Dihydrolycopodine
10		$C_{16}H_{21}NO_3$	276.3428	276.4	Annotinine authentic standard
11		$C_{16}H_{25}NO$	248.2009	248.3	Lycopodine authentic standard
12		$C_{15}H_{18}N_2O$	243.1492	243.1	Huperzine A authentic standard

Statistics

Statistical analysis was performed with Graph Pad Prism version 6.0 (GraphPad Software, San Diego, CA) using one-way analysis of variance (ANOVA) with the Newman-Keuls post-hoc test. Data are presented as means ± SEM. $P < 0.05$ was considered significant.

Results

In the present study to determine the content of alkaloids in *H. selago* and *D. complanatum* plants, dry alkaloid extracts were separated using column chromatography and were analysed using several methods. The results indicated that they contain numerous different types of alkaloids, previously classified by Ayer and Trifonow [4] into four structural classes: the lycopodine class, the lycodine class, the fawcettimine class and the miscellaneous group (Table I). The antioxidant activities of alkaloid fractions (AEF) in the cell-free system were assessed by measuring their capabilities for scavenging 2,2-diphenyl-1-picrylhydrazyl (DPPH) and via the analysis of their effect on dityrosine formation, that is a biomarker of oxidative stress in biological samples. Moreover, antioxidative properties of these compounds were analysed using rat brain cortex homogenate. Oxidative stress in the homogenate was evoked by Fenton's reaction generating the hydroxyl radical in the presence of $FeCl_2$ and ascorbic acid (Fe/Asc). The antiradical activity of all AEF examined by free radical DPPH scavenging tests

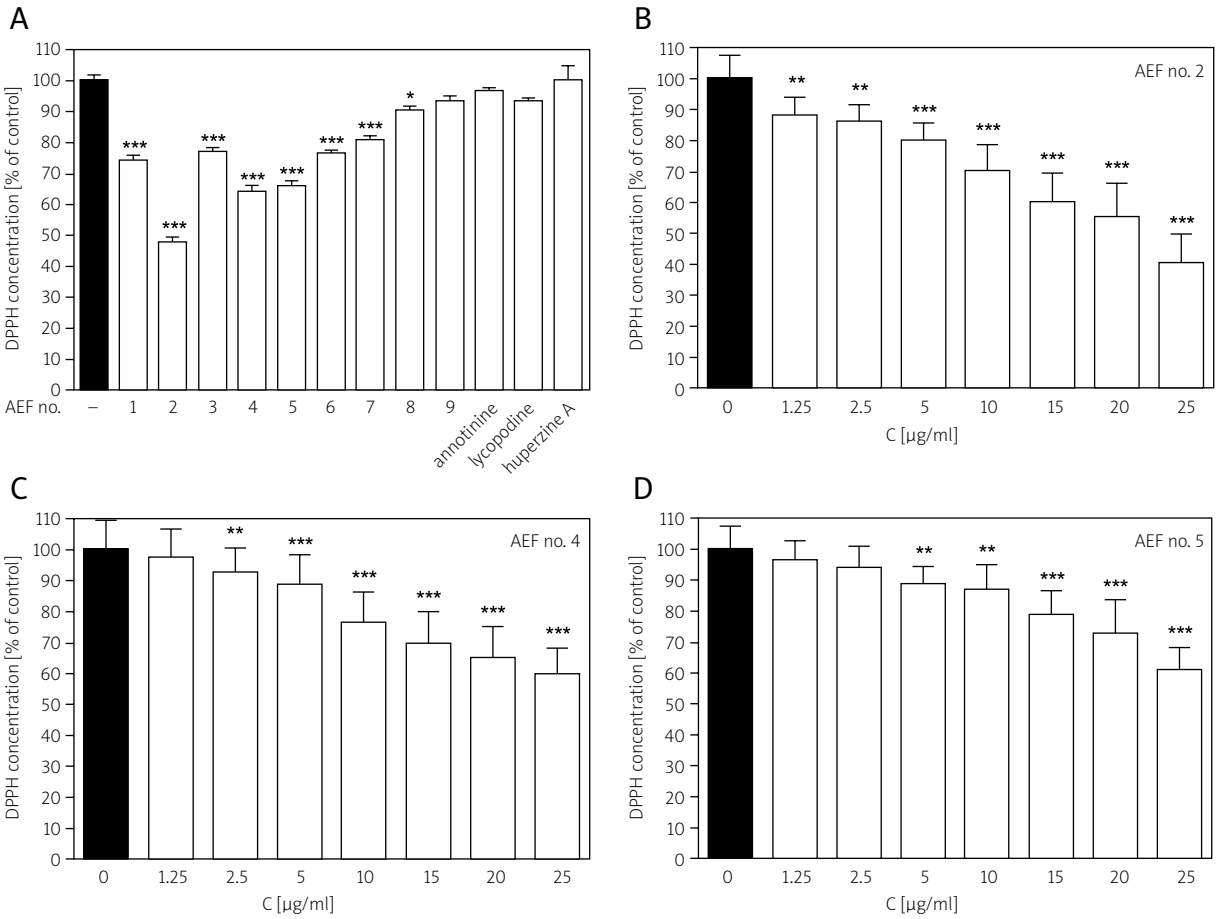

Fig. 1. Free radical scavenging properties of alkaloid fractions (AEF). The direct free radical scavenging properties of tested alkaloids were determined using the DPPH assay. **A)** The stable free radical DPPH was incubated for 20 min at room temperature in the presence of the tested AEF at 25 µg/ml, and then the concentration of DPPH was determined spectrophotometrically. **B-D)** The most powerful free radical scavengers were tested in the concentration range 0-25 µg/ml. Each chart represents a separate set of experiments. All values are the means ± SEM from three experiments. *, **, ***$p < 0.05$, 0.01 and 0.001, respectively, compared to the control.

demonstrated that AEF 1-8 at 25 µg/ml were capable of scavenging the DPPH radical (Fig. 1A). The most potent antioxidants, AEF-2, -4 and -5, were tested in the concentration range 0-25 µg/ml. As shown in Figure 1B-D, all these AEF scavenged the DPPH free radical in a concentration-dependent manner. The most powerful free radical scavenger was AEF-2, which affected the level of DPPH at a concentration of 1.25 µg/ml (IC50 = 21.9 µg/ml). AEF-4 and -5 were less efficient scavengers of the DPPH radical (IC50 > 25 µg/ml). These results indicated that selected AEF show proton-donating ability and could serve as free radical scavengers, acting possibly as primary antioxidants. Since the formation of dityrosine in a protein exposed to oxygen free radicals can serve as a marker of oxidative stress, we analysed the effect of all AEF on dityrosine level in the protein-free reaction in which oxidative stress was evoked by Fenton's reaction. Oxidation of L-tyrosine leads to formation of a tyrosyl radical that dimerizes to form dityrosine. As demonstrated in Figure 2, AEF-1, -4 and -5 caused a significant delay in formation of dityrosine evoked by $CuSO_4$, and H_2O_2, AEF-3, -6, -7 and lycopodine also subtly attenuated dityrosine formation. Other alkaloids had no effect. Lipid peroxidation involves the formation and propagation of lipid radicals with numerous deleterious effects, including destruction of membrane lipids, and production of malondialdehyde and other thiobarbituric acid-reactive substances (TBARS). The thiobarbituric

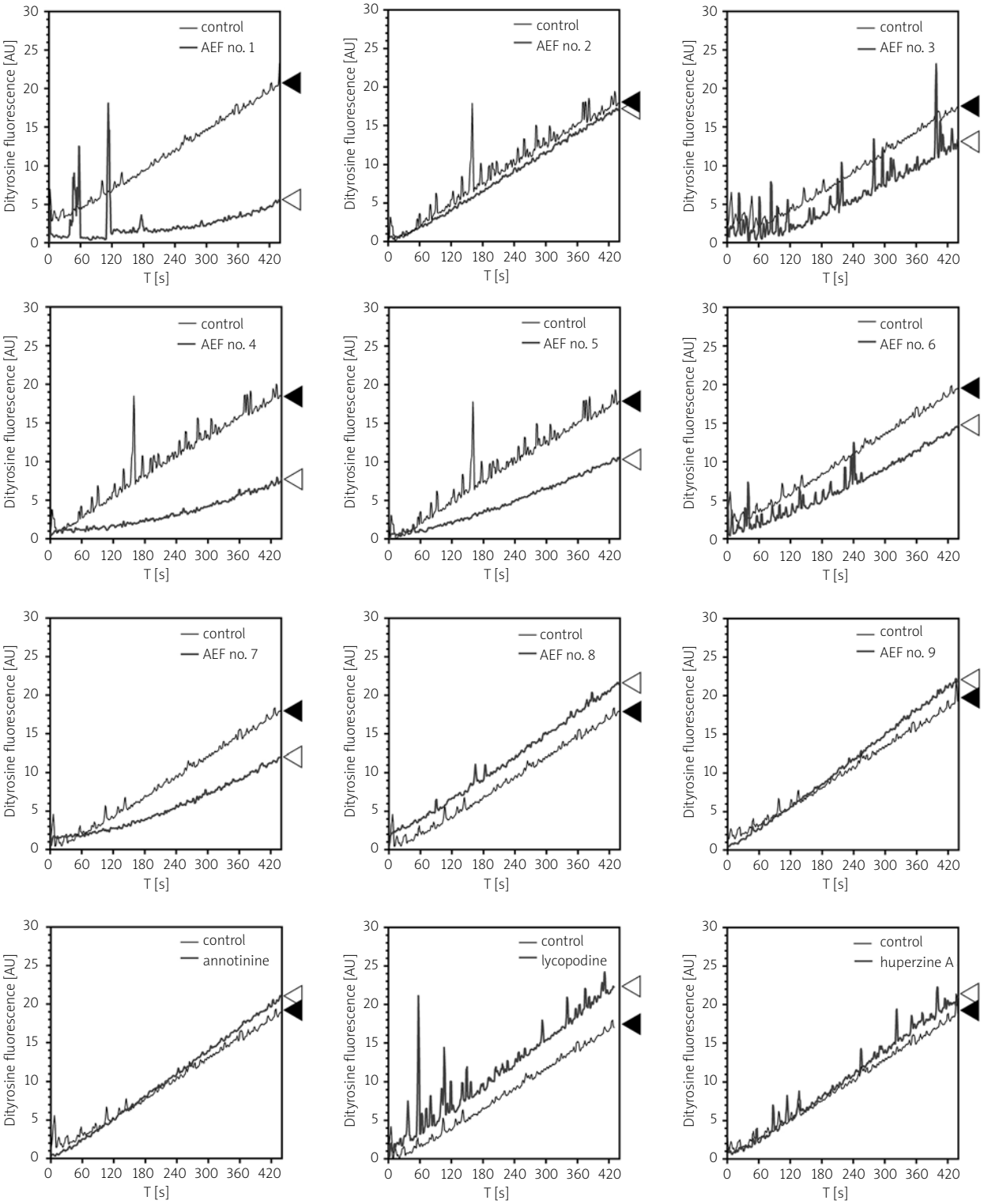

Fig. 2. The effect of alkaloid fractions (AEF) on dityrosine formation. L-tyrosine (0.5 mM) was incubated in PBS at room temperature in the absence (control ◀) and in the presence (◁) of tested alkaloids with gentle mixing. Oxidative stress was induced by $CuSO_4$ and H_2O_2. AEF were in a concentration of 2.5 µg/ml. Dityrosine concentration was determined by measurement of fluorescence (Ex, 325 nm; Em, 405 nm).

acid-reactive substances assay was used to measure formation of lipid peroxides in rat brain cortex homogenate, as a lipid-rich structure. Incubation of rat brain homogenate in the presence of Fe/Asc evoked a rapid increase in the level of lipid peroxidation (Fig. 3). AEF-2 and -4 used at a concentration of 25 µg/ml significantly reduced the level of Fe/Asc-evoked lipid peroxidation by ca. 20%. Other tested AEF had no effect on the level of TBARS (Fig. 3). In addition, AEF-5 reduced the level of Fe/Asc-induced protein oxidation by ca. 76%, and AEF-4 showed a strong tendency, leading to an approximately 52% decrease (Fig. 4). Therefore, these data indicate that selected alkaloids contributed significantly to the inhibition of lipid and protein oxidation.

Discussion

Oxidative stress is an extensive cellular process responsible for unspecific modification of macromolecules leading to impairment of major metabolic pathways [41]. Approaches to prevent oxidative damage usually involve enhancing antioxidant defence with nutritional supplements or vitamins. Although various antioxidative compounds have been tested in clinical studies, there is still a need for effective therapies against oxidative stress. The growing body of evidence approves the importance of natural products as lead compounds in drug discovery.

Pharmacological properties of alkaloids isolated from club moss have been described previously [6]. Cytoprotective properties of club moss extracts were suggested in neurodegenerative processes via their antioxidant and anti-inflammatory properties. Moreover, it was indicated that alkaloid extracts from *Lycopodium* species inhibited acetylcholinesterase (AChE) activity in rat brain [28]. HupA is reported to increase efficiency of learning and memory in animals, and it was shown to be a promising treatment of Alzheimer's disease. About 201 *Lycopodium* alkaloids from 54 species of *L. sensu lato* (including the genera *Huperzia* and *Diphasiastrum*) have been reported so far [30]. In the present study it was demonstrated that selected alkaloid fractions from *Huperzia selago* possess some antioxidative potential. AEF-2, -4 and -5 seem to be the most promising sources of antioxidative compounds.

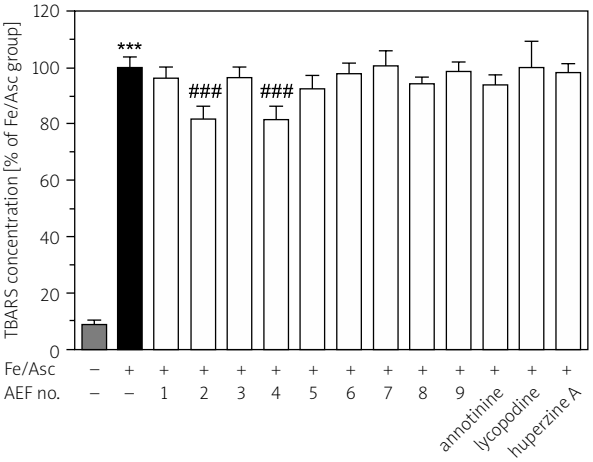

Fig. 3. The effect of alkaloid fractions (AEF) on lipid peroxidation in rat brain homogenate. The homogenate was incubated for 15 min at 37°C in the presence of $FeCl_2$ (25 µM), ascorbic acid (10 µM) and the tested alkaloids at a concentration of 25 µg/ml. Lipid peroxidation was determined by measuring thiobarbituric acid reactive substances (TBARS). All values are the means ± SEM from 4-5 experiments carried out in triplicate. Statistical significance $^{***}p < 0.001$, compared to untreated control. $^{###}p < 0.001$, compared to the Fe/Asc-treated group.

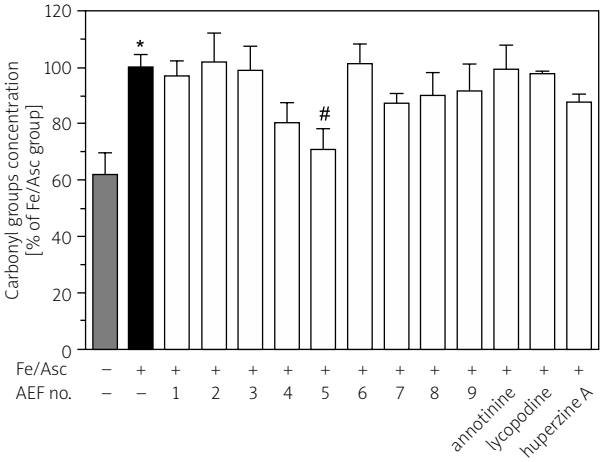

Fig. 4. The effect of alkaloid fractions (AEF) on protein oxidation in rat brain homogenate. The homogenate was incubated for 15 min at 37°C in the presence of $FeCl_2$ (25 µM), ascorbic acid (10 µM) and the tested AEF at a concentration of 25 µg/ml. The level of carbonyl groups was determined as described in Material and Methods. All values are the means ± SEM from 3-4 experiments carried out in triplicate. Statistical significance: $^{*}p < 0.05$, compared to the untreated control. $^{\#}p < 0.05$, compared to the Fe/Asc-treated group.

AEF-2 potently reduced the level of lipid peroxidation, but had no effect on the level of carbonyl groups and on dityrosine formation. AEF-2 very efficiently scavenged DPPH radicals in a concentration ≥ 1.25 µg/ml. The identified components of this fraction were huperzine B, des-*N*-methyl-β-obscurine, lycodine, lycopodine, fawcettidine, lycoposerramine-L or lycoposerramine-M and acrifoline (Table I). AEF-4 at a concentration of 25 µg/ml effectively reduced the level of lipid peroxidation and showed some tendency to reduce the level of carbonyl groups. It scavenged DPPH radicals at concentrations ≥ 2.5 µg/ml and significantly inhibited the rate of dityrosine formation. The identified components of this fraction were 6-β-hydroxyhuperzine, huperzine A, huperzine B, lycoposerramine-L or lycoposerramine-M, lycopodine, lycoposerramine-G, probably 8b-hydroxylycoposerramine K and lyconadin (Table I). AEF-5 significantly reduced the level of carbonyl groups and scavenged DPPH radicals at concentration ≥ 5 µg/ml. It also reduced the rate of dityrosine formation. The identified components of this fraction were lycopodine, serratidine, lycoposerramine-G and probably cermizine B (Table I).

Our study demonstrated that fractions AEF-2, -4 and -5 contain alkaloids which may possess potent and direct antioxidative activity. Analysis of components of tested fractions (Table I) revealed that lycodine, lycoposerramine-G, 8b-hydroxylycoposerramine K and cermizine B are exclusively present in AEF-2, -4 and -5, but not in other fractions; thus they might be responsible for the antioxidative properties of these fractions. Antioxidative potential of these compounds has not been studied before. Our data indicated that direct scavenging of free radicals may be a major way of antioxidative actions of AEF-2, -4 and -5, although some indirect effects cannot be excluded. Additional studies are necessary to reveal which components are responsible for antioxidative properties of the selected fractions, and to determine the exact mechanism of their antioxidative activity. It was previously suggested that HupA possesses potent antiapoptotic, neuroprotective and antioxidative properties [34,43,51,52,56]. Our study demonstrated that this alkaloid is not a direct scavenger of free radicals, and other mechanisms are responsible for its antioxidative potential. Further studies should reveal whether protection of mitochondrial function, stimulation of antioxidative enzymes or non-enzymatic defence may also be involved in antioxidative action of HupA as well as of AEF-2, -4 and -5.

Our results indicated for the first time that alkaloid extracts from *H. selago* possess antioxidative properties, scavenge free radicals and prevent lipid and protein oxidation, presenting the desired mechanism of action in neurodegenerative disorders. Therefore, we suggest that these alkaloids might be a promising source of lead compounds for drug discovery in the therapies for Alzheimer's and Parkinson's diseases and related processes. However, detailed investigation *in vitro* and *in vivo*, including identification of the most effective alkaloids, their mechanisms of action and possible interactions, is necessary.

Acknowledgments

The authors thank Ms Magdalena Piwowarczyk for technical assistance. This study was supported by the statutory budget of the Mossakowski Medical Research Centre, Polish Academy of Sciences (Theme No. 17) and by a grant from the Polish Ministry of Science and Higher Education, grant no. NN 405 362237.

Disclosure

Authors report no conflict of interest.

References

1. Armstrong RA. What causes Alzheimer's disease? Folia Neuropathol 2013; 51: 169-188.
2. Asakawa T, Matsushita S. Coloring conditions of thiobarbituric acid test for detecting lipid hydroperoxides. Lipids 1980; 15: 137-140.
3. Ayer WA, Kasitu GC. Some new Lycopodium alkaloids. Can J Chem-Rev Can Chim 1989; 67: 1077-1086.
4. Ayer WA, Trifonow LS. Lycopodium alkaloids. Academic Press, San Diego 1994.
5. Ayer WA, Browne LM, Orszanska H, Valenta Z, Liu JS. Alkaloids of *Lycopodium selago*: on the identity of selagine with huperzine a and the structure of a related alkaloid. Can J Chemistry 1989; 67: 1538-1540.
6. Banerjee J, Biswas S, Madhu NR, Karmakar SR, Biswas SJ. A better understanding of pharmacological activities and uses of phytochemicals of *Lycopodium clavatum*: a review. J Pharmacogn Phytochem 2014; 3: 207-210.
7. Bastos DHM, Saldanha LA, Catharino RR, Sawaya ACHF, Cunha IBS, Carvalho PO, Eberlin MN. Phenolic antioxidants identifled by ESI-MS from Yerba maté (*Ilex paraguariensis*) and green tea (Camelia sinensis) extracts. Molecules 2007; 12: 423-432.
8. Bishayee K, Chakraborty D, Ghosh S, Boujedaini N, Khuda-Bukhsh AR. Lycopodine triggers apoptosis by modulating 5-lipoxygenase, and depolarizing mitochondrial membrane poten-

tial in androgen sensitive and refractory prostate cancer cells without modulating p53 activity: Signaling cascade and drug-DNA interaction. Eur J Pharmacol 2013; 698: 110-121.
9. Blois MS. Antioxidant determinations by the use of a stable free radical. Nature 1958; 181: 1199-1200.
10. Brown DR. Neurodegeneration and oxidative stress: Prion disease results from loss of antioxidant defence. Folia Neuropathol 2005; 43: 229-243.
11. Chen CYO, Ribaya-Mercado JD, McKay DL, Croom E, Blumberg JB. Differential antioxidant and quinone reductase inducing activity of American, Asian, and Siberian ginseng. Food Chemistry 2010; 119: 445-451.
12. Czapski GA, Czubowicz K, Strosznajder RP. Evaluation of the antioxidative properties of lipoxygenase inhibitors. Pharmacol Rep 2012; 64: 1179-1188.
13. Czapski GA, Avram D, Sakharov DV, Wirtz KWA, Strosznajder JB, Pap EHW. Activated neutrophils oxidize extracellular proteins of endothelial cells in culture: Effect of nitric oxide donors. Biochem J 2002; 365: 897-902.
14. Czubowicz K, Czapski GA, Cieslik M, Strosznajder RP. Lipoxygenase inhibitors protect brain cortex macromolecules against oxidation evoked by nitrosative stress. Folia Neuropathol 2010; 48: 283-292.
15. Farhoosh R, Golmovahhed GA, Khodaparast MHH. Antioxidant activity of various extracts of old tea leaves and black tea wastes (*Camellia sinensis* L.). Food Chemistry 2007; 100: 231-236.
16. Ferdinandy P, Schulz R. Inhibition of peroxynitrite-induced dityrosine formation with oxidized and reduced thiols, nitric oxide donors, and purine derivatives. Antioxid Redox Signal 2001; 3: 165-171.
17. Friedman J. Why is the nervous system vulnerable to oxidative stress? In: Gadoth N, Göbel HH (eds.). Oxidative stress and free radical damage in neurology. Springer Science+Business Media, New York 2011; p. 19-27.
18. Galasko DR, Peskind E, Clark CM, Quinn JF, Ringman JM, Jicha GA, Cotman C, Cottrell B, Montine TJ, Thomas RG, Aisen P; Alzheimer's Disease Cooperative Study. Antioxidants for Alzheimer disease: a randomized clinical trial with cerebrospinal fluid biomarker measures. Arch Neurol 2012; 69: 836-841.
19. Gerard RV, Maclean DB. GC/MS examination of four Lycopodium species for alkaloid content. Phytochemistry 1986; 25: 1143-1150.
20. Halldorsdottir ES, Jaroszewski JW, Olafsdottir ES. Acetylcholinesterase inhibitory activity of lycopodane-type alkaloids from the Icelandic *Lycopodium annotinum* ssp. *alpestre*. Phytochemistry 2010; 71: 149-157.
21. Halldorsdottir ES, Palmadottir RH, Nyberg NT, Olafsdottir ES. Phytochemical analysis of alkaloids from the Icelandic club moss *Diphasiastrum alpinum*. Phytochem Lett 2013; 6: 355-359.
22. Hatcher H, Planalp R, Cho J, Torti FM, Torti SV. Curcumin: From ancient medicine to current clinical trials. Cellular and molecular life sciences. CMLS 2008; 65: 1631-1652.
23. Hirasawa Y, Morita H, Kobayashi J. Nankakurine A, a novel C16N2-type alkaloid from *Lycopodium hamiltonii*. Org Lett 2004; 6: 3389-3391.
24. Ishiuchi K, Park JJ, Long RM, Gang DR. Production of huperzine a and other Lycopodium alkaloids in *Huperzia* species grown under controlled conditions and in vitro. Phytochemistry 2013; 91: 208-219.
25. Ishiuchi K, Kubota T, Ishiyama H, Hayashi S, Shibata T, Mori K, et al. Lyconadins D and E, and complanadine E, new Lycopodium alkaloids from *Lycopodium complanatum*. Bioorg Med Chem 2011; 19: 749-753.
26. Jung CH, Seog HM, Choi IW, Choi HD, Cho HY. Effects of wild ginseng (Panax ginseng C.A. Meyer) leaves on lipid peroxidation levels and antioxidant enzyme activities in streptozotocin diabetic rats. J Ethnopharmacol 2005; 98: 245-250.
27. Kobayashi J, Hirasawa Y, Yoshida N, Morita H. Lyconadin A, a novel alkaloid from *Lycopodium complanatum*. J Org Chem 2001; 66: 5901-5904.
28. Konrath EL, Neves BM, Lunardi PS, Passos Cdos S, Simões-Pires A, Ortega MG, Gonçalves CA, Cabrera JL, Moreira JC, Henriques AT. Investigation of the in vitro and ex vivo acetylcholinesterase and antioxidant activities of traditionally used Lycopodium species from South America on alkaloid extracts. J Ethnopharmacol 2012; 139: 58-67.
29. Li H, Wang X, Lei X. Total syntheses of Lycopodium alkaloids (+)-fawcettimine, (+)-fawcettidine, and (–)-8-deoxyserratinine. Angew Chem Int Ed Engl 2012; 51: 491-495.
30. Ma X, Gang DR. The Lycopodium alkaloids. Nat Prod Rep 2004; 21: 752-772.
31. Ma X, Gang DR. In vitro production of huperzine A, a promising drug candidate for Alzheimer's disease. Phytochemistry 2008; 69: 2022-2028.
32. Ma X, Tan C, Zhu D, Gang DR, Xiao P. Huperzine A from Huperzia species – an ethnopharmacolgical review. J Ethnopharmacol 2007; 113: 15-34.
33. Morita H, Hirasawa Y, Shinzato T, Kobayashi J. New phlegmarane-type, cernuane-type, and quinolizidine alkaloids from two species of Lycopodium. Tetrahedron 2004; 60: 7015-7023.
34. Ning N, Hu JF, Yuan YH, Zhang XY, Dai JG, Chen NH. Huperzine A derivative M3 protects PC12 cells against sodium nitroprusside-induced apoptosis. Acta Pharmacol Sin 2012; 33: 34-40.
35. Oliver CN, Ahn BW, Moerman EJ, Goldstein S, Stadtman ER. Age-related-changes in oxidized proteins. J Biol Chem 1987; 262: 5488-5491.
36. Pan G, Williams RM. Unified total syntheses of fawcettimine class alkaloids: fawcettimine, fawcettidine, lycoflexine, and lycoposerramine B. J Org Chem 2012; 77: 4801-4811.
37. Park JH, Kim RY, Park E. Antioxidant and alpha-glucosidase inhibitory activities of different solvent extracts of skullcap (*Scutellaria baicalensis*). Food Sci Biotechnol 2011; 20: 1107-1112.
38. Peng-Fei L, Fu-Gen H, Bin-Bin D, Tian-Sheng D, Xiang-Lin H, Ming-Qin Z. Purification and antioxidant activities of baicalin isolated from the root of huangqin (*Scutellaria baicalensis gcorsi*). J Food Sci Tech 2013; 50: 615-619.
39. Piotrowski P, Wierzbicka K, Smialek M. Neuronal death in the rat hippocampus in experimental diabetes and cerebral ischaemia treated with antioxidants. Folia Neuropathol 2001; 39: 147-154.

40. Pocernich CB, Butterfield DA. Elevation of glutathione as a therapeutic strategy in Alzheimer disease. Biochim Biophys Acta 2012; 1822: 625-630.
41. Pradeep H, Diya JB, Shashikumar S, Rajanikant GK. Oxidative stress – assassin behind the ischemic stroke. Folia Neuropathol 2012; 50: 219-230.
42. Ronowicz J, Kupcewicz B, Budzisz E. Chemometric analysis of antioxidant properties of herbal products containing *Ginkgo biloba* extract. Cent Eur J Biol 2013; 8: 374-385.
43. Shi Q, Fu J, Ge D, He Y, Ran J, Liu Z, Wei J, Diao T, Lu Y. Huperzine A ameliorates cognitive deficits and oxidative stress in the hippocampus of rats exposed to acute hypobaric hypoxia. Neurochem Res 2012; 37: 2042-2052.
44. Singh G, Kapoor IPS, Singh P, de Heluani CS, de Lampasona MP, Catalan CAN. Comparative study of chemical composition and antioxidant activity of fresh and dry rhizomes of turmeric (*Curcuma longa* Linn.). Food Chem Toxicol 2010; 48: 1026-1031.
45. Staerk D, Larsen J, Larsen LA, Olafsdottir ES, Witt M, Jaroszewski JW. Selagoline, a new alkaloid from *Huperzia selago*. Nat Prod Res 2004; 18: 197-203.
46. Szypula W, Pietrosiuk A, Suchocki P, Olszowska O, Furmanowa M, Kazimierska O. Somatic embryogenesis and in vitro culture of *Huperzia selago* shoots as a potential source of huperzine A. Plant Sci 2005; 168: 1443-1452.
47. Szypula WJ, Mistrzak P, Olszowska O. A new and fast method to obtain in vitro cultures of *Huperzia selago* (Huperziaceae) sporophytes, a club moss which is a source of huperzine A. Acta Soc Bot Pol 2013; 82: 313-320.
48. Szypula WJ, Kiss AK, Pietrosiuk A, Swist M, Danikiewicz W, Olszowska O. Determination of huperzine A in *Huperzia selago* plants from wild population and obtained in in vitro culture by high-performance liquid chromatography using a chaotropic mobile phase. Acta Chromatogr 2011; 23: 339-352.
49. Takayama H, Katakawa K, Kitajima M, Yamaguchi K, Aimi N. Ten new Lycopodium alkaloids having the lycopodane skeleton isolated from *Lycopodium serratum* Thunb. Chem Pharm Bull 2003; 51: 1163-1169.
50. Vellas B, Coley N, Ousset PJ, Berrut G, Dartigues JF, Dubois B, Grandjean H, Pasquier F, Piette F, Robert P, Touchon J, Garnier P, Mathiex-Fortunet H, Andrieu S; GuidAge Study Group. Long-term use of standardised *Ginkgo biloba* extract for the prevention of Alzheimer's disease (GuidAge): a randomised placebo-controlled trial. Lancet Neurol 2012; 11: 851-859.
51. Wang LM, Han YF, Tang XC. Huperzine A improves cognitive deficits caused by chronic cerebral hypoperfusion in rats. Eur J Pharmacol 2000; 398: 65-72.
52. Wang R, Zhang HY, Tang XC. Huperzine A attenuates cognitive dysfunction and neuronal degeneration caused by beta-amyloid protein-(1-40) in rat. Eur J Pharmacol 2001; 421: 149-156.
53. Wang XJ, Li L, Yu SS, Ma SG, Qu J, Liu YB, Li Y, Wang Y, Tang W. Five new fawcettimine-related alkaloids from Lycopodium japonicum Thunb. Fitoterapia 2013; 91: 74-81.
54. Wiedenfeld H, Pietrosiuk A, Furmanowa M, Roeder E. Pyrrolizidine alkaloids from *Lithospermum canescens* Lehm. Z Naturforsch C 2003; 58: 173-176.
55. Wu QQ, Gu YH. Quantification of huperzine A in *Huperzia serrata* by HPLC-UV and identification of the major constituents in its alkaloid extracts by HPLC-DAD-MS-MS. J Pharm Biomed Anal 2006; 40: 993-998.
56. Xiao XQ, Wang R, Tang XC. Huperzine A and tacrine attenuate beta-amyloid peptide-induced oxidative injury. J Neurosci Res 2000; 61: 564-569.
57. Yang G, Wang Y, Tian J, Liu JP. Huperzine A for Alzheimer's disease: a systematic review and meta-analysis of randomized clinical trials. PloS one 2013; 8: e74916.
58. Yuan C, Chang CT, Axelrod A, Siegel D. Synthesis of (+)-complanadine A, an inducer of neurotrophic factor excretion. J Am Chem Soc 2010; 132: 5924-5925.
59. Zandi PP, Anthony JC, Khachaturian AS, Stone SV, Gustafson D, Tschanz JT, et al. Reduced risk of Alzheimer disease in users of antioxidant vitamin supplements: the Cache County Study. Arch Neurol 2004; 61: 82-88.
60. Zhang HY, Tang XC. Neuroprotective effects of huperzine A: new therapeutic targets for neurodegenerative disease. Trends Pharmacol Sci 2006; 27: 619-625.

Original article

Folia Neuropathologica

Non-woven nanofiber mats – a new perspective for experimental studies of the central nervous system?

Janina Rafalowska[1], Dorota Sulejczak[2], Stanisław J. Chrapusta[2], Roman Gadamski[1], Anna Taraszewska[1], Paweł Nakielski[3], Tomasz Kowalczyk[4], Dorota Dziewulska[1,5]

[1]Department of Experimental and Clinical Neuropathology, Mossakowski Medical Research Centre, Polish Academy of Sciences, Warsaw, [2]Department of Experimental Pharmacology, Mossakowski Medical Research Centre, Polish Academy of Sciences, Warsaw, [3]Department of Mechanics and Physics of Fluids, Institute of Fundamental Technological Research, Polish Academy of Sciences, Warsaw, [4]Department of Theory of Continuous Media, Institute of Fundamental Technological Research, Polish Academy of Sciences, Warsaw, [5]Department of Neurology, Medical University of Warsaw, Poland

Folia Neuropathol 2014; 52 (4): 407-416 DOI: 10.5114/fn.2014.47841

Abstract

(Sub)chronic local drug application is clearly superior to systemic administration, but may be associated with substantial obstacles, particularly regarding the applications to highly sensitive central nervous system (CNS) structures that are shielded from the outer environment by the blood-brain barrier. Violation of the integrity of the barrier and CNS tissues by a permanently implanted probe or cannula meant for prolonged administration of drugs into specific CNS structures can be a severe confounding factor because of the resulting inflammatory reactions. In this study, we tested the utility of a novel way for (sub)chronic local delivery of highly active (i.e., used in very low amounts) drugs to the rat spinal cord employing a non-woven nanofiber mat dressing. To this end, we compared the morphology and motoneuron ($\alpha + \gamma$) counts in spinal cord cervical and lumbar segments between rats with glutamate-loaded nanofiber mats applied to the lumbar enlargement and rats with analogical implants carrying no glutamate. Half of the rats with glutamate-loaded implants were given daily valproate treatment to test its potential for counteracting the detrimental effects of glutamate excess. The mats were prepared in-house by electrospinning of an emulsion made of a solution of the biocompatible and biodegradable poly(L-lactide-co-caprolactone) polymer in a mixture of organic solvents, an aqueous phase with or without monosodium glutamate, and sodium dodecyl sulfate as an emulsifier; the final glutamate content was 1.4 µg/mg of the mat. Three weeks after mat implantation there was no inflammation or considerable damage of the spinal cord motoneuron population in the rats with the subarachnoid dressing of a glutamate-free mat, whereas the spinal cords of the rats with glutamate-loaded nanofiber mats showed clear symptoms of excitotoxic damage and a substantial increase in dying/damaged motoneuron numbers in both segments studied. The rats given systemic valproate treatment showed significantly lower percentages of damaged/dying motoneurons in their lumbar enlargements. These results demonstrate the capacity of nanofiber mats for generation of neurotoxic glutamate in the rat CNS. However, the tested nanofiber mats need further improvements aimed at extending the period of effective drug release and rendering the release more steady.

Key words: *CNS injury, electrospinning, excitotoxicity, glutamate, motoneuron, nanofibers, neurodegeneration, spinal cord, valproate.*

Communicating author:

Dorota Sulejczak, Department of Experimental Pharmacology, Mossakowski Medical Research Centre, Polish Academy of Sciences, 5 Pawińskiego St., 02-106 Warsaw, Poland, phone: +48 22 608 65 23, fax: +48 22 668 65 27, e-mail: dsulejczak@imdik.pan.pl

Introduction

Targeted administration of active substances has clear advantages over systemic application. However, it may be associated with considerable obstacles in some cases, particularly regarding the chronic administration of drugs meant to affect specific central nervous system (CNS) structures that are shielded from the outer environment by the blood-brain barrier [10,13]. In most cases it is necessary to mechanically disturb the integrity of the meninges and the barrier. Such interventions additionally carry a risk of CNS tissues being damaged by the permanently implanted probe or cannula, which may be a severe confounding factor due to the consequential inflammatory reaction. This is why there is an ongoing search for alternative ways for delivering medicines to the CNS that lessen the risk of such complications [6,12,13,15].

In the case of drugs that are used in small (in mass and volume) quantities, an ideal solution would be to employ a carrier that: 1) is small enough to pose no problems at its implantation, and 2) degrades gradually to harmless metabolites over time, e.g., see [9], simultaneously releasing its active load at a rate necessary to create an effective concentration of the active principle. An effective solution of this problem may be in the use of nanomaterials, and particularly those made of electrospun fibers prepared from biocompatible/biodegradable polymers that have already been accepted for medical use.

Electrospinning is a process of forming nanofibers by interaction of a viscoelastic liquid stream (e.g., a polymer solution or melt, an emulsion, or other liquid-liquid systems) with a strong electric field. Such nanofibers have a thickness of several tens of nm to several μm and can be easily made into non-woven mats that can be used as drug carriers; for a review see [23].

The aim of this study was to test the utility of a novel way for (sub)chronic local delivery of active substances to the CNS with the use of such mats. To avoid instant discharge of the entire drug load and ensure long-term action of such a drug delivery system, the drug must be somehow enclosed within the nanofiber structural material. In the case of substances that cannot be dissolved in the latter, the nanofibers can be formed by emulsion electrospinning, with the drug being a component of the aqueous phase, or by coaxial electrospinning (core-shell system) [23]. A considerable potential for such applications is shown by nanofibers made of polycarbonates or aliphatic polyesters, which degrade *in vivo* relatively slowly (over many weeks, see [9]) by non-enzymatic random hydrolytic scission of esters linkage, to form small molecules identical to or homologous with endogenous metabolites or their analogs; the process is slow enough to cause no inflammation. Nanofibers made of these polymers can also aid appropriate healing of possible CNS trauma [1,24], which is likely due to their forming a temporary biocompatible scaffold for the cells taking part in this process [5].

To test the capacity of such material for effective delivery of an active substance *in vivo*, we chose mats carrying glutamate. As evidenced by many animal studies and clinical and post-mortem observations in humans, excessive glutamate accumulation in the interstitial space plays an important role in pathogenesis of many CNS disorders by causing injury and death of cells, and particularly of motoneurons, in both the brain and the spinal cord [14,22].

In the last decade, much attention was paid to the function of the excitatory amino acid receptors and their role in excitotoxicity, e.g., see [4,8,16,26]. Many of those experiments were performed with the use of microdialysis, which involves placement of the microdialysis probe (i.e., of a "foreign body") within the CNS, and the consequential nervous tissue damage and the emergence of (pro)inflammatory cytokines and other potentially harmful reactions. Establishing precisely the relationship between the effects of various noxious/pathogenic factors in such an experimental setup may be difficult or not feasible.

Neurotoxicity of exogenous and endogenous glutamate manifests itself, *inter alia*, in morphological changes occurring both in the cytoplasm and in the cell nucleus. Nuclear chromatin structure is mostly determined by the interaction of DNA with basic proteins – histones [21]. Increased histone deacetylase (HDAC) activity leads to condensation of the chromatin and silencing of gene expression, whereas inhibition of this activity causes rarefaction of chromatin and facilitates interaction between transcription factors and gene promoters, resulting in enhanced gene expression [7,28]. Perturbations of the acetylation/deacetylation balance can result in pathology and were found in various neurological disorders as well as in brain ischemia, in which HDAC inhibition usually plays an anti-inflammatory, neuroprotec-

tive and neurotrophic role [3,11,17,28]. Among many HDAC inhibitors, valproic acid [21] and its derivatives are widely used. Beside its utility in the treatment of bipolar disorders, epilepsy and migraine, it is also employed in a variety of acute CNS injuries [2]. Valproic acid was found to increase the expression of the survival motor neuron (SMN) protein in fibroblasts from patients with spinal muscular atrophy [25]. It also improves memory and inhibits neuritic plaque formation in a mouse model of Alzheimer disease [19]. Hence, in this study, we decided to test also the possibility of attenuating, with systemic valproate treatment, the pathomorphological changes evoked in the rat spinal cord by the glutamate released from the locally applied nanofiber mat.

Material and methods

Reagents for nanofiber mat production and analysis

Poly(L-lactide-*co*-caprolactone) Purasorb PLC 7015 (PLCL) containing 70% L-lactide and 30% caprolactone units was bought from Corbion Purac (Gorinchem, The Netherlands). Monosodium glutamate, *o*-phthalaldehyde and 2-mercaptoethanol were purchased from Sigma-Aldrich, and sodium dodecyl sulfate, chloroform, dimethylformamide, boric acid and sodium hydroxide were obtained from POCh S.A. (presently Avantor Performance Materials Poland S.A., Gliwice, Poland). All the chemicals were used without further purification.

Nanofiber mat preparation and characterization

Non-woven nanofiber mats were prepared by emulsion electrospinning, using a custom-made system as described elsewhere [18,23]. The emulsion was prepared as follows: 40 mg of sodium dodecyl sulfate was mixed with 1 g of 9% (w/w) solution of PLCL in a chloroform-dimethylformamide mixture (16 : 1, w/w). Fifty mg of 5% (w/w) monosodium glutamate solution in deionized water was added dropwise, with 30-s vortexing intervals, to the polymer/sodium dodecyl sulfate mixture. Next, the entire mixture was vortexed vigorously for 15 min in a tightly closed tube. Electrospinning was performed in a polycarbonate chamber of about 1 m^3 volume that shielded the working personnel from the high voltage employed and the final product from contamination with dust. The electrospinning setup was as follows: spinneret nozzle (made of 26G needle) to collector distance 15 cm, voltage 20 kV, and the emulsion flow of 0.2 ml/h. The forming nanofibers were collected on a rotating (1800 rpm) polypropylene cylinder (15 mm diameter) covered with grounded aluminum foil, to form a non-woven mat. The "empty" (glutamate-free) nanofiber mat was prepared by the same method except that the emulsion was devoid of glutamate. The mats were left on the collector for 24 h to release internal tension and avoid mat shrinkage, and then were removed from the collector together with the underlying aluminum foil and cut to the needed size with a fresh disposable surgical blade.

The morphology of the glutamate-loaded nanofiber mat was examined by scanning electron microscopy, using a model JSM 6390 LV microscope (Jeol, Japan). For the analysis, the mat was sputtered with gold using a model SC7620 Polaron mini sputter coater (Quorum Technologies Ltd., Ashford, UK). The analysis showed a network of partially adhering fibers of average diameter of 549 ± 206 nm (mean ± SD); see Fig. 1.

The capacity of the mat for gradual release of monosodium glutamate was evaluated *in vitro* as follows: a single sample of the mat (11 mg, about 11 mm × 11 mm) was placed in an Eppendorf tube with 1 ml of phosphate-buffered (10 mM, pH 7.4) 0.9% (w/v) solution of NaCl in deionized water (PBS), capped and incubated at 37°C. The incubation medium was sampled and replaced with fresh PBS at predetermined time intervals. The used medium

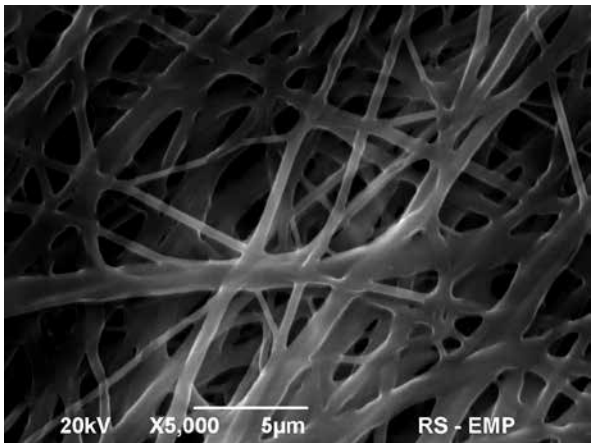

Fig. 1. Scanning electron microscope micrograph of the monosodium glutamate-containing PLCL nanofiber mat prepared by emulsion electrospinning.

samples were kept frozen at –20°C until analyzed. The concentration of glutamate in the samples was assessed after its conversion into a fluorescent derivative as described by Roth [20], with minor modifications. Briefly, the assay was performed in 96-well plates, using the reagent made by mixing 0.05 M borate buffer solution with ethanolic *o*-phthalaldehyde (10 mg/ml) and 2-mercaptoethanol solutions (5 µl/ml) 60 : 1 : 1 (v/v/v). Seventy-five µl aliquots (6 each) of fresh incubation medium (blank samples), used incubation medium samples and monosodium glutamate dilutions in PBS (standard samples) were pipetted into separate wells. Next, 75 µl of the borate buffer-mercaptoethanol-*o*-phthalaldehyde reagent mixture was added to each well and all samples were mixed immediately. Fluorescence intensity was measured within the next 5 min, using a model Fluoroskan Ascent spectrofluorimeter (Thermo Scientific, Rockford, IL, USA), with monochromators set at 355 nm (excitation) and 460 nm (emission measurement). The analysis (data not shown) revealed that the mat released about 0.8 µg of monosodium glutamate per mg of the mat during the first week; about 50% of this amount was released within the first few hours. After two weeks, the total amount released was 1.2 µg of the drug per mg of the mat (i.e., 8.4% of the initial content), and the estimated total amount released during 3 weeks (the planned duration of the *in vivo* rat experiment) was 1.7 µg per mg of the mat (12% of the initial content).

Animals and experimental design

Twelve adult male Wistar rats from the stock of the Mossakowski Medical Research Centre, Warsaw, Poland, initial body weight 250-300 g, were used for the study. The rats were housed three per opaque plastic cage (55 cm × 33 cm floor size) in an air-conditioned environment (21 ± 2°C, 60-70% relative humidity) under a 12 h light/12 h dark day cycle (lights on at 7 a.m.), with free access to standard laboratory rodent chow and tap water. The rats were randomly divided between four experimental groups: 1) intact rats (group I, $n = 3$); 2) rats subjected to surgical placement of a drug-free nanofiber mat into the spinal cord subarachnoid space at the lumbar level (group II, $n = 3$); 3) rats subjected to surgical placement of a monosodium glutamate-containing nanofiber mat into the spinal cord subarachnoid space at the lumbar level (group III, $n = 3$); and 4) rats subjected to surgical placement of a glutamate-loaded mat into the spinal cord subarachnoid space at the lumbar level and additionally given daily one dose of sodium valproate (Convulex syrup 50 mg/ml, Gerot Pharmazeutika, Vienna, Austria) by gavage (group IV, $n = 3$), beginning on the day of the surgery. The starting valproate dose was 33.3 mg/kg; the dosage was increased by 8.3 mg/kg each day for 4 consecutive days and then was kept constant for the rest of the study period.

The surgical procedure employed for submeningeal implantation of nanofiber mat pieces (approximately 5 mm × 5 mm size) into rat spinal cords (at the lumbar enlargement level) was as described elsewhere [1]. Three weeks after implantation of nanofiber mats, all rats were anesthetized with a lethal dose of sodium pentobarbital (80 mg/kg, i.p.) and decapitated. Spinal cords were excised and fixed in 4% formaldehyde in PBS and then embedded in paraffin using a standard procedure. All animal use procedures were in strict compliance with the European Union directive on the protection of laboratory animals (86/609/EEC) and with the current laws of Poland. All efforts were made to keep the number of rats used at a minimum and minimize animal discomfort. The experimental protocol has been accepted by the 4th Local Animal Experimentation Ethics Committee at the National Medicines Institute, Warsaw, Poland (Permit No. 43/210).

Histology and immunohistochemistry

The formalin-fixed and paraffin-embedded samples of rat spinal cords were cut transversely into 8 µm-thick sections. After deparaffinization and rehydration in a water-ethanol solution series, part of the sections were stained with violet cresyl using a routine procedure. Their sister slices were incubated with primary antibodies against synaptophysin (Dako Cytomation A/S, Denmark, cat. no. M0776; dilution 1 : 100), or GFAP (Dako cat. no. Z0334; dil. 1 : 2000), or neurofilament (Dako cat. no. M0762; dil. 1 : 100). Next, the samples were incubated with the respective secondary antibody (Beckman Coulter Inc., France, cat. no. IM0816, or IM0830; dil. 1 : 100) and then with streptavidin-horseradish peroxidase solution (Beckman Coulter cat. no. IM0309; dil. 1 : 500). The final immune complexes were visualized by a standard procedure employing diaminobenzidine as the chromogen, counterstained with hematoxylin, and assessed by light microscopy.

Ultrastructural studies

For electron microscopy studies, samples of lumbar spinal cord were taken and immediately fixed in a solution of 2% formaldehyde and 2.5% glutaraldehyde in cacodylate buffer pH 7.4 for 4 h, then they were divided into smaller pieces, rinsed in cacodylate buffer, postfixed in 1.0% OsO_4 for 1 h, dehydrated in a series of ethanol dilutions and embedded in Epon resin. Semi-thin sections stained with 1% toluidine blue were viewed in a light microscope for identification of motoneurons. Ultrathin sections were prepared from selected blocks, counterstained with uranyl acetate and lead citrate and then examined in a model JEOL 1200EX (Jeol, Japan) transmission electron microscope.

Assessment of the extent of damage to spinal cord motoneuron populations

Spinal cord samples used for motoneuron counting were taken from both the cervical enlargement (C4-C8 level) and the lumbar enlargement (L2-L6 level). The samples were fixed in 4% formaldehyde solution pH 7.4, dehydrated in a series of ethanol dilutions, embedded in paraffin, cut transversally into 8 µm thickness serial sections, and stained with cresyl violet using the routine procedure. Different sections from the same segment of the spinal cord can contain differing numbers of motoneurons. Therefore, three such sections from each of the two spinal cord segments of each rat, each section covering the whole of both ventral horns of the spinal cord, were used for quantitation. The sections were separated by at least 40 µm (along the spinal cord length) to avoid double counting of the same motoneurons. To facilitate the counting and avoid double counting the same cells, especially the relatively small γ-motoneurons, a 10 mm × 10 mm reticle with 20 divisions along each side was placed in the microscope eyepiece to overlap with the cross-section view of the spinal cord. The counting was performed in three "fields of observation" for each spinal horn (i.e., in six fields/section), and the counts from all six fields were added up for calculation of the percentage of damaged/dying motoneurons in a given rat and spinal cord segment.

Statistical analysis

Data on spinal cord motoneuron numbers were analyzed by repeated measures two-way ANOVA with group (I-IV) as the main factor and spinal cord segment (cervical enlargement and lumbar enlargement) as the repeated measures factor, followed by Fisher's least significant difference test. In all cases, $p < 0.05$ was considered significant.

Results

Spinal cord morphology and immunohistochemistry findings

Spinal cords of intact control rats showed normal morphology, with no detectable astrocytic reaction (Fig. 2). Morphological assessment revealed that implantation of nanofiber mats caused neither spinal cord damage nor inflammation in the rats with the subarachnoid dressing of an "empty" (glutamate-free) nanofiber mat (group II). The surface of their spinal cord motoneurons (both α and γ) showed a rosary-like arrangement of synapses; only a few of the cells showed symptoms of partial tigrolysis.

The rats with the subarachnoid dressing of a glutamate-carrying nanofiber mat (group III) revealed tigrolysis in a considerable fraction of their spinal cord motoneurons, including central tigrolysis in a number of the cells. In these rats, synaptophysin immunostaining showed substantial irregularities in the rosary-like arrangement of synapses on the surface of the cells, including loss of some synapses and only a residual thin band of reactivity in some cases. The astrocytic reaction was very weak, but hypertrophy and clasmatodendrosis were occasionally found. Spinal cord cross-sections also revealed distinct vasodilation, particularly of capillaries and venules, and the presence of subarachnoid hemorrhages as well as ecchymoses within the spinal cord (Fig. 2).

In group IV rats (with glutamate-loaded spinal cord dressing and systemic valproic acid treatment), the morphological changes in the ventral horns closely resembled those seen in the group III rats, except for a diminished number of tigrolytic cells (Fig. 2).

Results of neurofilament immunohistochemistry in rats from all experimental groups were very similar. The only difference was slightly stronger neurofilament immunoreactivity of the spinal cord gray matter due to increased density of immunoreactive neurofilament fibers and/or their more intense immunolabelling in group IV in comparison to group III (Fig. 2).

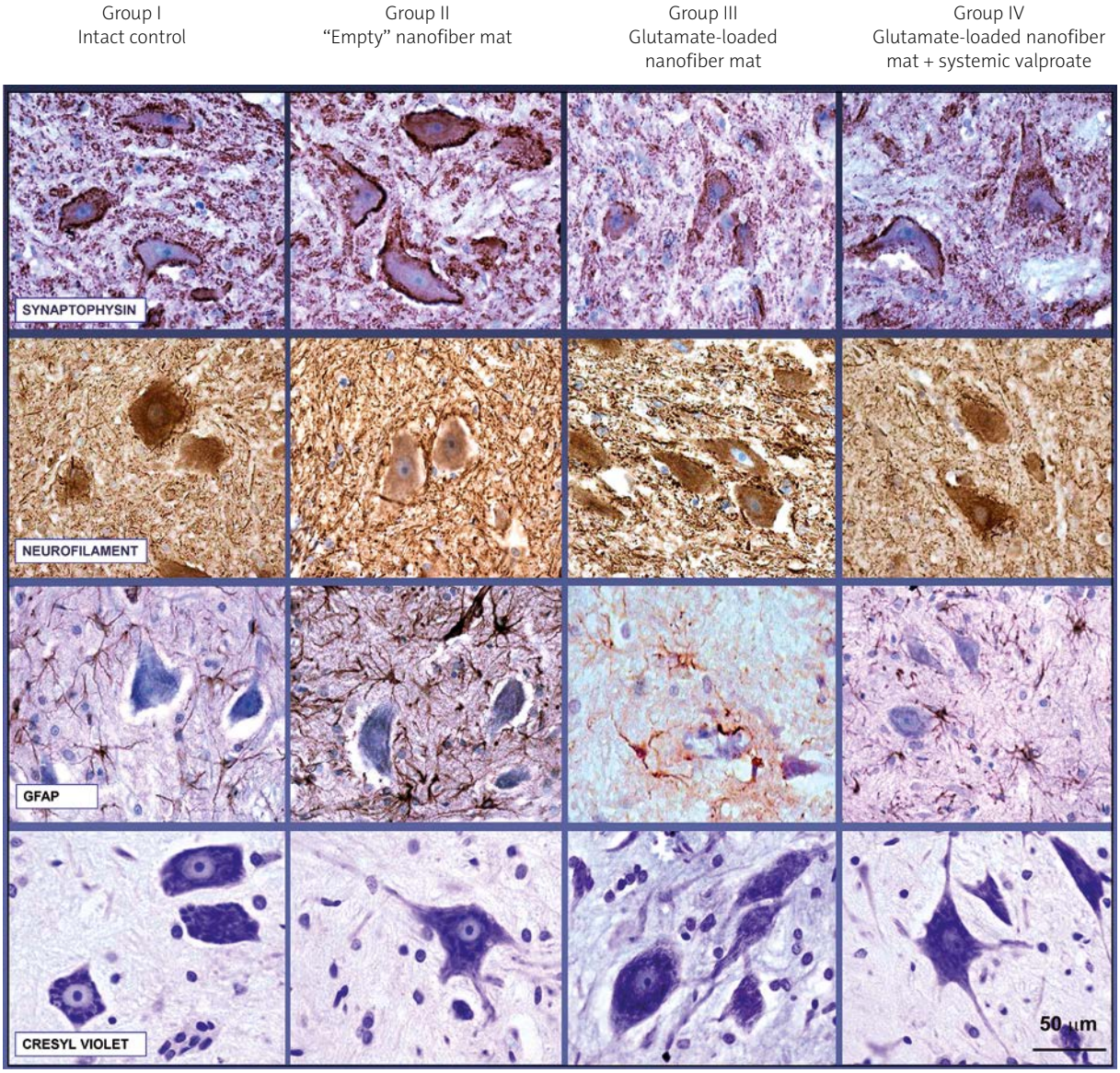

Fig. 2. Representative microphotographs illustrating the results of histological (cresyl violet staining) and immunohistochemical (synaptophysin, neurofilament and GFAP immunoreactivities) examination of spinal cords from all experimental rat groups.

Ultrastructural findings

In the control groups I and II, the motoneurons showed normal ultrastructure of their perikaryal cytoplasm with aggregates of long profiles of rough endoplasmic reticulum and the nucleus rich in hetero- and euchromatin (Fig. 3A). Mitochondria in the perikaryal cytoplasm, dendrites and axons were small and electron-dense. The neuropil showed the presence of numerous synaptic contacts on the neuronal somata and dendrites, and narrow spaces between cellular processes; see Fig. 3B.

In the group III rats, motoneuron perikaryal cytoplasm displayed depletion and dispersion of the rough endoplasmic reticulum (Fig. 3C), increased numbers of small vesicles and cisterns of the Golgi apparatus, and prominent swelling of the mitochondria (Fig. 3D); rarefaction of nuclear chromatin was evident as well. Dendrites were swollen and showed commonly the presence of numerous vesicles and disintegrated organelles; see Figs. 3C-D. Pathological changes (microvacuolization of cytoplasm and mitochondrial swelling) were also found in astrocytes and satellite

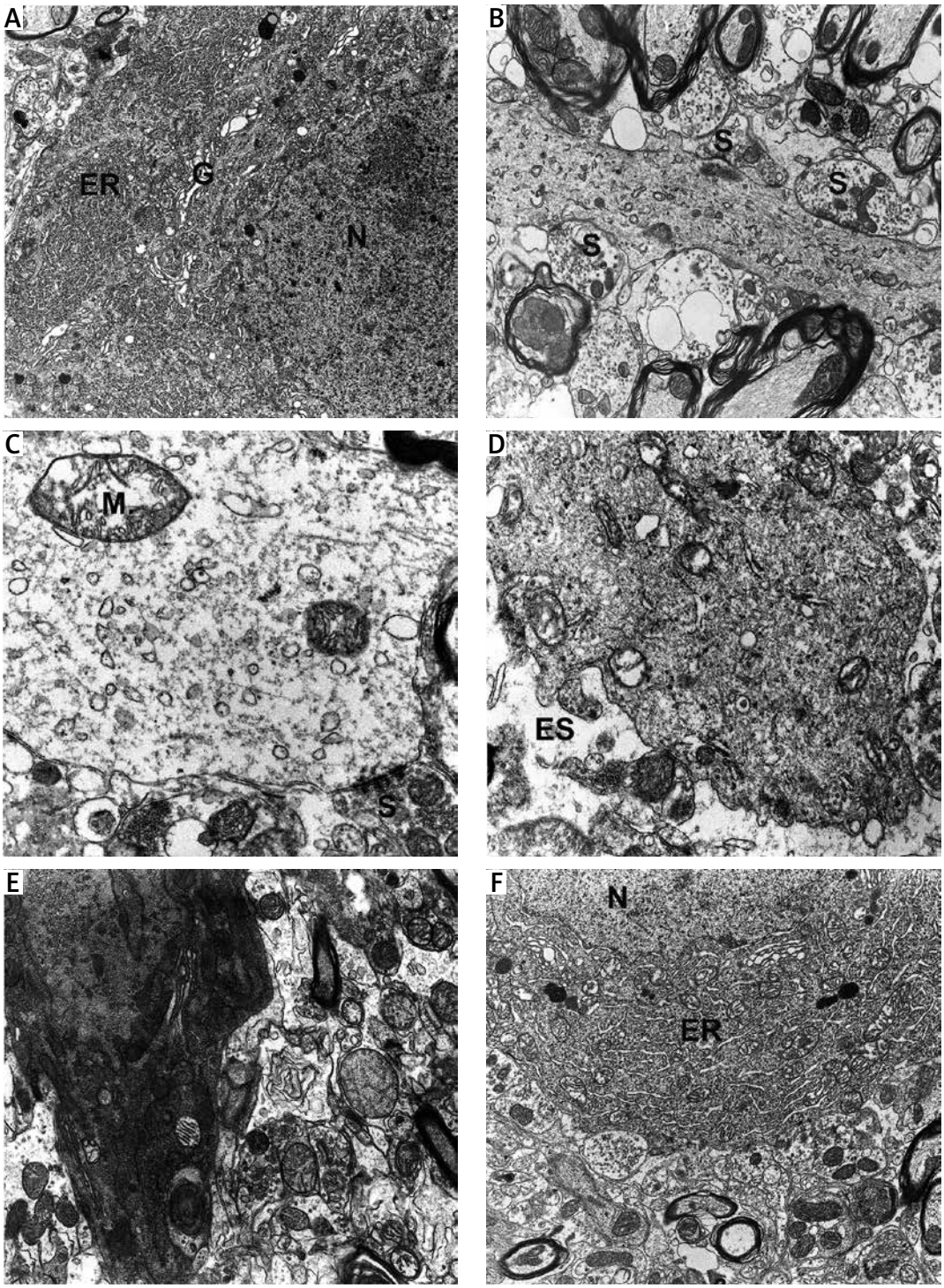

Fig. 3. Representative electronographs showing the ultrastructure of spinal cords from all experimental rat groups. **A-B)** Groups I and II. Note a well-preserved motoneuron cell body (in **A**) and a dendrite (in **B**). ER – endoplasmic reticulum, G – Golgi apparatus, N – nucleus, S – axo-dendritic synapse. Original magnification: × 3000 **(A)**; × 6000 **(B)**. **C-E)** Group III. Note swelling and microvacuolization of the dendrite cytoplasm (in **C** and **D**), and a "dark" motoneuron (in **E**). ES – enlarged extracellular space, M – swollen mitochondrium, S – axo-dendritic synapse. Original magnification: × 10 000 **(C, D)**; × 7500 **(E)**. **F)** Group IV. Motoneuron cell body with normal looking nuclear chromatin (N) and elongated profiles of rough endoplasmic reticulum (ER). Original magnification: × 5000.

oligodendrocytes, and in endothelial cells. The cellular changes were often associated with pericellular edema and loss of the axo-dendritic and axo-somatic synapses (Fig. 3E). Spinal cord motoneurons of group IV rats showed increased density of the nuclear chromatin and striking augmentation of the long profiles of rough endoplasmic reticulum in perikaryal cytoplasm (Fig. 3F).

Transmission electron microscopy also revealed partial degradation of the implanted mats (data not shown).

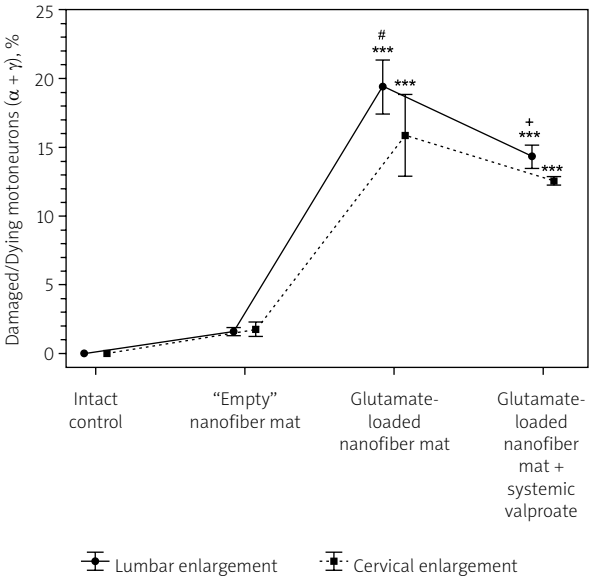

Fig. 4. Comparison of the damage to combined (α + γ) cervical and lumbar motoneuron populations in the various experimental groups. Note that the data for intact controls are shown only for illustration and were not included in statistical analyses. Repeated measures two-way ANOVA yielded a significant effect of both experimental group ($F_{2,6}$ = 410.6, $p < 10^{-3}$) and spinal cord region ($F_{1,6}$ = 8.74, p = 0.025) but no significant group × spinal cord region interaction on the combined percentages of damaged/dying motoneurons ($F_{2,6}$ = 3.39, p = 0.103). ***$p < 0.001$ vs. the respective value for the rats with implanted "empty" nanofiber mat, $^{\#}$< 0.05 vs. the respective value for the cervical enlargement of the same rats, $^{+}$< 0.05 vs. the respective value for the lumbar enlargement of the rats given no valproate.

Quantitative assessment of damage to spinal cord motoneuron population (see Fig. 4)

There was no difference between the experimental groups in the density of the combined motoneuron (α + γ) population in the studied spinal cord sections/segments (data not shown). No damaged/dying motoneurons were found in the ventral horns of control intact rats in either spinal cord segment studied. The rats with "empty" nanofiber mat application showed only a minute fraction of such cells, which was identical for the cervical and lumbar region. The rats given the spinal cord dressing of a glutamate-loaded nanofiber mat compared to both the intact rats and rats with the dressing of an "empty" nanofiber mat showed significant motoneuron damage in both these spinal cord segments; the damage was slightly but significantly greater in the lumbar region. The rats with an implanted glutamate-loaded nanofiber mat given systemic valproate treatment showed significantly but slightly lower percentages of damaged/dying motoneurons in their lumbar enlargements than their counterparts given no valproate, and a similar tendency (p = 0.062) was apparent for their cervical motoneurons.

Discussion

The toxicity of endogenous and exogenous glutamate is well established. In this study, we assessed the toxicity of exogenous glutamate to verify the idea of using, instead of probes permanently implanted into the CNS, which can cause major tissue damage, nanofiber mats as drug carriers. Importantly, probe implantation-related tissue damage can induce a variety of pathological phenomena that hinder the interpretation of experimental data.

We could not find, in the existing body of published scientific reports, any data on the use of nanofiber-based mats as drug carriers for chronic experiments. One of the questions to be answered was whether the amount of nanofiber mat that can be safely applied to the rat spinal cord using the laminectomy approach will be sufficient to provide an effective (as judged by a clear biological effect) drug dose. The subarachnoid space of the spinal cord is very narrow, which greatly limits the applicable size of the mat dressing. The use of smaller nanofiber mat fragments may necessitate a reduction of the mat-carried drug

dose, which may render it ineffective. Increasing drug concentration in the emulsion used for nanofiber mat production, with the aim of compensating the lessened size, may not be feasible because of some electrospinning-related physicochemical phenomena (e.g., those involving interactions of drug-derived ions; this was the case in this experiment, too). We were quite lucky in this regard because the amount of glutamate released during the 3-week *in vivo* study period, which represented but a minor fraction of the total drug contents of the implanted nanofiber mat pieces, exerted unambiguous toxic effects both in the spinal cord region adjacent to the location of the mat implant and in the more distant cervical segment of the spinal cord. The symptoms identified in the rats carrying glutamate-loaded nanofiber mat implants were typical of excitotoxic CNS insult (tigrolysis, postsynaptic dendrite swelling, clasmatodendrosis, and synaptic and neurofilament damage). Furthermore, numerous hemorrhages found in multiple locations of the spinal cord cross-sections and in the subarachnoid space clearly indicated blood-brain barrier damage, with thickening of small blood vessels possibly forecasting an increase in blood-brain barrier permeability. The absence of similar damage in the rats carrying "empty" nanofiber mat implants demonstrated that the PLCL mat itself was safe for the spinal cord and did not cause mere mechanical contact/size-related irritation either. The latter observation is in line with earlier studies performed in Mossakowski Medical Research Centre [1,24].

The beneficial effect of systemic valproate treatment on spinal cord motoneuron counts and morphology (decrease in the number of tigrolytic cells), as well as on synaptophysin immunoreactivity in the rats carrying glutamate-loaded nanofiber mat implants, suggested that the glutamate-induced damage was related to the effects of glutamate excess on histone acetylation/deacetylation. However, an alternative/additional explanation may be sought in the stimulatory effect of valproate on expression of the *SMN* gene [25]. Surprisingly, the valproate treatment did not improve blood-brain barrier impermeability, a finding that contrasts with the results of an earlier rat study [27]. This discrepancy was most likely related to the relatively low valproate dosage in our study and to its administration by gavage instead of the intraperitoneal route.

In summary, this study showed the potential of the tested nanofiber mat-based drug delivery system for (sub)chronic (a few weeks at least) administration of medicines to the CNS. The implanted nanofibrous carrier did not induce inflammatory changes either in the neighboring lumbar spinal cord region, or in the more distant cervical segment, or in the meninges, and underwent gradual biodegradation over time. As evidenced by the various approaches used for detecting glutamate-induced pathomorphological changes in our study, the tested PLCL nanofiber mat is suitable for generation of neurotoxic levels of excitatory amino acids in rat spinal cord as an alternative to mechanical probes that cause much more tissue damage. However, the tested nanofiber mat-based drug delivery system needs further improvements aimed at: 1) extending the period of effective drug release, 2) rendering the release more steady, and 3) eliminating the initial phase of 'burst' (of a few hours' duration) release of the carried drug.

Acknowledgments

This work was supported by grant no. NN 401 014640 from the Ministry of Science and Higher Education of Poland and by statutory funds from the Mossakowski Research Institute, Polish Academy of Science. The technical assistance of Tomasz Chmielewski and Aleksandra Kiszko of the Institute of Fundamental Technological Research, PAS, with preparation and *in vitro* characterization of the nanofiber mats is gratefully acknowledged.

Disclosure

Authors report no conflict of interest.

References

1. Andrychowski J, Frontczak-Baniewicz M, Sulejczak D, Kowalczyk T, Chmielewski T, Czernicki Z, Kowalewski TA. Nanofiber nets in prevention of cicatrization in spinal procedures. Experimental study. Folia Neuropathol 2013; 51: 147-157.
2. Chen S, Wu H, Klebe D, Hong Y, Zhang J. Valproic acid: a new candidate of therapeutic application for the acute central nervous system injuries. Neurochem Res 2014; 39: 1621-1633.
3. Chuang DM, Leng Y, Marinova Z, Kim HJ, Chiu CT. Multiple roles of HDAC inhibition in neurodegenerative conditions. Trends Neurosci 2009; 32: 591-601.
4. Corona JC, Tapia R. Ca^{2+}-permeable AMPA receptors and intracellular Ca^{2+} determine motoneuron vulnerability in rat spinal cord in vivo. Neuropharmacology 2007; 52: 1219-1228.
5. Delaine-Smith RM, Green NH, Matcher SJ, MacNeil S, Reilly GC. Monitoring fibrous scaffold guidance of three-dimensional collagen organisation using minimally-invasive second harmonic generation. PLoS One 2014; 9: e89761.

6. Gilmore JL, Yi X, Quan L, Kabanov AV. Novel nanomaterials for clinical neuroscience. J Neuroimmune Pharmacol 2008; 3: 83-94.
7. Hauser AT, Jung M, Jung M. Assays for histone deacetylases. Curr Top Med Chem 2009; 9: 227-234.
8. Hirata A, Nakamura R, Kwak S, Nagata N, Kamakura K. AMPA receptor-mediated slow neuronal death in the rat spinal cord induced by long-term blockade of glutamate transporters with THA. Brain Res 1997; 771: 37-44.
9. Jeong SI, Kim BS, Kang SW, Kwon JH, Lee YM, Kim SH, Kim YH. In vivo biocompatibilty and degradation behavior of elastic poly(L-lactide-co-ε-caprolactone) scaffolds. Biomaterials 2004; 25: 5939-5946.
10. Jiang X. Brain drug delivery systems. Pharm Res 2013; 30: 2427-2428.
11. Kazantsev AG, Thompson LM. Therapeutic application of histone deacetylase inhibitors for central nervous system disorders. Nat Rev Drug Discov 2008; 7: 854-868.
12. Kubinová S, Syková E. Nanotechnology for treatment of stroke and spinal cord injury. Nanomedicine (Lond) 2010; 5: 99-108.
13. Labuzek K, Gorki K, Jaroszek H, Jarzabek K, Gabryel B, Okopien B. Highly organized nanostructures for brain drug delivery – new hope or just a fad? CNS Neurol Disord Drug Targets 2013; 12: 1271-1285.
14. Leigh PN, Meldrum BS. Excitotoxicity in ALS. Neurology 1996; 47 (Suppl 4): S221-S227.
15. Liu T, Xu J, Chan BP, Chew SY. Sustained release of neurotrophin-3 and chondroitinase ABC from electrospun collagen nanofiber scaffold for spinal cord injury repair. J Biomed Mater Res A 2012; 100: 236-242.
16. Massieu L, Tapia R. Glutamate uptake impairment and neuronal damage in young and aged rats in vivo. J Neurochem 1997; 69: 1151-1160.
17. Meisel A, Harms C, Yildirim F, Bösel J, Kronenberg G, Harms U, Fink KB, Endres M. Inhibition of histone deacetylation protects wild-type but not gelsolin-deficient neurons from oxygen/glucose deprivation. J Neurochem 2006; 98: 1019-1031.
18. Nakielski P, Kowalczyk T, Zembrzycki K, Kowalewski TA. Experimental and numerical evaluation of drug release from nanofiber mats to brain tissue. J Biomed Mater Res B Appl Biomater 2014 May 13 [Epub ahead of print]. doi: 10.1002/jbm.b.33197.
19. Qing H, He G, Ly PT, Fox CJ, Staufenbiel M, Cai F, Zhang Z, Wei S, Sun X, Chen CH, Zhou W, Wang K, Song W. Valproic acid inhibits Aβ production, neuritic plaque formation, and behavioral deficits in Alzheimer's disease mouse models. J Exp Med 2008; 205: 2781-2789.
20. Roth M. Fluorescence reaction for amino acids. Anal Chem 1971; 43: 880-882.
21. Santini V, Gozzini A, Ferrari G. Histone deacetylase inhibitors: molecular and biological activity as a premise to clinical application. Curr Drug Metab 2007; 8: 383-393.
22. Shaw PJ, Eggett CJ. Molecular factors underlying selective vulnerability of motor neurons to neurodegeneration in amyotrophic lateral sclerosis. J Neurol 2000; 247 (Suppl 1): I17-I27.
23. Sill TJ, von Recum HA. Electrospinning: applications in drug delivery and tissue engineering. Biomaterials 2008; 29: 1989-2006.
24. Sulejczak D, Andrychowski J, Kowalczyk T, Nakielski P, Frontczak-Baniewicz M, Kowalewski T. Electrospun nanofiber mat as a protector against the consequences of brain injury. Folia Neuropathol 2014; 52: 56-69.
25. Sumner CJ, Huynh TN, Markowitz JA, Perhac JS, Hill B, Coovert DD, Schussler K, Chen X, Jarecki J, Burghes AH, Taylor JP, Fischbeck KH. Valproic acid increases SMN levels in spinal muscular atrophy patient cells. Ann Neurol 2003; 54: 647-654.
26. Wang Z, Leng Y, Tsai LK, Leeds P, Chuang DM. Valproic acid attenuates blood–brain barrier disruption in a rat model of transient focal cerebral ischemia: the roles of HDAC and MMP-9 inhibition. J Cereb Blood Flow Metabol 2011; 31: 52-57.
27. Yildirim F, Gertz K, Kronenberg G, Harms C, Fink KB, Meisel A, Endres M. Inhibition of histone deacetylation protects wildtype but not gelsolin-deficient mice from ischemic brain injury. Exp Neurol 2008; 210: 531-542.

Original article

Folia Neuropathologica

On the lack of a clear-cut association between alpha-2-macroglobulin deletion and the risk of Alzheimer disease in Poland

Grażyna Michałowska-Wender[1,2], Alicja Wawrzynek[1], Grzegorz Rossa[3], Wojciech Kozubski[4], Mieczysław Wender[2]

[1]Laboratory of Neurogenetics, Department of Neurology, University of Medical Sciences, Poznań, Poland, [2]Neuroimmunological Unit, Mossakowski Medical Research Centre, Polish Academy of Sciences, Poznań, Poland, [3]Regional Hospital for Neurological and Psychiatric Diseases, Cibórz, Poland, [4]Department of Neurology, University of Medical Sciences, Poznań, Poland

Folia Neuropathol 2014; 52 (4): 417-420 DOI: 10.5114/fn.2014.47842

Abstract

Alzheimer disease (AD) is a complex, multi-factorial disease with the potential involvement of several genes. Alpha-2-macroglobulin (A2M) has been implicated in AD on the basis of its ability to mediate the clearance and degradation of β-amyloid peptide. Nevertheless, it is not clear whether there are racial differences in frequency of polymorphisms of A2M in AD. We examined a group of 50 unrelated patients from Poland (38 women and 12 men), who were diagnosed clinically as probably developing AD (according to the N1NCD3 – ADR PA criteria). The patients were examined by a neurologist and a psychologist and had a CT or MRI scan of the brain. Fifty individuals of matched age, without any signs of dementia, were studied as a control group. DNA was extracted by a routine method from a blood sample. Amplification and genotyping at A2M was performed as described by Blacker et al. (1997). The genotypic distribution in A2M exon 18 in patients with AD and genotype TT in A2M exon 24 was similar to that in the controls. Significant differences were noted only in early onset AD in males and for old onset disease in females. The deletions were found more frequently in AD; however, they were found in only a small proportion of studied patients. These findings indicate that A2M is not the only biological candidate gene for AD determination.

Key words: *Alzheimer disease, alpha-2-macroglobulin, polymorphism.*

Introduction

Alzheimer disease (AD) is a complex multi-factorial disease with the potential involvement of several genes. Alpha-2-macroglobulin (A2M) has been implicated in AD on the basis of its ability to mediate the clearance and degradation of β-amyloid peptide. Nevertheless, it is not clear whether there are racial differences in frequency of polymorphisms of A2M in AD.

Association of A2M deletion polymorphism with sporadic AD was reported in Korea [11] and in southern Italy [23]. Genetic association of A2M with AD was also noted in the Finnish elderly population [16]. Similar results were reported in the USA [5,7,13]. These data seem to support the view about susceptibility for AD, linked to A2M polymorphism.

However, there are also many studies with negative results, including in Poland [21], Hungary [10],

Communicating author:
Grazyna Michalowska-Wender, Neuroimmunological Unit, Mossakowski Medical Research Centre, Polish Academy of Sciences, 49 Przybyszewskiego St., 60-355 Poznań, Poland, phone/fax: +48 61 869 17 91, e-mail: grazynawender@wp.pl

Japan [9], China [20], USA [22], Italy [17], Germany [3], France [8] and Sweden [6].

The discussed differences between various human populations may be explained by the known gene expression variability between different human populations, with the impact on disease susceptibility [14], and by biochemical individuality probably with potential relevance to AD [15].

The above, briefly presented differences regarding whether existing data point to an association between A2M polymorphism and AD justify our interest in this problem.

Material and methods

We examined a group of 50 unrelated patients from Poland (38 women and 12 men), who were diagnosed clinically as probably developing AD (according to the N1NCD3 – ADR PA criteria), including 35 patients with an onset of over 65 years of age (late AD) and 15 with an early AD (onset before the 65th year of age). The patients were examined by the neurologist and psychologist and had a CT or MRI scan of the brain. Fifty individuals of matched age, without any signs of dementia, were studied as control subjects.

DNA was extracted by a routine method from a 1 ml EDTA blood sample. All patients were pseudosporadic ones, without evident familiar association. Amplification and genotyping at A2M was performed as described by Blacker *et al*. [5].

Results

The genotype and allelic distribution were compared between controls and patients with AD. In the control group the genotype WW in A2M exon 18 was detected in 74% of individuals. Heterozygous W/Δ was found in 24%, and ΔΔ was found in only 2% of control group individuals. Allelic distribution in the control group was 86% for W and 14% for Δ.

The genotypic distribution in A2M exon 18 in patients with AD was similar to that in the controls. The genotype WW was detected in 32 cases (64%), while heterozygous W/Δ was detected in 3 cases (6%). A polymorphism (deletion) was uncovered in 4 cases. The allelic distribution was found to be 78% for W and 22% for Δ. The comparisons of genotype and allele frequencies between the early (before 65 years) and late onset (older than 65 years) as well as between male and female patients with AD are presented in Table I. Statistically significant differences were not found.

The genotype TT in A2M exon 24 of the control group was detected in 52%, TC in 30% and CC in 18% instances. In the control group the allelic distribution was as follows: T 67% and C 33%. In AD the TT genotype in A2M exon 24 was found in 19 patients (38%), TC in 19 individuals (38%) and CC in 12 cases (29%), and the allelic distribution was C 43% and T 57%. The genotype and allele frequencies, divided according to gender, in early onset AD are presented in Table II. Significant differences were detected between the subgroup of males in early onset AD and the controls, as well as between the subgroup of females with late onset AD and the respective controls.

Discussion

The molecular basis of AD is of general interest and in recent years has been broadly discussed in

Table I. Genotype and allele frequencies for alpha-2-macroglobulin (A2M) exon 18 in Alzheimer disease and control groups

	Age < 65, *n* = 15			Age > 65, *n* = 35			Control, *n* = 50			
		Female	Male		Female	Male		Female	Male	
W/W	12	4	8	20	13	7	37	26	11	
W/Δ	3	1	2	11	5	6	12	9	3	
Δ/Δ	0	0	0	4	3	1	1	1	0	
W	27	9	18	51	31	20	86	61	25	
Δ	3	1	2	19	11	8	14	11	3	
ratio W : Δ	9 : 1	9 : 1	9 : 1	2.5 : 1	3 : 1	2 : 1	8 : 1	6 : 1	0.8 : 1	

*OR = 0.6162; p = 0.6609 (*1)*
*OR = 0.9259; p = 0.9364 (*2)*
*OR = 1.9677; p = 0.1585 (*3)*
*OR = 3.3333; p = 0.1040 (*4)*

Table II. Genotype and allele frequencies for alpha-2-macroglobulin (A2M) exon 24 in Alzheimer disease and control groups

	Age < 65, *n* = 15			Age > 65, *n* = 35			Control, *n* = 50		
		Female	Male		Female	Male		Female	Male
T/T	5	0	5	14	8	6	26	24	2
T/C	9	4	5	10	5	5	15	6	9
C/C	1	1	0	11	8	3	9	6	3
T	19	4 *1	15 *2	38	21 *3	17 *4	67	54 *1*3	13 *2*4
C	11	2	0	32	21	11	33	18	15
ratio T : C	2 : 1	2 : 1	15 : 0	3.8 : 3.2 1 : 1	1 : 1	1.7 : 1	2 : 1	3 : 1	1 : 1

*OR = 15000; p = 0.6551 (*1)*
*OR = 0.02810; p = 0.0161 (*2)*
*OR = 3.0000; p = 0.0076 (*3)*
*OR = 0.5608; p = 0.2855 (*4)*

very interesting review papers [1,2,18,19]. Among several genetic factors which have been implicated in AD, only a few are thought to be causative for the disease. In the majority of sporadic AD cases, genetic factors act as predisposing agents, without the capacity to induce the disease but able to increase the risk of disease above that found in the general population. They may also interact among themselves to further enhance the probability of inducing the disease (synergic effect) [21].

In our studies we have used the typical approach to evaluate the genetic contribution to the risk of AD by analyzing the frequency distribution of the allelic variants at polymorphic sites of the candidate gene, A2M, in cases of the disease and in controls. Alpha-2-macroglobulin is a serum pan-protease inhibitor, also expressed in the brain, which has been implicated in AD on the basis of its ability to mediate the clearance and degradation of Aβ, the major component of β-amyloid deposits. Alpha-2-macroglobulin is a component of senile plaques. The A2M gene, mapped to chromosome 12p, became a candidate as a disease locus for late-onset AD. Based on the positional information about the candidate gene, Blacker *et al.* [5] focused on a 5 bp deletion/insertion polymorphism of the A2M gene, located in the 5' splice site of exon 18. By using a family-based association test method, they found an association between the deletion allele (A2M-D) and late-onset AD. With a deletion, A2M may be less effective in β-amyloid binding and clearance and in preventing its deposition in senile plaques. Sequencing of the RT-PCR products from the deletion and insertion homozygotes revealed no alteration in sequence from that expected, despite the loss of 5 bp adjacent to exon 18. These molecular findings suggest that A2M deletion might be nonfunctional [6].

In our studied material we have not found any clear-cut differences in the frequency of genotype and allele frequency between AD and controls. Significant differences were noted only in early onset AD in males and for old onset disease in females. The deletions were found more frequently in AD; however, they were found in only a small proportion of studied patients.

There are three biological manifestations of the Aβ-A2M interactions that may be directly relevant to the etiology of AD [13]. First, the interaction between A2M and Aβ prevents Aβ fibril formation and fibril-associated neurotoxicity. Secondly, protease activation of Aβ-A2M complexes or protease activation of A2M followed by Aβ binding can promote the protease-mediated degradation of A2M-bound Aβ. And thirdly, protease activated Aβ-A2M complexes may undergo LPR-mediated endocytosis followed by trafficking of Aβ to lysosomes for degradation. The established late-onset risk factor ApoE ε4 accelerates Aβ deposition, and ApoE is found in a complex with A2M in plasma. Taken together, these findings indicate that A2M is not the only biological candidate gene for AD determination. So far, only the ApoE ε4 allele is known to be a genetic risk factor for the later onset sporadic AD.

Similar negative results in the Polish population were obtained in studies of CR1, PICALM and CLU gene polymorphisms [12]. Therefore the slightly positive results obtained in studies by Bednarska-Makaruk *et al.* [4] are very interesting. The authors con-

cluded that paraoxonase 1 (PON1) gene promoter polymorphism may have a role in AD development. However, the role seems to be only an additional one.

Disclosure

Authors report no conflict of interest.

References

1. Armstrong RA. On the 'classification' of neurodegenerative disorders: discrete entities, overlap or continuum? Folia Neuropathol 2012; 50: 201-218.
2. Armstrong RA. What causes Alzheimer's disease? Folia Neuropathol 2013; 51: 169-188.
3. Bagli M, Papassotiropoulos A, Jessen F, Schmitz S, Rao ML, Maier W, Heun R. Identical distribution of the alpha 2-macroglobulin pentanucleotide deletion in subjects with Alzheimer disease and controls in a German population. Am J Med Genet 2000; 96: 775-777.
4. Bednarska-Makaruk ME, Krzywkowski T, Graban A, Lipczyńska-Łojkowska W, Bochyńska A, Rodo M, Wehr H, Ryglewicz DK. Paraoxonase 1 (PON1) gene –108C>T and p.Q192R polymorphisms and arylesterase activity of the enzyme in patients with dementia. Folia Neuropathol 2013; 51: 111-119.
5. Blacker D, Wilcox MA, Laird NM, Rodes L, Horvath SM, Go RC, Perry R, Watson B Jr,Basset SS, McInnisMG, Albert MS, Hyman BT, Tanzi RE. Alpha-2 macroglobulin is genetically associated with Alzheimer disease. Nat Genet 1998; 19: 357-360.
6. Blennow K, Ricksten A, Prince JA, Brookes AJ, Emahazion T, Wasslavik C, Bogdanovic N, Andreasen N, Båtsman S, Marcusson J, Nägga K, Wallin A, Regland B, Olofsson H, Hesse C, Davidsson P, Minthon L, Jansson A, Palmqvist L, Rymo L. No association between the alpha2-macroglobulin (A2M) deletion and Alzheimer's disease, and no change in A2M mRNA, protein, or protein expression. J Neural Transm 2000; 107: 1065-1107.
7. Dodel RC, Du Y, Bales KR, Gao F, Eastwood B, Glazier B, Zimmer R, Cordell B, Hake A, Evans R, Gallagher-Thompson D, Thompson LW, Tinklenberg JR, Pfefferbaum A, Sullivan EV, Yesavage J, Alstiel L, Gasser T, Farlow MR, Murphy GM Jr, Paul SM. Alpha2 macroglobulin and the risk of Alzheimer's disease. Neurology 2000; 54: 438-442.
8. Halimi G, Duplan L, Bideau C, Iniesta D, Berthézène P, Oddoze C, Verdier JM, Michel B, Bergé-Lefranc JL. Association of APOE promoter but not A2M polymophisms with risk of developing Alzheimer's disease. Neuroreport 2000; 11: 3599-3601.
9. Higuchi S, Matsushita S, Nakane J, Arai H, Matsui T, Urakami K, Yuzuriha T, Takeda A. Alpha2-macroglobulin gene polymorphisms show racial diversity and are not associated with Alzheimer's disease. Neuroreport 2000; 11: 1167-1171.
10. Janka Z, Juhász A, Rimanóczy A, Boda K, Márki-Zay J, Palotás M, Kuk I, Zöllei M, Jakab K, Kálmán J. Alpha2-macroglobulin exon 24 (Val-1000-Ile) polymorphisms is not associated with late-onset sporadic Alzheimer's dementia in the Hungarian population. Psychiatr Genet 2002; 12: 49-54.
11. Jhoo JH, Kim KW, Lee DY, Lee KU, Lee JH, Kim SY, Youn JC, Woo JI. Association of alpha-2-macroglobulin deletion polymorphism with sporadic Alzheimer's disease in Koreans. J Neurol Sci 2001; 184: 21-25.
12. Klimkowicz-Mrowiec A, Sado M, Dziubek A, Dziedzic T, Pera J, Szczudlik A, Slowik A. Lack of association of CR1, PICALM and CLU gene polymorphisms with Alzheimer disease in a Polish population. Neurol Neurochir Pol 2013; 47: 157-160.
13. Kovacs DM. Alpha2-macroglobulin in late-onset Alzheimer's disease. Exp Gerontol 2000; 35: 473-479.
14. Li J, Liu Y, Kim T, Min R, Zhang Z. Gene expression variability within and between human populations and implications toward disease susceptibility. PLoS Comput Biol 2010; 6: 1-10.
15. Lukiw WJ. Variability in micro RNA (miRNA) abundance, speciation andcomplexity amongst different human populations and potential relevance toAlzheimer's disease (AD). Front Cell Neurosci 2013; 7: 1-4.
16. Myllykangas L, Polvikoski T, Sulkava R, Verkkoniemi A, Crook R, Tienari PS, Pusa AK, Niinistö L, O`Brien P, Kontula K, Hardy J, Haltia M, Pérez-Tur J. Genetic association of alpha2-macroglobulin with Alzheimer`s disease in a Finnish elderly population. Ann Neurol 1999; 46: 382-390.
17. Nacmias B, Tedde A, Cellini E, Forleo P, Orlacchio A, Guarnieri BM, Petruzzi C, D'Andrea F, Serio A, Sorbi S. Alpha2-macroglobulin polymorphism in Italian sporadic and familial Alzheimer's disease. Neurosci Lett 2001; 16: 9-12.
18. Pluta R, Kocki J, Maciejewski R, Ułamek-Kozioł M, Jabłoński M, Bogucka-Kocka A, Czuczwar SJ. Ischemia signalling to Alzheimer-related genes. Folia Neuropathol 2012; 50: 322-329.
19. Šerý O, Povová J, Mišek I, Pešák L, Janout V. Molecular mechanisms of neuropathological changes in Alzheimer's disease: a review. Folia Neuropathol 2013; 51: 1-9.
20. Shi J, Ma C, Lao H, Feng R, Guo Y, Mu N, Li Q, Tan Y, Wang D. No evidence for association between the alpha 2-macroglobulin polymorphism and Alzheimer's disease in the Han Chinese. Zhonghua Yi Xue Yi Chuan Xue Za Zhi 2001; 18: 299-302.
21. Styczynska M, Religa D, Pfeffer A, Luczywek E, Wasiak B, Styczynski G, Peplonska B, Gabryelewicz T, Golebiowski M, Kobrys M, Barcikowska M. Simultaneous analysis of five factors in Polish patients with Alzheimer's disease. Neurosci Lett 2003; 344: 99-102.
22. Wang X, Luedecking EK, Minster RL, Ganguli M, DeKosky ST, Kamboh MI. Lack of association between alpha2-macroglobulin polymorphisms and Alzheimer's disease. Hum Genet 2001; 108: 105-108.
23. Zappia M, Cittadella R, Manna I, Nicoletti G, Andreoli V, Bonavita S, Gambardella A, Quattrone A. Genetic association of alpha2-macroglobulin polymorphisms with AD in southern Italy. Neurology 2002; 59: 756-758.

Original article

Folia Neuropathologica

Prevalence of small cerebral bleeds in patients with progressive supranuclear palsy: a neuropathological study with 7.0-Tesla magnetic resonance imaging correlates

Jacques De Reuck[1,2], Dominique Caparros-Lefebvre[3], Vincent Deramecourt[1,2,4,5], Luc Defebvre[1,4,6], Florent Auger[1,2], Nicolas Durieux[1,2], Regis Bordet[1,2], Florence Pasquier[1,2,4], Claude-Alain Maurage[1,4,5]

[1]Université Lille Nord de France, F-59000 Lille, [2]UDSL, EA 1046, F-59000 Lille, [3]Centre Hospitalier, F-59150 Wattrelos, [4]CHULille, F-59000 Lille, [5]INSERM U837, F-59000 Lille, [6]UDSL, EA 4559, F-59000 Lille, France

Folia Neuropathol 2014; 52 (4): 421-427 DOI: 10.5114/fn.2014.47843

Abstract

Introduction: *Progressive supranuclear palsy (PSP) is a degenerative disease affecting mainly the brain stem, basal ganglia and cerebellum. Associated cerebrovascular lesions, mainly small cerebral bleeds, are frequently observed in some neurodegenerative diseases such as Alzheimer dementia and rare in others such as frontotemporal lobar degeneration. The present post-mortem study investigates the prevalence and distribution of small cerebral bleeds in PSP brains.*

Material and methods: *Nineteen brains of PSP patients were compared to 12 age-matched controls. The prevalence and distribution of mini-bleeds were investigated on a coronal section of a cerebral hemisphere at the level of the mamillary bodies and on a horizontal section through the pons and cerebellum. In addition, out of these series T2*-weighted gradient-echo 7.0-Tesla magnetic resonance imaging (MRI) of 3 coronal sections of a cerebral hemisphere and of a brain stem and cerebellum was performed in 14 PSP and 11 control brains.*

Results: *Although the total number of mini-bleeds was the same on neuropathological examination of both groups, they prevailed around the dentate nucleus of the cerebellum ($p = 0.05$) and in the tegmentum pontis ($p = 0.05$) of the PSP brains. On MRI the small bleeds were also more frequent around the dentate nucleus of the cerebellum ($p = 0.02$) and in the pons ($p = 0.04$) of PSP brains.*

Discussion: *In PSP brains, mini-bleeds only prevail in the regions affected by the neurodegenerative process, similarly to what happens in frontotemporal lobar degeneration. They should be considered as the result of increased angiogenesis and microglial activation, leading to associated disturbances of the blood-brain barrier in the most affected regions of PSP. They are not indicative of cerebrovascular disease.*

Key words: *progressive supranuclear palsy, neuropathology, T2*-weighted gradient-echo 7.0-T MRI, tauopathies, small cerebral bleeds, cerebellum, pons.*

Communicating author:

J. De Reuck, MD, PhD, Leopold II laan 96, BE–9000 Ghent, Belgium, phone: +32 9 221 8844; fax: +32 9 3324971, e-mail: dereuck.j@gmail.com

Introduction

Progressive supranuclear palsy (PSP) was first described in 1964 by Steele, Richardson and Olszewski as a heterogeneous degeneration involving the brain stem, basal ganglia and cerebellum with clinically a vertical gaze and pseudobulbar palsy, nuchal dystonia and dementia [21]. Progressive supranuclear palsy is now increasingly recognized, with an average prevalence of 3.5 per 100 000 [19]. It belongs to the family of tauopathies with the classical picture, consisting of a symmetrical akinetic-rigid syndrome, vertical supranuclear gaze palsy, frontal deficits, prominent postural instability and falls, now referred to as Richardson's syndrome (PSP-RS). However, several variants in the clinical presentation complicate the early differential diagnosis [20]. It now includes a progressive supranuclear palsy-parkinsonism (PSP-P) form and one with pure akinesia and gait freezing (PAGF) [22].

Vascular factors have sometimes been implicated, leading to the description of a vascular progressive supranuclear palsy syndrome [15]. A pre-symptomatic history of arterial hypertension as a major feature in the diagnosis of PSP remains controversial [3,13].

Although the co-existence of argyrophilic grains, corticobasal degeneration, Alzheimer features and Lewy bodies was rather frequent in a large post-mortem series of PSP patients, the severity of cerebrovascular pathology was found to be too limited to explain any clinical symptomatology [17]. These findings are in contrast to the high incidence of small bleeds observed in brains of patients with Alzheimer dementia (AD) and Lewy body dementia (LBD) [4,5,9].

The present neuropathological and post-mortem 7.0-Tesla magnetic resonance imaging (MRI) study investigates the prevalence and the distribution of small cerebral bleeds and other cerebrovascular lesions in patients with PSP.

Material and methods

Progressive supranuclear palsy and control population

From January 2000 until February 2013, 212 consecutive patients with a clinical history of a neurodegenerative disease came to autopsy: in 19 (9%) of them the neuropathological diagnosis of PSP was made.

During the same period, 12 post-mortem brains of age-matched controls were obtained. The controls consisted of brains of elderly patients who died from an illness not related to a cerebral disease.

All patients had well-documented clinical files including a prior history of vascular risk factors and of the use of antithrombotic agents.

Neuropathological analyses

Post-mortem brains were obtained by informed consent of the patients or from the nearest family, who allowed an autopsy for a post-mortem diagnosis and the use of brain samples for scientific purposes. The brain tissue samples were first used for diagnosis and afterward integrated in the Lille Neuro-Bank, dependent on the University of Lille and co-federated by the "Centre des Resources Biologiques", acting as the institutional review board. The neuropathological evaluation was performed blinded to history and clinical data.

Neurodegenerative lesions

After 3-week fixation in formalin, many samples were taken according to a standard protocol [4]. Slides from paraffin-embedded sections were immuno-stained for tau protein, β-amyloid, α-synuclein, prion protein, TDP-43 and ubiquitin.

The post-mortem diagnosis of PSP was made according to the NINDs neuropathological criteria for Steele-Richardson-Olszewski syndrome (progressive supranuclear palsy) [14]. Additional AD features were staged according to the classification of Braak and Braak [1].

Cerebrovascular lesions

The prevalence and severity of cerebrovascular lesions were compared between the brains of PSP patients and controls. In addition, a semi-quantitative evaluation of small microscopic lesions was performed on a whole coronal section of a cerebral hemisphere, at the level of the mamillary bodies, and a horizontal section through the mid-pons and cerebellar hemispheres, after staining with hematoxylin-eosin, Luxol Fast Blue and Perl's Prussian Blue. The considered cerebrovascular lesions were bleeds, infarcts, lacunes and white matter changes.

A semi-quantitative scale, with ranking (R) 0 to 3, was used to evaluate the severity of the white matter changes and the frequency of micro-infarcts and of micro- and mini-bleeds. The white matter changes were restricted to the periventricular regions (R1),

scattered in the centrum semiovale (R2) or forming confluent lesions (R3) of myelin and axonal loss. For the micro-infarcts, micro- and mini-bleeds R1 corresponded to 1 to 2, R2 up to 5 and R3 to more than 5 lesions per region [4].

Magnetic resonance imaging examination

Out of the neuropathological series, 14 PSP and 11 control brains were available for MRI examination. On a 7.0-Tesla MRI Bruker BioSpec SA (Ettlingen, Germany) three MRI sequences were used: a positioning sequence, a T2 sequence and a gradient echo T2* sequence. Three coronal sections of a formalin-fixed cerebral hemisphere and one section of brain stem and cerebellar hemisphere, placed in a plastic box filled with physiological serum, were examined according to the previously described method [6]. The mean number of cortical small bleeds detected on each examined section was compared between the PSP and control brains. The majority of the brain stem sections consisted of a horizontal section through the pons. Only in one PSP and one control brain was a sagittal section of the whole brain stem available.

Statistical analyses

The statistical analysis compared the items of the PSP with the control group. Univariate comparisons of unpaired groups were done with Fisher's exact test for categorical data. The non-parametric Mann-Whitney *U*-test was used to compare continuous variables. The significance level was set at 0.05, two-tailed.

Results

The demographic and main clinical data of the 19 patients with proven PSP are labeled in Table I.

Table I. Demographic, clinical and associated neuropathological features of the 19 patients with progressive supranuclear palsy

Age at disease onset (years)	Gender	Clinical syndrome	Age at death (years)	Associated pathology
50	Female	Richardson	55	
50	Male	Richardson	57	
51	Male	Richardson	57	
56	Female	Parkinson	65	
59	Female	Richardson	72	
59	Female	Parkinson	74	
61	Male	Parkinson	68	Alzheimer II
66	Female	Richardson	69	
67	Female	Richardson	82	
68	Female	Richardson	77	
71	Female	Parkinson	77	
71	Male	Parkinson	83	
72	Female	Parkinson	77	
72	Male	Richardson	82	
73	Male	Parkinson	75	Alzheimer III
73	Female	Parkinson	87	
75	Female	Parkinson	79	
78	Male	Richardson	87	
79	Male	Richardson	83	Alzheimer II

Table II. Comparison of the number (percentage) of patients with vascular risk factors and the use of antithrombotic medication among the group with progressive supranuclear palsy (PSP) and among controls

Items	PSP (n = 19)	Controls (n = 12)	p value
Arterial hypertension	7 (37)	3 (25)	0.70
Diabetes	1 (5)	1 (8)	1.0
Hypercholesterolemia	1 (5)	2 (17)	0.54
Smoking	1 (5)	1 (8)	1.0
Antithrombotic treatment	6 (32)	3 (25)	1.0

The median age at onset of the PSP was 67 (interquartile range [IQR]: 56-73) years). Ten patients presented clinically as a PSP-RS and 9 as a PSP-P. The average disease duration was 8.5 (SD 4.3) years. The median age of the patients at death was 75 (IQR: 68-82) years. This was not statistically different from the 70 (IQR 65-77) years in the controls. Gender distribution was also similar, with 42% males in the former and 75% in the latter group.

The vascular risk factors of both groups were rare and not significantly different between the groups. Antithrombotic agents had been used by 32% of the PSP patients and by 25% of the controls (Table II).

The global severity of mini-bleeds was low in the PSP brains and comparable to the controls on neuropathological examination. Only mini-bleeds in the cerebellum (p = 0.05) and in the pons (p = 0.05) were significantly more frequent in PSP brains. In the cerebellum the mini-bleeds were exclusively found around the dentate nucleus, while in the pons they predominated in the tegmentum (Fig. 1A-B). The incidence of other cerebrovascular lesions was low in the PSP as well as in the control brains (Table III).

Table IV shows the mean values of hypo-intensity signals, representing small bleeds, in the cerebral cortex of the 3 coronal slides of a cerebral hemisphere, the hippocampus, pons and cerebellum on T2*-weighted gradient-echo MRI. Only around the dentate nucleus of the cerebellum and in the tegmentum pontis of the PSP brains, significantly more small bleeds were observed compared to the controls (p < 0.5) (Fig. 2A-B). One sagittal sample of a whole PSP brainstem could be compared to a normal control. In addition to the global atrophy and the

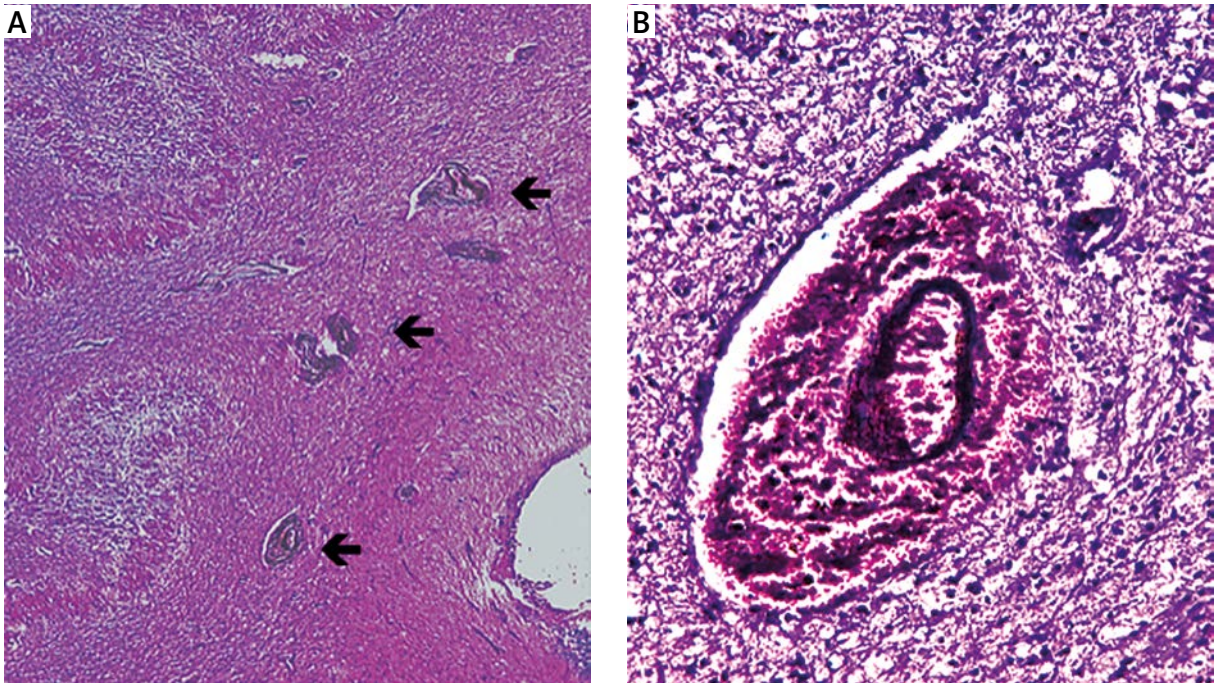

Fig. 1. Histological sections of cerebellum and pons, stained with hematoxylin-eosin, of a patient with progressive supranuclear palsy. **A)** Presence of three small perivascular bleeds (arrows) near the dentate nucleus of the cerebellum. **B)** Small perivascular bleed in the dorsal part of the pons.

Table III. Neuropathological comparison of the mean ranking scores (standard deviations) of the severity of cerebrovascular lesions among patients with progressive supranuclear palsy (PSP) and among controls

Items	PSP (n = 19)	Controls (n = 12)	p value
White matter changes	0.6 (1.0)	0.3 (0.9)	0.33
Amyloid angiopathy	0.1 (0.2)	0.0 (0.0)	0.82
Lacunar infarcts	0.1 (0.2)	0.1 (0.3)	0.91
Territorial infarcts	0.2 (0.5)	0.0 (0.0)	0.62
Cortical micro-infarcts	0.2 (0.5)	0.0 (0.0)	0.43
Hematomas	0.1 (0.2)	0.0 (0.0)	0.82
Micro-bleeds	0.0 (0.0)	0.0 (0.0)	1.0
Mini-bleeds			
Total	1.3 (1.0)	0.5 (0.5)	0.07
Cortico-subcortical	0.5 (0.9)	0.4 (0.5)	1.0
White matter	0.8 (0.8)	0.5 (0.7)	0.38
Striatum	0.4 (0.6)	0.2 (0.4)	0.61
Thalamus	0.1 (0.2)	0.1 (0.3)	0.89
Pons	0.6 (0.9)	0.0 (0.0)	0.05
Cerebellum	1.2 (1.3)	0.1 (0.3)	0.05

Table IV. Comparison of the mean number (standard deviation) of small bleeds on T2*-weighted gradient-echo MRI in post-mortem brains among patients with progressive supranuclear palsy (PSP) and among controls

Items	PSP (n = 14)	Controls (n = 11)	p value
Frontal cerebral cortex	2.5 (2.3)	3.2 (2.5)	0.40
Central cerebral cortex	2.3 (2.0)	1.6 (1.6)	0.47
Occipital cerebral cortex	5.2 (4.0)	3.2 (2.4)	0.34
Hippocampus	0.1 (0.4)	0.5 (1.0)	0.57
Pons	1.8 (1.4)	0.3 (0.5)	0.04
Cerebellum	3.1 (2.3)	0.6 (0.9)	0.02

loss of hypo-intensity in the substantia nigra and red nucleus, small bleeds were observed in the dorsal part of the whole brain stem (Fig. 3).

Discussion

No overall increase of small cerebral bleeds is observed in PSP brains on neuropathological examination or on MRI. This is similar to what happens in frontotemporal lobar degeneration, which in most cases also belongs to the family of tauopathies [7]

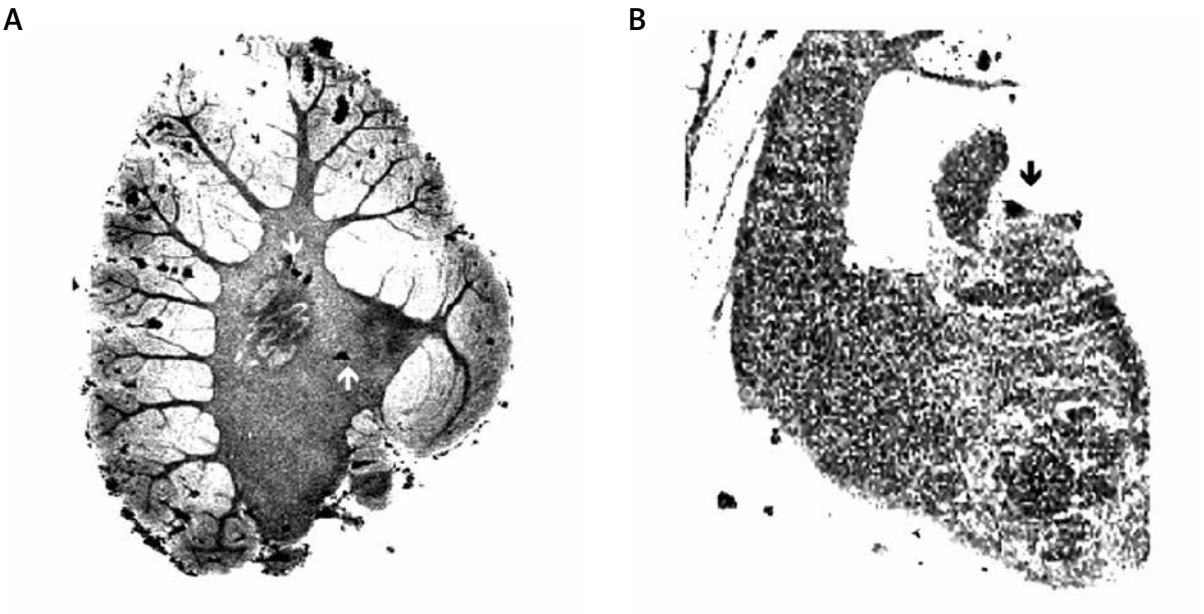

Fig. 2. T2*-weighted gradient-echo 7.0-T magnetic resonance imaging of a horizontal hemi-section of a cerebellar hemisphere and pons in progressive supranuclear palsy. **A)** Presence of small bleeds around the dentate nucleus (arrows). **B)** One small subependymal bleed in the pons (arrow).

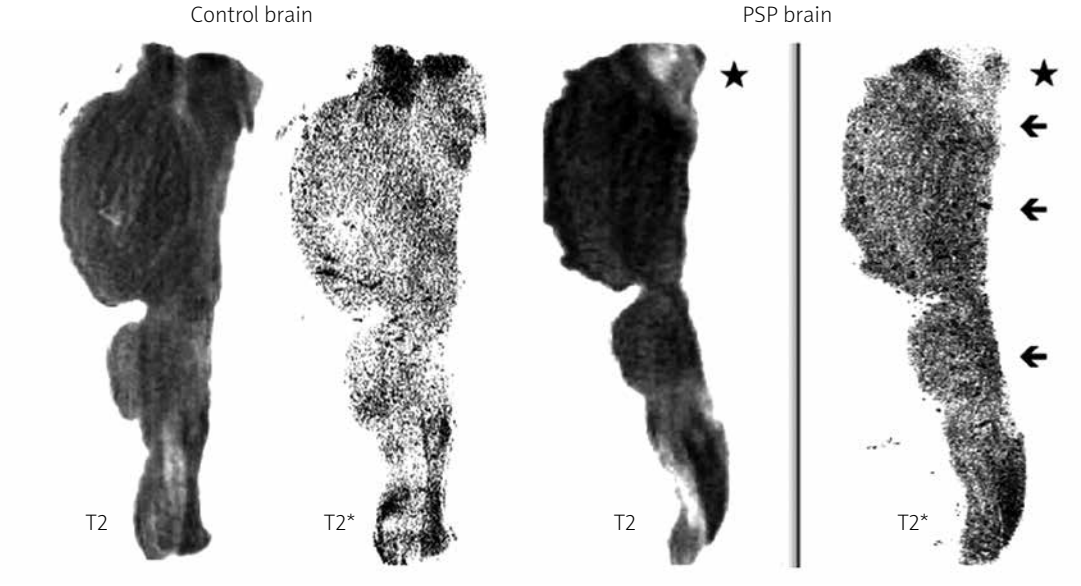

Fig. 3. T2 and T2-weighted gradient-echo 7.0-T magnetic resonance imaging of a sagittal section through the whole brain stem of a control and of a patient with progressive supranuclear palsy (PSP). Note the global atrophy of the PSP brain stem as well as the decreased iron content in the substantia nigra and red nucleus (asterisks). Small bleeds are more prominent in the dorsal part of the whole brain stem in the PSP compared to the control (arrows).

and is in contrast to the overall prevalence of small bleeds in AD and in the cerebral cortex of LBD [4,5,9]. However, compared to age-matched controls, an increased number of mini-bleeds is observed around the dentate nucleus of the cerebellum and in the tegmentum pontis of PSP brains.

Ponto-cerebellar micro-bleeds are frequently observed in patients with cerebral micro-angiopathy due to arterial hypertension [12] and in those using antithrombotic agents [2]. These bleeds are mainly observed around the dentate nucleus of the cerebellum, similar to our cases, and in the central portion of the pons [18] instead of in the tegmentum as in the PSP brains. Our patients with PSP have a low incidence of vascular risk factors, similar to the controls.

Our 7.0-Tesla MRI study confirms the neuropathological findings of an increased incidence of small bleeds in the pons and cerebellum. In the sample covering the whole brain stem, one can suspect that the small bleeds extend over the whole length of the brain stem.

The selective presence of mini-bleeds must be linked to the neurodegenerative process of the PSP itself. The clinical and the neuropathological findings in PSP are heterogeneous and can affect the cerebellum to various degrees [16,22].

The findings in PSP share similarity with those observed in our post-mortem 7.0-Tesla MRI study of frontotemporal lobar degeneration, in which mini-bleeds predominated in the frontal cortex, where the major neurodegenerative changes occur [8].

There is now evidence for increased angiogenesis and microglial activation in the neuropathologically most affected regions of PSP. Such angiogenic vessels could contribute to neuroinflammation and lead to disruption of the blood-brain barrier [11]. Also in Alzheimer's disease ongoing angiogenesis is mainly observed in the hippocampus and is correlated with the presence of neurofibrillary tangles [10].

In any case, the presence of these mini-bleeds in the pons and cerebellum are not to be considered as evidence of cerebrovascular involvement in the pathogenesis of PSP.

Disclosure

Authors report no conflict of interest.

References

1. Braak H, Braak E. Evolution of neuronal changes in the course of Alzheimer's disease. J Neural Transm 1998; 53 (Suppl): 127-140.

2. Chang YY, Liu JS, Lai SL, Wu HU, Lan MY. Cerebellar hemorrhage provoked by combined use of natokinase and aspirin in a patient with cerebral microbleeds. Inter Med 2008; 47: 467-469.
3. Colosimo C, Osaki Y, Vanacore N, Lees AJ. Lack of association between progressive supranuclear palsy and arterial hypertension: a clinicopathological study. Mov Dis 2003; 18: 694-697.
4. De Reuck J, Deramecourt V, Cordonnier C, Leys D, Pasquier F, Maurage CA. Prevalence of small cerebral bleeds in patients with a neurodegenerative dementia: a neuropathological study. J Neurol Sci 2011; 300: 63-66.
5. De Reuck J, Deramecourt V, Cordonnier C, Leys D, Maurage CA, Pasquier F. The impact of cerebral amyloid angiopathy on the occurrence of cerebrovascular lesions in demented patients with Alzheimer features: a neuropathological study. Eur J Neurol 2011; 18: 313-318.
6. De Reuck J, Auger F, Cordonnier C, et al. Comparison of 7.0-T T2*-magnetic resonance imaging of cerebral bleeds in post-mortem brain sections of Alzheimer patients with their neuropathological correlates. Cerebrovasc Dis 2011; 31: 511-517.
7. De Reuck J, Deramecourt V, Cordonnier C, Leys D, Pasquier F, Maurage CA. Cerebrovascular lesions in patients with frontotemporal lobar degeneration: a neuropathological study. Neurodegenerative Dis 2012; 9: 170-175.
8. De Reuck J, Deramecourt V, Cordonnier C, et al. Detection of microbleeds in post-mortem brains of patients with frontotemporal lobar degeneration: A 7.0 tesla magnetic resonance imaging study with neuropathological correlates. Eur J Neurol 2012; 19: 1355-1360.
9. De Reuck J, Deramecourt V, Cordonnier C, Leys D, Pasquier F, Maurage CA. Prevalence of cerebrovascular lesions in patients with Lewy body dementia: A neuropathological study. Clin Neurol Neurosurg 2013; 115: 1094-1097.
10. Desai BS, Schneider JA, Li JL, Carvey PM, Hendey B. Evidence of angiogenetic vessels in Alzheimer's disease. J Neural Transm 2009; 116: 587-579.
11. Desai Bradaric B, Patel A, Schneider JA, Carvey PM, Hendey B. Evidence of angiogenesis in Parkinson's disease, incidental Lewy body disease, and progressive supranuclear palsy. J Neural Transm 2012; 119: 59-71.
12. Fazekas F, Kleinert R, Roob G, et al. Histopathologic analysis of foci of signal loss on gradient-echo T2*-weighted MR images in patients with spontaneous intracerebral hemorrhage: evidence of microangiopathy-related microbleeds. Am J Neuroradiol 1999; 20: 637-642.
13. Ghika J, Bogousslavsky J. Presymptomatic hypertension is a major feature in the diagnosis of progressive supranuclear palsy. Arch Neurol 1997; 54: 1104-1108.
14. Hauw JJ, Daniel SE, Dickson D, et al. Preliminary NINDS neuropathological criteria for Steele-Richardson-Olszewski syndrome (progressive supranuclear palsy); Neurology 1994; 44: 2015-2019.
15. Joseph KA, Ishizawa T, Tsuboi Y, Cookson N, Dickson DW. A clinico-pathological study of vascular progressive supranuclear palsy. A multi-infarct disorder presenting as progressive supranuclear palsy. Arch Neurol 2002; 59: 1597-1601.
16. Kanzawa M, Shimohata T, Toyoshima Y, et al. Cerebellar involvement in progressive supranuclear palsy: A clinicopathological study. Mov Dis 2009; 24: 1312-1318.
17. Keith-Rokosh J, Ang LC. Progressive supranuclear palsy: a review of co-existing neurodegeneration. Can J Neurol Sci 2008; 35: 602-608.
18. Lee SH, Kwon SJ, Kim KS, Yoon BW, Roh JK. Topographic distribution of pontocerebellar microbleeds. Am J Neuroradiol 2004; 25: 1337-1341.
19. Nath U, Ben-Shlomo Y, Thompson RG, et al. The prevalence of progressive supranuclear palsy (Steele-Richardson-Olszewski) in the UK. Brain 2001; 124: 1438-1449.
20. Stamelou M, de Silva R, Arias-Carrion O, et al. Rational therapeutic approaches to progressive supranuclear palsy. Brain 2010; 133: 1578-1590.
21. Steele JC, Richardson C, Olszewski J. Progressive supranuclear palsy. A heterogeneous degeneration involving the brain stem, basal ganglia and cerebellum with vertical gaze and pseudobulbar palsy, nuchal dystonia and dementia. Arch Neurol 1964; 10: 333-359.
22. Williams DR, Holton JL, Strand C, et al. Pathological tau burden and distribution distinguishes progressive supranuclear palsy-parkinsonism from Richardson's syndrome. Brain 2007; 130: 1566-1576.

Original article

Folia Neuropathologica

Methyl-CpG binding protein 2, receptors of innate immunity and receptor for advanced glycation end-products in human viral meningoencephalitis

Danuta Maslinska[1,2], Milena Laure-Kamionowska[1], Sławomir Maslinski[2]

[1]Department of Experimental and Clinical Neuropathology, Mossakowski Medical Research Centre, Polish Academy of Sciences, Warsaw, [2]Department of General and Experimental Pathology, Warsaw Medical University, Warsaw, Poland

Folia Neuropathol 2014; 52 (4): 428-435 DOI: 10.5114/fn.2014.47844

Abstract

Inflammation is a normal host defense reaction to infections and tissue injury. In pathology, the process of inflammation is deregulated by various environmental factors, prolonged activation of Toll-like receptors (TLRs), induction of epigenetic machinery or expression of receptors for advanced glycation end-products (RAGE). In the present study, we examined immunoexpression of proteins participating in the above-mentioned mechanisms, in the brain of patients with viral meningoencephalitis. The results showed that depending on the period of the disease, the process of inflammation is deregulated in different ways. In an early period of viral meningoencephalitis, we found numerous so-called microglial nodules which were strongly immunopositive to methyl-CpG protein 2 (MeCP2). This protein is an epigenetic factor important for methylation of DNA; therefore, our results suggest that cells collected in the nodules may participate in modification of the host defense reaction. Moreover, in the early period of viral meningoencephalitis, we found that Purkinje cells of the cerebellum contain TLR3 or TLR9 receptors that can recognize viral pathogens and may activate a self-destructive mechanism in these neurons. In the later (advanced) period of viral meningoencephalitis, despite some of the above observations, RAGE protein was detected in the brain of adult and aging patients. It means that in this period of the disease, the inflammatory process may be deregulated by numerous post-translationally modified proteins that are transported to the brain after binding with activated RAGE. In addition, young patients appeared more susceptible to viral infections than adult and aging patients, because most of them died during the early period of meningoencephalitis.

Key words: *viral meningoencephalitis, glial nodules, methyl-CpG binding protein 2, Toll-like receptors, receptor for advanced glycation end-products.*

Introduction

The human defense reaction to infections includes activation of innate immunity, inflammation, and acquired immunity [4]. The first line of this rescue strategy relates to the function of innate immunity and pathogen detection. Cells participating in this process recognize pathogens via pattern recognition receptors (PRRs), of which the most well-studied are the Toll-like receptors (TLRs). Toll-like receptors are expressed on the surface of the cells or on the intra-

Communicating author:

Prof. Danuta Maślińska, Department of Clinical and Experimental Neuropathology, Mossakowski Medical Research Centre, PASci, 5 Pawinskiego St., 02-106 Warsaw, e-mail: maslinskad@imdik.pan.pl

cellular vesicles and are stimulated by the presence of pathogen-associated molecular patterns (PAMPs) such as cell membrane components, intracellular wall organelle components, and single or double stranded RNA or DNA fragments [10,19]. Following TLR stimulation, second messenger-specific intracellular signaling cascades are activated that result in expression of genes for production of key inflammatory mediators [7] such as cytokines, chemokines or adhesion molecules. The integrated activity and release of all these mediators by innate immunity cells contribute to the normal inflammatory response [2,14] and determine the course and severity of the host response to infection. Thus, the second step of the defense strategy of the organism is inflammation. The main role of inflammation is removal of necrotic cells from the injured tissue and stimulation of the repair processes. However, prolonged activation of innate immunity receptors and production of proinflammatory proteins may deregulate the course of inflammation, leading to chronic diseases. In addition, the course of inflammation may be deregulated by endogenous proteins that undergo non-enzymatic transformations. The structure and function of such proteins are changed. They bind to receptors for advanced glycation end-products (RAGE) and are transported into the inflamed tissue, where they modify the host defense reaction [5,8]. Inflammation may also be modified by numerous environmental factors through activation of epigenetic processes that change the expression of genes in host cells. The biological machinery of this system comprises a variety of regulatory proteins including DNA methyltransferases, putative demethylases, methyl-CpG binding proteins such as MeCP2, histone-modifying enzymes and chromatin remodeling complexes [15]. One of the major epigenetic mechanisms is DNA cytosine methylation, which modulates many cellular events including developmental gene regulation, genome defense, and genomic imprinting [16]. Alterations in DNA methylation have been linked to human diseases such as cancer and several mental retardation disorders, suggesting an important role for DNA methylation in brain function [9]. The above-mentioned intrinsic programs and environmental factors that may modulate the human defense reaction require further study with respect to neuroinflammation such as that induced in the central nervous system (CNS) by viral infection. In the human brain, the defense response to viral infection is almost invariably associated with meningeal inflammation and sometimes with involvement of the spinal cord. Despite the diversity of viral causative agents, the reactions of the CNS are rather stereotyped and display similar morphological features in all forms of encephalitis [17]. However, the morphological changes vary both in the emphasis on one or another type of reaction and in their distribution through the cerebrospinal axis. Histologically, viral meningitis and the meningitic component of viral meningoencephalitis are characterized by sparse inflammatory cell infiltrates in the meninges and in the subarachnoid space. Histologic features of viral encephalitis include perivascular and parenchymal mononuclear cell infiltrates, glial cell reactions, and neuronal degeneration. The characteristic glial reaction to viral infection is formation of focal cell collections of "microglial nodules". The nodules are scattered throughout the brain gray and white matter, either in relation to dying neurons or independently of them. The cause of glial nodule formation and their function in viral infected brains are not well known; therefore, in the present study we paid special attention to such cell collections and their participation in above-mentioned mechanisms suspected to have a modulatory effect on inflammation.

Material and methods

Brain samples were obtained at autopsy of 24 patients with clinical diagnosis of viral meningoencephalitis. The clinical diagnosis was confirmed by neuropathological examination. Tissue samples were fixed in formalin and embedded in paraffin. For the purpose of the present study, brain paraffin blocks of patients were drawn from the archive (Table I) of the Medical Research Institute, Polish Academy of Sciences, Warsaw, Poland. These blocks contained six different brain regions (cerebellum, brain stem, spinal cord, and cerebral cortex of parietal, frontal and temporal lobes) of each patient and were cut into 5 µm thick serial sections. Sections were stained with cresyl violet for routine histological examination, and sections containing glial nodules were selected for immunohistochemical study.

The same procedures were employed to study brain sections of 22 control, age-matched patients who died suddenly because of non-neurological disorders, in whom no brain morphological lesions were found and no neurological symptoms were observed before they died.

The study was carried out according to the national ethics guidelines and legal regulations regarding the use of archival post-mortem material.

Table I. Groups of infected patients

Group of patients	Age	Number	Sex (F/M)	Brains with "glial nodules"
Neonates	2-7 ms	7	2/5	7/7
Children	1-3 ys	6	2/4	6/6
Teenagers	11-13 ys	5	4/1	4/5
Adults	55-57 ys	3	1/2	1/3
Aging	65-78 ys	3	2/1	0/3

ms – months of life, ys – years of age

Immunohistochemistry

Immunohistochemistry was performed using the avidin-biotin-peroxidase complex system, according to the manufacturer's recommendations (Vectastain Elite ABC Peroxidase Kit; Vector Laboratories).

Briefly, sections were dewaxed and hydrated through descending alcohols to water. For non-enzymatic antigen retrieval, some sections were heated in 0.01 M sodium citrate buffer (pH 6.0) to 95°C and allowed to cool for 20 min at room temperature and washed with PBS. Then, sections were incubated in methanol/3% H_2O_2 solution for 20 min to quench endogenous peroxidase. After being washed again in PBS and blocked with solution containing PBS/5% normal serum of goat, rabbit or mouse for 2 h at room temperature, sections were incubated overnight at 4°C in solutions of primary antibodies (Table II).

Immunoreactions were visualized using biotinylated secondary antibodies and ABComplex/HRP conjugate. All sections were lightly counterstained with Mayer's hematoxylin.

For negative controls, primary antibodies were replaced with an appropriate isotypic normal mouse, rabbit or goat immunoglobulin fraction at matched protein concentration. These were included for the examination of each specimen and consistently produced negative results.

Results

In brain specimens of all our patients affected by viral meningoencephalitis, the morphological chang-

Table II. Antibodies used in the study

Antigen name	Antigen origin	Antigen domain	Catalogue	Antibody type	Dilution
GFAP	human	n-terminus	sc-6171	polyclonal	1 : 50
GFAP	human	c-terminus	sc-6170	polyclonal	1 : 50
Ferritin	human	full length	DAKO	polyclonal	1 : 100
MeCP2	human	c-terminus	sc-5758	polyclonal	1 : 50
MeCP2	human	187-486 aa	sc-20700	polyclonal	1 : 50
MeCP2	human	n-terminus	sc-5755	polyclonal	1 : 50
TLR2	human	n-terminus	sc-8689	polyclonal	1 : 50
TLR3	mouse	extracellular	sc-23323	polyclonal	1 : 50
TLR4	human	c-terminus	sc-8694	polyclonal	1 : 50
TLR9	human	near n-term	sc-13215	polyclonal	1 : 50
RAGE	human	n-terminus	sc-8230	polyclonal	1 : 50
RAGE	human	c-terminus	sc-8229	polyclonal	1 : 50

sc – Santa Cruz, USA
GFAP – glial fibrillary acidic protein, ferritin – marker of microglial cells L, TLR – Toll-like receptor, MeCP2 – methyl-CpG binding protein 2, RAGE – receptors for advanced glycation end-products

es varied with the stage of the disease at which the patient died. Generally, in the early stage, the brain was infiltrated with small cells, and most of them appear to be lymphocytes and histiocytes, probably of microglial origin. These cells formed numerous focal "stars" or "microglial nodules". The nodules differed in size and cell density from a few up to 100 or more cells per nodule (Fig. 1). All such cell collections were strongly immunoreactive for methyl-CpG binding protein 2 (MeCP2) (Table III). MeCP2 immunopositive nodules were scattered throughout the cerebral gray (Fig. 2) and white matter (Fig. 3). Some nodules were seen in the close vicinity of dying nerve cells, suggesting that MeCP2 immunopositive cells of the nodules participated in neuronal degeneration and/or neuronophagia (Fig. 4). Corresponding to these lesions, prominent multifocal, MeCP2 immunopositive glial nodules were also observed in the cerebellar cortex (Table III). Generally, glial nodules were most numerous in brains of neonates, infants and teenagers (Table I), suggesting that young patients were more susceptible than adults to viral infection and died in the early period of the disease.

In the cerebellum of all infected patients, innate immunity receptors that recognize viral pathogens such as TLR3 and TLR9 were found. They were detected in the cytoplasm of Purkinje cells and, depending on the virus type which caused infection of the patient, in some patients these cells were immunopositive for TLR3 and in others for TLR9 (Fig. 5).

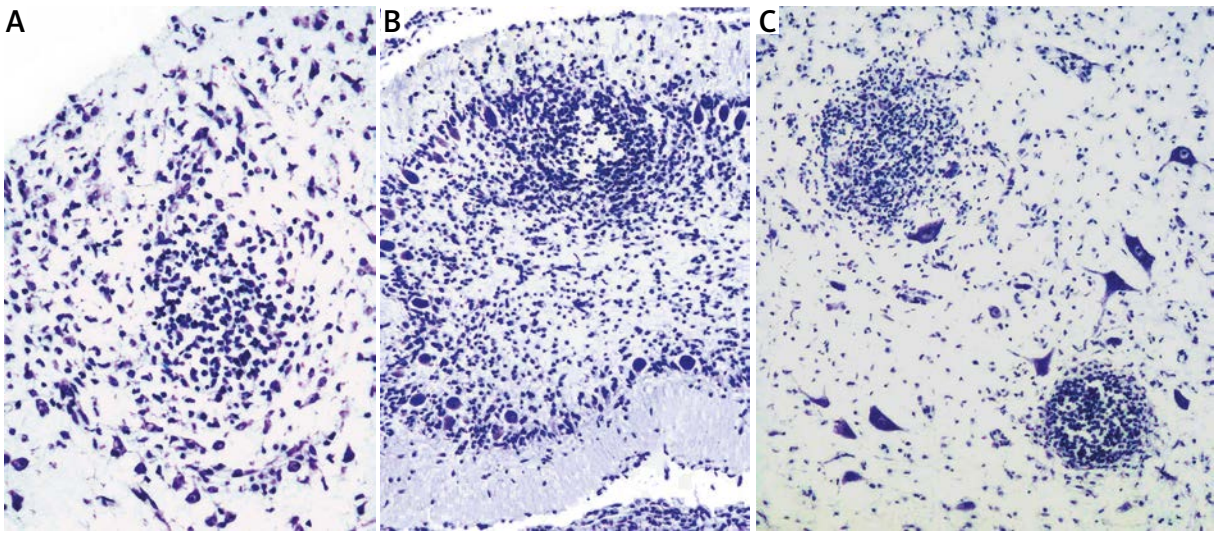

Fig. 1. Different size and cell density of microglial nodules in patients with viral meningoencephalitis (cresyl violet, 500×). **A)** Microglial nodule in the cerebral cortex gray matter of a 2-year-old patient. **B)** Microglial nodule in the cortex of the cerebellum of a 2-month-old infant. **C)** Microglial nodule in the ventral horn of the spinal cord of a 55-year-old patient.

Table III. Antigens in "glial nodules" detected by antibodies used in the study

Antigens	Localization of nodules in the brain			
	cerebral cortex	brain white matter	Purkinje cell degeneration	neuronophagia in spinal cord
GFAP	–	–	–	–
MeCP2	+	+	+	+
TLR2	–	–	–	–
TLR3	–	–	–	–
TLR4	–	–	–	–
TLR9	–	–	–	–
RAGE	–	–	–	–

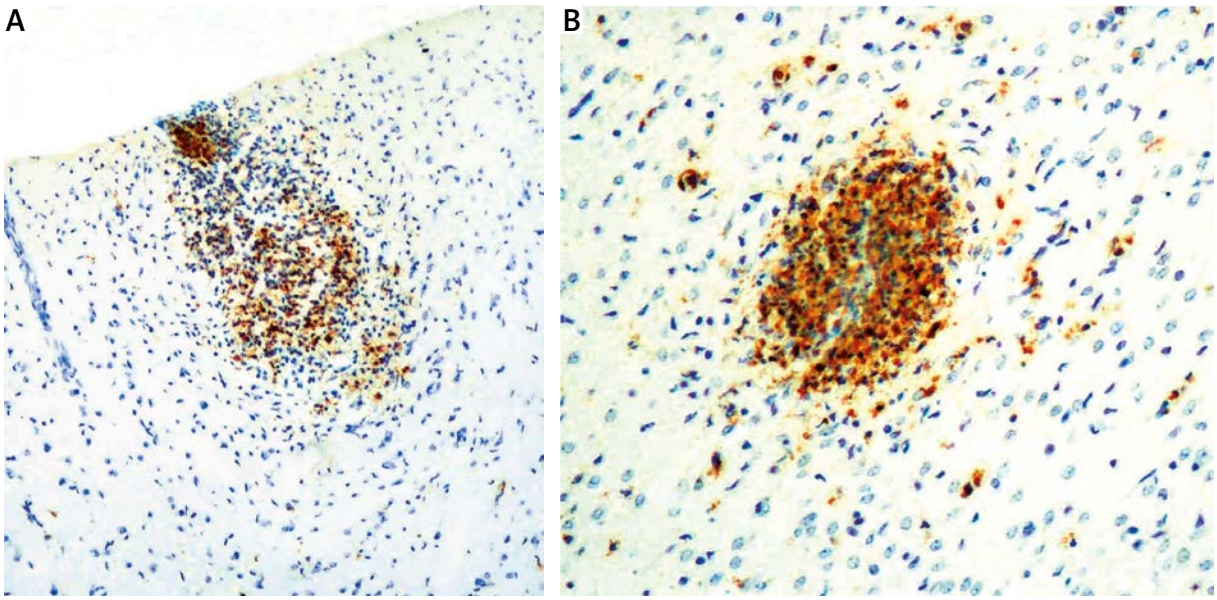

Fig. 2. Methyl-CpG binding protein (MeCP2) detected in immunopositive cells of glial nodules localized in gray matter of the cerebral cortex of patients with viral meningoencephalitis (immunostaining with diaminobenzidine/cresyl violet 350×). **A)** Nodule in the brain of a 2-year-old patient. **B)** Nodule in the brain of a 12-year-old patient.

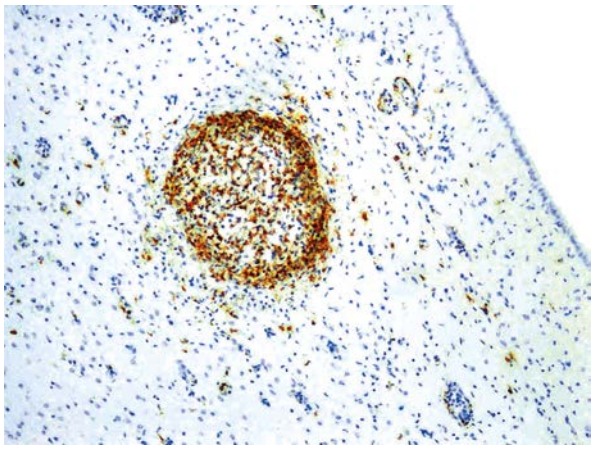

Fig. 3. Methyl-CpG binding protein (MeCP2) detected in immunopositive cells of glial nodules localized in white matter of periventricular area of the brain of a 2-year-old patient with viral meningoencephalitis (immunostaining with diaminobenzidine/cresyl violet 350×).

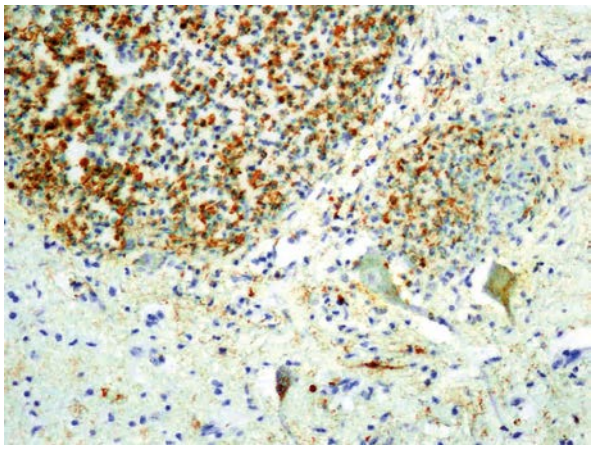

Fig. 4. Methyl-CpG binding protein (MeCP2) detected in immunopositive cells of glial nodules localized in the vicinity of degenerating nerve cells of the ventral horn of the spinal cord in a 55-year-old patient (immunostaining with diaminobenzidine/cresyl violet 500×).

Such immunoreactivity was observed only in cells with no signs of degeneration, suggesting that in these cells, the process of degeneration could be initiated following recognition of the viral pathogen. In no brain regions were there detected TLR2 and TLR4 receptors that recognize bacterial pathogens. Thus we suspect that bacterial infections were not involved in the process of meningoencephalitis observed in our patients.

In addition, in our adult patients, the inflammatory process could also be modulated by ligands of RAGE receptors, because we found numerous foci of immunoreactivity to RAGE in brain areas with widespread tissue necrosis (Fig. 6A), in hypertrophied gli-

al cells (Fig. 6B) and in cells localized in the vicinity of blood vessels (Fig. 6C).

Discussion

Most viral infections of the CNS are potentially serious complications of systemic infections caused by common viral agents. Thus, the initial infection may be acquired through the gastrointestinal tract, respiratory tract, genital tract, percutaneous inoculation, or by transplacental passage. Depending on the particular virus, several pathways are at least potentially available for access to the CNS. Regardless of the route of entry to the CNS, infection with neurotropic viruses activates innate immune responses of macrophages that release proinflammatory cytokines [7]. The brain inflammatory reactions to viral infection tend to be similar in all forms of encephalitis and almost constant are microglial hyperplasia and proliferation [17]. Characteristic for this reaction are also clusters of cells commonly termed "microglial nodules". Microglial nodules are a well-known phenomenon in viral encephalitis, and we observed them most often in the early period of the disease. In the brains of our young patients, nodules were identified in the absence of leukocyte infiltration, tissue necrosis and astrogliosis. In cells of the nodules we found MeCP2 protein, which is an important factor of epigenetic mechanisms. This result suggests that cells of nodules are involved in the process of viral deregulation of the host defense reaction. In previous studies, authors have found MeCP2 to be abundantly expressed in neurons and reported that this protein functions as both a transcriptional suppressor and an activator [3,12,13,20]. Although information concerning the relationship between viral infection and MeCP2 is limited, several investigations have been reported. Thus, it was found that MeCP2 binds to the latency-associated nuclear antigen (LANA) of Kaposi sarcoma-associated herpesvirus [11], and that MeCP2 was detected in viral infected glial cells [18]; however, the role of MeCP2 in deregulation of the host inflammatory response following viral infection was not considered.

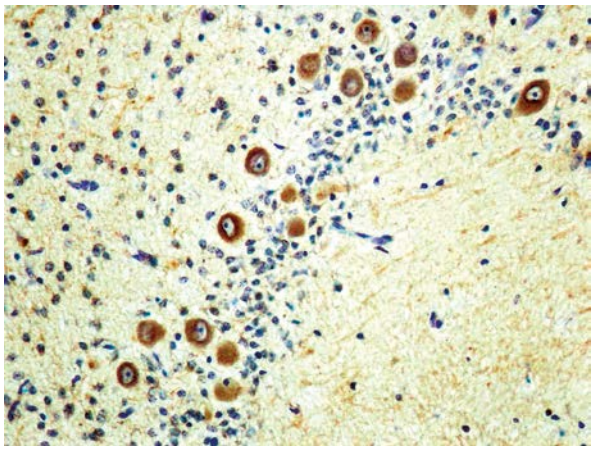

Fig. 5. Immunohistochemical detection of Toll-like receptor 3 (TLR3) protein in cytoplasm of Purkinje cells in the cerebellum of a 2-month-old infant with viral meningoencephalitis (immunostaining with diaminobenzidine/cresyl violet 350×).

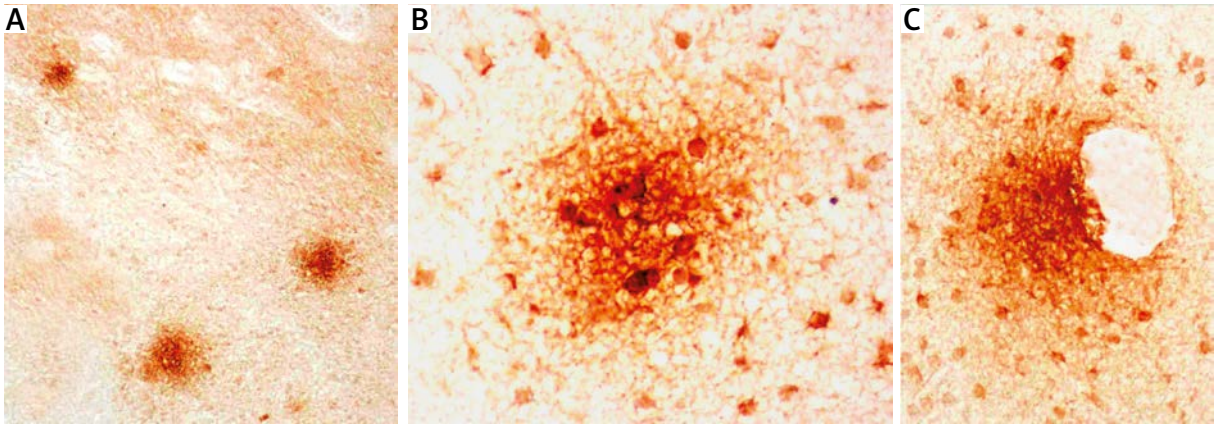

Fig. 6. Immunohistochemical detection of RAGE protein in the brain of a 75-year-old patient with viral meningoencephalitis (immunostaining with diaminobenzidine). **A)** Focal immunoreactivity to RAGE in white matter of the brain (350×). **B)** RAGE immunopositive hypertrophied glial cells (500×). **C)** Perivascular localization of RAGE immunoreactive cells (500×).

In the later, more advanced period of viral meningoencephalitis, activated microglia can secrete a variety of pro-inflammatory and neurotoxic factors that are necessary to destroy invading pathogens, but these factors can also induce apoptosis of host cells. Additionally, microglia activation is thought to be a causative factor in many neurological diseases, including viral encephalitis [6]. Viruses can injure neurons in a number of ways, including direct killing and induction of apoptosis. Neurotropic viruses can induce neuronal dysfunction of specific neuronal populations, leading to life-threatening consequences for the host [1]. The results of our study suggest that in viral meningoencephalitis, Purkinje cells of the human cerebellum possess one more pathway to neurodegeneration, because we found in their cytoplasm TLR3 or TLR9 receptors that may directly recognize viral pathogens and initiate production of proinflammatory factors.

In the brain of adult and aging patients with viral meningoencephalitis we detected numerous RAGE immunopositive blood vessels and hypertrophied astroglial cells. Specific ligands for this receptor are normal endogenous proteins that spontaneously undergo non-enzymatic transformations, which change their structure and function [5,8]. Accumulation of such proteins, termed advanced glycation end-products (AGE), is characteristic of aging, but accelerated accumulation was observed in different neurological disorders as well. The increased activation of RAGE was observed following oxidative stress, immune and/or inflammatory responses, and upon altered cell functions, suggesting that AGE accumulation also occurs during these processes. Engagement of RAGE introduces transformed proteins into inflamed tissue, modifying the host defense reaction, and induces the release of pro-inflammatory cytokines and free radicals, thus perpetuating a cycle of damage.

In summary, the results of our study suggest that depending on the period of the viral meningoencephalitis, the process of inflammation in CNS may be deregulated by various mechanisms, in which TLR3, TLR9, RAGE and MeCP2 proteins participate. Moreover, for the first time we document that cells collected in glial nodules contain the protein MeCP2, and therefore these cells may play an important but still unknown role in the host defense reaction following viral infection.

Disclosure

Authors report no conflict of interest.

References

1. Amor S. Virus infections of the central nervous system. In: Mansons' Tropical Diseases. Cook G, Zumla A (eds.). Sounders Elsevier, London 2008; pp. 853-883.
2. Beutler B. Inferences, questions and possibilities in Toll-like receptor signaling. Nature 2004; 430: 257-263.
3. Chahrour M, Jung SY, Shaw C, Zhou X, Wong ST, Qin J, Zoghbi HY. MeCP2, a key contributor to neurological disease, activates and repress transcription. Science 2008; 320: 1224-1229.
4. Cuenca AG, Wynn JL, Moldawer LL, Levy O. Role of innate immunity in neonatal infection. Am J Perinatol 2013; 30: 105-112.
5. Donato R. RAGE: A single receptor for several ligands and different cellular responses: the case of certain S 100 proteins. Curr Mol Med 2007; 7: 711-724.
6. Ghoshal A, Das S, Ghosh S, Mishra MK, Sharma V, Koli P, Sen E, Basu A. Proinflammatory mediators released by activated microglia induces neuronal death in Japanese encephalitis. Glia 2007; 55: 483-496.
7. Hanke ML, Kielian T. Toll-like receptors in health and disease in the brain: mechanisms and therapeutic potential. Clin Sci (Lond) 2011; 121: 367-387.
8. Hori O, Brett J, Slattery T, Cao R, Zhang J, Chen JX, Nagashima M, Lundh ER, Vijay S, Nitecki D. The receptor for advanced glycation end products (RAGE) is a cellular binding sites for amphoterin. Mediation of neurite outgrowth and co-expression of rage and amphoterin in the developing nervous system. J Biol Chem 1995; 270: 25752-25761.
9. Jaenisch R, Bird A. Epigenetic regulation of gene expression: how the genome integrates intrinsic and environmental signals. Nat Genet 2003; 33 Suppl: 245-254.
10. Kawai T, Akira S. Toll-like receptors and their crosstalk with other innate receptors in infection and immunity. Immunity 2011; 34: 637-650.
11. Krithivas A, Fujimuro M, Weidner M, Young DB, Hayward SD. Protein interactions targeting the latency-associated nuclear antigen of Kaposi's sarcoma-associated herpesvirus to cell chromosomes. J Virol 2002; 76: 11506-11604.
12. Nan X, Campoy FJ, Bird A. MeCP2 is a transcriptional repressor with abundant binding sites in genomic chromatin. Cell 1997; 88: 471-481.
13. Nan X, Ng HH, Johnson CA, Laherty CD, Turner BM, Eisenman RN, Bird A. Transcriptional repression by the methyl-CpG-binding protein MeCP2 involves a histone deacetylase complex. Nature 1998; 393: 386-389.
14. Perry AK, Chen G, Zheng D, Tang H, Cheng G. The host type I interferon response to viral and bacterial infections. Cell Res 2005; 15: 407-442.
15. Robertson KD, Wolffe AP. DNA methylation in health and disease. Nat Rev Genet 2000; 1: 11-19.
16. Rodríguez-Dorantes M, Téllez-Ascencio N, Cerbón MA, López M, Cervantes A. DNA methylation: an epigenetic process of medical importance. Rev Invest Clin 2004; 56: 56-71.

17. Schochet SS. Infectious Diseases. In: Clinical Neurosciences. Rosenberg RN (ed.). Churchill Livingston, New York, Edinburgh, London, Melbourne 1983; sec III; pp. 195-240.
18. Shirai S, Takahashi K, Kohsaka S, Tsukamoto T, Isogai H, Kudo S, Sawa H, Nagashima K, Tanaka S. High expression of MeCP2 in JC virus-infected cells of progressive multifocal leukoencephalopathy brains. Neuropathology 2011; 31: 38-41.
19. Trinchieri G, Sher A. Cooperation of Toll-like receptor signals in innate immune defence. Nat Rev Immunol 2007; 7: 179-190.
20. Yasui DH, Peddada S, Bieda MC, Vallero RO, Hogart A, Nagarajan RP, Thatcher KN, Farnham PJ, Lasalle JM. Integrated epigenomic analyses of neuronal MeCP2 reveal a role for long-range interaction with active genes. Proc Natl Acad Sci U S A 2007; 104: 19416-19421.

Original article

Folia Neuropathologica

Mitofusin 2 expression dominates over mitofusin 1 exclusively in mouse dorsal root ganglia – a possible explanation for peripheral nervous system involvement in Charcot-Marie-Tooth 2A

Maria Kawalec[1], Barbara Zabłocka[1], Dagmara Kabzińska[2], Jacek Neska[1], Małgorzata Beręsewicz[1]

[1]Molecular Biology Unit, Mossakowski Medical Research Centre, Polish Academy of Sciences, Warsaw, [2]Neuromuscular Unit, Mossakowski Medical Research Centre, Polish Academy of Sciences, Warsaw, Poland

Folia Neuropathol 2014; 52 (4): 436-442 DOI: 10.5114/fn.2014.47845

Abstract

Mitofusin 2 (Mfn2), a protein of the mitochondrial outer membrane, is essential for mitochondrial fusion and contributes to the maintenance and operation of the mitochondrial network. Mutations in the mitofusin 2 gene cause axonal Charcot-Marie-Tooth type 2A (CMT2A), an inherited disease affecting peripheral nerve axons. The precise mechanism by which mutations in MFN2 selectively cause the degeneration of long peripheral axons is not known. There is a hypothesis suggesting the involvement of reduced expression of a homologous protein, mitofusin 1 (Mfn1), in the peripheral nervous system, and less effective compensation of defective mitofusin 2 by mitofusin 1. We therefore aimed to perform an analysis of the mitofusin 1 and mitofusin 2 mRNA and protein expression profiles in different mouse tissues, with special attention paid to dorsal root ganglia (DRGs), as parts of the peripheral nervous system. Quantitative measurement relating to mRNA revealed that expression of the Mfn2 gene dominates over Mfn1 mainly in mouse DRG, as opposed to other nervous system samples and other tissues studied. This result was further supported by Western blot evaluation. Both these sets of data confirm the hypothesis that the cellular consequences of mutations in the mitofusin 2 gene can mostly be manifested in the peripheral nervous system.

Key words: *mitofusins, peripheral nervous system, CMT2A, Mfn2 mutation manifestation.*

Introduction

Defects in mitochondrial dynamics – mitogenesis, mitophagy and fission/fusion events – are thought to underlie a variety of disorders in humans, such as metabolic diseases (diabetes, hypertension) and neuronal disorders (Parkinson's disease, Alzheimer's disease and Charcot-Marie-Tooth disease [CMT]) [2,4, 7,8,11,16,20]. One of the earliest indicators of a role for abnormal mitochondrial dynamics in neurological diseases derives from the analysis of genetic mutations leading to CMT, i.e. a group of inherited diseases affecting peripheral nerves [21].

Charcot-Marie-Tooth diseases can be caused by several different mutations in various genes in which an unusual number of mutations occur in mitochondrial-associated proteins, including proteins involved in the regulation of mitochondrial dynamics (e.g. mitofusin 2 [Mfn2] and ganglioside-induced differentiation-associated protein 1 [GDAP1]). For example,

Communicating author:

Małgorzata Beręsewicz, PhD, Molecular Biology Unit, Mossakowski Medical Research Centre, Polish Academy of Sciences, Warsaw, Poland, e-mail: mberesewicz@imdik.pan.pl

a large subset of patients with CMT type 2A (CMT2A) have been found to manifest mutations in the mitofusin 2 gene.

While disease-associated mutations in *MFN2* are seen to lead to abnormal formation of mitochondrial networks in peripheral nerve axons [14], the precise cellular physiological mechanisms underlying the CMT2A pathology are still poorly understood. One puzzling aspect of CMT2A is that symptoms are restricted to very specific tissues or cell types, despite the fact that mutant *MFN2* alleles are expressed in every cell [10]. Hence, one of the hypotheses explaining this problem holds that the axonal neuropathy manifestations of CMT2A could be due to impaired expression of homologous protein – mitofusin 1 (MFN1) – in the peripheral nervous system as compared with other tissues, as well as less effective compensation for defective mitofusin 2 by mitofusin 1 [9,10,18].

Mitofusins 1 and 2 are mitochondrial GTPases, implicated in the tethering of adjacent outer mitochondrial membranes (OMMs) through the formation of homo- or heterodimers [5]. Murine Mfn1 and Mfn2 are approximately 63% identical at the amino acid level, and in several contexts they exhibit functional overlap or complementation in the mediation of OMM fusion [23]. However, there is growing evidence to indicate differences in function. Since Mfn1 knockout has presented more severe aberrations in mitochondrial network formation than Mfn2-deficient cells, Mfn1 is considered to have stronger fusion activity [19]. Moreover, it is suggested that fusion of outer and inner mitochondrial membranes mainly entails Mfn1 [12]. On the other hand, Mfn2, rather than Mfn1, is present on the endoplasmic reticulum (ER), tethering it to mitochondria facilitating calcium flux and autophagy [9,23]. Finally, Mfn2 seems to have some regulatory effect on the cell cycle extending beyond its fusion activity, with impaired expression seemingly correlating with insulin resistance and hyperproliferation in hypertension [23].

In the current study seeking to verify the hypothesis regarding a low level of MFN1 in peripheral nerves as an additional factor responsible for axonal neuropathy manifestation in CMT2A, we aimed to analyse both the mRNA and protein expression profiles regarding Mfn1 and 2 in different mouse tissues, paying special attention to the dorsal root ganglia as parts of the peripheral nervous system [12].

Material and methods

Animals

All animal procedures were conducted in accordance with instructions from the Local Commission for Ethics of Experiments on Animals, with every effort being made to minimise animal suffering and the number of animals needed for reliable scientific data to be obtained. Adult C57BL/6 mice obtained from the Animal House of the Mossakowski Medical Research Centre, Polish Academy of Sciences, were decapitated under deep anaesthesia, with subsequent dissecting out of the dorsal root ganglia (DRG), cerebral cortex, cerebellum, spinal cord, heart, muscle (*quadriceps femoris*), liver, and kidney, as well as a fragment of skin. Tissues were frozen and then crushed into a fine powder under liquid nitrogen, portioned for both protein and mRNA expression analysis and stored at –80°C until used. Due to the small amount of material, DRGs were homogenised immediately after dissection, with neither the freezing nor the crushing in liquid nitrogen steps. Hence, in the case of DRGs, at least three mice were used for gene expression studies and another three for protein detection.

Gene expression

RNA from freshly dissected DRGs was isolated using a Qiagen RNeasy Micro Kit (74004), while isolations from fatty tissues (such as kidney and liver) and other tissues were performed using a Qiagen RNeasy Lipid Tissue Mini Kit (74804) and Qiazol Lysis Reagent (Qiagen, 79306) respectively. RNA samples were subjected to DNase I digestion (Thermo Scientific, EN0521) to remove genomic DNA, and then cleaned using a Thermo Scientific Gene Jet RNA Purification Kit (K0731). For RT-PCR, a First Strand cDNA Synthesis Kit (Thermo Scientific, K1612) was used. Quantitative real-time PCR was then performed, the TaqMan primers and probes (from Life Technologies) being: Gene expression assay Mm00612599_m1 for Mfn1; FAM; Gene expression assay Mm00500120_m1 for Mfn2; FAM; Gene expression assay Mm03928990_g1 for 18s ribosomal RNA; VIC. 18s RNA was used as an internal control. Results were calculated automatically using the $\Delta\Delta$Ct method, presented by reference to the relative expression of Mfn1 and Mfn2, and shown as the Mfn1/Mfn2 ratio ± standard deviation (Fig. 1A). For particular samples from the nervous system the

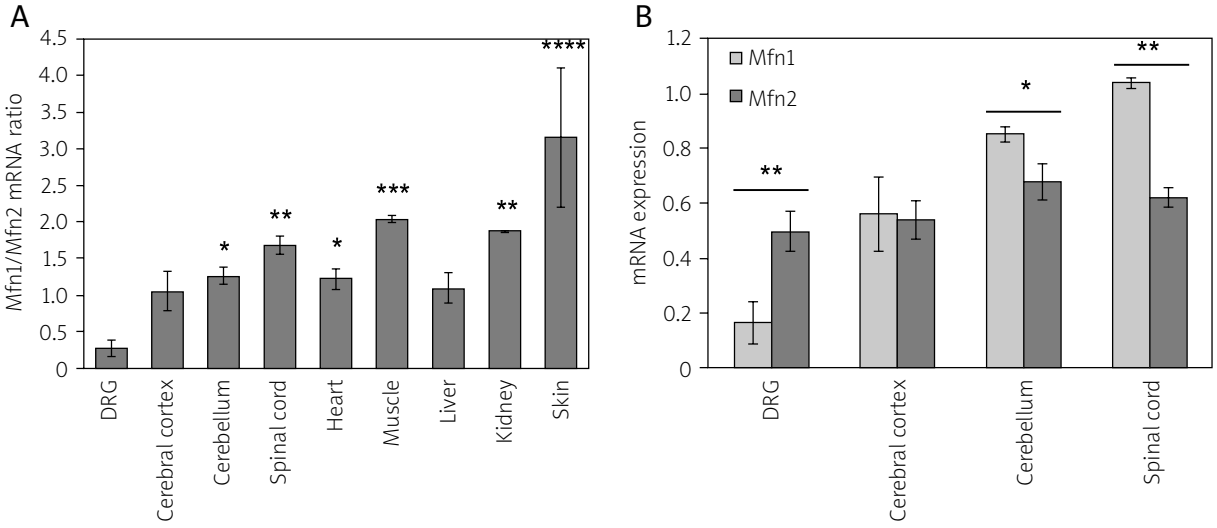

Fig. 1. Comparative analysis of Mfn1 and Mfn2 mRNA expression in different mouse tissue revealed that mitofusin 2 expression only prevails over that of mitofusin 1 in dorsal root ganglia (DRG). In DRG samples the Mfn1/Mfn2 ratio gave an average value of 0.27 ± 0.08, indicating Mfn2 expression three times greater than that of Mfn1. Real-time PCR results were calculated using the ΔΔCt method and are presented **(A)** as means for the Mfn1 to Mfn2 mRNA ratio ± standard deviations (*$p < 0.05$, **$p < 0.01$, ***$p < 0.001$, ****$p < 0.0001$ vs. DRG) and **(B)** as relative values of Mfn1 and Mfn2 mRNA expression (*$p < 0.05$, **$p < 0.01$). Statistical significance was determined using one-way ANOVA with the Bonferroni test in 1A or Student's *t*-test in 1B.

relative expression of both Mfn1 and Mfn2 mRNA is presented as mean mRNA expression ± standard deviation (Fig. 1B).

SDS-PAGE and immunodetection

Tissue powder and freshly dissected DRGs were homogenized in lysis buffer containing 20 mM Tris-HCl at pH 7.5, 150 mM NaCl, 1 mM Na_2EDTA, 1 mM EGTA, 1% Triton X-100, 2.5 mM sodium pyrophosphate, 1 mM β-glycerophosphate, 1 mM Na_3VO_4, 1 µg/ml leupeptin and 1 mM PMSF (Cell Signalling, 9803). Following homogenisation, samples were sonicated and centrifuged at 14 000 × g at 4°C for 10 min so that clear tissue lysates were obtained. 20 µg portions of these were separated by electrophoresis on 10% SDS-polyacrylamide gels, before being transferred to nitrocellulose membrane (Healthcare Life Sciences, RPN203E GE). Blots were blocked for 1 hour in TBS-T (10 mM Tris-HCl, pH 7.5, 150 mM NaCl, 0.05% Tween 20) containing 5% skimmed milk, and then incubated for 2 hours with primary antibodies against mitofusin 1 (mouse monoclonal) and mitofusin 2 (rabbit polyclonal) (Sigma Aldrich, WH0055669M4, M6319, 1 : 500 and 1 : 1000 respectively), as well as against glyceraldehyde-3-phosphate dehydrogenase (GAPDH, Chemicon, MAB374, 1 : 1000), to verify the equal loading of protein per lane. Secondary antibodies conjugated with horseradish peroxidase were visualized using a chemiluminescent kit (Bio-Rad 170-5061), in line with the manufacturer's protocol. To confirm anti-Mfn1 and anti-Mfn2 antibody specificity, mouse embryonic fibroblast (MEF) lysates were also loaded onto each gel (wild type MEF [MEFwt] and Mfn1/Mfn2-null MEFs [$MEF^{Mfn1-/-Mfn2-/-}$], as positive and negative controls, respectively). In order to present the results graphically, densitometric analysis of Western blots was performed using Gel Expert Image analysis software (Nucleo Vision). Obtained values for Mfn1 and Mfn2 were normalized to values of Mfn1 and Mfn2 from wild type MEF respectively and presented in terms of the relative expression of Mfn1 versus Mfn2, i.e. as the Mfn1/Mfn2 ratio ± standard deviation.

Statistical analysis

The statistical significances of Mfn1/Mfn2 ratios were determined using one-way ANOVA with the Bonferroni test for simultaneous analysis of multiple test groups (Figs. 1A and 2B). Student's *t*-test was used to evaluate the statistical significance of dif-

ferences between Mfn1 and Mfn2 mRNA expression in particular tissues (Fig. 1B). Data are presented as means ± standard deviations. The differences are considered significant where $p < 0.05$.

Results

Mitofusin 2 mRNA expression dominates over that of mitofusin 1 in dorsal root ganglia

Real-time PCR showed that values for the Mfn1 to Mfn2 mRNA ratio were substantially lower in dorsal root ganglia than in other samples from the nervous system (cerebral cortex, cerebellum and spinal cord), as well as other tested organs (heart, muscle, liver, kidney and skin) (Figs. 1A and 1B). In the DRG samples the Mfn1/Mfn2 ratio was 0.27 ± 0.08, which is to say that expression of Mfn2 was at a level three times higher than that of Mfn1. In contrast, in the cerebral cortex, cerebellum and spinal cord samples, Mfn1/Mfn2 ratios were 1.05 ± 0.27, 1.26 ± 0.12 and 1.67 ± 0.12 respectively, indicating similar intensities of expression of the two mitofusins in the cerebral cortex, as well as a dominance of Mfn1 over Mfn2 in the cerebellum and spinal cord (Fig. 1A). The Mfn1/Mfn2 ratios in the cases of non-nervous-system tissues were above 1, the average values being: heart: 1.22 ± 0.14, muscle: 2.04 ± 0.05, liver: 1.10 ± 0.20, kidney: 1.87 ± 0.01 and skin: 3.15 ± 0.95. This indicates similar levels of expression of the two mitofusins in heart and liver, and marked dominance of Mfn1 expression in muscle, kidney and skin.

Moreover, comparison of Mfn1 and Mfn2 mRNA expression – in particular in samples from the nervous system (the DRG, cerebral cortex, cerebellum and spinal cord) – made it clear that Mfn1 expression in the nervous system varies significantly ($p < 0.01$ DRG vs. cerebral cortex, cerebellum and spinal cord; $p < 0.05$ cerebral cortex vs. cerebellum and spinal cord; $p < 0.05$ cerebellum vs. spinal cord) – and much more so than that of Mfn2, whose expression was comparable between the samples (the one-way ANOVA followed by the Bonferroni test revealing no significant differences) (Fig. 1B).

Lower protein level of Mfn1 than Mfn2 in dorsal root ganglia

Western blot evaluation for the two mitofusins suggests differing Mfn1/Mfn2 ratios in various mouse tissues that were consistent with the mRNA expression ratios (Fig. 2). In DRG the protein Mfn1/Mfn2 ratio was 0.87 ± 0.18, indicating a lower level of Mfn1 than of Mfn2 there (Fig. 2B). As with the dorsal root ganglia, so in the muscle sample an Mfn1/Mfn2 ratio below 1 was detected, the values being 0.75 ± 0.04. In the case of other tissues, the protein Mfn1/Mfn2 ratio was found to be equal to or above 1, with average values of: 1.36 ± 0.04 for cerebral cortex, 1.30 ± 0.04 for cerebellum, 1.30 ± 0.26 for spinal cord, 1.27 ± 0.04 for heart, 0.93 ± 0.1 for liver, 1.02 ± 0.16 for kidney and 2.12 ± 0.20 for skin. Furthermore, in the cases of muscle and skin samples in particular, Western blots revealed an additional, higher molecular weight band detected with the anti-Mfn2 antibody (Fig. 2A).

Discussion

Mutations in the *MFN2* gene cause axonal Charcot-Marie-Tooth type 2A disease affecting long peripheral axons [22]. While it is already well known that disease-associated mutations in the mitofusin 2 gene lead to abnormal formation of mitochondrial networks [10], as well as disrupting mitochondrial transport [1,13] and ER-mitochondrial interactions, the precise pathomechanism of CMT2A has remained poorly understood. One of the still-unsolved aspects of CMT2A is the way in which symptoms of this disease are limited to very specific tissues or cells, despite the fact that the mutant *MFN2* alleles are expressed in every cell. It is on this basis that one hypothesis (proposed by Detmer *et al.*) suggests that it is predominantly peripheral nerves that are affected in CMT2A patients, because they express low levels of MFN1 and rely primarily on MFN2 [10], which is mutated, malfunctioned and insufficient for the proper fusion process among patients with CMT2A. To elucidate this issue further, we analysed the mRNA expression of Mfn1 and Mfn2 in various mouse tissues, paying special attention to the dorsal root ganglia as parts of the peripheral nervous system. In parallel, Western blot analysis was performed to evaluate the mitofusins protein profile.

Quantitative PCR revealed that values for the Mfn1 to Mfn2 mRNA ratio were substantially lower in DRG than in other tissues. This phenomenon was not observed in other tissues, Mfn1 mRNA being expressed abundantly, especially in spinal cord as well as in muscle, kidney and skin. While a few studies comparing the expression profiles for the two mitofusins in different tissues have been published

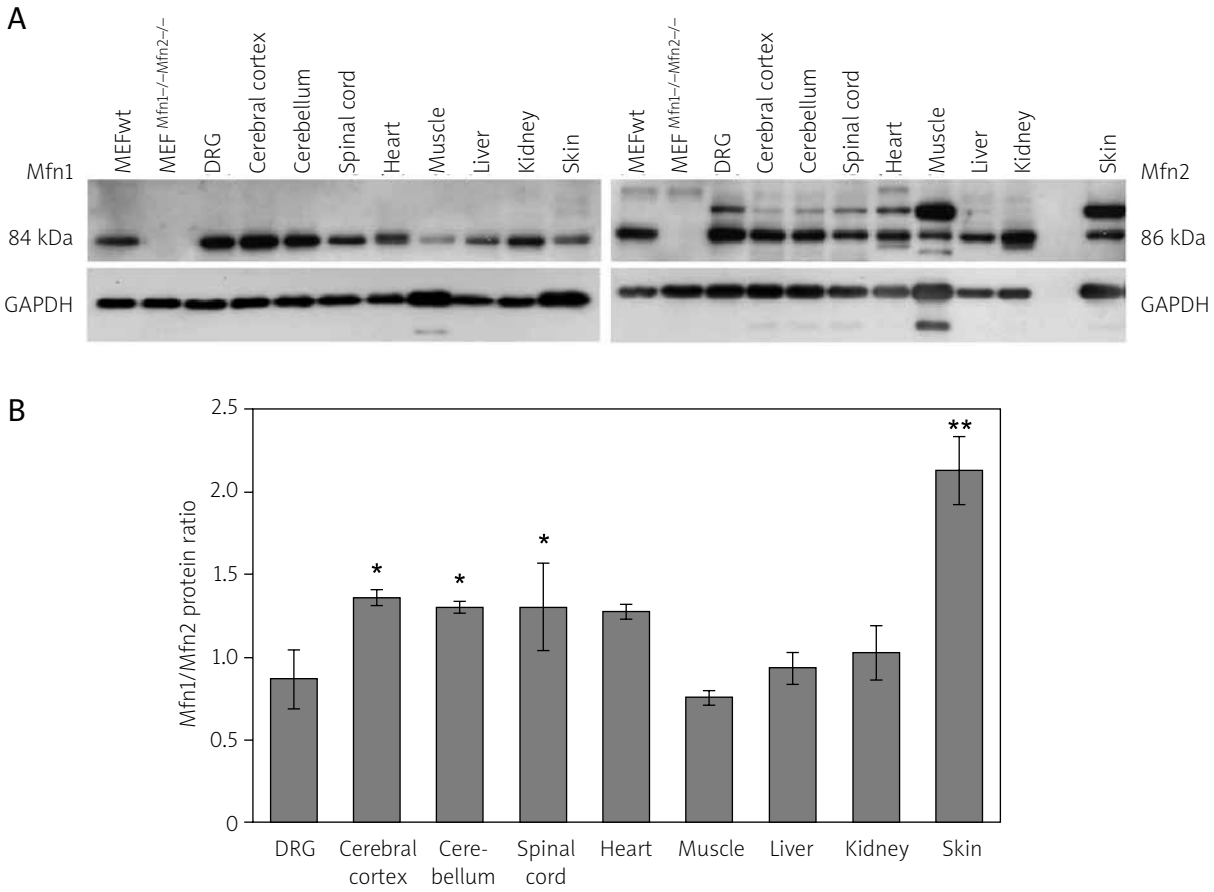

Fig. 2. Comparison of Mfn1 and Mfn2 immunoreactivity suggests a slightly lower level of Mfn1 than Mfn2 in dorsal root ganglia (DRG). **A)** Tissue lysates (20 µg) from different mouse tissue were loaded on 10% polyacrylamide gel and analysed with anti-Mfn1 (84 kDa) and anti-Mfn2 (86 kDa) antibodies by Western blot. To confirm anti-Mfn1 and anti-Mfn2 antibody specificity, mouse embryonic fibroblast (MEF) lysates were also loaded onto gel (wild type MEF [MEFwt] and Mfn1/Mfn2-null MEFs [$MEF^{Mfn1-/-Mfn2-/-}$]), as positive and negative controls. GAPDH immunoreactivity was assayed for loading control. Immunoblots shown are representative of at least three independent experiments. **B)** Quantitative analysis of Western blot bands normalized to Mfn1 or Mfn2 in MEFwt and expressed as the relative immunoreactivity of Mfn1 vs. Mfn2 (Mfn1/Mfn2 ratio). Results are presented as means ± standard deviations; *$p < 0.05$, **$p < 0.01$ vs. DRG.

previously, these have never included an analysis of the peripheral nervous system [19]. For example, a Northern blot analysis showed that Mfn1 transcripts could be detected at similar levels in a variety of human tissues and were elevated intensely in the heart, while Mfn2 mRNA was expressed abundantly in heart and muscle tissue, but only present at low levels in many other tissues [19]. In addition, Cao *et al*. (2013) detected the presence of equal amounts of the two mitofusins in rat spinal cord [3].

To recap, the data for mRNA expression offer quite firm evidence of axonal damage to peripheral nerves in CMT2A being due to inadequate compensation for dysfunctional MFN2 by MFN1, which is fully functional, but not expressed at a sufficient level.

In our study, the comparative evaluation of Mfn1 and Mfn2 protein expression in different mouse tissues suggests lower protein expression for Mfn1 as compared with Mfn2 in the DRG, as well as levels of mitofusin 1 higher than those of mitofusin 2 in the cerebral cortex, cerebellum and spinal cord. Similarly, Mfn1 seems to dominate over Mfn2 in skin and heart tissue. Unexpectedly, the estimated ratio of Mfn1/Mfn2 proteins in muscle is seen to be as low as in the dorsal root ganglia, suggesting a higher level of Mfn2 protein there. The significance of this

observation is unclear, but it is tempting to speculate that over-expression of Mfn1 mRNA is not fully translated to protein, or regulated in a special manner. It is worth noting that in the case of muscle tissue an additional, higher than 86 kDa, dense band was detected in the Western blot by the anti-Mfn2 antibody. A similar band pattern is visible in the skin sample, which may suggest muscle-cell content or a similar modification pattern for Mfn2 protein in various cell types. A parallel fine band is also visible in DRG and heart samples, which suggests a common level for the two forms of Mfn2 protein. It has been reported that mitofusin 2 binds to MARCH-V – mitochondrial ubiquitin ligase – and may possibly undergo ubiquitylation [15]. There are also data regarding Mfn2 phosphorylation [6]. These post-translational modifications increase molecular mass and can alter cellular localisation and protein function. It is possible that Mfn2 plays additional roles in skeletal muscle cells, e.g. in calcium signalling, trafficking or selective mitophagic elimination of damaged mitochondria, as was described recently for heart tissue, through mechanisms requiring the mitochondrial kinase PINK1 and the cytosolic ubiquitin ligase Parkin [6]. Similarly, it has been reported that Mfn1 may be a ubiquitylation substrate, undergoing modification that in this case is necessary for proper mitochondrial network formation [17].

Although the progress in understanding the molecular machinery and role of mitofusins in mitochondrial dynamics and the regulation of mitochondrial metabolism is notable, several issues regarding mitofusin 2 function and its relationship with mitofusin 1 remain poorly understood. First, the extent to which there is complementation among mitofusins is unclear. Are they functionally interchangeable? Second, the correlation between mitochondria and neuromuscular junction formation and function remains unknown. The existence of unresolved questions of this magnitude points to the significance of the topic and the necessity for additional studies.

Acknowledgments

The project was supported by NSC grant NN 4024 74640.

Disclosure

Authors report no conflict of interest.

References

1. Baloh RH, Schmidt RE, Pestronk A, Milbrandt J. Altered axonal mitochondrial transport in the pathogenesis of Charcot-Marie-Tooth disease from mitofusin 2 mutations. J Neurosci 2007; 27: 422-430.
2. Beal MF. Mitochondria take center stage in aging and neurodegeneration. Ann Neurol 2005; 58: 495-505.
3. Cao Y, Lv G, Wang YS, Fan ZK, Bi YL, Zhao L, Guo ZP. Mitochondrial fusion and fission after spinal sacord injury in rats. Brain Res 2013; 1522: 59-66.
4. Chan PH. Mitochondria and neuronal death/survival signaling pathways in cerebral ischemia. Neurochem Res 2004; 29: 1943-1949.
5. Chen H, Detmer SA, Ewald AJ, Griffin EE, Fraser SE, Chan DC. Mitofusins Mfn1 and Mfn2 coordinately regulate mitochondrial fusion and are essential for embryonic development. J Cell Biol 2003; 160: 189-200.
6. Chen Y, Dorn GW. PINK1-phosphorylated mitofusin 2 is a Parkin receptor for culling damaged mitochondria. Science 2013; 340: 471-475.
7. Cho DH, Nakamura T, Lipton SA. Mitochondrial dynamics in cell death and neurodegeneration. Cell Mol Life Sci 2010; 67: 3435-3447.
8. de Brito OM, Scorrano L. Mitofusin 2: a mitochondria-shaping protein with signaling roles beyond fusion. Antioxid Redox Signal 2008; 10: 621-633.
9. Del Bo R, Moggio M, Rango M, Bonato S, D'Angelo MG, Ghezzi S, Airoldi G, Bassi MT, Guglieri M, Napoli L, Lamperti C, Corti S, Federico A, Bresolin N, Comi GP. Mutated mitofusin 2 presents with intrafamilial variability and brain mitochondrial dysfunction. Neurology 2008; 71: 1959-1966.
10. Detmer SA, Chan DC. Complementation between mouse Mfn1 and Mfn2 protects mitochondrial fusion defects caused by CMT2A disease mutations. J Cell Biol 2007; 176: 405-414.
11. Fujimoto M, Hayashi T. New insights into the role of mitochondria-associated endoplasmic reticulum membrane. Int Rev Cell Mol Biol 2011; 292: 73-117.
12. Melli G, Hoke A. Dorsal Root Ganglia Sensory Neuronal Cultures: a tool for drug discovery for peripheral neuropathies. Expert Opin Drug Discov 2009; 4: 1035-1045.
13. Misko A, Jiang S, Wegorzewska I, Milbrandt J, Baloh RH. Mitofusin 2 is necessary for transport of axonal mitochondria and interacts with the Miro/Milton complex. J Neurosci 2010; 30: 4232-4240.
14. Misko AL, Sasaki Y, Tuck E, Milbrandt J, Baloh RH. Mitofusin2 mutations disrupt axonal mitochondrial positioning and promote axon degeneration. J Neurosci 2012; 32: 4145-4155.
15. Nakamura N, Kimura Y, Tokuda M, Honda S, Hirose S. MARCH-V is a novel mitofusin 2- and Drp1-binding protein able to change mitochondrial morphology. EMBO Rep 2006; 7: 1019-1022.
16. Oettinghaus B, Licci M, Scorrano L, Frank S. Less than perfect divorces: dysregulated mitochondrial fission and neurodegeneration. Acta Neuropathol 2012; 123: 189-203.
17. Park YY, Lee S, Karbowski M, Neutzner A, Youle RJ, Cho H. Loss of MARCH5 mitochondrial E3 ubiquitin ligase induces cellular senescence through dynamin-related protein 1 and mitofusin 1. J Cell Sci 2010; 123: 619-626.

18. Rouzier C, Bannwarth S, Chaussenot A, Chevrollier A, Verschueren A, Bonello-Palot N, Fragaki K, Cano A, Pouget J, Pellissier JF, Procaccio V, Chabrol B, Paquis-Flucklinger V. The MFN2 gene is responsible for mitochondrial DNA instability and optic atrophy 'plus' phenotype. Brain 2012; 135: 23-34.
19. Santel A, Frank S, Gaume B, Herrler M, Youle RJ, Fuller MT. Mitofusin-1 protein is a generally expressed mediator of mitochondrial fusion in mammalian cells. J Cell Sci 2003; 116: 2763-2774.
20. Schon EA, Przedborski S. Mitochondria: the next (neurode)generation. Neuron 2011; 70: 1033-1053.
21. Stetler AR, Leak RK, Gao Y, Chen J. The dynamics of the mitochondrial organelle as a potential therapeutic target. Cereb Blood Flow Metab 2013; 33: 22-32.
22. Verhoeven K, Claeys KG, Zuchner S, Schroder JM, Weis J, Ceuterick C, Jordanova A, Nelis E, De Vriendt E, Van Hul M, Seeman P, Mazanec R, Saifi GM, Szigeti K, Mancias P, Butler IJ, Kochanski A, Ryniewicz B, De Bleecker J, Van den BP, Verellen C, Van Coster R, Goemans N, Auer-Grumbach M, Robberecht W, Milic R, V, Nevo Y, Tournev I, Guergueltcheva V, Roelens F, Vieregge P, Vinci P, Moreno MT, Christen HJ, Shy ME, Lupski JR, Vance JM, De Jonghe P, Timmerman V. MFN2 mutation distribution and genotype/phenotype correlation in Charcot-Marie-Tooth type 2. Brain 2006; 129: 2093-2102.
23. Zorzano A, Liesa M, Sebastian D, Segales J, Palacin M. Mitochondrial fusion proteins: Dual regulators of morphology and metabolism. Semin Cell Dev Biol 2010; 21: 566-574.

Case report

Folia Neuropathologica

Blood vessel ultrastructural picture in a CADASIL patient diagnosed at an advanced age

Eliza Lewandowska[1], Paulina Felczak[1], Julia Buczek[2], Karolina Gramza[3], Janina Rafałowska[4]

[1]Department of Neuropathology, Institute of Psychiatry and Neurology, Warsaw, [2]Department of Neurology, Institute of Psychiatry and Neurology, Warsaw, [3]Neuroimmunology Laboratory at the 2nd Department of Neurology, Institute of Psychiatry and Neurology, Warsaw, [4]Department of Experimental and Clinical Neuropathology, Mossakowski Medical Research Institute, Polish Academy of Sciences, Warsaw, Poland

Folia Neuropathol 2014; 52 (4): 443-451 DOI: 10.5114/fn.2014.47846

Abstract

We report the case of an 84-year-old male patient afflicted by cerebral autosomal dominant arteriopathy with subcortical infarcts and leukoencephalopathy (CADASIL) showing minimal symptoms of disease. The patient was diagnosed on the basis of ultrastructural and genetic examinations. Ultrastructurally, a typical vascular pathology was found. However, in abnormal capillary vessel walls no granular osmiophilic material (GOM) was found. In the arteriole there were only a few GOM deposits that revealed various structures, of which only some resembled typical round GOM. The arteriolar walls showed severe damage, including fragmentation, degeneration and loss of vascular smooth muscle cells (VSMCs) with numerous deposits of elastin, mucosubstances, different granular debris, as well as collagen fibres in the basement membrane. Lysosomal inclusions with fingerprint morphology, atypical for CADASIL, were located in some of the VSMCs. Very old age at the onset of the disease may suggest that morphological changes in blood vessels, described in this report, may be due to both the disease and the patient's age. To our best knowledge it is the first description of pathology of blood vessels and GOM morphology in a CADASIL patient diagnosed at an advanced age.

Key words: *CADASIL, morphology of GOM deposits, aging, ultrastructure.*

Introduction

Cerebral autosomal dominant arteriopathy with subcortical infarcts and leukoencephalopathy (CADASIL) is hereditary systemic vascular disease caused by mutations in the *NOTCH3* gene. Clinically CADASIL is characterized by migraine, recurrent ischaemic events, dementia, depression and less commonly epileptic seizures [7]. These symptoms usually occur in the fourth or fifth decade of life. However, a few cases of CADASIL diagnosed in a person beyond the age of 20 and even in a 3-year-old child [1,5,10-12] or in the elderly [15,19] have been described.

Degeneration and loss of vascular smooth muscle cells (VSMCs) or pericytes, thickening of basement membrane and the presence of granular osmiophilic material (GOM) deposits are typical vascular changes in CADASIL [8,22]. Granular osmiophilic material deposits, a specific diagnostic feature of CADASIL,

Communicating author:
Eliza Lewandowska, Department of Neuropathology, Institute of Psychiatry and Neurology, 9 Sobieskiego St., 02-957 Warsaw, Poland, phone/fax: +48 22 458 25 24, e-mail: lewandow@ipin.edu.pl

along with the genetic analysis of the *NOTCH3* gene, permit the diagnosis of this disease.

The youngest patient in whom GOM deposits were found was 19 years old [13]. A single and inaccurate case report, describing vascular pathology in a patient with the onset of CADASIL symptoms at a very late age, has been published, but the data on the presence and morphology of GOM deposits are incomplete because the diagnosis was made on the basis of genetic testing only [19].

In this report we present an ultrastructural examination of vascular changes with particular regard to GOM deposits in the skin and skeletal muscle biopsies in an 84-year-old patient with minimal symptoms of CADASIL.

Case report

An 84-year-old patient was admitted to the Department of Neurology, because his son at the age of 58 was diagnosed with CADASIL (described elsewhere) [17] previously under the care of the Outpatient Clinic of Neurology. The patient has suffered from hypertension for many years. At the age of 67 he had a heart attack, and at the age of 79 the first epileptic seizures occurred. At that time he had a computed tomography (CT) scan of the brain, which showed multiple ischaemic lesions and leukoaraiosis in both hemispheres, as well as moderate atrophy of the brain and cerebellum. Treatment with anti-epileptics drugs was started after admission. Epileptic seizures recurred sporadically. His family history revealed that his mother died at the age of 62 due to heart disease; she was also under psychiatric care probably due to depression. His father's medical history was not known. The patient has no siblings. His granddaughter suffered from epilepsy and migraine headaches; she did not decide to be tested for CADASIL.

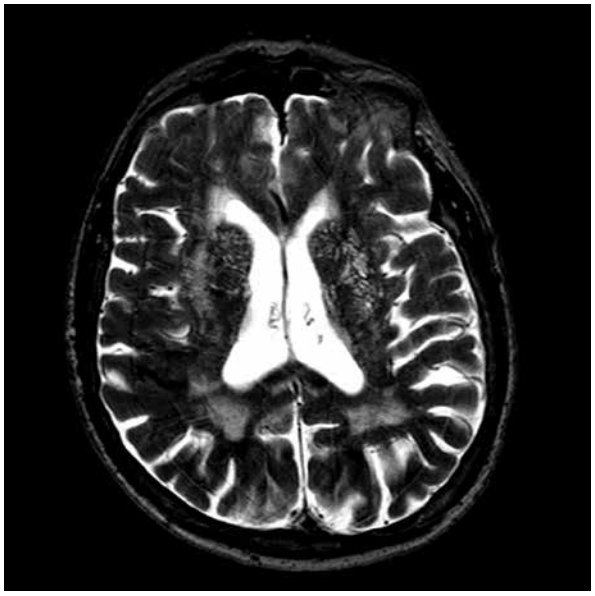

Fig. 1. Axial T2 weighted MR image shows hyperintense signal of bilateral external capsules and periventricular white matter.

On neurological examination only small asymmetry of the face was revealed. Neuropsychological evaluation showed normal cognitive function. A magnetic resonance imaging (MRI) scan of the brain revealed widespread lesions in the bilateral periventricular and subcortical white matter, external capsules and significant brain atrophy (Fig. 1). By sequencing of exon 12 of the *NOTCH3* gene, the same mutation that was detected previously in the patient's son was identified. To date, the patient remains stable and is independent in activities of daily living.

Material and methods

The samples of skin and muscle biopsy were fixed in 2.5% glutaraldehyde and post-fixed in 2% osmium tetroxide. After dehydration, tissue samples were embedded in epoxy resin. Semithin sections stained with toluidine blue were examined in the light microscope to select blood vessels. Ultrathin sections were counterstained with uranyl acetate and lead citrate and examined with a transmission electron microscope (Opton DPS 109).

Results

The capillaries in the skin and muscle biopsies were characterized by very thickened basement membrane and degenerated mural cells, pericytes in particular, but they did not contain any GOM deposits (Fig. 2A). In the extreme state only clusters of thickened basement membrane with debris of degenerated mural cells were noted (Fig. 2B).

In the muscle and skin biopsies only a few arterioles were found. They revealed typical features of CADASIL vessels, as well as damage to endothelial cells, degeneration and loss of VSMC thickening of the basement membrane, but only a few GOM deposits varied in electron density. Endothelial cells were often irregular in shape with clear vacuoles

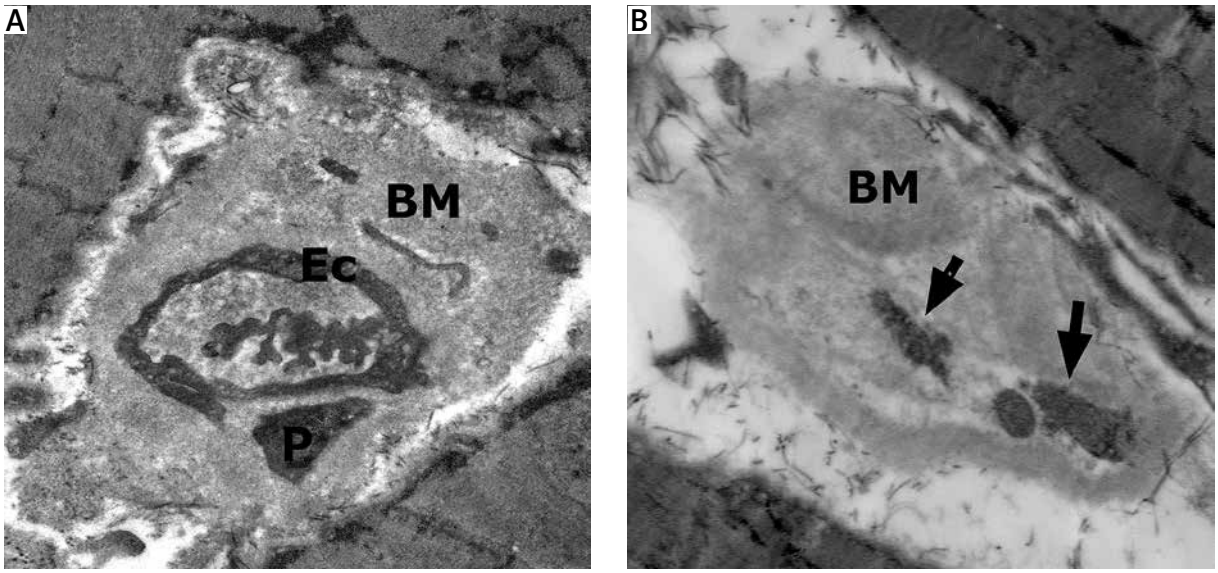

Fig. 2. Degenerative changes in capillary vessels. **A)** Thickened basement membrane (BM), thin endothelial cells (Ec) and disappearing pericytes (P). Orig. magn. × 4400. **B)** Cluster of thickened basement membrane (BM) with debris of disappearing mural cells (arrows). Orig. magn. × 4400.

of different sizes, dense mitochondria and sometimes numerous microfilaments in the cytoplasm. They formed characteristic thin sharp projections towards/in the direction of VSMCs. Some of these cells were arranged perpendicularly to the lumen of the vessel (Fig. 3).

Granular osmiophilic material deposits were located in the indentation of VSMCs (Fig. 4). The majority of them were round or oval and composed of typical electron-dense granules (Fig. 5A), but other deposits demonstrated a lower electron density of granules and irregular shape (Fig. 5B) or blurred gran-

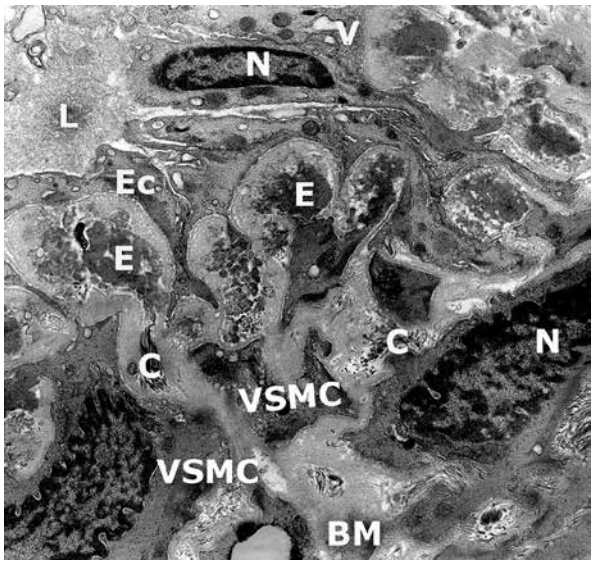

Fig. 3. Arteriolar wall. Endothelial cells (Ec) with vacuoles (V). Vascular smooth muscle cells (VSMC) with different size and shape and misshapen nuclei (N). Basement membrane (BM) with clusters of collagen (C), elastin (E). Lumen (L). Orig. magn. × 7000.

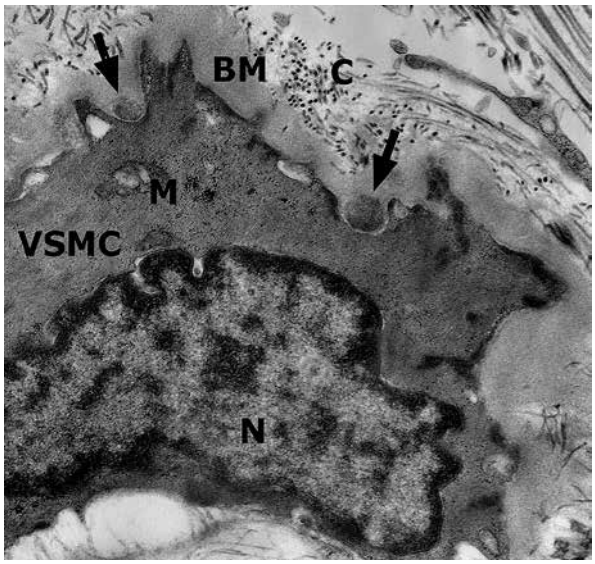

Fig. 4. Granular osmiophilic material deposits (arrows) in vascular smooth muscle cell (VSMC) infolding. Nucleus (N), swollen mitochondrium (M), basement membrane (BM), collagen (C). Orig. magn. × 7000.

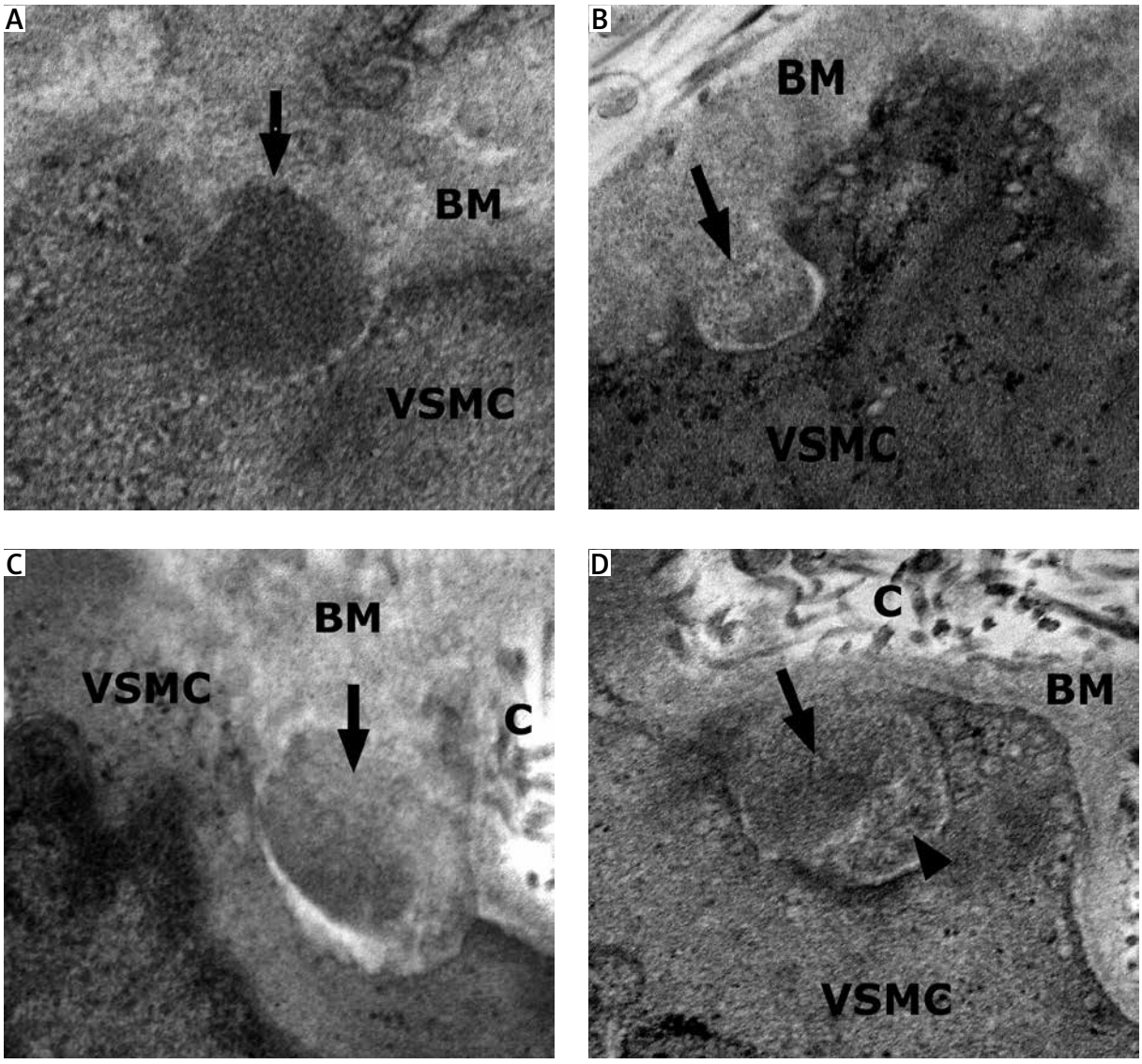

Fig. 5. Different morphology of GOM deposits (arrows) in arteriolar walls. **A)** GOM (arrow) with typical granular structure and electron density. Basement membrane (BM), vascular smooth muscle cell (VSMC). Orig. magn. × 12 000. **B)** GOM (arrow) with different electron density and bizarre shape. Orig. magn. × 12 000. **C)** GOM (arrow) with blurred structure and density similar to basement membrane (BM). Collagen (C). Orig. magn. × 12 000. **D)** GOM-like with heterogeneous structure: granular (arrow) and filamentous (arrowhead). Collagen (C). Orig. magn. × 12 000.

ular structure (GOM-like). However, their shape and location resembled GOM (Fig. 5C). GOM or "GOM-like" deposits comprising two different parts, granular or filamentous, sometimes difficult to identify, were also present (Fig. 5D). In the same arteriole, the ultrastructural picture of VSMCs was widely different. The majority of VSMCs were irregular in shape, shrunken, and fragmented, with a small diameter; however, large cells were also visible (Fig. 6). They were loosely arranged and separated from neighbouring cells by basement membrane (Fig. 3, 6). In their cytoplasm different numbers of organelles including vacuoles of various size, clusters of glycogen, lipofuscin granules and mitochondria were visible (Fig. 6, 7A). Individual VSMCs in the same arteriole revealed different numbers of mitochondria.

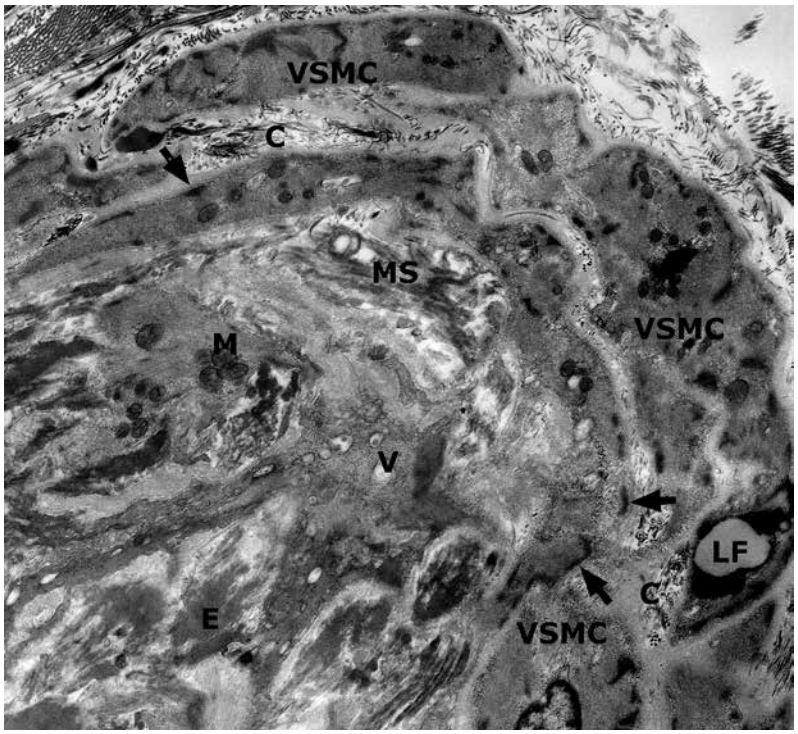

Fig. 6. Degenerative changes in arteriolar wall. Different size and shape of vascular smooth muscle cells (VSMC) with lipofuscin (LF), prominent dense bodies (arrows), vacuole (V) and dense or swollen mitochondria (M). In irregular thickened basement membrane deposits of elastin (E), collagen (C) and mucosubstances (MS) are visible. Orig. magn. × 4400.

The mitochondria were often swollen and grouped in clusters or very numerous mitochondria filled the whole cell (Fig. 7B). Numerous VSMCs exhibited misshapen nuclei and well-marked dense bodies (Fig. 7C, 7D).

In some VSMCs, abundant, large deposits, demonstrating fingerprint profiles, were visible. The majority of these deposits showed mixed complexes of fingerprint and curvilinear profiles together with lipofuscin (Fig. 8A). In the cytoplasm of VSMCs with deposits, only a few organelles, mainly clusters of mitochondria, were present (Fig. 8A, 8B).

The wall of arterioles was markedly damaged. In the thickened basement membrane numerous collagen fibres, a large amount of elastin, "pigtails" of mucosubstances and clumps of non-specific granular debris were noted (Fig. 6, 7C, 7D). Hyaline material was also visible in some parts of arteriolar walls (Fig. 7C).

Discussion

The 84-year-old patient did not show typical clinical features of CADASIL. A detailed description of clinical condition of the patient is presented in our earlier paper [3 in press]. The patient was tested for CADASIL because his son had previously been diagnosed with this disease on the basis of ultrastructural and genetic examination [17]. Genetic testing of both father and son showed the same mutation in exon 12 of the *NOTCH3* gene; however, the picture of vascular pathology was different. In the CADASIL patient presented in this paper, all the capillaries were negative for GOM deposits although their basement membrane was thickened and mural cells were degenerating and disappearing. In the extreme state only the looped basement membrane with remnants of cells was visible. The capillaries of his son revealed GOM deposits occasionally, but in his arterioles very numerous typical GOM deposits were visible [17]. In contrast, in the present CADASIL patient, GOM deposits were observed only in arteriolar walls, but they were rare and sometimes difficult to identify because they were less osmiophilic and granular.

This is consistent with the observation made by Brulin *et al*. [2] that in some elderly CADASIL patients

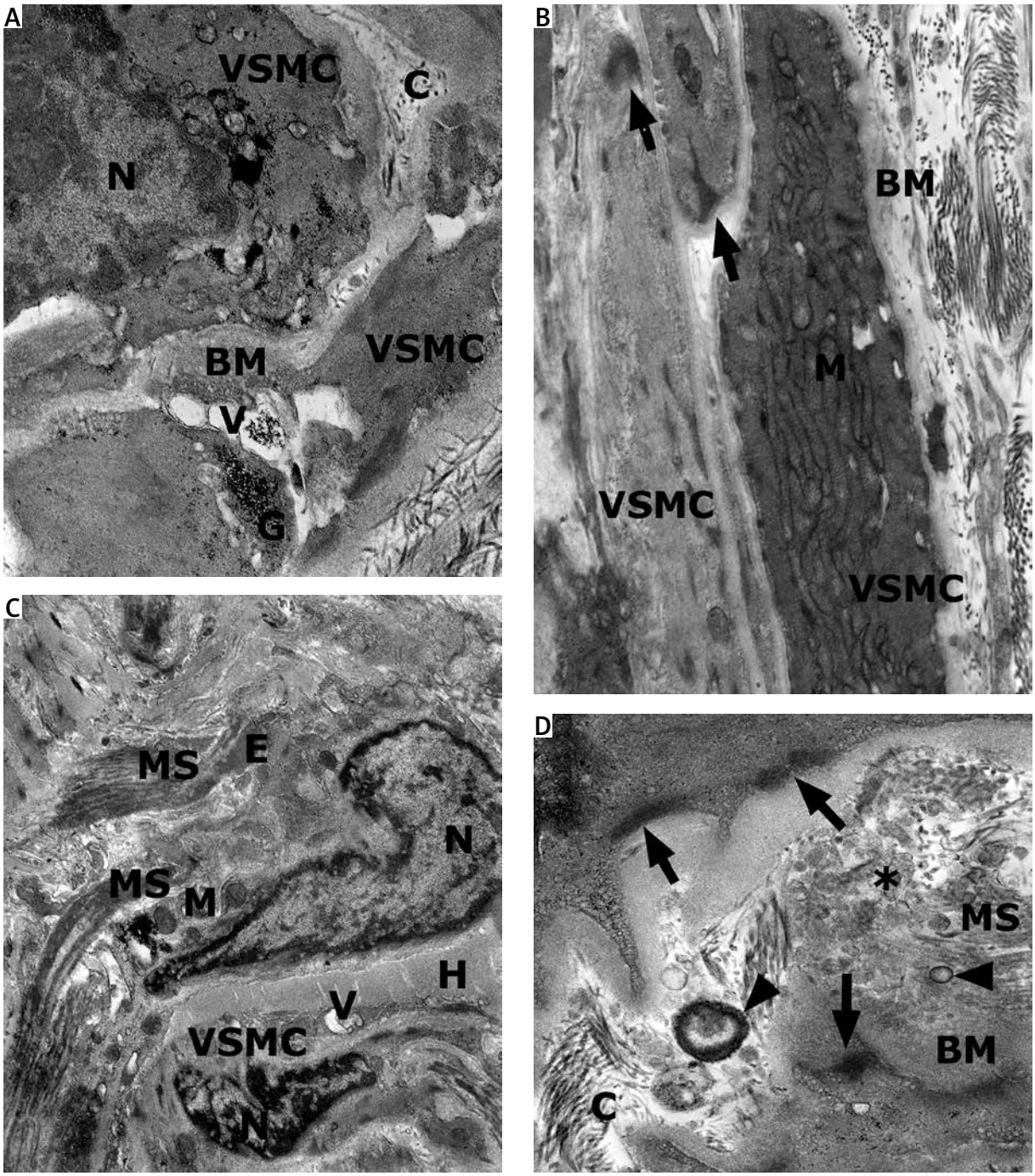

Fig. 7. Different degenerative changes of vascular smooth muscle cells (VSMC) and basement membrane (BM). **A)** VSMC with numerous vacuoles (V) or swollen mitochondria (M) and glycogen (G). Nucleus (N), collagen (C). Orig. magn. × 12 000. **B)** VSMC filled with numerous mitochondria (M) with different morphology or with prominent dense bodies (arrows). Basement membrane (BM). Orig. magn. × 7000. **C)** VSMC with misshapen nucleus (N), vacuole (V). Between VSMC, hyaline (H), elastin (E) and mucosubstances (MS) deposits are visible. Orig. magn. × 4400. **D)** Single deposits of extracellular calcium (arrowheads) in the degenerated basement membrane (BM), collagen (C), mucosubstances (MS) and numerous debris of different morphology (asterisk). Prominent dense bodies (arrows) at surface of VSMC. Orig. magn. × 12 000.

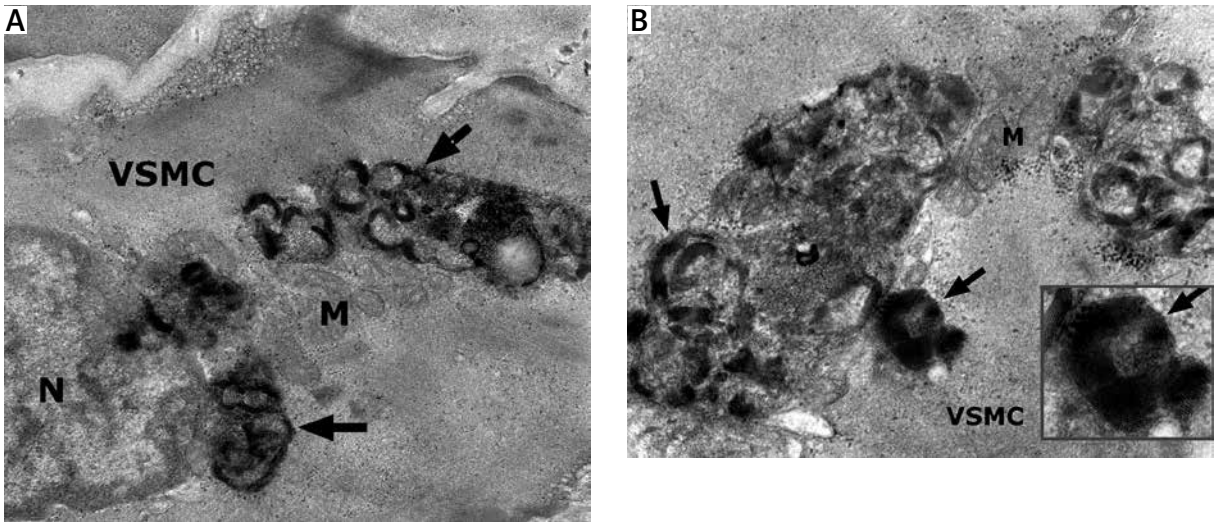

Fig. 8. A) Mixed fingerprint and curvilinear profiles (arrows) located in vascular smooth muscle cells (VSMC). Nucleus (N), mitochondria (M). Orig. magn. × 12 000. **B)** Higher magnified fingerprint and curvilinear profiles (arrows). In the inset higher magnification of fingerprint deposits. Orig. magn. × 20 000.

GOM become rare and difficult to identify. They also demonstrated that the highest numbers of GOM deposits per vessel and per patient were found in CADASIL patients at the age around 50 years. In elderly patients (65-75 years) the mean number of GOM deposits per vessel and per patient decreased. Similarly, a small amount of GOM was present in a 19-year-old patient [13]. It is known that GOM deposits are composed of 10-15 nm granules, but their morphological picture varies, including size, shape and electron density [14,18,22,26], which may suggest that they undergo changes. Based on our observations together with morphometric analysis of the age-related mean number of GOM deposits per skin vessel [2] and early reports [22,26], it can be suggested that GOM deposits disappear, which could lead to the decreased number of GOM deposits in elderly patients. On the other hand, vessels in a human fetus with a *Notch3* mutation did not contain GOM deposits, and morphology of VSMCs, as well as other vascular wall structures, was normal, which suggests that the vessel wall abnormalities are initiated and progressed in the course of the first two decades of life [16]. In a 19-year-old CADASIL patient, only a small amount of GOM deposits was visible [13].

Although a small number of GOM deposits was found in our patient, electron microscopy revealed severe and common changes in arterioles, including VSMCs, endothelial cells and basement membrane. Endothelial cells in our material exhibited changes similar to those previously described in CADASIL patients [2,23].

The pathology of VSMCs varied greatly. They showed differences in size, shape and degenerative changes, including their loss. The degeneration and loss of VSMCs is a typical feature of CADASIL arterioles [2,21,25]. In the oldest patients (aged 55-65 years), VSMCs were totally destroyed [21]. In our patient, in general, VSMCs contained only a few organelles, but some differences were observed between cells.

Some of the VSMCs were filled by numerous and closely packed mitochondria with abnormal ultrastructure while others contained only a few mitochondria or clusters of distended mitochondria. It has been previously demonstrated that the mean number of abnormal mitochondria was higher in VSMCs in CADASIL as compared to control cells, which might have an effect on vital cellular functions important for CADASIL pathology [27]. The ultrastructural picture of the degenerating VSMCs demonstrates different numbers and morphology of mitochondria; therefore, it may be assumed that the mechanisms of the degeneration process may also differ in these cells. The presence of lysosomal inclusions in VSMCs with fingerprint profiles was a very interesting observation. Some of them revealed mixed morphology. Those inclusions are observed in neuronal ceroid lipofuscinosis, but they were also found in

skeletal muscles in "fingerprint body myopathy" [9]. The interpretation of their presence in VSMCs of our patient is difficult, especially since they seem to be non-specific.

Electron microscopy analysis of an arteriolar wall revealed the presence of collagen fibres, elastin, hyaline, mucosubstances and different granular debris in basement membrane probably derived from massive degeneration of VSMCs. These findings have been described both in CADASIL pathology and the aging process [2,6,13,20]. In irregularly thickened subendothelial space, large aggregates mainly of elastin were observed. In CADASIL patients, increased production of elastin [4], as well as fibrous and hyaline thickening of the vessel walls, was observed [6,24]. On the other hand, hyaline is observed in different processes, such as aging and hypertension [20], and it is not specific for CADASIL pathology such as collagen fibres usually visible in the form of clusters scattered throughout the basement membrane of our patient.

It is important that our patient was diagnosed at the age above 80. It should also be remembered that vascular pathology probably results from typical CADASIL and age-related pathologies. The patient diagnosed with CADASIL at an advanced age showed minimal symptoms, in contrast to his son [17], as well as a different picture of vascular pathology and in particular the number and morphology of GOM deposits. This indicates that a clinical phenotype, such as vascular pathology, may be different despite the same mutation. The reason remains an open question.

Acknowledgments

This study was supported by grant NN402375039 from the Polish Ministry of Science and Higher Education.

Disclosure

Authors report no conflict of interest.

References

1. Benabu Y, Beland M, Ferguson N, Maranda B, Boucher RM. Genetically proven cerebral autosomal–dominant arteriopathy with subcortical infarcts and leukoencephalopathy (CADASIL) in a 3-year-old. Pediatr Radiol 2013; 43: 1227-1230.
2. Brulin P, Godfraind C, Leteurtre E, Ruchoux MM. Morphometric analysis of ultrastructural vascular changes in CADASIL: analysis of 50 skin biopsy specimens and pathogenic implications. Acta Neuropathol 2002; 104: 241-248.
3. Buczek J, Gramza K, Lewandowska E, Błażejewska-Hyżorek B, Kurkowska-Jastrzębska J. CADASIL – opis przypadku osiemdziesięcioletniego pacjenta z niewielkimi objawami klinicznymi choroby. Medycyna Praktyczna – Neurologia [in press].
4. Caronti B, Calandriello L, Francia A, Scorretti L, Manfredi M, Sansolini T, Pennisi EM, Calderaro C, Palladini G. Cerebral autosomal dominant arteriopathy with subcortical infarcts and leucoencephalopathy (CADASIL) Neuropathological and in vitro studies of abnormal elastogenesis. Acta Neurol Scand 1998; 98: 259-267.
5. Cleves C, Friedman NR, Rothner AD, Hussain MS. Genetically confirmed CADASIL in a pediatric patient. Pediatrics 2010; 126: 1603-1607.
6. Davous P. CADASIL: a review with proposed diagnostic criteria. Eur J Neurol 1998; 5: 219-233.
7. Dichgans M, Mayer M, Uttner I, Brüning R, Müller-Höcker J, Rungger G, Ebke M, Klockgether T, Gasser T. The phenotypic spectrum of CADASIL: clinical findings in 102 cases. Ann Neurol 1998; 44: 791-839.
8. Dziewulska D, Lewandowska E. Pericytes as a new target for pathological processes in CADASIL. Neuropthol 2012; 32: 515-521.
9. Engel AG, Angelini C, Gomez MR. Fingerprint body miopathy. Mayo Clinic Proceedings 1972; 47: 377-388.
10. Golomb MR, Sokol DK, Walsh EL, Christensen CK, Garg BP. Recurrent hemiplegia, normal MRI, and NOTCH3 mutation in a 14-year-old: Is this early CADASIL? Neurology 2004; 22: 2331-2332.
11. Granild-Jensen J, Jensen UB, Schwartz M, Hansen US. Cerebral autosomal dominant arteriopathy with subcortical infarcts and leukoencephalopathy resulting in stroke in an 11-year-old male. Dev Med Child Neurol 2009; 51: 754-757.
12. Hartley J, Westmacott R, Decker J, Shroff M, Yoon G. Childhood-onset CADASIL: clinical, imaging, and neurocognitive features. J Child Neurol 2010; 25: 623-627.
13. Kalimo H, Miao Q, Tikka S, Mykkänen K, Junna M, Roine S, Viitanen M, Pöyhönen M, Baumann M. CADASIL: the most common hereditary subcortical vascular dementia. Future Neurol 2008; 3: 683-704.
14. Lačković V, Bajčetič M, Šternić N, KoskićV, Zidverc J, Pavlović A, Lačković M, Kočica M. Ultrastructural analysis of small blood vessels in skin biopsies in CADASIL. Arch Biol Sci 2008; 60: 573-580.
15. Lee YC, Yang AH, Soong BW. The remarkably variable expressivity of CADASIL: report of a minimally symptomatic man at an advanced age. J Neurol 2009; 256: 1026-1027.
16. Lesnik Oberstein SAJ, Maat–Schieman MLC, Boon EMJ, Haan J, Breuning MH, van Duinen SG. No vessel wall abnormalities in a human foetus with a NOTCH 3 mutation. Acta Neuropathol 2008; 115: 369-370.
17. Lewandowska E, Wierzba-Bobrowicz T, Buczek J, Gromadzka G, Dziewulska D. CADASIL patient with extracellular calcium deposits. Folia Neuropathol 2013; 51: 302-311.
18. Lewandowska E, Dziewulska D, Parys M, Pasennik E. Ultrastructure of granular osmiophilic material deposits (GOM) in arterioles of CADASIL patients. Folia Neuropathol 2011; 49: 174-180.
19. Mourad A, Levasseur M, Bousser MG, Chabriat H. CADASIL with minimal symptoms after 60 years. Revue Neurologique 2006; 162: 827-831.

20. Pavelka M, Roth J. Collagen and elastic fibres. In: Functional Ultrastructure Atlas of tissue biology and pathology. 2nd ed. Springer-Verlag, Wien 2010; pp. 278-279.
21. Ruchoux MM, Guerouaou D, Vandenhaute B, Pruvo JP, Vermersch P, Leys D. Systemic vascular smooth muscle cell impairment in cerebral autosomal dominant arteriopathy with subcortical infarcts and leucoencephalopathy. Acta Neuropathol 1995; 89: 500-512.
22. Ruchoux MM, Maurage CA. CADASIL: Cerebral autosomal dominant arteriopathy with subcortical infarcts and leukoencephalopathy. J Neuropathol Exp Neurol 1997; 56: 947-964.
23. Ruchoux MM, Maurage CA. Endothelial changes in muscle and skin biopsies in patients with CADASIL. Neuropathol Appl Neurobiol 1997; 23: 60-65.
24. Schröder JM, Sellhaus B, Jörg J. Identification of the characteristic vascular changes in a sural nerve biopsy of a case with cerebral autosomal dominant arteriopathy with subcortical infarcts and leukoencephalopathy (CADASIL). Acta Neuropathol 1995; 89: 116-121.
25. Schröder JM, Züchner S, Dichgans M, Nagy Z, Molnar MJ. Peripheral nerve and skeletal muscle involvement in CADASIL. Acta Neuropathol 2005; 110: 587-599.
26. Tikka S, Mykkänen K, Ruchoux MM, Bergholm R, Junna M, Pöyhönen M, Yki-Järvinen H, Joutel A, Viitanen M, Baumann M, Kalimo H. Congruence between NOTCH3 mutations and GOM in 131 CADASIL patients. Brain J Neurol 2009; 132: 933-939.
27. Viitanen M, Sundström E, Baumann M, Poyhonen M, Tikka S, Behbahani H. Experimental studies of mitochondrial function in CADASIL vascular smooth muscle cells. Exp Cell Res 2013; 319: 134-143.

Folia Neuropathologica

Case report of an adolescent girl with limb-girdle muscular dystrophy type 2B – the usefulness of muscle protein immunostaining in the diagnosis of dysferlinopathies

Sylwia Szymanska[1], Dariusz Rokicki[2], Agnieszka Karkucinska-Wieckowska[1], Tamara Szymanska-Debinska[1], Elzbieta Ciara[3], Rafal Ploski[4], Wieslawa Grajkowska[1,5], Maciej Pronicki[1]

[1]Department of Pathology, The Children's Memorial Health Institute, Warsaw, [2]Department of Pediatrics, Nutrition and Metabolic Disorders, The Children's Memorial Health Institute, Warsaw, [3]Department of Medical Genetics, The Children's Memorial Health Institute, Warsaw, [4]Department of Medical Genetics, Centre of Biostructure, Medical University of Warsaw, [5]Department of Clinical and Experimental Neuropathology, Mossakowski Medical Research Centre, Polish Academy of Sciences, Warsaw, Poland

Folia Neuropathol 2014; 52 (4): 452-456 DOI: 10.5114/fn.2014.47847

Abstract

Dysferlinopathies are rare disorders of muscle that present two main phenotypes: Miyoshi myopathy with primarily distal weakness and limb-girdle muscular dystrophy type 2B (LGMD2B) with primarily proximal weakness. They are caused by mutations in the gene encoding the skeletal muscle protein dysferlin, which is involved in muscle repair. The clinical presentation of the disease is rather uncharacteristic, and molecular genetic testing is long-lasting; thus muscle biopsy may be essential in the diagnostic process. Histology itself reveals non-specific changes, but a variety of currently available muscle protein immunostains may be very helpful. We present a 19-year-old girl with epilepsy and elevated creatine phosphokinase (CPK) concentration. Due to increased CPK, myopathy was suspected and muscle biopsy was performed. Light microscopy showed no distinctive myopathic changes, and electron microscopy showed no abnormalities. Extended immunohistochemistry, performed much later, showed complete absence of dysferlin immunostaining. Based on that result, the diagnosis of LGMD2B was made, with subsequent genetic testing to be done. Two known pathogenic variants were found in the DYSF gene, confirming the diagnosis of LGMD2B and allowing proper genetic counseling.

Key words: *dysferlinopathies, limb-girdle muscular dystrophy type 2B (LGMD2B), dysferlin, immunohistochemistry, muscle, DYSF gene.*

Introduction

Limb-girdle muscular dystrophy type 2B (LGMD2B) is an autosomal recessive phenotype of dysferlinopathies, muscle disorders caused by mutations in the dysferlin gene (*DYSF*) [9]. The *DYSF* gene is located on chromosome 2p12-14 and encompasses 55 exons spanning over 150 kb of genomic DNA. It encodes a 230-kDa type-II transmembrane protein, dysferlin, which contains a large intracellular cytoplasmic *N*-terminal domain, an extreme *C*-terminal transmembrane domain, and a short *C*-terminal extracel-

Communicating author:
Maciej Pronicki, Department of Pathology, The Children's Memorial Health Institute, Al. Dzieci Polskich 20, 04-730 Warsaw, Poland, phone: +48 228151960, fax: +48 228151975, e-mail: m.pronicki@czd.pl

lular domain. Its expression is widespread in different tissues, especially in skeletal muscles and cardiac muscle [2]. In skeletal muscle, dysferlin is located at the plasma membrane, as well as in cytoplasmic vesicles [3]. Its role is associated with muscle repair. In human patients with LGMD2B, dysferlin expression is absent. Clinically, it is characterized by weakness in the proximal muscles at onset, involving predominantly the lower limbs. At late stages of the disease, loss of muscle bulk in the pelvic girdle and calf may appear. This may result in frequent falls, and difficulty in climbing stairs, rising from the floor, and running. With the progression of the condition, patients may have problems with walking [1,4]. Onset is typically in the late teens or early adulthood, with no previous history of muscle weakness. Laboratory tests show increased levels of the muscle enzyme creatine kinase, typically 10 to 150 times above normal levels. Cardiac muscle and respiratory muscles are not involved in this disorder [9]. Symptoms are not specific enough; thus LGMD2B should be confirmed by identifying a defect either in the *DYSF* gene, which is done on a DNA sample from the blood, or by Western blot analysis of skeletal muscle biopsy. It was proved [5] that the reduction of dysferlin expression to 20% of normal values in skeletal muscle or in peripheral blood monocytes is associated with 100% coexistence of pathogenic mutations in the *DYSF* gene; however, long *DYSF* gene sequencing is time-consuming. Therefore, microscopic analysis of muscle biopsy may be essential in the diagnostic process. Histology itself reveals non-specific changes such as centrally located nuclei, fiber splitting, scattered necrotic and regenerating fibers, and an occasional perivascular infiltrate comprising lymphocytes and macrophages, sometimes leading to a misdiagnosis of polymyositis. There is increased connective tissue in the endomysium and perimysium. Fiber type distribution is normal and rimmed vacuoles and ragged red fibers are absent [6,8,13,14]. These microscopic findings may also be seen in other limb-girdle muscular dystrophies, caveolinopathies and dystrophinopathies; thus immunohistochemistry seems to be essentially helpful. In healthy muscle, dysferlin immunoreactivity is localized along the plasma membrane of muscle fibers. The pathological pattern of immunostaining is either complete absence of or marked reduction in LGMD2B, depending on the nature of the genetic mutation [11]. We present a 19-year-old girl with epilepsy and elevated creatine phosphokinase (CPK) concentration. Due to increased CPK a myopathy was suspected and muscle biopsy was performed. Light microscopy showed no distinctive myopathic changes, and electron microscopy showed no abnormalities. Extended immunohistochemistry performed much later within our research project showed complete absence of dysferlin immunostaining. The diagnosis of LGMD2B was then made.

Case report

We present a case report of a 19-year-old girl who was suspected of myopathy at the age of 10. She was born as a second child of her parents; pregnancy and delivery were not complicated. The period of infancy was uneventful. Psychomotor development was normal. At the age of one, she presented an episode of convulsions that happened again when she was two and a half. The epilepsy was diagnosed with consecutive introduction of treatment (valproic acid). Epilepsy attacks subsided but increased levels of transaminases (up to 170 U/l) occurred with time. The medication was changed without a satisfactory effect on hypertransaminasemia. In 2004 the patient was admitted to The Children's Memorial Health Institute because of a persistent increase in transaminase levels. Laboratory tests performed at the time showed increased transaminases (AlAT 163 U/l; AspAT 96 U/l) and elevated CPK concentration (2402 U/l). Because of elevated CPK, she has been suspected of having a myopathic disorder since then. In 2005, during her follow-up visit to the Outpatient Metabolic Clinic, she complained of occasional muscle pain. Otherwise, she was in good general condition. Physical examination did not reveal muscle weakness, atrophy or hypertrophy of muscles, and muscle tension was correct. Cardiological consultation did not reveal cardiomyopathy. Electromyography (EMG) was also performed, but the result was within the normal range. The most sensitive and specific parameter for myopathy in conventional EMG, which is decreased duration of motor unit potentials (MUP), was not observed. Muscle biopsy was planned but had to be postponed due to the patient's infection. One year later, the girl was admitted to the hospital again to undergo muscle biopsy. She remained in good condition; levels of transaminases were lower, but constantly increased (AlAT 107 U/l; AspAT 72 U/l); CPK > 3000 U/l. Histological findings in the performed muscle biopsy were consistent with moderate myo-

pathic changes including an increased number of centrally located, single necrotic fibers, and unequally intensive NADH-D reaction. There were no features of regeneration or endomysial fibrosis. Findings characteristic of neurogenic disorders were not present. In electron microscopy there were no diagnostic ultrastructural changes. Spectrophotometric analysis of mitochondrial respiratory chain complex enzyme activities revealed decreased complex IV activity (6.6%; normal levels 19-33.8%) and complex I activity (6.8%; normal levels 8.2-18%). Frozen samples of muscle were protected for further examination. The patient was discharged from hospital with suspicion of undefined myopathy. In 2008, additional immunostainings were performed from frozen samples (merosin, adhalin and dystrophin [DYS.1, DYS.2, DYS.3]), but expression was normal. Recently, we decided to assess her muscle biopsy once again within a research project, using an extended panel of muscle protein immunostains. This time, second-look examination revealed a pattern of complete absence of dysferlin immunostaining. In view of the clinical presentation and histologic findings, the diagnosis of LGMD2B was made (Figs. 1 and 2). Whole exome sequencing (WES) was conducted to identify the molecular basis of the disease. Whole exome sequencing was performed on a HiSeq 1500 using an Exome Enrichment Kit (Illumina) [12]. Generated reads were aligned to the hg19 reference human genome. Alignments were viewed with Integrative Genomics Viewer v.2.2.34.

Two known pathogenic variants in the *DYSF* gene were revealed: missense mutation c.6124C>T in exon 54 and splice-site mutation c.1180+5G>A in intron 12 (Fig. 3). The missense change is associated with severe reduction of dysferlin activity, and the intronic variant is predicted to create a cryptic splice donor site, but its protein effect is unknown yet. This has to be further validated at the transcriptional level. Mutation numbering is based on the cDNA sequence (human *DYSF*, GenBank NM_003494.3) according to journal guidelines (www.hgvs.org/mutnomen).

Discussion

LGMD2B is a rare autosomal recessive muscle disorder caused by mutation in the *DYSF* gene, mostly missense or null alleles [10]. Onset of the disease is usually in the proximal lower-limb musculature in the late teens or later, most commonly between 20 and 30 years of age. Progress is rather slow [4]. Our patient presented the first symptoms when she was 10 years old, which was relatively early; thus suspicion of LGMD2B was not obvious. Recently, Fanin *et al*. [7] found that males with LGMD may be clinically more severely affected than females, although the mechanism remains elusive. Our patient has always remained in good general condition, and sporadic muscle pain has been her only complaint while CPK has been constantly and significantly increased (> 3000 U/l). Massive elevation of serum CK concentration is thought [4,13] to be one of the typical LGMD2B symptoms, but it is not a specific marker – it

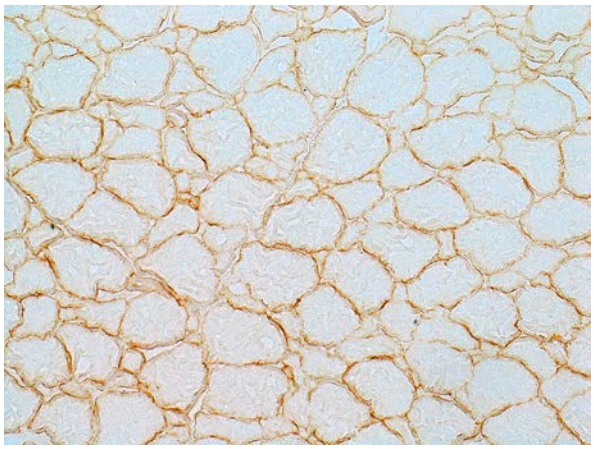

Fig. 1. Image of skeletal muscle dysferlin IHC control positive reaction. Original magnification × 400.

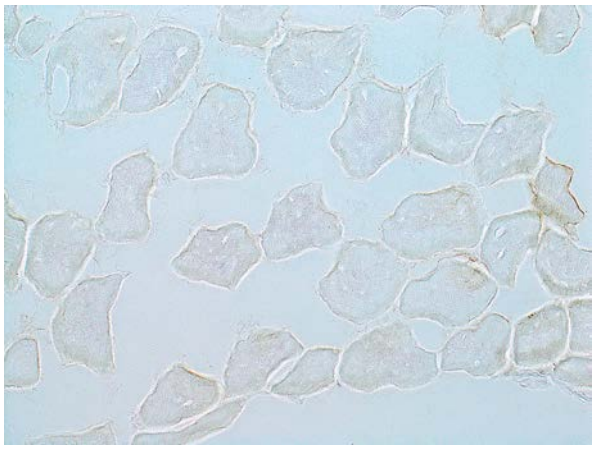

Fig. 2. Image of skeletal muscle dysferlin IHC negative reaction in our patient's muscle biopsy. Original magnification × 400.

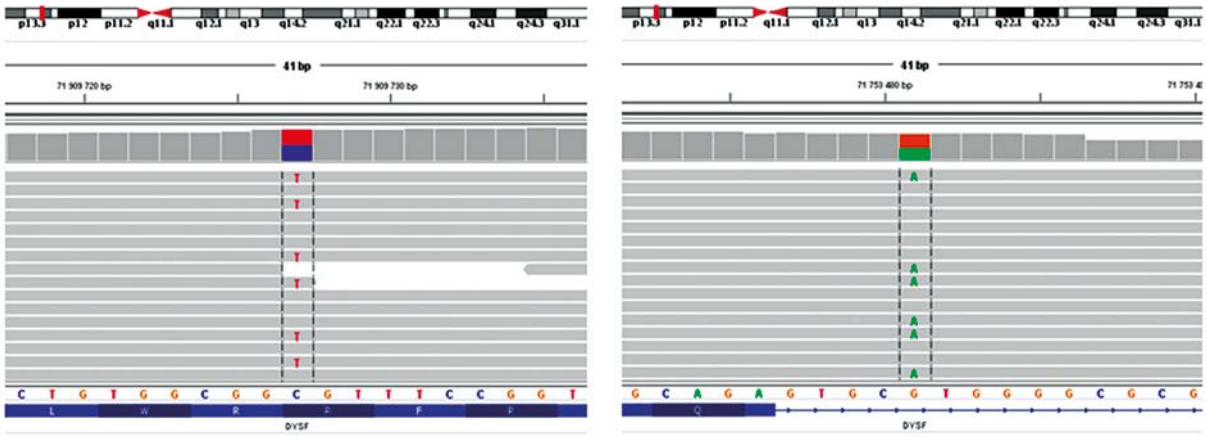

Fig. 3. Integrative Genomics Viewer view of DYSF mutations: c.6124C>T (left) and c.1180+5G>A (right) in the patient by whole-exome sequencing.

only indicates muscle damage. One method that leads to a firm LGMD2B diagnosis is molecular genetic testing. Muscle biopsy Western immunoblotting almost always indicates a primary dysferlinopathy. *DYSF* is the only gene known to be associated with dysferlinopathy [1]. There were three testing possibilities – targeted mutation analysis focused on the two most common mutations among Jews [1] (1624delG, and 927delG); *DYSF* gene sequencing [1]; and mutation scanning that detects sequence variants but only in 80% of individuals [15]. Although genetic tests are the most precise methods and they must be done to confirm the LGMD2B diagnosis, they are time-consuming and expensive, and are often done following a clue from the muscle biopsy or examination. As histologic light microscopic features are non-characteristic, immunostaining is essential. Our patient was first suspected of having a muscle disorder almost 10 years ago when immunohistochemistry was limited, and thus the exact diagnosis was established only recently, after performing additional staining within our research project. LGMD2B is genetically transferred, but the risk that offspring will inherit one faulty copy of the dysferlin gene and therefore will all be carriers but unaffected is unlikely. Therefore, carrier testing is not necessary unless the risks are increased due to intra-familial marriage. We present this case as an example of the practical usefulness of immunostaining in the diagnosis of LGMD2B. We believe that an extended immunohistochemical panel of muscle proteins should be examined in all patients with non-specific histologic features of myopathy to increase the detection rate of known limb girdle muscle dystrophies.

An alternative diagnostic approach in the described patient was provided by fast and cost-effective next generation sequencing (NGS). This method, simultaneously identifying mutations affecting both the most frequent and rare genes, will greatly improve the precise diagnosis of heterogeneous limb-girdle muscular dystrophies, especially for patients with mild, non-specific or atypical phenotype.

Acknowledgments

The work was supported by grants of The Children's Memorial Health Institute for young researchers, no. M4/2012 and 136/2013, Polish National Science Centre (NCN) grant 2011/01/B/NZ4/03455, and EU Structural Funds, project POIG.02.01.00-14-059/09.

References

1. Aoki M. Dysferlinopathy. In: Pagon RA, Adam MP, Ardinger HH, Bird TD, Dolan CR, Fong CT, Smith RJH, Stephens K (eds.). GeneReviews® University of Washington, Seattle 2004.
2. Bansal D, Campbell KP. Dysferlin and the plasma membrane repair in muscular dystrophy. Trends Cell Biol 2004; 4: 206-213.
3. Bansal D, Miyake K, Vogel SS, Groh S, Chen CC, Williamson R, McNeil PL, Campbell KP. Defective membrane repair in dysferlin-deficient muscular dystrophy. Nature 2003; 423: 168-172.
4. Bushby KMD, Straub V, Lochmuller H, Eagle M, Guglier M, Hastings L. National Commissioning Group (NCG) and the Clinical team at Newcastle, LGMD 2B – Muscular Dystrophy Campaign. www.muscular-dystrophy.org
5. Cacciottolo M, Numitone G, Aurino S, Caserta IR, Fanin M, Politano L, Minetti C, Ricci E, Piluso G, Angelini C, Nigro V. Muscular dystrophy with marked dysferlin deficiency is consistently caused by primary dysferlin gene mutations. Europ J Hum Genet 2011; 19: 974-980.

6. Fanin M, Angelini C. Muscle pathology in dysferlin deficiency. Neuropathol Appl Neurobiol 2002; 28: 461-470.
7. Fanin M, Nascimbeni AC, Angelini C. Gender difference in limb-girdle muscular dystrophy: a muscle fiber morphometric study in 101 patients. Clin Neuropathol 2014; 33: 179-185.
8. Gallardo E, Rojas-Garcia R, de Luna N, Pou A, Brown RH, Illa I. Inflammation in dysferlin myopathy: immunohistochemical characterization of 13 patients. Neurology 2001; 57: 2136-2138.
9. Karpati G. Structural and Molecular Basis of Skeletal Muscle Diseases. Diseases associated with sarcolemmal and extracellular matrix defects: Dysferlinopathies. ISN Neuropath Press, Basel 2002; pp. 29-39.
10. Nigro V, Savarese M. Genetic basis of limb-girdle muscular dystrophies: the 2014 update. Acta Myol 2014; 33: 1-12.
11. Piccolo F, Moore SA, Ford GC, Campbell KP. Intracellular accumulation and reduced sarcolemmal expression of dysferlin in limb-girdle muscular dystrophies. Ann Neurol 2000; 48: 902-912.
12. Ploski R, Pollak A, Müller S, Franaszczyk M, Michalak E, Kosinska J, Stawinski P, Spiewak M, Seggewiss H, Bilinska ZT. Does p.Q247X in TRIM63 cause human hypertrophic cardiomyopathy? Circ Res 2014; 114: e2-5.
13. Prelle A, Sciacco M, Tancredi L, Fagiolari G, Comi GP, Ciscato P, Serafini M, Fortunato F, Zecca C, Gallanti A, Chiveri L, Bresolin N, Scarlato G, Moggio M. Clinical, morphological and immunological evaluation of six patients with dysferlin deficiency. Acta Neuropathol (Berl) 2003; 105: 537-542.
14. Serratrice G, Pellissier JF, N'Guyen V, Attarian S, Pouget J. Dysferlinopathy. Example of a new myopathy. Bull Acad Natl Med 2002; 186: 1025-1032.
15. Takahashi T, Aoki M, Tateyama M. Mutational and clinical features of Japanese patients with dysferlinopathy. Neurology 2003; 60 Suppl: A233.

Folia Neuropathologica

Frontotemporal lobar degeneration with *MAPT* mutation in an Italian-Polish family. A case report

Teresa Wierzba-Bobrowicz[1], Eliza Lewandowska[1], Jacek Zaremba[2], Mariusz Berdyński[3], Cezary Żekanowski[3], Tomasz Stępień[1], Paulina Felczak[1], Sylwia Tarka[4]

[1]Department of Neuropathology, Institute of Psychiatry and Neurology, Warsaw, [2]Department of Genetics, Institute of Psychiatry and Neurology, Warsaw, [3]Department of Neurodegenerative Disorders and Neurogenetic Unit, Mossakowski Medical Research Institute, Polish Academy of Sciences, Warsaw, [4]Department of Forensic Medicine, Warsaw Medical University, Poland

Folia Neuropathol 2014; 52 (4): 457-466 DOI: 10.5114/fn.2014.47848

Abstract

Frontotemporal lobar degeneration (FTLD) with mutations in the MAPT (microtubule-associated protein tau) gene (FTLD with MAPT mutation) is a neurodegenerative disease with various clinical phenotypes. We present an Italian-Polish family with a IVS10+3G>A mutation in the MAPT gene, linked with haplotype H1s in a male proband (Fig. 2, II.2, H1s/H1b diplotype) and his sister (Fig. 2, II.1, the H1s/H1j diplotype). This report presents clinical, neuropathological and genetic testing of the proband and his affected sister, two members of an Italian-Polish family consisting of 25 family members. Their clinical history includes dementia as well as movement and cardiovascular disorders. Magnetic resonance imaging showed frontal and temporal cerebral atrophy. Neuropathological studies of the brain samples showed loss of neurons, gliosis, and the occurrence of neurofibrillary tangles, numerous neuropil threads, coiled bodies and abundant deposits of tau protein, including 3- and 4-repeated isoforms in neurons and glial cells. Only in the male proband brain, there were Pick body-like deposits in granule neurons of the hippocampus. Pathology of vascular walls was found in both cases. Ultrastructurally, the male proband showed clusters of collagen fibers mainly in a pericyte position. Beside the typical neurofibrillary pathology, aggregated gliofilaments and lipofuscin deposits in astroglia are described. Our report suggests that FTLD with IVS10+3G>A MAPT mutation causes damage mainly to the central nervous system and induces neuropathological changes, depending on the haplotypes of MAPT. In the clinical course of this disease, damage of the cardiovascular system may also be observed.

Key words: *FTLD, MAPT, H1 haplotypes, diplotypes H1s/H1j and H1s/H1b, tau isoforms.*

Introduction

Frontotemporal lobar degeneration (FTLD) represents a large heterogeneous group of familial and sporadic diseases, in which the neurodegenerative process involves mainly the frontal and temporal lobes (Fig. 1) [3]. The group of these diseases constitutes about 20% of presenile dementia cases [18]. Hereditary forms of FTLD are associated with mutations of multiple genes, including *MAPT* (microtubule-associated protein tau gene), *PGRN* (progranulin gene), *VCP* (valosin-containing protein gene), *$CHMP_2B$* (charged multivesicular body protein $_2$B gene),

Communicating author:
Prof. Teresa Wierzba-Bobrowicz, Department of Neuropathology, Institute of Psychiatry and Neurology, 9 Sobieskiego St., 02-957 Warsaw, Poland, e-mail: bobrow@ipin.edu.pl

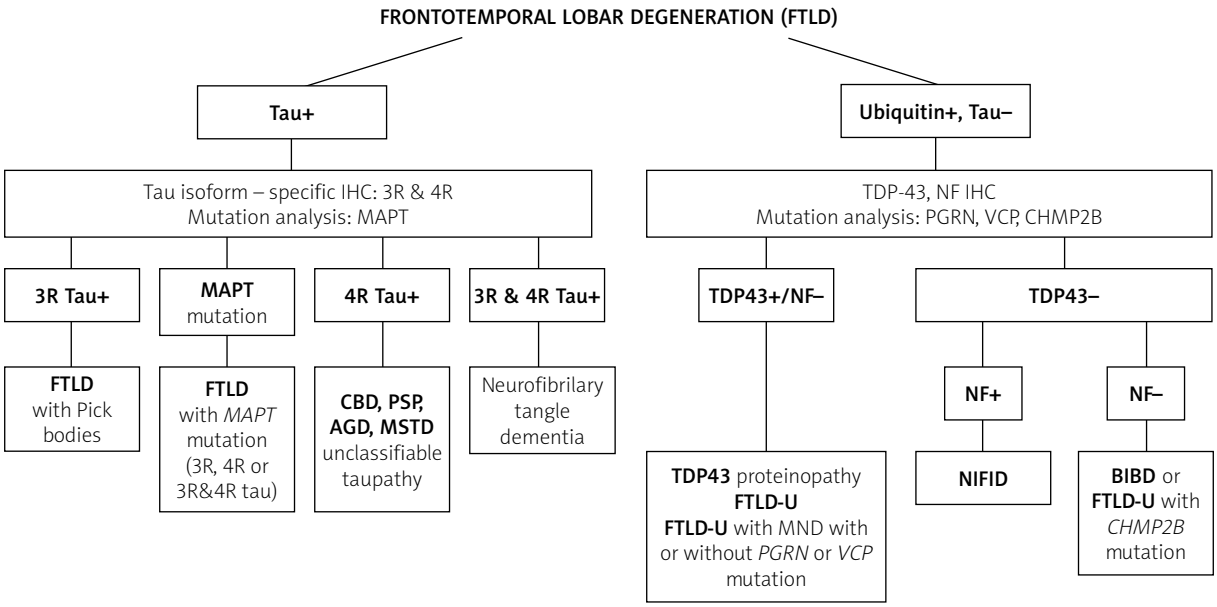

Fig. 1. Neuropathology algorithm flow chart for the diagnosis of frontotemporal lobar degeneration (FTLD) by Cairns *et al*. (Acta Neuropathol 2007; 114: 5-22). AGD – argyrophilic grain disease, BIBD – basophilic inclusion body disease, CBD – corticobasal degeneration, CHMP2B – charged multivesicular body protein 2B gene, FTLD-U – FTLD with ubiquitin-positive, tau-negative inclusions, IHC – immunohistochemistry, MAPT – microtubule-associated protein tau gene, MSTD – sporadic multiple system tauopathy with dementia, NIFID – neuronal intermediate filament inclusion disease, NF – neurofilament, PGRN – progranulin gene, PSP – progressive supranuclear palsy, TDP-43 – TAR DNA-binding protein 43, Tau – tau protein, VCP – valosin-containing protein gene.

TDP-43 (TAR DNA-binding protein 43) and other mutations [4,17]. *MAPT* mutations are identified in up to 20% of familial FTLD [9,20]. The *MAPT* gene codes the microtubule-associated protein tau, which is involved in microtubule assembly and stabilization, neuronal polarity, and axonal transport in the brain [7,20]. The tau protein is mainly synthesized in the peripheral and central nervous system (central nervous system [CNS], neurons and neuroglia), but it is also expressed in other tissues (heart, skeletal muscle, lung, kidney and others) [1,8,16]. The *MAPT* gene locus on chromosome 17 q21 has two major haplotypes, H1 and H2. *MAPT* consists of 16 exons and encodes 6 human brain isoforms of tau protein with 3 or 4 repeat domains (3R and 4R) [2,5,15]. Tau protein inclusions in different tauopathies have specific morphology and distribution. In the nervous system of FTLD patients carrying the *MAPT* mutation, inclusions of both 3R tau and 4R isoforms of tau protein are found. The 3R isoform of tau protein inclusions are observed in FTLD with Pick bodies, while the 4R isoform of tau protein occurs, inter alia, in such diseases as corticobasal degeneration, progressive supranuclear palsy and argyrophilic grain disease [6]. More than 40 mutations have been identified in the *MAPT* gene in individuals from more than 100 families with FTLD [6,12,27]. Depending on the mutation in the *MAPT* gene, we can observe different neuropathologic and clinical symptoms. There are also differences between family members and families suffering from FTLD with the same *MAPT* mutations. The main hallmarks of this disease are neurofibrillary pathology, neuronal inclusions, tau-positive neuroglial inclusions, both in astrocytic and oligodendrocytic cells and also the coiled bodies [5,11,13,26]. In this study, we investigated immunohistochemically, using antibodies against 3R- and 4R-tau isoforms, genetic and ultrastructural features of two members of Italian-Polish familial FTLD with dementia and movement disorders.

Material and methods

The reported cases

The pedigree consists of 25 Italian-Polish family members in four generations. The first tested pro-

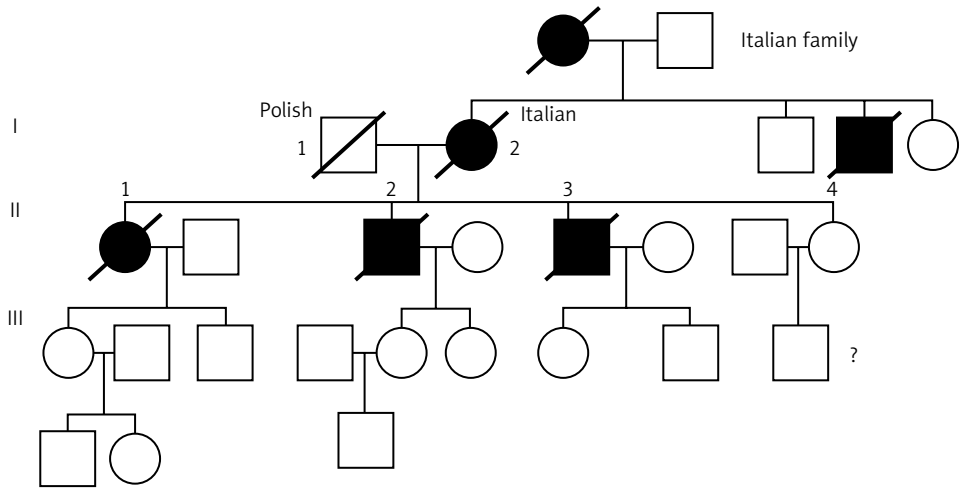

Fig. 2. Pedigree of the frontotemporal lobar degeneration with *MAPT* mutation of the Italian- Polish family. I.2 Italian grandmother, her mother and brother also with dementia and movement disorders in the family medical history. **I.1** grandfather (Pole) without symptoms. **II.2** the first tested male proband with mutation in *MAPT* gene, **II.1** his sister with mutation in *MAPT* gene, **II.3** brother with dementia and movement disorders in the family medical history, **III.** family members were not examined, currently without clinical symptoms.

band, a 58-year-old man (Fig. 2, II.2), died one year after the onset of the first dementia symptoms. At the age of 49, he had a cardiac pacemaker implanted. The patient complained of muscle weakness. At the end of his life, bulbar syndrome occurred. The diagnosis of Alzheimer's disease was suspected. The proband's sister (Fig. 2, II.1) died at the age of 68. She presented with behavioral abnormalities from the age of 59. Primarily, the loss of awareness, memory, interest and empathy was noted. Gradually social withdrawal and logopenic aphasia progressed. At the age of 61 she was afflicted by brain hemorrhagic stroke. At the end of her life, pyramidal and Parkinsonian syndromes were reported. Magnetic resonance imaging (MRI) showed cerebral atrophy in frontal and temporal lobes (Fig. 3).

Methods

Brain examinations were performed. Samples were taken from the brain structures of the affected male proband (II.2) and his sister (II.1). They were fixed in 10% buffered formalin and paraffin embedded. The specimens were stained with hematoxylin-eosin, Bielshowsky, Yamamoto, and Gallyas methods. Immunohistochemical studies were performed with antibodies to glial fibrillary acidic protein (GFAP, DAKO 1 : 70), anti-tau (DAKO 1 : 100), anti-Tau, 3R-re-

Fig. 3. Magnetic resonance imaging scans of frontotemporal lobar degeneration with *MAPT* mutation. Case II.1 sister (6 years of disease). Atrophy of frontal and temporal lobes.

peated isoform RD3 (Millipore, 1 : 1000), anti-tau-4R repeated isoform RD4 (Millipore, 1 : 1000), ubiquitin (DAKO, 1 : 35), β-amyloid (DAKO, 1 : 70) and α-synuclein (Leica, 1 : 20). For electron microscope evaluation small fragments of brains were taken from formalin or paraffin blocks. After deparaffinizing and/or washing in water, the material was fixed in 2.5% glutaraldehyde and postfixed in 2% OsO4, then routinely processed to Spurr resin. Ultrathin sections were stained with uranyl acetate and lead citrate and examined in an electron microscope (Opton DPS 109). Blood samples for DNA analysis were protected. Genomic DNA was isolated from peripheral blood leukocytes using standard methods. The male proband was screened for mutations in: *PSEN1*, *APP*, *PGRN*, *MAPT*, and *C9ORF72*. The presence of the mutation also was confirmed in the proband's sister. The absence of the mutation IVS10+3G> A *MAPT* was confirmed in the control group of 150 elderly, neurologically healthy subjects from the Polish population. Haplotype associated with the mutation was identified by the presence or absence of 238 bp deletion in intron 9 and by genotyping five SNPs (rs1467967, rs242557, rs3785883, rs2471738 and rs7521) [22]. The mutation-associated haplotype was determined based on the comparison of diplotypes identified in the male proband and his sister.

Results

In both cases, the gross examination of the brains showed moderate symmetrical cortical atrophy in the frontal and temporal lobes. There was mild atrophy of the anterior part of the caudate nucleus, while other subcortical structures were normal. The lateral ventricles were intensively dilated. The substantia nigra of the mesencephalon and locus coeruleus of the pons were moderately depigmented. The cerebellum seemed to be normal. Routine histology of the light microscopy examination showed neocortical neuronal loss, mostly in the frontal and temporal lobes in layers II and III and also in the substantia nigra. This change was accompanied by moderate spongiosis and astrogliosis. Sections stained with either the Bielschowski, Yammamoto or Gallyas silver technique showed neurofibrillary tangles (NFTs) and neuropil threads (NTs) (Fig. 4A,B). Silver-stained fibrillary inclusions were found in Purkinje cells and neurons of the substantia nigra and also in the locus coeruleus (Fig. 4C-E). Numerous coiled bodies were observed in the white matter in frontal and temporal lobes (Fig. 4F,G). Ballooned neurons were detected in the pons and in the cerebral and cerebellar cortices (Fig. 4H). Tau-immunoreactive methods detected many more NFTs, coiled bodies and NTs than silver methods. Tau-immunoreactive deposits were abundant in the frontal and temporal cortex but also in the brainstem. They were visible in the form of granular deposits, tau-positive abundant neurites, neuropil threads, coiled bodies, Pick bodies, ballooned neurons and grain-like deposits (Fig. 5 and 6). Tau-3 repeated isoform positive Pick bodies in the granule neurons of the dentate gyrus of the hippocampus occurred only in the male proband (Fig. 5C), whereas intracytoplasmic deposits of tau-4 repeated isoform were observed in both cases (Fig. 5D and 6E). In the frontal cortex of the sister, tau-positive Pick bodies-like deposits were visible (Fig. 6F). A GFAP-positive tufted and monstrous astrocytes were observed mainly in the sister (Fig. 2, II.1) (Fig. 6H and 6J). Pathology of vascular walls was visible in both cases (Fig. 5J and 6J). Ultrastructural analysis of fibrillary inclusions showed tightly aggregated filaments of neurofibrillary tangles in the cytoplasm of nerve cells (Fig. 7). Astrocytes were often swollen with only a few short gliofilaments or with numerous gliofilaments filling the cytoplasm (Fig. 8). In their cytoplasm, lipofuscin deposits were located in the adjacent gliofilaments (Fig. 8). In capillaries, abundant collagen fibers were frequently found in the pericyte position and small clusters in different locations of the basement membrane (Fig. 9).

The analysis of the nucleotide sequence of the *MAPT* gene revealed an intron 10+3-splice site mutation (IVS10+3G>A, g.123806G>A) in both affected siblings. The analysis of diplotypes associated with mutation in the male proband and his sister showed that the IVS10+3G>A mutation was in the haplotype H1s background. The *MAPT* diplotype of the male proband was H1s/H1b, and that of his sister was H1s/H1j (Table I).

Discussion

We present a comprehensive analysis of members of the first Italian-Polish family with genetically confirmed FTLD with the IVS10+3G>A *MAPT* mutation. The mutation was previously reported as pathologic in another European population [19,26,28] and was absent in 138 patients with FTLD in the Polish population (data not published). The analysis of the *MAPT* gene in the two described cases showed

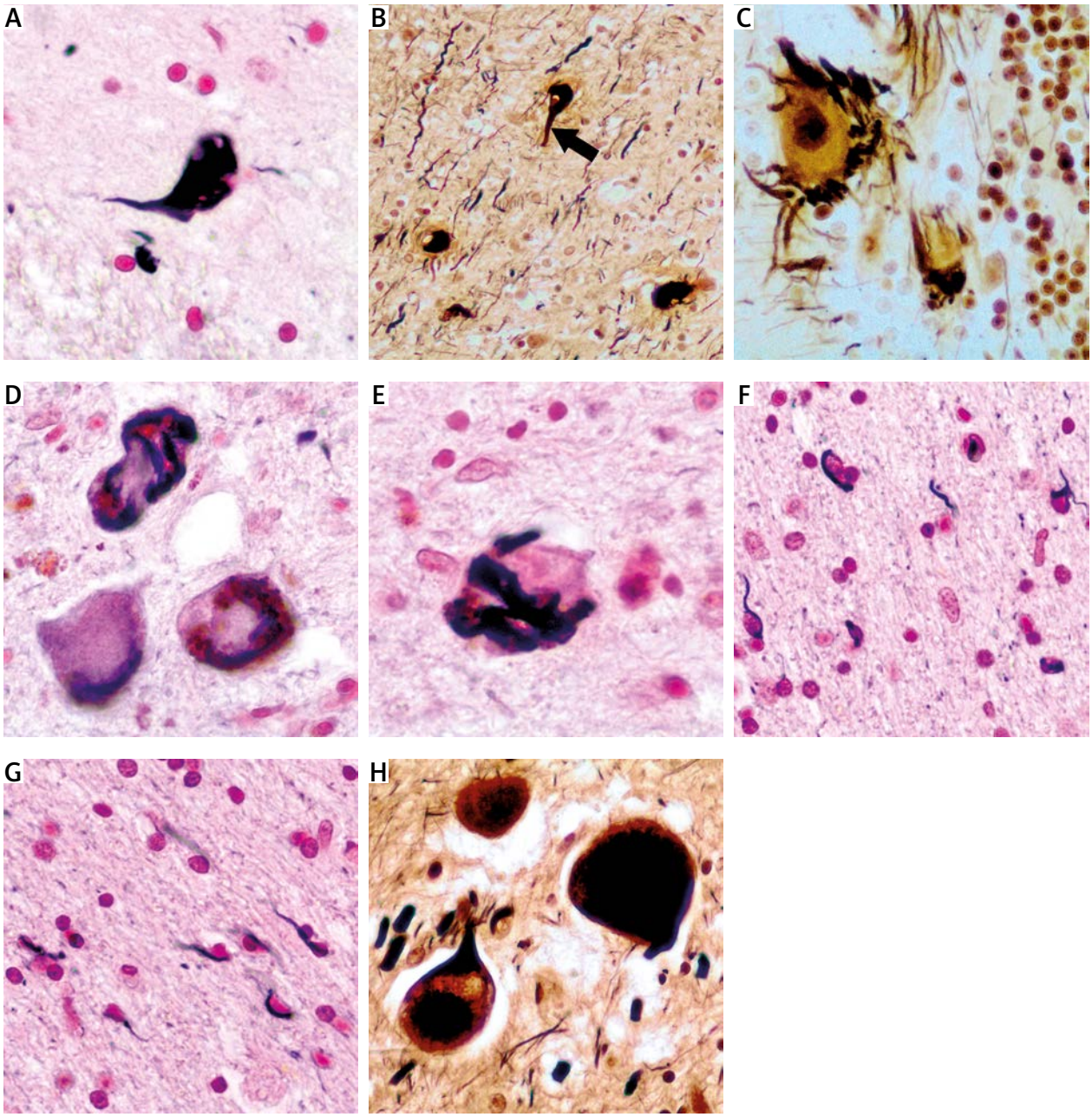

Fig. 4. Frontotemporal lobar degeneration (FTLD) with *MAPT* mutation. Silver techniques. **A)** Proband II.2. Pons. Neurofibrillary tangle (NFT). Gallyash. × 20. **B)** Case II.2. Temporal lobe, case II.2. Fibrillary material surrounds the nucleus and extends into the axon (arrow). Numerous neuropil threads. Yamamoto × 20. **C)** Case II.2. Purkinje cell. Nucleus surrounded by densely packed neurofibers. Yamammoto. × 40. **D)** Case II.1. Mesencephalon. Intracytoplasmic argyrophilic depots. Gallyas. × 40. **E)** Case II.1. Pons. Argyrophilic deposits. Gallyas. × 40. **F)** Case II.2. Coiled bodies in white matter of frontal lobe. Gallyas. × 40. **G)** Case II.1. Coiled bodies in white matter of temporal bodies. Gallyas. × 40. **H)** Case II.2. Ballooned neurons in the pons. Yamammoto. × 40.

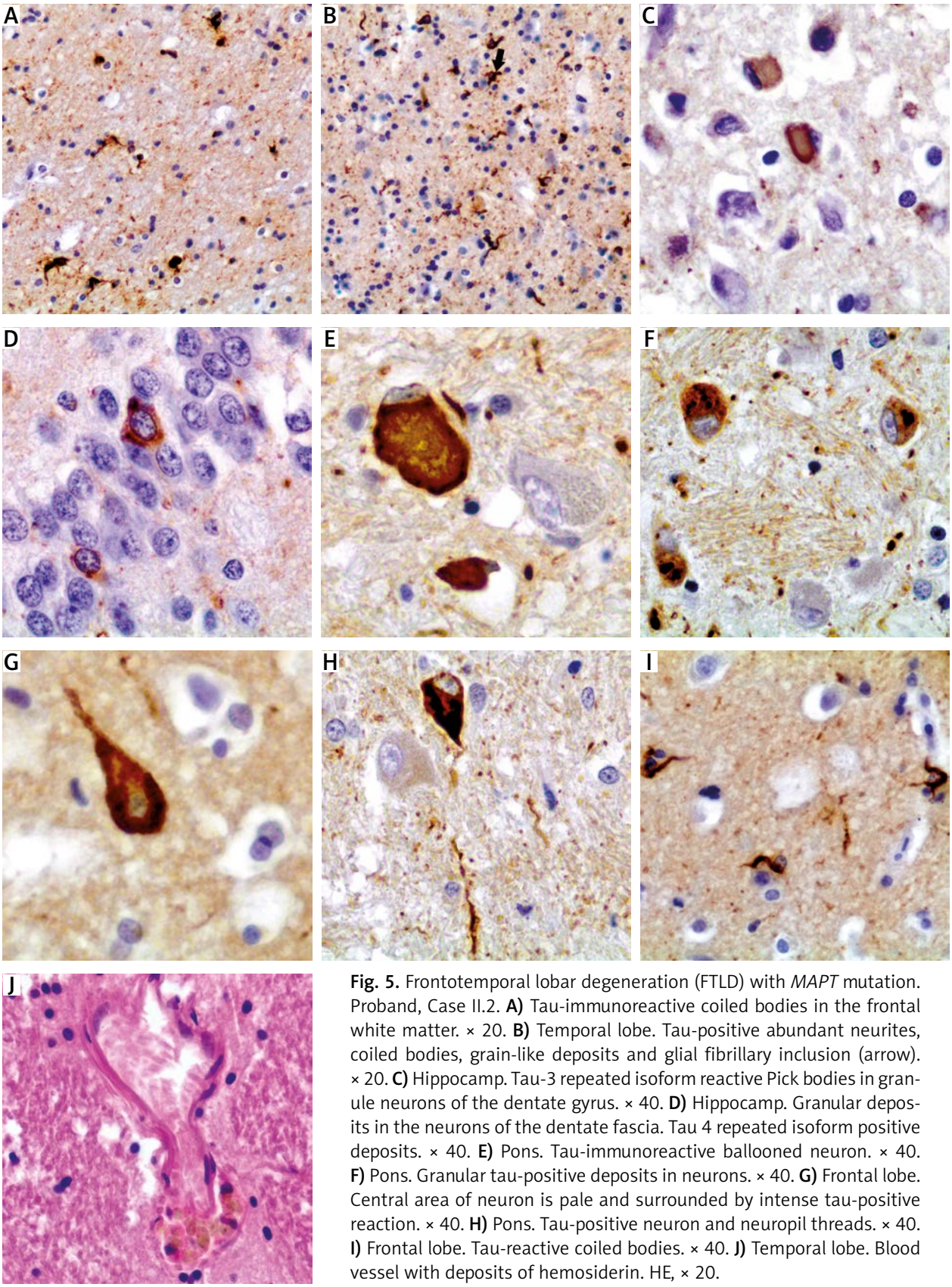

Fig. 5. Frontotemporal lobar degeneration (FTLD) with *MAPT* mutation. Proband, Case II.2. **A)** Tau-immunoreactive coiled bodies in the frontal white matter. × 20. **B)** Temporal lobe. Tau-positive abundant neurites, coiled bodies, grain-like deposits and glial fibrillary inclusion (arrow). × 20. **C)** Hippocamp. Tau-3 repeated isoform reactive Pick bodies in granule neurons of the dentate gyrus. × 40. **D)** Hippocamp. Granular deposits in the neurons of the dentate fascia. Tau 4 repeated isoform positive deposits. × 40. **E)** Pons. Tau-immunoreactive ballooned neuron. × 40. **F)** Pons. Granular tau-positive deposits in neurons. × 40. **G)** Frontal lobe. Central area of neuron is pale and surrounded by intense tau-positive reaction. × 40. **H)** Pons. Tau-positive neuron and neuropil threads. × 40. **I)** Frontal lobe. Tau-reactive coiled bodies. × 40. **J)** Temporal lobe. Blood vessel with deposits of hemosiderin. HE, × 20.

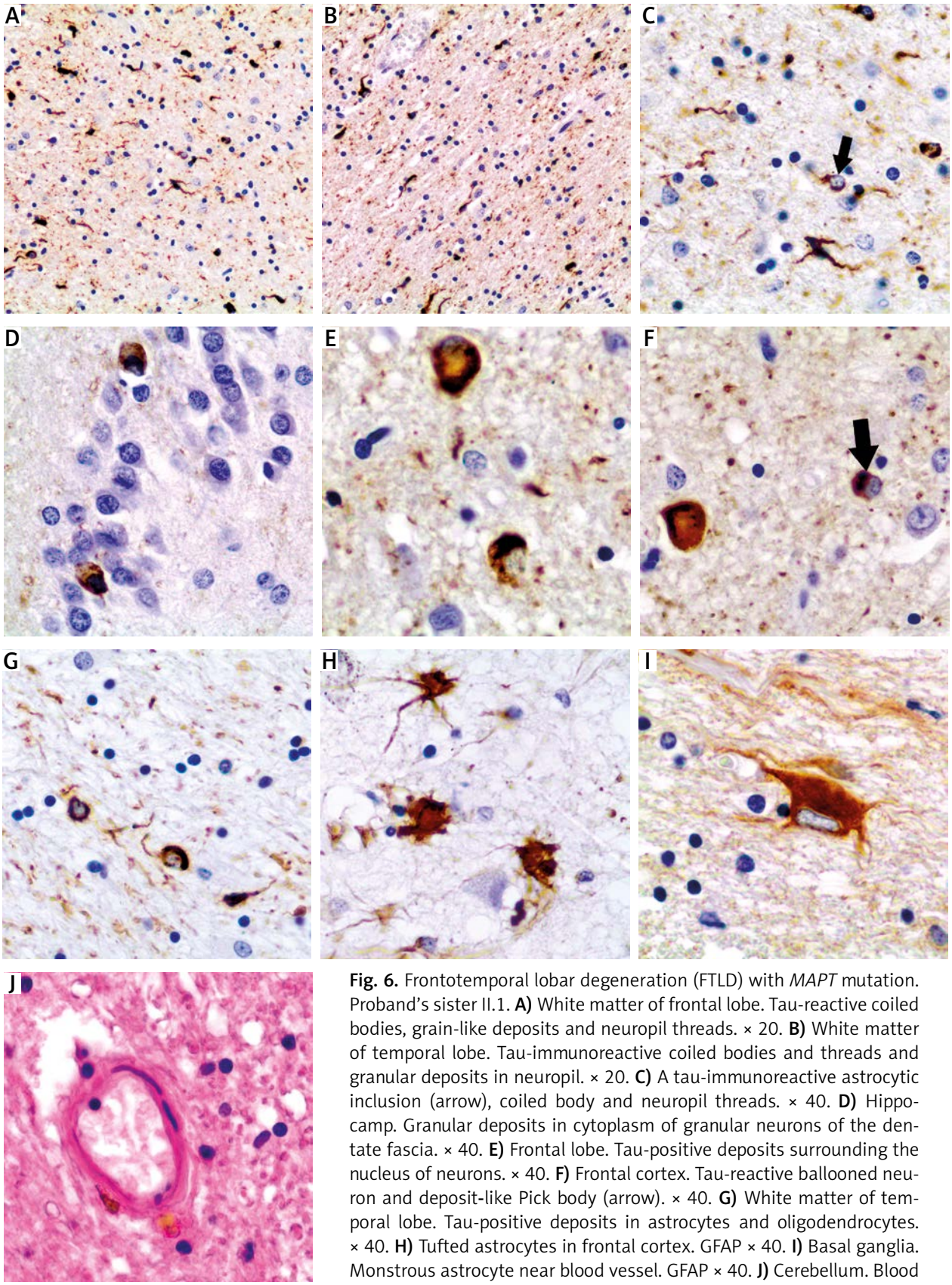

Fig. 6. Frontotemporal lobar degeneration (FTLD) with *MAPT* mutation. Proband's sister II.1. **A)** White matter of frontal lobe. Tau-reactive coiled bodies, grain-like deposits and neuropil threads. × 20. **B)** White matter of temporal lobe. Tau-immunoreactive coiled bodies and threads and granular deposits in neuropil. × 20. **C)** A tau-immunoreactive astrocytic inclusion (arrow), coiled body and neuropil threads. × 40. **D)** Hippocamp. Granular deposits in cytoplasm of granular neurons of the dentate fascia. × 40. **E)** Frontal lobe. Tau-positive deposits surrounding the nucleus of neurons. × 40. **F)** Frontal cortex. Tau-reactive ballooned neuron and deposit-like Pick body (arrow). × 40. **G)** White matter of temporal lobe. Tau-positive deposits in astrocytes and oligodendrocytes. × 40. **H)** Tufted astrocytes in frontal cortex. GFAP × 40. **I)** Basal ganglia. Monstrous astrocyte near blood vessel. GFAP × 40. **J)** Cerebellum. Blood vessel with deposits of hemosiderin. HE × 40.

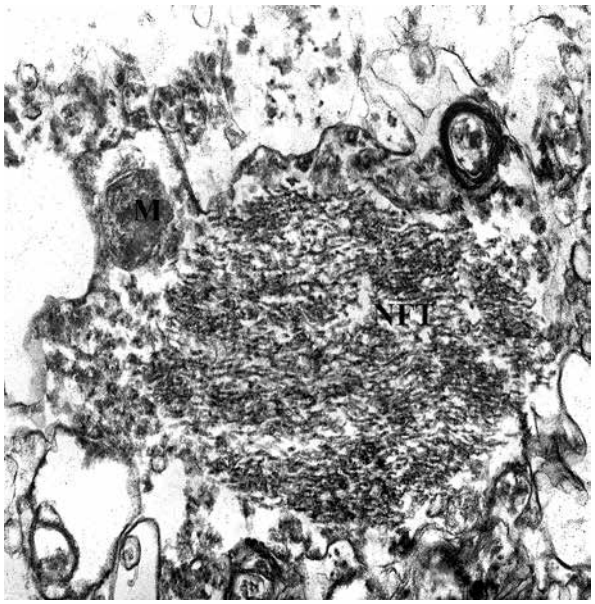

Fig. 7. Case II.1. Nerve cell cytoplasm with tightly aggregated filaments of neurofibrillary tangles (NFT). M – mitochondrium. Org. mag. × 12000.

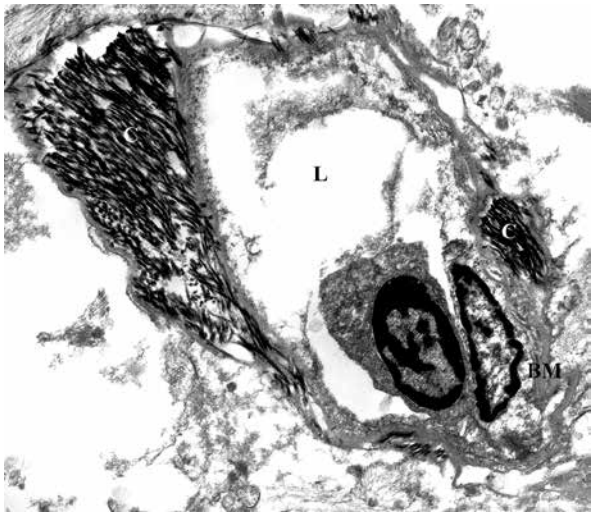

Fig. 9. Proband. Case II.2. Capillary. Collagen fibers (C) in the basement membrane (BM) and in the pericyte position. L – lumen. Orig. mag. × 4400.

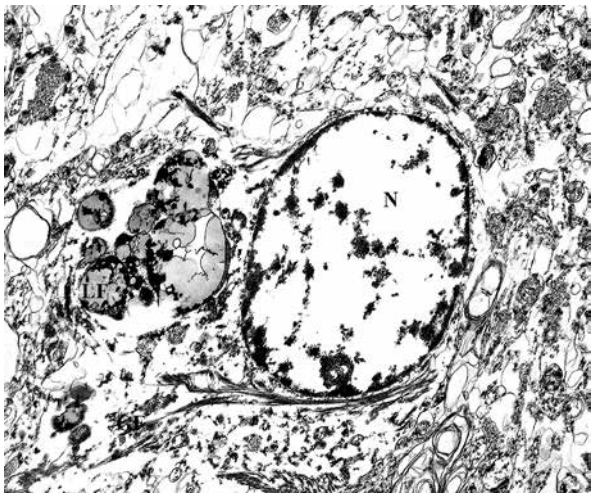

Fig. 8. Case II.1. Astrocyte with numerous bundles of gliofilaments (GF) and lipofuscin (LF) in the cytoplasm. N – nucleus. Orig. mag. × 4400.

that the IVS10+3G>A mutation was in the haplotype H1s background. There were differences in the *MAPT* diplotypes. The male proband's diplotype was H1s/H1b, while his sister's was H1s/H1j. It is possible that these variations affected the differences in the clinical course of the disease and in its neuropathological picture [28]. The male proband died one year after the onset of symptoms of dementia and 9 years after implantation of a cardiac pacemaker. The sister of the proband experienced brain hemorrhagic stroke 2 years after disease onset and died 9 years after the first symptoms of dementia. The mutation in the microtubule protein tau (*MAPT*) gene locus into haplotype H1 affected tau microtubule assembly and tau mRNA splicing. In addition, the increased inclusion of exon 10 in transcripts show an imbalance in the 3R and 4R tau isoforms [2,9,15].

The ratio of these two isoforms in normal conditions is generally equal (1 : 1), but it varies depending on the type of mutation [24]. Corticobasal degeneration (CBD) is characterized by increased 4R tau,

Table I. Mutation analysis of *MAPT* gene – ideogram

	Rs1467967	Rs242557	Rs3785883	Rs2471738	Del-in9	IVS10+3	Rs7521
Proband	G/G	G/G	G/G	C/C	H1/H1	G/A	G/A
Shared alleles	G	G	G	C	H1	A	G
Sister	A/G	G/G	G/G	C/C	H1/H1	G/A	G/G

whereas frontotemporal lobar degeneration with Pick bodies shares an overabundance of 3R tau (Fig. 1). FTLD with *MAPT* mutation is a biochemically heterogeneous disease associated with 3R and 4R tau deposits in various proportions, influencing the type of neuropathological changes. The main cellular function of tau protein is to assemble and stabilize microtubules and neural integrity. The aggregation of microtubules and creation of NFTs may be regarded as "toxic intensification" of their function in neurons [21,23]. These disorders may start aging processes leading finally to apoptosis. The clinical course of FTLD with *MAPT* mutation is also heterogeneous, because of the tau protein function in the cells outside the nervous system [1,8,16]. Ultrastructurally, in both cases, we observed neurofibrillary pathology and deposits of collagen in the vessel walls of the male proband's brain [10]. Šerý *et al*. [24] suggest that vascular pathology influences pathological processes in Alzheimer's disease [14]. Our report suggests that FTLD with *MAPT* mutation affects mainly the CNS, and neuropathological changes depend on the variant of the mutation. In the clinical course of this disease, damage of the cardiovascular system may also be observed.

Disclosure

Authors report no conflict of interest.

References

1. Birukova AA, Birukov KG, Gorshkov B, Liu F, Garcia JGN, Verin AD. MAP kinases in lung endothelial permeability induced by microtubule disaessembly. AMJ Physiol Lung Cell Mol Physiol 2005; 289: L75-L-84.
2. Caffrey TM, Wade-Martins R. Functional MAPT haplotypes: Bridging the gap between genotype and neuropathology. Neurobiol Dis 2007; 27: 1-10.
3. Cainrs NJ, Bigio EH, Mackenzie IRA, Neumann M, Lee V M-Y, Hatanpaa KJ, White III ChL, Schneider JA, Grinberg LT, Halliday G, Duyckaert Ch, Lowe JS, Holm IE, Tolnay M, Okamoto K, Yokoo H, Murayama S, Woulfe J. Munoz DG, Dickson DW, Ince PG, Trojanowski JQ, Mann DMA. Neuropathologic diagnostic and nosologic criteria for frontotemporal lobar degeneration: consensus of the Consortium for Frontotemporal Lobar Degeneration. Acta Neuropathol 2007; 114: 5-22.
4. Cainrs NJ, Neumann M, Bigio EH, Holm IE, Troost D, Hatanpaa KJ, Foong Ch, White III CHL, Schneider JA, Kretzschmar HA, Carter D, Taylor-Reinwald L, Paulsmeyer K, Strider J, Gitcho M, Goate AM, Morris JC, Mishra M, Kwong LK, Stieber A, Xu Y, Forman MS, Trojanowski JQ, Lee VM-Y, Mackenzie JRA. TDP-43 in familial and sporadic frontotemporal lobar degeneration with ubiquitin inclusions. Am J Pathol 2007; 171: 227-240.
5. de Silva R, Lashley T, Gibb G, Hanger D, Hope A, Reid A, Brandopadhyay R, Utton M, Strand C, Jowett T, Khan N, Anderton B, Wood N, Holton J, Revesz T, Lees A. Pathological inclusion bodies in tauopathies contain distinct complements of tau with three or four microtubule-binding repeat domains as demonstrated by new specific monoclonal antibodies. Neuropathol Appl Neurobiol 2003; 29: 288-302.
6. de Silva R, Lashley T, Strand C, Shiarli AM, Shi J, Tian J, Bailey KL, Davies P, Murayama S, Kretzschmar H, Neumann M, Lippa C, Halliday G, Mackenzie J, Ravid R, Dickson D, Wszolek Z, Iwatsubo T, Pickering-Brown SM, Holton J, Lees A, Revesz T, Mann DMA. An immunohistochemical study of cases of sporadic and inherited frontotemporal lobar degeneration using 3R- and 4R-specific tau monoclonal antibodies. Acta Neuropathol 2006; 111: 329-340.
7. Goedert M, Ghetti B, Spillantini MG. Frontotemporal dementia: implication for understanding Alzheimer's disease. Cold Spring Harb Perspect Med 2012; 2: a006254.
8. Ingelson M, Vanmechelen E, Lannfelt L. Microtubule-associated protein tau in human fibroblasts with the Swedish Alzheimer mutation. Neuroscience Lett 1996; 220: 9-12.
9. Iovino M, Pfisterer U, Holton JL, Lashley T, Swingler RJ, Calo L, Treacy R, Revesz T, Parmar M. Goedert M, Muqit MMK, Spillantini MG. The novel MAPT mutation K298E: mechanisms of mutant tau toxicity, brain pathology and tau expression in induced fibroblast-derived neurons. Acta Neuropathol 2014; 127: 283-295.
10. Kato S, Nakamura H, Otomo E. Reappraisal of neurofibrillary tangles. Immunohistochemical, ultrastructural and immunoelectron microscopical studies. Acta Neuropathol 1989; 77: 258-266.
11. Komori T. Tau-positive glial inclusions in progressive supranuclear palsy, corticobasal degeneration and Pick's disease. Brain Pathol 1999; 9: 663-679.
12. Kowalska A. The genetics of dementias. Part 1: Molecular basis of frontotemporal dementia and parkinsonism linked to chromosome 17 (FTDP-17). Postepy Hig Med Dosw 2009; 63: 278-286.
13. Kovacs GG, Rozemuller AJM, van Swieten JC, Gelpi E, Majtenyi K, A-Sarraj S, Troakes C, Bodi I, King A, Hortobagyi T, Esiri MM, Ansorge O, Giaccone G, Ferrer I, Arzbeger T, Bogdanovic N, Nilsson T, Leisser I, Alafuzoff I, Ironside JW, Kretzschmar H, Budka H. Neuropathology of the hippocampus in FTLD-Tau with Pick bodies: A study of the BrainNet Europe Consortium. Neuropathol Appl Neurobiol 2013; 39: 166-178.
14. Lipiński B, Pretorius E. Iron-induced fibrin formation may explain vascular pathology in Alzheimer's disease. Folia Neuropathol 2014; 52: 205.
15. Myers AJ, Pittman AM, Zhao AS, Rohrer K, Kaleem M, Marlowe L. Lees A, Leung D, McKeith IG, Perry RH, Morris ChM, Trojanowski JQ, Clark Ch, Karlawish J, Arnold S, Forman MS, Deerlin VV, de Silva R, Hardy J. The MAPT H1c risk haplotype is associated with increased expression of tau and especially of 4 repeat containing transcripts. Neurobiol Dis 2007; 25: 561-570.
16. Nagao SI, Kumamoto T, Masuda T, Uekyama H, Toyoshima I, Tsuda T. Tau expression in denervated rat muscles. Muscle Nerve 1999; 22: 61-70.

17. Narożańska E, Jasińska-Myga B, Sitek EJ, Robowski P, Brockhuis B, Lass P, Dubaniewicz M, Wieczorek D, Baker M, Rademakers R, Wszołek ZK, Sławek J. Frontotemporal dementia and parkinsonism linked to chromosome 17 – the first Polish family. Eur J Neurol 2011; 18: 535-537.
18. Neary D, Snowden JS, Mann DM. Classification and description of frontotemporal dementias. Ann NY Acad Sci 2000; 920: 46-51.
19. Neumann M, Mittelbronn M, Simon P, Vanmassenhove B, de Silva R, Lees A, Klapp J, Meyermann R, Kretzschmar HA. A new family with frontotemporal dementia with intronic 10+3 splice site mutation in the tau gene: neuropathology and molecular effects. Neuropathol Appl Neurobiol 2005; 31: 362-373.
20. Onyike CU, Diehl-Schmid J. The epidemiology of frontotemporal dementia. Int Rev Psychiatry 2013; 25: 130-137.
21. Pickering-Brown SM, Baker M, Nonaka T, Ikeda K, Sharma S, Mackenzie J, Simpson SA, Moore JW, Snowden JS, de Silva R, Revesz T, Hasegawa M, Hutton M, Mann DMA. Frontotemporal dementia with Pick-type histology associated with Q336R mutation in the tau gene. Brain 2004; 127: 1415-1426.
22. Pittman AM, Myers AJ, Abou-Sleiman P, Fung HC, Kaeleem M, Marlowe L, Duckworth J, Leung D, Williams D, Kilford L, Thomas N, Morris CM, Dickson D, Wood NW, Hardy J, Lees AJ, de Silva R. Linkage disequilibrium fine mapping and haplotype associatrion analysis of the tau gene in progressive supranuclear palsy and corticobasal degeneration. J Med Genet 2005; 42: 837-846.
23. Rossi G, Bastone A, Piccoli E, Mazzoleni G, Morbin M, Uggetti A, Giaccone G, Sperber S, Beeg M, Salmona M, Tagliavini F. New mutations in MAPT gene causing frontotemporal lobar degeneration: biochemical and structural characterization. Neurobiol Aging 2012; 33: 834.el-6.
24. Šerý O, Popová J, Míšek I, Pešák L, Janout V. Molecular mechanisms of neuropathological changes in Alzheimer's disease: a review. Folia Neuropathol 2013; 51: 1-9.
25. See TM, LaMarre AK, Lee SE, Miller BL. Genetic causes of frontotemporal degeneration. J Geriatr Psych Neurol 2010; 23: 260-268.
26. Spillantini MG, Murrell JR, Goedert M, Farlow MR, Klug A, Ghetti B. Mutation in the tau gene in familial multiple system taupathy with presenile dementia. Proc Natl Acad Sci U S A 1998; 95: 7737-7774.
27. Spina S, Farlow MR, Unverzagt FW, Kareken DA, Murrell JR, Fraser G, Epperson F, Crowther A, Spillantini MG, Goedert M, Ghetti B. The tuopathy associated with mutation +3 in intron 10 of Tau: characterization of the MSTD family. Brain 2008; 131: 72-89.
28. Tolnay M, Spillantini MG, Rizzini C, Eccles D, Lowe J, Ellison D. A new case of frontotemporal dementia and parkinsonism resulting from an intron 10 + 3-splice site mutation in the tau gene: clinical and pathological features. Neuropathol Appl Neurobiol 2000; 2: 368-378.

Abstracts from the Conference of the Team of Oncologic Neuropathology of the Committee on Neurological Sciences, Polish Academy of Sciences

"STRUCTURAL AND MOLECULAR BACKGROUND OF THE DRUG-RESISTANT EPILEPSY"

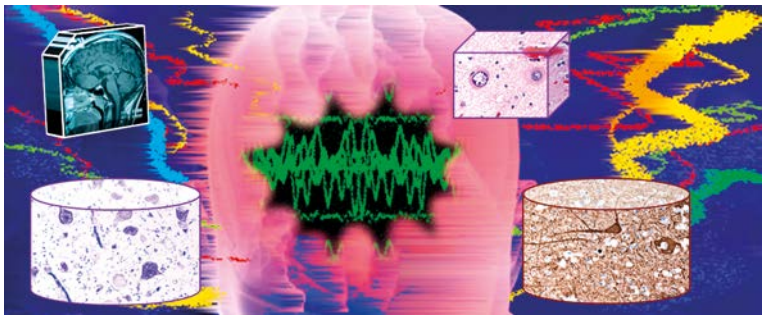

October 17, 2014

Warsaw, Poland

ORGANIZERS

The Team of Oncologic Neuropathology of the Committee of Neurological Sciences

Mossakowski Medical Research Centre,
Polish Academy of Sciences

SCIENTIFIC PROGRAMME COMMITTEE

Ewa Matyja – chairman
Teresa Wierzba-Bobrowicz
Milena Laure-Kamionowska
Wiesława Grajkowska

Conference was financially supported by Polish Academy of Sciences
and Mossakowski Medical Research Centre, Polish Academy of Sciences

Neuropathology behind symptomatic epilepsy. A bird's eye view over this vast stretch of land of neuropathology with some dives toward elected targets

Dariusz Adamek

Department of Neuropathology,
Jagiellonian University Medical College, Kraków, Poland

Seizures/epilepsy make one of the most significant symptoms of neurological/neurosurgical disorders. Secondary (symptomatic) epilepsy by its definition requires or assumes the presence of morphological pathology of the brain. Though new ILAE (International League Against Epilepsy) proposals of seizures/epilepsy classification discard the term "symptomatic" (epilepsy), this term has very important practical medical meaning, since it, at least implicitly, reminds the physician/neurologist/neurosurgeon, that seizures may have morphological and (supposedly, or hypothetically) operable cause (focal brain lesion). One has to exclude such "simple" (?) lesion first, before starting thinking of genetics or metabolic cause of epilepsy. Yet correlation between neuropathology and secondary epilepsy is complicated. The scope of all conceivable pathologies, that may underlie seizures is enormous and seems to cover almost all, if not verbatim all known disorders with morphological changes in the brain, however frequency of epilepsy/seizures is different in different conditions. Neoplastic, vascular, metabolic, developmental, inflammatory, toxic, and even neurodegenerative diseases, let alone posttraumatic lesions, may manifest with secondary epilepsy. Two main causes of secondary epilepsy may be distinguished: firstly, epilepsy with prevailing genetic and/or developmental background, and secondly epilepsy due to acquired causes (though this division is by far not perfect). From the practical neuropathological point of view, there is definite difference between the way one has to approach autopsy cases (especially those of children, in which developmental or inborn metabolic disturbances play very important role), and biopsy cases, in which tumors or other focal lesions of whatever nature predominate. In "surgical neuropathology" special attention has to be paid to any forms of lesions in which epilepsy is amenable to treatment by neurosurgical methods. This relates first of all to tumors, esp. to some particular tumors typically associated with epilepsy (so called LEATs) and focal malformations of cortical development. For the neuropathologist the information of the type of seizure has relatively limited importance since the phenotype of seizures and a character of pathology in general do not have direct relations. Of much consequence is first of all information on the duration of seizures (epilepsy), and its severity, which may truly help pathologist in difficult cases. He/she also has to be aware that some changes like Chaslin gliosis, hippocampal sclerosis and other unspecific changes maybe secondary to epilepsy. Nevertheless the general knowledge of epilepsy, at least at relatively basic level and its relations with the particular pathologies of brain is necessary for the neuropathologist. Special attention will be turned to epilepsy in relation tofakomatoses (including neurofibromatoses), perinatal brain lesions, and Rasmussen's encephalitis, and to secondary changes (due to epilepsy).

The work was financially supported by Jagiellonian University fund K/ZDS/003862.

Clinical heterogeneity of West syndrome – the possibilities and limitations of molecular diagnostics

Agnieszka Charzewska, Magdalena Nawara, Iwona Terczyńska, Monika Gos, Paulina Górka-Skoczylas, Kinga Duszyc, Dorota Hoffman-Zacharska

Department of Medical Genetics, Institute of Mother and Child, Warsaw, Poland

Background: West syndrome, also described as early infantile epileptic encephalopathy type 1 (EIEE1), is an age-specific, heterogenic epilepsy syndrome characterized by a triad of symptoms: infantile spasms, hypsarrhythmia on EEG, and arrest of psychomotor development. The syndrome has been divided into subtypes with known (symptomatic) and unknown (cryptogenic) aetiology. Mutations in the *ARX* gene are one of the causes of EIEE1, but in most patients with clinical recognition of the syndrome, the genetic background of the disease is very difficult to establish.

Aim: The purpose of the study is to present molecular approaches aiming to establish molecular basis of encephalopathy in patients with clinical recognition of cryptogenic West syndrome.

Material and methods: We used Sanger sequencing of the *ARX* gene and the Next Generation Sequencing using TruSight One sequencing panel (Illumina). The panel consists of 4813 genes with clinical relevance. Obtained data were filtered with custom designed panel containing 405 genes reported as causative for epilepsy using VariantStudio software (Illumina), and visualised with IGV software (Broad Institute). The pathogenicity of obtained variants was predicted using Polyphen2, Sift and Mutation Taster software.

Results: In one patient we found a deletion of 15 nucleotides (c.451_465delGCGGCCGCCGCGGCC) resulting in a loss of 5 alanines in a second polyalanine tract of the *ARX* gene. Although the shortening of polyalanine tracts is still contro-

versial, the X inactivation analysis performed for the family suggests that the deletion might be a pathogenic one. For two patients with West syndrome we obtained several variants in known genes causative for epilepsy. The variants are predicted to be pathogenic. They need to be further confirmed by sequencing analysis of family members.

Conclusions: The analysis of the *ARX* gene should be performed as a first-tier test in West syndrome patients even though exome sequencing is planned, since a high GC content of the *ARX* gene results in a very poor coverage in exome sequencing. The variants obtained by exome sequencing should be further confirmed by sequencing analysis of parents in order to establish *de novo* or inherited character of the variant. In families with a X-linked pattern of inheritance a cosegregation analysis should be performed in order to prove that examined variant segregates with EIEE phenotype.

Mutations in the *SCN1A* gene and what else... analysis of the molecular background of epileptic encephalopathy in Polish patients clinically diagnosed with Dravet syndrome

Paulina Górka-Skoczylas[1,2], Iwona Terczyńska[2], Anna Nykel[3], Kinga Duszyc[1], Agnieszka Pollak[4], Agnieszka Charzewska[1], Rafał Płoski[4], Dorota Hoffman-Zacharska[1,4]

[1]Department of Medical Genetics, Institute of Mother and Child, Warsaw, Poland
[2]Clinic of Neurology of Children and Adolescents, Institute of Mother and Child, Warsaw, Poland
[3]Faculty of Biology and Environmental Sciences, Cardinal Stefan Wyszynski University of Warsaw, Poland
[4]Institue of Genetics and Biotechnology, University of Warsaw, Poland

Epileptic encephalopathies (EEs) are an intractable group of severe childhood epilepsy disorders in which the epileptic electrical discharges themselves may contribute to progressive psychomotor dysfunctions. Epileptic encephalopathies are genetically heterogeneous diseases that may be caused by mutations in the genes which products are involved in controlling the neuronal excitability. Among the various EEs, Dravet syndrome (DS) has become one of the best-defined phenotype and the highest frequency of mutation detection. 75-80% of the DS cases have a demonstrable mutation in the *SCN1A* gene. Despite this high probability of a mutation identification, in individuals with a typical DS phenotype, up to 25% patients do not carry the *SCN1A* mutations. These cases are described as Dravet sydrome like (DS-like) and suggest the involvement of other genes such as *PCDH19*, *SCN2A*, *SCN1B* and *GABRG2*. About 25% of *SCN1A*-negative female Dravet-like patients carry a mutation in the *PCDH19* gene. Mutations in the other genes have been reported only in single cases with DS-like phenotype.

The aim of this study was to characterize prevalence of mutations in the *SCN1A*, *PCDH19*, *SCN2A*, *SCN1B* and *GABRG2* genes in two groups of patients with epileptic encephalopathies diagnosed as DS or DS-like.

The investigated group comprised Polish patients clinically diagnosed with DS or DS-like. All patients were screened for *SCN1A* point mutations by direct sequencing; subsequent rearrangement analysis (MLPA) was performed only for individuals without an identified point mutation. *SCN1A*-negative patients with phenotypes resembling DS were checked for the *PCDH19*, *SCN2A*, *SCN1B* and *GABRG2* mutations.

In order to identify new genes associated with a DS, affected individuals without *SCN1A* or *PCDH19* mutations were studied by using Next Generation Sequencing (NGS) – Exome Analysis with TrueSight One panel containing the 4,813 genes associated with known clinical phenotypes including epileptic disorders.

In the studied group, *SCN1A* mutations were identified in 85% individuals clinically diagnosed with DS. Mutations in the *PCDH19* gene were identified in 4 patients (females). No mutations within the *SCN2A*, *SCN1B* or *GABRG2* genes were identified, which confirms that mutations in these genes constitute a rare cause of DS-like phenotype.

Angiocentric glioma – a rare intractable epileptogenic tumour with heterogenous histopathology

Wiesława Grajkowska[1,2], Ewa Matyja[1,3], Paweł Daszkiewicz[4], Marcin Roszkowski[4], Peregud-Jarosław Pogorzelski[5], Mariola Zielińska[3]

[1]Department of Neurosurgery, M. Sklodowska-Curie Memorial Cancer Centre and Institute of Oncology, Warsaw, Poland
[2]Department of Pathology, The Children's Memorial Health Institute, Warsaw, Poland
[3]Department of Experimental and Clinical Neuropathology, Mossakowski Medical Research Centre, Polish Academy of Sciences, Warsaw, Poland
[4]Department of Neurosurgery, The Children's Memorial Health Institute, Warsaw, Poland
[5]Department of Pediatrics, Pediatric Hematology and Oncology, Pomeranian Medical University, Szczecin, Poland

Angiocentric glioma (AG) is a rare, low-grade tumour included into the group of "other neuroepithelial tumours"

in the 2007 WHO Classification of Tumours of the Central Nervous System. This is slowly growing neoplasm, classified as WHO grade I, with benign biological behavior. Typically, it occurs in children and young adults with a long-standing, intractable epilepsy.

Angiocentric glioma is typically localized within the cerebral cortex but may extend into the adjacent white matter and is often associated with foci of cortical dysplasia. The typical histopathological features of this tumour is angiocentric growth pattern with the presence of elongated, spindle-shaped cells, arranged around the blood vessels. Such perivascular, pesudorosette-like formations are present also in some other gliomas, particularly in ependymoma, astroblastoma or pilomyxoid astrocytoma. Moreover, AG might display histopathological features with palisading arrangement of tumour cells, resembling schwannoma-like pattern. Infiltration of elongated cells could be also observed in the subpial layers of cerebral cortex. Due to such morphological heterogeneity, the proper diagnosis of AG might be difficult, particularly considering the small biopsy material. Imunohistochemical studies provide the evidence of glial origin of neoplastic cells with expression of glial fibrillary acidic protein and S-100 protein. Moreover, a "dot-like" intracytoplasmic EMA staining, typical for ependymal differentiation of neoplastic cells, might be documented.

We present additional three cases of angiocentric variant of glioma in young adults with documented long follow-up. All tumours displayed characteristic perivascular orientation of neoplastic cells. The distinctive palisading arrangement of tumour cells, resembling schwannoma-like pattern were also documented. The neoplastic cells were positive for GFAP, S-100 protein and vimentin. In numerous cells, a "dot-like" intracytoplasmic EMA staining, were evidenced. The overall MIB-1 labelling index was less than 1%.

The histogenesis of AG is controversial. Angiocentric growth, "dot-like" EMA positivity and ultrastructural features might suggest ependymal differentiation. The appropriate diagnosis of this peculiar type of glial tumour is important for successful treatment without application of aggressive therapy.

Histopathology of brain tumours associated with epilepsy

Wieslawa Grajkowska[1], Ewa Matyja[2]

[1]Department of Pathology, The Children's Memorial Health Institute, Warsaw, Poland
[2]Department of Experimental and Clinical Neuropathology, Mossakowski Medical Research Centre, Polish Academy of Science, Warsaw, Poland

The neoplasms associated with epilepsy present with a broad spectrum of low-grade glial and glio-neuronal tumours, mostly corresponding to WHO grade I. These tumours usually manifest with epilepsy with early seizure onset, which is poorly controlled by antiepileptic drugs. Recently, the name "long-term epilepsy associated tumours" (LEATs) or epileptomas was introduced for these particular neoplastic lesions. Long-term epilepsy associated tumours are likely appear during brain development and they are preferential localized in the temporal lobe. The most frequent histopathological types of epileptogenic tumours include ganglioglioma (GG), dysembryoplastic neuroepithelial tumour (DNT), pleomorphic xanthoastrocytoma (PXA), pilocytic astrocytoma (PA), oligodendroglioma, and angiocentric glioma (AG). These tumours are frequently accompanied by focal cortical dysplasia (FCD) type IIIb. Blumcke *et al.* has proposed a novel, clinically useful, so-called A-B-C terminology to classify the large spectrum of epileptogenic brain tumours (Acta Neuropathol 2014; 128: 39-54). This classification recommends to use the standardized parameters based on selected immunohistochemical markers i.e. CD34, MAP2 and IDH1. The A-B-C terminology of neuropathological diagnosis of epileptomas includes: 1) "BNET" (basic neuroepithelial tumor) with CD34 expression, proposed to define the broad spectrum of GGs with dysplastic neuronal and neoplastic glial components; 2) "GNET", without CD34 expression, proposed to describe gangliocytic neuroepithelial tumor; 3) "DNET", exhibiting the multinodular appearance and specific glio-neuronal element, remains unchanged, as originally described by Daumas-Duport; 4) "CNET", proposed to define composite neuroepithelial tumours, characterized by the co-existence of at least two distinct LEAT entities; 5) "ANET", proposed as synonymous to the AG with ependymoma-like features; 6) "INET", which lacks any CD34 and glial MAP2 labeling, considered as an isomorphic neuroepithelial tumor, previously described as isomorphic astrocytoma corresponding to WHO Grade I; 7) "ENET-Epileptoma/NOS", proposed to describe any other epileptogenic neuroepithelial tumor that does not match the proposed A-B-C terminology.

Surgical resection of LEATs may be directed to oncological issue and/or to prevent epilepsy progression.

The perturbations in the neuronal interaction – a possible cause of the epileptic encephalopathy related to mutations in the *PCDH19* gene

Dorota Hoffman-Zacharska[1], Kinga Duszyc[1], Iwona Terczyńska[2], Marta Jurek[1], Ewa Obersztyn[1], Anna Winczewska-Wiktor[3], Tomasz Mazurczak[2], Jerzy Bal[1]

[1]Department of Medical Genetics, Institute of Mother and Child, Warsaw, Poland
[2]Clinic of Neurology of Child and Adolecents, Institute of Mother and Child, Warsaw, Poland
[3]Pediatric Neurology of Developmental Age Clinic, Poznan Medical University, Poland

Epilepsy and mental retardation limited to females (EFMR), caused by mutations in the X-linked *PCDH19* gene, is classified as an early infantile encephalopathy. It is characterized by a wide spectrum of phenotypes, varying from the severe cases resembling Dravet syndrome to more benign ones with normal intelligence. The *PCDH19* gene mutations in most cases arise *de novo*, but if not, the EFMR is characterized by an unusual mode of X-linked inheritance. Heterozygous females are generally affected, but hemizygous male carriers are not. Currently, this pattern of inheritance is explained by the model of "cellular interference" and tissue mosaicism due to the presence of the normal and mutated allele of the *PCDH19* gene in heterozygous females/mosaic males.

Mutations in the *PCDH19* gene are mainly localized in the extracellular cadherin domain (> 90%) building the homophilic interactions between the protocadherin 19 molecules. Deletions of the part or the whole gene are less common.

Three cases of the molecularly confirmed EFMR are presented. We identified mutations in the *PCDH19* gene – missense and nonsense in the region encoding cadherin domain and microdeletion of the X chromosome encompassing the whole *PCDH19* gene. Analysis of the phenotype-genotype correlations has shown that the mutation's type may influence the disease course but only in the relation to developmental delay and intellectual disability. Loss of one copy of the gene, or lack of protein synthesis (due to a nonsense mutation) may be less harmful than expression of two different forms of the protocadherin 19 interacting on the neuronal surface (missense mutation).

New concepts in definition and classification of the epilepsies. Proposal of International League Against Epilepsy

Joanna Jędrzejczak

Department of Neurology and Epileptology, Medical Center for Postgraduate Education, Warsaw, Poland

Over the past several decades, significant advances in neuroimaging, genomic technologies, and molecular biology have improved the understanding of the pathogenesis of seizures and epilepsy. In addition, many epilepsy syndromes have been delineated. As a result, the International League Against Epilepsy (ILAE) Commission on Classification and Terminology has prepared a new manuscript on the organization of the epilepsies, based on the 2010 proposal. Epilepsies can be organized in a flexible, multidimensional way depending on the purpose eg. by age, etiology, seizure type, EEG abnormality. A quick overview will be presented. It is unfortunate that most of the proposals in this report are modified interpretations and nomenclature of previous ILAE classifications; new terms are not better than the old ones, and recent advances have not been incorporated. Hence, the new ILAE report met with considerable protest from several expert epileptologists (*Panayiotopoulos. The new ILAE report on terminology and concepts for organization of epileptic seizures: A clinician's critical view and contribution*. Epilepsia 2011; 52: 2155-60). New terminology and concepts update the classification to be consistent with current understanding of the epilepsies in clinical practice. Currently there is no biologically based classification of the epilepsies.

In 2005 a Task Force of the ILAE formulated conceptual definitions of "seizure and epilepsy" (Fisher *et al.* 2005). The definitions were not sufficiently detailed to indicate in individual cases whether a person did or did not have epilepsy. Therefore, the ILAE commissioned a second task force to develop a practical (operational) definition of epilepsy, designed for use by doctors and patients. The results of several years of deliberations on this issue have now been published (Fisher *et al. A practical clinical definition of epilepsy*. Epilepsia 2014; 55: 475-82) and adopted as a position of the ILAE. This practical definition is designed for clinical use.

A person is considered to have epilepsy if they meet any of the following conditions:

1. At least two unprovoked (or reflex) seizures occurring greater than 24 hours apart.
2. One unprovoked (or reflex) seizure and a probability of further seizures similar to the general recurrence risk (at least 60%) after two unprovoked seizures, occurring over 10 years.

3. Diagnosis of an epilepsy syndrome. Epilepsy is considered to be resolved for individuals who had an age-dependent epilepsy syndrome but are now past the applicable age or those who have remained seizure-free for the last 10 years, with no seizure medicines for the last 5 years. The revised definition is not perfect. It will become more useful over time as we gain better information on seizure recurrence risks. But for now, the new definition better reflects the way clinicians think about epilepsy.

Progress in epilepsy treatment in tuberous sclerosis complex (TSC) – prevention is better than treatment

Sergiusz Jozwiak

The Children's Memorial Health Institute, Warsaw, Poland

Introduction of new antiepileptic drugs (AEDs) in the last decades was intended to reduce the number of patients with drug-resistant epilepsy. However, new agents have been characterized by better safety and lower ratio of interactions, but their efficacy remained at the similar level. The search of newer and more efficacious therapeutic interventions resulted in the concept of earlier, preventative treatment of epilepsy.

The search for new therapeutic approaches led to a renewed interest in the process of epileptogenesis. This cascade of molecular and cellular alterations (including changes in expression and function of receptors and ion channels) begins with an insult, brain injury, or genetic predisposition. Beginning from the insult there is often a latent period lasting weeks to months prior to the onset of seizures, followed by the development of clinical epilepsy and its comorbidities. This latent period of epilepsy development may offer a time window when an appropriate medication may stop or modify the epileptogenic process.

With improvement of tuberous sclerosis complex (TSC) diagnostics we are currently able to diagnose the disease prenatally or during the early infantile period. During the recent years in these patients treated in the Children's Memorial Health Institute in Warsaw carried out EEG studies every 4 weeks in the first 6 months of life or every 6 weeks in the next months until 24 months of age. Those with permanently normal EEG did not require any intervention. These patients whose EEG demonstrated paroxysmal activity received antiepileptic treatment with vigabatrin. The treatment has been continued until 24 months of age unless the patients developed clinical seizures.

Such approach has been assessed in 14 patients and resulted in significantly lower incidence of drug-resistant epilepsy. We have not observed any severe forms of mental retardation at 24 month of age comparing to 38% in the control group treated with standard approach.

Our results confirm that epilepsy prevention is possible and that antiepileptogenic (not antiepileptic) treatment may provide a new strategy for preventing epilepsy in susceptible individuals. Currently we conduct the EPISTOP project within 7th Framework Programme of the European Commission, which is intended to discover changes in the molecular biomarkers within the epileptogenic process leading to the clinical seizures.

Acknowledgments

This abstract was partially supported by the 7th Framework Programme of European Commission within the Large-scale Integrating Project EPISTOP (Proposal No: 602391-2; Proposal title: "Long term , prospective study evaluating clinical and molecular biomarkers of epileptogenesis in a genetic model of epilepsy – tuberous sclerosis complex").

The role of mTOR pathway in epilepsy treatment

Katarzyna Kotulska

The Children's Memorial Health Institute, Warsaw, Poland

Epilepsy affects about 1% of the general population and in one third of patients the seizures are refractory to medical treatment. Most currently available antiepileptic drugs suppress seizures but do not influence the process of epileptogenesis, thus change neither the natural history of the disease nor the burden of epilepsy-related neuropsychiatric problems. Recently, much attention is paid to the research on the mechanisms of epileptogenesis. It has been showed both in animal models and clinical settings that Mammalian Target of Rapamycin (mTOR) pathway is involved in development of wide spectrum of epilepsies. mTOR is a serine-threonine kinase regulating cell growth, differentiation, proliferation, and metabolism. Up-regulation of mTOR pathway is a key finding in many disorders associated with epilepsy, like tuberous sclerosis complex (TSC), cortical dysplasias, Cowden syndrome, and others. It has also been reported in brain tissue obtained from epileptogenic foci. Many studies showed that in animal models, mTOR inhibitor, rapamycin, or its derivate, mayameliorate the development of seizures and reduce the risk of epilepsy comorbidities. In mouse model of TSC, rapa-

mycin introduced after the onset of seizures reduced epilepsy severity and prolonged survival, whereas introduced before the onset of clinical seizures prevented epilepsy and premature death of the animals.

mTOR inhibitor, everolimus, was approved by EMA and FDA for the treatment of brain and kidney tumors associated with TSC. Accumulating data indicate that mTOR inhibitors may alleviate epilepsy in TSC patients. Clinical studies aimed to investigate the impact of everolimus on drug-resistant focal epilepsy in TSC are currently ongoing.

In conclusion, mTOR pathway presents a promising possible target for antiepileptogenic treatment, however, further studies are needed.

Prominent microcolumnar cortical architecture in the case of pontocerebellar hypoplasia

Milena Laure-Kamionowska[1], Krystyna Szymańska[1,2], Elżbieta Lipińska[3], Justyna Romańska[4], Monika Bekiesińska-Figatowska[5], Jolanta Toborowicz[1], Barbara Raczkowska[1]

[1]Department of Experimental and Clinical Neuropathology, Mossakowski Medical Research Centre, Polish Academy of Science, Warsaw, Poland
[2]Department of Child Psychiatry, Medical University of Warsaw, Poland
[3]Department of Pediatric Neurology, SPDSK, Warsaw, Poland
[4]Clinic of Neonatology and Neonate Intensive Care, Medical University of Warsaw, Poland
[5]Department of Diagnostic Imaging, Institute of Mother and Child, Warsaw, Poland

Pontocerebellar hypoplasia is congenital neurodevelopmental disorder characterized by hypoplasia of the cerebellar cortex, dentate nuclei, pontine and olivar nuclei. This report presents a case of 22-week-old infant born at 25 gestational weeks by cesarean section (adjusted age 7 weeks). During hospitalization the neonate underwent sepsis and surgery due to meconium ileus. The infant had seizures treated with phenobarbital and phenytoin. He clinically presented failure to thrive, hypotonia, episodes of irritability. An ultrasonography of the brain revealed intraventricular hemorrhage. Magnetic resonance imaging (MRI) examination of the head showed posthemorrhagic changes in the cerebellar vermis and cerebellar hemispheres with destruction of cerebellar hemispheres. Child died suddenly due to respiratory insufficiency. Postmortem examination of the brain revealed microencephaly, hypoplastic cerebellum and narrow basal part of the pons. Neuropathological abnormalities included hypoplasia of the cerebellar hemispheres with the exception of the vermis and flocculi. Complete loss of Purkinje and granule cells in the cerebellar hemispheres cortex with astrocytic reaction, and a normal microscopic appearance of the floccular and vermal cortex were stated. Loss of the majority of neurons in the dentate nucleus with remaining dentate neurons clustered in islands, loss of pontine nuclei with near absence of transverse pontine fibers and dysplastic olivary nuclei with reactive changes were noted. The morphological picture of brain abnormalities correspond with the diagnosis of pontocerebellar hypoplasia. The changes within brain stem and cerebellum in the presented case coexisted with generalised persistent fetal radial columnar architecture. The minicolumnar arrangement was visible in all regions of the cerebral hemispheres with predominance in the temporal and frontal lobes. Prominent microcolumnar cortical architectonic pattern is regarded as separate type Ia of focal cortical dysplasias according to International League Against Epilepsy classification. There is a dilemma whether persistent fetal cerebral cortical circuit is the result of maturational arrest in histogenesis of neocortex or primary cortical dysplasia. Sarnat concludes that columnar architecture is a maturational arrest in histogenesis of the neocortical plate and becomes a component of cortical dysplasia in the perinatal period. It seems that in the presented case the persistent prominent columnar organization of neurons is a result of maturational delay in the cortical development accompanying pontocerebellar hypoplasia.

State-of-the-art imaging of patients with refractory epilepsy

Edyta Maj

2nd Department of Clinical Radiology, Medical University of Warsaw, Poland

The crucial issue in surgical treatment of patients with refractory epilepsy is an accurate detection, localization and characterization of brain lesion. There is significant improvement in clinical status after surgery in over 70% of patients with refractory epilepsy if abnormal focal lesions were correctly diagnosed.

The diagnosis is difficult, due to a broad spectrum of underlying pathologies (e.g. hipocampal sclerosis, congenital abnormalities, epileptomas) which are often very subtle or invisible in available neuroimaging techniques.

The imaging procedure of choice in the investigation of patients with epilepsy is magnetic resonance imaging (MRI) performed on high-field systems (1.5 T and 3.0 T)

using dedicated protocol. Acquired images should be evaluated by experienced neuroradiologists.

Besides the standard sequences, such as T1, T2, FLAIR, DWI in axial plane, T2 in coronal and saggital planes (4-5 mm slice thickness), applied in brain imaging, it is vital to use higher spatial resolution sequences like FLAIR in a plane perpendicular to the long axis of the hippocampus (2-3 mm), 3D T1-weighted inversion recovery (3D T1 IR) with isotropic voxel (1 mm) and sequence sensitive for the detection of hemosiderin and calcium (T2*/SWI).

Contrast enhanced images can be helpful in characterization of epileptogenic lesions. Furthermore, functional MRI and MR tractography is useful for mapping of the speech-eloquent areas and preoperative planning.

Magnetic resonance imaging allows morphologic evaluation of the brain, whereas positron emission tomography (PET) is a functional imaging technique which enables, by visualization of the regional glucose uptake, to assess the metabolic activity of the brain. Another valuable method is computed tomography, which allows detection of calcifications and hemorrhage.

The important issue in the identification of focal epileptogenic lesions is the correlation of radiological findings with clinical status and the results of other tests, including electroencephalography (EEG). Such analysis facilitates accurate characterization of abnormalities detected on imaging, helping in discrimination of epileptogenic and non-epileptogenic lesions.

Refractory epilepsy: radiologic – pathologic correlation

Edyta Maj[1], Andrzej Rysz[2], Aleksandra Łężak[3], Ewa Matyja[4], Andrzej Marchel[2], Andrzej Cieszanowski[1], Marek Gołębiowski[1], Olgierd Rowiński[1]

[1]2nd Department of Clinical Radiology, Medical University of Warsaw, Poland
[2]Department of Neurosurgery, Medical University of Warsaw, Poland
[3]1st Department of Clinical Radiology, Medical University of Warsaw, Poland
[4]Department of Experimental and Clinical Neuropathology, Mossakowski Medical Research Centre, Polish Academy of Sciences, Poland

Aims and objectives: We aimed to assess the sensitivity of magnetic resonance imaging (MRI) for the detection and characterization of focal brain lesions in patients who subsequently underwent operation due to refractory epilepsy. MRI findings were correlated with histopathology results based on a new classification of focal cortical dysplasia (FCD) proposed by ILAE (International League Against Epilepsy) Diagnostic Methods Commission in 2011.

Material and methods: Analysis included 71 patients aged 20-62 years (mean = 35) with right (n = 31) and left (n = 36) temporal lobe epilepsy, right (n = 1) and left (n = 1) frontal lobe epilepsy, left parietal lobe epilepsy (n = 1), gelastic epilepsy (n = 1). MRI (1.5 T) was performed using following sequences: T1SE (axial-5 mm), T2TSE (axial-5 mm), FLAIR (axial-5 mm), DWI (axial-5 mm), T2TSE (saggital-5 mm), T2TSE (coronal-5 mm), IR (coronal-2 mm), FLAIR (coronal-2 mm) and contrast-enhanced T1SE (axial-5 mm), 3DT1GRE (1 mm). MRI findings were correlated with histopathology results.

Results: In 57 of 71 patients MRI detected focal lesions (80% sensitivity), failing to demonstrate abnormalities in 14 patients: FCDIIA (n = 10), "dual pathology" (n = 3), FCDIB (n = 1). Of 74 abnormalities revealed by histopathology, MRI correctly characterized 42 lesions (57% sensitivity), including all of FCDIIB, FCDIIIA, FCDIIIB, FCDIIID, double pathologies, DNTs, gangliogliomas, hamartomas (100% sensitivity), 80% of glial scars and post-infarct malacia, 68% of "dual pathologies", 17% of FCDIIA. None of FCDIA, FDAIB, oligodendrogliomas and tuberous sclerosis were correctly characterized by MRI.

Conclusions: MRI is feasible for the detection and characterization of some lesions in refractory epilepsy, including FCDIIB, FCDIIIA, FCDIIIB, FCDIIID and epileptomas. The demonstration and characterization by MRI of more than one lesion is often not possible.

The current histopathological classifications of cortical dysplasia

Ewa Matyja[1], Wiesława Grajkowska[1,2]

[1]Department of Experimental and Clinical Neuropathology, Mossakowski Medical Research Centre, Polish Academy of Sciences, Warsaw, Poland
[2]Department of Pathology, Children's Memorial Health Institute, Warsaw, Poland

There is a wide variability of pathological presentation of cerebral cortex lesions, associated with pharmacoresistant epilepsy, that linked to cortical dysplasia. The first description of epilepsy-related cortical abnormality was reported by Taylor *et al.* (1971). Since then, the term "focal cortical dysplasia" (FCD) has been widely accepted to describe a large spectrum of lesions characterized by disorganization of cortical lamination and various cytoarchitectural abnormalities. During the last years, numerous FCD classifications have been proposed. The scheme introduced by Palmini *et al.* (2004), dividing FCD into distinct histopathological type I and type II, have appeared to be most acceptable in international community. According to

Palmini's classification, FCD type I included type IA with architectural disturbances of cortical lamination, and type IB with additional hypertrophic pyramidal neurons outside layer 5. Focal cortical dysplasia type II was also divided into type IIA with dysmorphic neurons and type IIB with dysmorphic neurons and large, eosinophilic balloon cells.

A revised clinicopathologic classification system was proposed by ILAE (International League Against Epilepsy) Task Force in 2011 (Blümcke *et al.*, 2011). This is a three-tiered classification system of focal cortical dysplasia that distinguishes isolated forms of FCD (FCD types I and II) from variants associated with another epileptogenic lesions (FCD type III). This scheme seems to provide a better characterization of clinical, imaging, pathologic and genetic features of distinct FCD subtypes and is helpful for clinical practice. According to ILAE histopathological classification, focal cortical dysplasia type I is a malformation presenting with abnormal radial (FCD type Ia) or tangential (FCD type Ib) cortical lamination. Moreover, the combination of both this variants is considered as FCD type Ic. Focal cortical dysplasia type II represents a malformation with disrupted cortical lamination and specific cytologic abnormalities, which differentiates FCD type IIa with dysmorphic, bizarre neurons in grey and/or white matter from FCD type IIb with dysmorphic neurons and so-called "balloon cells", similar to those observed in tuberous sclerosis. Cells with an intermediate phenotype between dysplastic neurons and balloon cells could be also encountered. Immunohistochemical studies reveal expression of both, neuronal and glial markers in dysmorphic and some balloon cells. The neuronal anomalies are usually accompanied by advanced astroglial gliosis in surrounding tissue. Focal cortical dysplasia type III refers to cortical lamination abnormalities associated with a principal lesion, usually adjacent to or affecting the same cortical area/lobe. Four variants of FCD type III are distinguished: FCD type IIIa – associated with hippocampal sclerosis (HS); FCD type IIIb – associated with glioneuronal tumours (ganglioglioma, dysembryoplastic neuroepithelial tumor – DNT) or other epilepsy-associated neoplasms; FCD type IIIc – associated with vascular malformations (cavernous or arteriovenous malformations, leptomeningeal vascular malformations, telangiectasias, meningioangiomatosis) and FCD type IIId – associated with any other principal lesion, acquired during early life (traumatic brain injury, perinatal ischemic injury, inflammatory or infectious diseases i.e. Rasmussen encephalitis, bacterial or viral infections). Moreover, so-called FCD type III not otherwise specified (NOS) is introduced to identify a clinically/radiologically suspected principal lesion in cases when tissue is not available for microscopic analysis.

The rare association between FCD types IIa and IIb with hippocampal sclerosis, tumour, or vascular malformation should be classified as "double pathology", not as FCD type III variant. Such pathology are suspected to be association of two epileptogenic lesions with independent pathogenesis.

It is worth noting, that any classification system using histopathologic examination requires representative surgical biopsy material and standardized laboratory techniques.

References

1. Blumcke I, Thom M, Aronica E, Armstrong DD, Vinters HV, Palmini A, Jacques TS, Avanzini G, Barkovich AJ, Battaglia G, Becker A, Cepeda C, Cendes F, Colombo N, Crino P, Cross JH, Delalande O, Dubeau F, Duncan JS, Guerrini R, Kahane P, Mathern GW, Najm I, Özkara C, Raybaud C, Represa A, Roper SN, Salamon N, Schulze-Bonhage A, Tassi L, Vezzani A, Spreafico R. The clinico-pathological spectrum of Focal Cortical Dysplasias: a consensus classification proposed by an ad hoc Task Force of the ILAE Diagnostic Methods Commission. Epilepsia 2011; 52: 158-174.
2. Palmini A, Najm I, Avanzini G, Babb T, Guerrini R, Foldvary-Schaefer N, Jackson G, Luders HO, Prayson R, Spreafico R, Vinters HV. Terminology and classification of the cortical dysplasias. Neurology 2004; 62: S2-S8.
3. Taylor DC, Falconer MA, Bruton CJ, Corsellis JA. Focal dysplasia of the cerebral cortex in epilepsy. J Neurol Neurosurg Psychiatry 1971; 34: 369-387.

A non-specific histopathological form of dysembrioplastic neuroepithelial tumour – diagnostic dilemmas

Ewa Matyja[1,2], Wiesława Grajkowska[3,4], Przemysław Kunert[4], Andrzej Marchel[4]

[1]Department of Experimental and Clinical Neuropathology, Mossakowski Medical Research Centre, Polish Academy of Sciences, Warsaw, Poland
[2]Department of Neurosurgery, M. Sklodowska-Curie Memorial Cancer Centre and Institute of Oncology, Warsaw, Poland
[3]Department of Pathology, Children's Memorial Health Institute, Warsaw, Poland
[4]Department of Neurosurgery, Warsaw Medical University, Poland

Dysembrioplastic neuroepithelial tumour (DNT) is a distinct clinic-pathological entity related with a drug resistant, intractable epilepsy with the onset in childhood or young adolescence. The tumour was originally described as a benign lesion with characteristic histopathological features, including intracortical topography, nodular structure and presence of unique glial and neuronal components, called "specific glio-neuronal element". Such lesion was often accompanied by cortical dysplasia of the adja-

cent cerebral cortex and/or bone deformity. However, DNT might present a large spectrum of morphological picture that results in some difficulties in differential diagnosis.

Three different histopathological subtypes of DNT could be identified: 1) simple form, that is composed exclusively of specific glioneuronal element, 2) complex form with nodular architecture, including nodules that resemble conventional gliomas, accompanied by specific glio-neuronal element and 3) non-specific form of DNT that lacks the specific glio-neuronal element and resemble other conventional types of glial or glio-neuronal neoplasms. The non-specific histopathological form of DNT is controversial. Occasionally, tumors exhibiting a mixed pattern, with features of DNT and additional neuronal or glioneuronal components. All subtypes of DNT are characterized by clinical stability with long-follow up with a normal life without recurrences and seizures.

The aim of this study was to present an unique morphological patterns of non-specific form of DNT composed of multinodular intracortical lesions with various histological components. Considering the non-specific form of DNT, other tumours presenting with epilepsy must be considered in differential diagnosis i.e.: low grade glial tumours as pilocytic astrocytoma, oligodendroglioma, astrocytoma or mixed oligoastrocytoma and high-grade glial neoplasms as anaplastic astrocytoma, anaplastic oligoastrocytoma or astroblastoma. Moreover, mixed glio-neuronal tumour as ganglioglioma ought to be taken into consideration. The distinction of DNT lesion from other forms of gliomas allows to avoid unnecessary aggressive radio- or chemotherapy in children or young adults.

Gelastic epilepsy as a result of hypothalamic hamartoma

Ewa Nagańska[1], Andrzej Marchel[2], Leszek Królicki[3], Ewa Matyja[4]

[1]Department of Neurology and Epileptology, Medical Center for Postgraduate Education, Warsaw, Poland
[2]Department of Neurosurgery, Warsaw Medical University, Poland
[3]Department of Nuclear Medicine, Warsaw Medical University, Poland
[4]Department of Experimental and Clinical Neuropathology, Mossakowski Medical Research Centre, Polish Academy of Sciences, Warsaw, Poland

Gelastic epilepsy is a type of epilepsy in which seizures may begin at any age, but usually before three or four years of age. The seizures usually start with laughter, often described as 'empty' and not very pleasant. The laughter occurs suddenly, comes on for no obvious reason. Children may also have other types of seizures, including tonic-clonic and atonic seizures. Gelastic epilepsy is slightly more common in boys than in girls. It is, however, very rare and of every 1,000 children with epilepsy, only one – two children will have gelastic epilepsy. In the clinical features they can be found also signs of precocious puberty, learning and behavioural problems.

The most common areas of the brain which give rise to gelastic seizures are the hypothalamus, the temporal lobes and the frontal lobes. A common cause of gelastic epilepsy is a small tumor in the hypothalamus. This tumor may be either a hamartoma or an astrocytoma. A hamartoma is a benign tumor mass, made up of an abnormal mixture of cells. The majority of these tumors are benign. This means that they may grow only very slowly, and do not spread to other parts of the brain or body.

The aim of the presentation is the case of 21 yrs old woman with drug resistant gelastic epileptic seizures, treated with many different antiepileptic drugs for 17 years. The diagnostic MRI scans were performed four times, and described as "normal". In repeated MRI of the brain in 2013 the tumor mass in hypothalamus was diagnosed, what was proved in PET CT. The patient was surgically treated. The neuropathological examination revealed the typical features for hypothalamic hamartoma. The postoperative course complicated by paresis and impairment of memory functions. After intensive rehabilitation lasting for several months, she has no neurological problems. From the operation the gelastic seizures don't exist any longer. She suffers from complex partial seizures, 2-3/moth, and still needs the antiepileptic pharmacological treatment. Surgery, or a special form of radiotherapy, is only available in the high specialized neurosurgical centres.

Reactive gliosis – in the search of new elements of its immunohistochemical signature

Edyta Radwańska[1], Ewelina Grzywna[2], Anastazja Stój[1], Dariusz Adamek[1], Artur Surówka[3], Magdalena Szczerbowska-Boruchowska[3], Marek Lankosz[3], Marek Moskała[2]

[1]Department of Neuropathology, Jagiellonian University Medical College, Krakow, Poland
[2]Department of Neurosurgery and Neurotraumatology University Hospital, Krakow, Poland
[3]Department of Medical Physics and Biophysics, Faculty of Physics and Applied Computer Science, AGH University of Science and Technology, Krakow, Poland

Reactive gliosis is unspecific response of astrocytes in many different conditions. Reactive gliosis of astrocytes is possibly is most often unspecific morphological change observed in central nervous system in neoplasms, inflammations, malformations, vascular pathologies, demyelinations, toxic conditions, metabolic disturbances and neurodegeneration. Though having the same name and similar morphology, supposedly molecular and metabolic properties of gliosis differ with regard to its underlying condition. There is still need to find ways for more specific immunohistochemical characterization of gliosis. The aim of the study was the estimation of relatively little known proteins.

Astrocyte elevated gene 1 (AEG-1)/LYRIC/MTDH and Mesencephalic astrocyte-derived neurotrophic factor (MANF)/ARMET. Astrocyte elevated gene 1, also known as metadherin, regulates key cells processes in oncogenesis like angiogenesis, migration, invasion and metabolism of tumour cells. MANF belongs to evolutionary conservative group of neurotrophicfactors. Moreover we tested expression of cytokeratins and mutated IDH1. Material: 96 cases of gliosis concomitant to following pathologies: primary and secondary tumours, abscesses, infarcts, vascular malformations. The regions of special interest were areas of gliosis in aforementioned lesions. The immunoexpression of the proteins was investigated using the following antibodies: Anti-human cytokeratin clone AE1/AE3, Rabbit monoclonal anti-Lyric clone EP 4445, Mouse monoclonal anti IDH1 R132H, Rabbit anti-human polyclonal MANF LS-B2688, Anti-human monoclonal antibody GFAP. AEG-1 imunopositivity was noted in 28/46 cases of gliosis and in 14/50 gliomas. MANF immunopositivity was noted in 20/46 cases of gliosis and in 15/50 gliomas (mostly glioblastomas). Moreover expression of MANF and AEG-1 was observed in cytoplasm and dendrites of neurons. Almost all cases of gliosis showed distinct expression of cytokeratins AE1/AE3 in astrocytes which was always limited to unequivocally smaller number of astrocytes when compared with GFAP what confirms that AE1/AE3+ cytokeratins are much more selective marker of reactive astrocytes than GFAP. No cases of gliosis showed positivity mutated IDH1, though 26% of gliomas (80% of oligodendrogliomas) were IDH1 positive. Only part of gliosis and of gliomaswas AEG-1 and/or MANF positive. Further research is necessary to find the answer for the cause of these differences.

The work was financially supported by Jagiellonian University fund K/ZDS/003862.

Current recommendations in cavernoma related epilepsy – diagnostic evaluation and management

Marcin Roszkowski[1], Paweł Daszkiewicz[1], Krzysztof Drabik[1], Wiesława Grajkowska[2]

[1]Department of Neurosurgery, The Children's Memorial Health Institute, Warsaw, Poland
[2]Department of Pathology, The Children's Memorial Health Institute, Warsaw, Poland

Cerebral cavernous malformations (CCMs) are well-defined lesions occur in 0.4-0.9% of the population. Seizures and epilepsy are frequent clinical manifestations, represent the most common symptomatic presentation of supratentorial lesions and have a great impact on social function and quality of life. Patients with CCM-related epilepsy (CRE) who undergo surgical resection achieve postoperative seizure freedom in only about 75% of cases, because insufficient efforts are made to adequately define and resect the epileptogenic zone. The authors present current pathophysiological concepts related to epilepsy associated with CCMs, definitions of definitive and probable CRE, and recommendations regarding the diagnostic evaluation. They also discuss the spectrum of disorders associated with these lesions and review the natural history, prognosis, and options for etiology-specific management of patients with CRE. At the time being published data do not permit the proposal of an evidence-based treatment guideline with regards to the resection of CCM in patients with CRE, although authors recommend excision of at least the cortical parts of the surrounding gliotic hemosiderin stained tissue.

A case of tuberous sclerosis complex associated with hemimegalencephaly in an infant of 32 weeks gestational age

Anna Taraszewska[1,2], Jacek M. Witwicki[3], Milena Laure-Kamionowska[1], Wiesława Grajkowska[1], Ryszard Szopiński[4]

[1]Department of Experimental and Clinical Neuropathology, Mossakowski Medical Research Centre, Polish Academy of Sciences, Warsaw, Poland
[2]Department of Pathomorphology, Bielanski District Hospital, Warsaw, Poland
[3]Department of Neonatology, Bielanski District Hospital, Warsaw, Poland
[4]Laboratory of Photographic Documentation, Mossakowski Medical Research Centre, Polish Academy of Sciences, Warsaw, Poland

Hemimegalencephaly (HME) and tuberous sclerosis complex (TSC) are distinct and unrelated conditions that both are characterized by an early abnormality in cortical development, responsible for the intractable epilepsy. The association of hemimegalencephaly and TSC is extremely rare, with only a few cases published in the literature so far.

This report presents a case of a preterm male infant born at 32 week of gestational age by emergency cesarean section because of intrauterine asphyxia danger. Examination by ultrasonography disclosed cardiomegaly, multiple cardiac tumors corresponding to rhabdomyoma, cysts in the kidneys and the brain abnormality exhibiting marked enlargement and pachygyria of the left hemisphere. The baby died in the second day of age. Postmortem gross examination of the brain showed left hemimegalencephaly with features of pachygyria and agyria, hardened centrum semiovale and dilated left lateral ventricle, whereas contralateral hemisphere, brain stem and cerebellum appeared unaffected. By microscopic study of the brain the lesions were characteristic for TSC and consisted of cortical and subcortical tubers and subependymal nodules in both hemispheres and subependymal giant cell astrocytoma in the left hemisphere. The changes in the left hemimegalencephalic hemisphere were more extensive, with massive aggregates of gemistocyte-like balloon cell, extending from the cortical surface into the subcortical white matter and the subventricular germinal matrix. Some of the alterations and cellular abnormalities in hemimegalencephalic hemisphere had common characteristics for both TSC and HME and were difficult to separate between them and to consider, whether they represent two separate malformations or one process connected with the early development of TSC with extraordinarily extensive cerebral lesions.

Focal cortical dysplasia in patients with drug resistant epilepsy. Neuropathological features

Teresa Wierzba-Bobrowicz[1], Sylwia Tarka[2], Tomasz Stępień[1], Henryk Koziara[3], Bartosz Królicki[3]

[1]Department of Neuropathology, Warsaw Medical University, Poland
[2]The Department of Forensic Medicine, Warsaw Medical University, Poland
[3]Department of Neurosurgery, Institute of Psychiatry and Neurology, Warsaw, Poland

Focal cortical dysplasia (FCD) is very common in patients with drug refractory epilepsy in both children and adult patients. The ILAE (International League Against Epilepsy) Diagnostic Methods Commission, proposed a three-tiered classification system to characterize clinicopathological FCD entities.

We analyzed the neuropathological changes in two females (one aged 28; epilepsy diagnosed at the age of 10 years and the other 59 years old; epilepsy since the age of 12) treated neurosurgically because of drug-resistant epilepsy.

A neuroimaging study, showed in both cases focal cortical thickening and/or blurring of the grey-white matter interface in frontal lobes. The neuropathological findings (using histochemical and immunohistochemical methods) in cortical dysplasia showed cortical laminar disorganization and various pathological forms of neurons. Immature neurons were usually seen as round homogeneous cells with large nuclei and dysmorphic neurons with distorted cell body and pathological accumulation of neurofilaments. Immature neurons were sometimes immunoreactive to neuronal antibodies. The observed giant cells had large cytoplasm, usually normal in shape, sometimes had multiple nuclei. Balloon cells, considered the most characteristic of FCD, occurred in both cases. These cells showed large body size, eosinophilic cytoplasm and eccentric, sometimes multi-lobed nucleus. They had both neuronal and glial features like-intermediate cells. In the younger woman hypertrophy and proliferation of astroglia in areas of dysplasia were observed. Focal cortical dysplasia type II b with dysmorphic neurons and balloon cells was diagnosed in both described cases. The frequency of seizures decreased after neurosurgery.

Instructions to Authors

This instruction is based upon *Uniform Requirements for Manuscripts Submitted to Biomedical Reviews* (the complete document appears in N Engl J Med 1997; 336, 309-315).

Aims and scope

Folia Neuropathologica is an official journal of the Mossakowski Medical Research Centre Polish Academy of Sciences and the Polish Association of Neuropathologists. The journal publishes original articles and reviews that deal with all aspects of clinical and experimental neuropathology and related fields of neuroscience research. The scope of journal includes surgical and experimental pathomorphology, ultrastructure, immunohistochemistry, biochemistry and molecular biology of the nervous tissue. Papers on surgical neuropathology and neuroimaging are also welcome. The reports in other fields relevant to the understanding of human neuropathology might be considered.

Ethical consideration

Papers describing animal experiments can be accepted for publication only if the experiment conforms to the legal requirements in Poland as well as with the European Communities Council Directive of November 24, 1986 or the National Institute of Health Guide (National Institute of Health Publications No. 80-23, Revised 1978) for the care and use of Laboratory Animals for experimental procedure. Authors must provide a full description of their anesthetics and surgical procedures. Papers describing experiments on human subjects must include a statement that experiments were performed with the understanding and consent of each subject, with the approval of the appropriate local ethics committee.

Submission of manuscripts

Articles should be written in English. All new manuscripts should be submitted through the online submission at http://panel2.termedia.pl/fn
For authors unable to submit their manuscript online, please contact with Prof. E. Matyja, Editor-in-Chief of *Folia Neuropathologica*, ematyja@imdik.pan.pl
The Editorial Board reserves the right to reject a paper without reviewers' opinion if the content or the form of the paper does not meet minimum acceptance criteria or if the subject of the paper is beyond the aims and scope of the journal.

Legal aspects

In sending the manuscript the author(s) confirm(s) that (s)he has (they have) not previously submitted it to another journal (except for abstracts of no more than 400 words) or published it elsewhere. The author(s) also agree(s), if and when the manuscript is accepted for publication, to automatic and free transfer of copyright to the Publisher allowing for the publication and distribution of the material submitted in all available forms and fields of exploitation. The author(s) accept(s) that the manuscript will not be published elsewhere in any language without the written consent of the copyright holder, i.e. the Publisher.
All manuscripts submitted should be accompanied by an authors' statement including signed confirmation of the above and confirming that this publication has been approved by all co-authors (if any), as well as by the responsible authorities at the institution where the work has been carried out. The authors' statement should be signed by ALL co-authors. Additionally, the author(s) confirm(s) that (s)he is (they are) familiar with and will observe the "Instruction to Authors" included in *Folia Neuropathologica* and also that all sources of financial support have been fully disclosed. Materials previously published should be accompanied by written consent for reprinting from the relevant Publishers. In the case of photographs of identifiable persons, their written consent should also be provided. Any potential conflict of interest will be dealt with by the local court specific to the Publisher. Legal relations between the Publisher and the author(s) are in accordance with Polish law and with international conventions binding on Poland.
Authors agree to waive their royalties.

Anonymous review

All manuscripts will be subject to a process of anonymous editorial review.

Preparation of manuscripts

Articles must be written in English, with British spelling used consistently throughout. Authors not entirely familiar with English are advised to correct the style by professional language editors or native English speakers.

- The length of original article should not exceed 20 printed pages including text, illustrations, tables, and references.
- Manuscripts should be typed using 12pts.font, double-spaced, and fully corrected. Allow a margin at least 2.5 cm at the top, bottom and left side of the page. Text should not be justified.

- The title page should contain: the author's full names, title of the paper, all authors' affiliations, full name and address of the communicating author (including e-mail address and fax number), running title (not exceed 40 characters including spaces).
- The abstract should not exceed 350 words. A list of 3–10 key words is recommended below the abstract.
- The manuscript body should be organized in a standard form with separate sections: Introduction, Material and Methods, Results, Discussion, and References. Review articles should be divided into sections and subsections as appropriate without numbering.
- Do not underline in the text. Avoid footnotes.
- All dimensions and measurements must be specified in the metric system.
- The source of any drug and special reagent should be identified.
- Particular attention needs to be paid to the selection of appropriate analysis of data and the results of statistical test should be incorporated in the results section.
- The nomenclature used should conform to the current edition of the Nomina Anatomica or Nomina Anatomica Veterinaria.
- Acknowledgements should be made in a separate sheet following Discussion and before References. These should contain a list of dedications, acknowledgements, and funding sources.
- Legends of figures and tables should be typed on separate pages.
- The editor reserves the right to make corrections.

Tables

- Tables numbered in Roman numerals require a brief but descriptive heading.
- The major divisions of the table should be indicated by horizontal rules.
- Explanatory matter should be included in footnotes, indicated in the body of the table in order of their appearance.
- Tables must not duplicate material in the text or in illustration.

Illustrations

All figures should be supplied electronically at resolution 300dpi in all standard formats (tiff, jpg, Adobe Photoshop, Corel Draw, and EPS). Name your figure files with "Fig" and the figure number, e.g., Fig1.tif

- The maximum figure size is 84 mm or 174 mm for use in a single or double column width, respectively.
- When possible, group several illustrations on one block for reproduction. Like all other figures, block should be prepared within a rectangular frame to fit within a single or double column width of 84 and 174 mm, respectively, and a maximum page height of 226 mm.
- Each figure should include scale magnification bar; do not use magnification factors in the figure legends.
- All figures, whether photographs, graphs or diagrams, should be numbered using Arabic numerals and cited in the text in consecutive numerical order
- **Immunohistochemical study requires color illustrations of very good quality. The papers with white and black immunohistochemistry will not be accepted.**
- **The expense of color illustrations must be borne by the authors.** The cost of color print for every successive 8 pages is 200 euro irrespective of the number of color pages, i.e., the price remains the same whether there is one or eight pages.

The Publisher makes out the bill to the communicating Author.

References

The list of references (written on a separate page) should include only those publications that are cited in the text. Avoid citation of academic books, manuals and atlases. References may be arranged alphabetically and numbered consecutively. References should be given in square brackets with no space between the comma and the consecutive number, e.g. [3,4,6-12].

References should be written as follows:

Journal papers: initials and names of all authors, full title of paper, journal abbreviation (according to Index Medicus), year of publication, volume (in Arabic numerals), first and last page (example below):

1. Valverde F. The organization of area 18 in the monkey. Anat Embryol 1978; 154: 305-334.
2. Uray NJ, Gona AG. Calbindin immunoreactivity in the auricular lobe and interauricular granular band of the cerebellum in bullfrogs. Brain Behav Evol 1999; 53: 10-19.

Book and monographs: initials and names of all authors, full title, edition, publisher, place, year (examples below):

1. Pollack RS. Tumor surgery of the head and neck. Karger, Basel 1975.
2. Amaral DG, Price JL, Pitkänen A, Carmichael ST. Anatomical organization of the primate amygdaloid complex. In: Aggleton JP (ed.). The amygdala. Wiley-Liss, New York 1992; pp. 1-66.

Reference to articles that are accepted for publication may be cited as „in press" or Epub.

Proofs

Corrections to the proofs should be restricted to printer's errors only; other alterations will be charged to the authors. In order to maintain rapid publication, proofs should be returned within 48 hours, preferably by e-mail, fax or courier mail. If the Publisher receives no response from the authors after 10 days, it will be assumed that there are no errors to correct and the article will be published.

Subscription information

The journal is published in one volume per year consisting of four numbers. The annual subscription price is 160 PLN for Institutions from Poland and 80 PLN for individual subscribers from Poland and 140 Euro for foreign Institutions and 70 Euro for foreign individual subscribers.
Payment should be made to:
Termedia sp. z o.o., ul. Kleeberga 8, 61-615 Poznań
BZ WBK III O/Poznań PL 61 1090 1359 0000 0000 3505 2645
SWIFT: WBKPPLPP

The publisher must be notified of a cancellation of a subscription not later than two months before the end of the calendar year. After that date the subscription is automatically prolonged for another year.
Publishing, Subscription and Advertising Office:
TERMEDIA Publishing House
ul. Kleeberga 2
61-615 Poznań, Poland
phone/fax +48 61 822 77 81
e-mail: termedia@termedia.pl
http://www.folianeuro.termedia.pl

Folia Neuropathologica

AUTHOR'S STATEMENT

Title of the article

.....

.....

.....

The author(s) hereby confirm(s) that:

☐ The above-mentioned work has not previously been published and that it has not been submitted to the Publishers of any other journal (with the exception of abstracts not exceeding 400 words).

☐ All co-authors named and the relevant authorities of the scientific institutions at which the work has been carried out are familiar with the contents of this work and have agreed to its publication.

☐ In sending the manuscript together with illustrations and tables agree(s) to automatic and free transfer of copyright to the Publisher allowing for the publication and distribution of the material submitted in all available forms and fields of exploitation, without limits of territory or language, provided that the material is accepted for publication. At the same time the author(s) accept(s) that the submitted work will not be published elsewhere and in whatever language without the earlier written permission of the copyright holder, i.e. the Publisher.

☐ (S)he (they) agree to waive his(her)(their) royalties (fees).

☐ (S)he (they) empower(s) the Publisher to make any necessary editorial changes to the submitted manuscript.

☐ All sources of funding of the work have been fully disclosed.

☐ The manuscript has been prepared in accordance with the Publisher's requirements.

☐ (S)he (they) is (are) familiar with the regulations governing the acceptance of works as published in *Folia Neuropathologica* and agree(s) to follow them.

☐ (S)he (they) agree to accept appropriate invoice from the Publisher in case colour illustrations are implemented.

Date *Signatures of* ***all authors***

The covering letter formula can be found at: www.folianeuro.termedia.pl
-The covering letter should be sent to Associate Editor:

Milena Laure-Kamionowska
-Editorial Office of Folia Neuropathologica
Mossakowski Medical Research Centre, Polish Academy of Sciences
Poland Medical Research Centre
ul. Pawinskiego 5
02-106 Warszawa, Poland

CONTENTS